Development of Catalysts for Alkyne Metathesis: Synthesis of Functionalised Molybdenum Benzylidyne Complexes and Related Species

Von der Fakultät für Lebenswissenschaften

der Technischen Universität Carolo-Wilhelmina zu Braunschweig

zur Erlangung des Grades eines

Doktors der Naturwissenschaften (Dr. rer. nat.)

genehmigte

D i s s e r t a t i o n

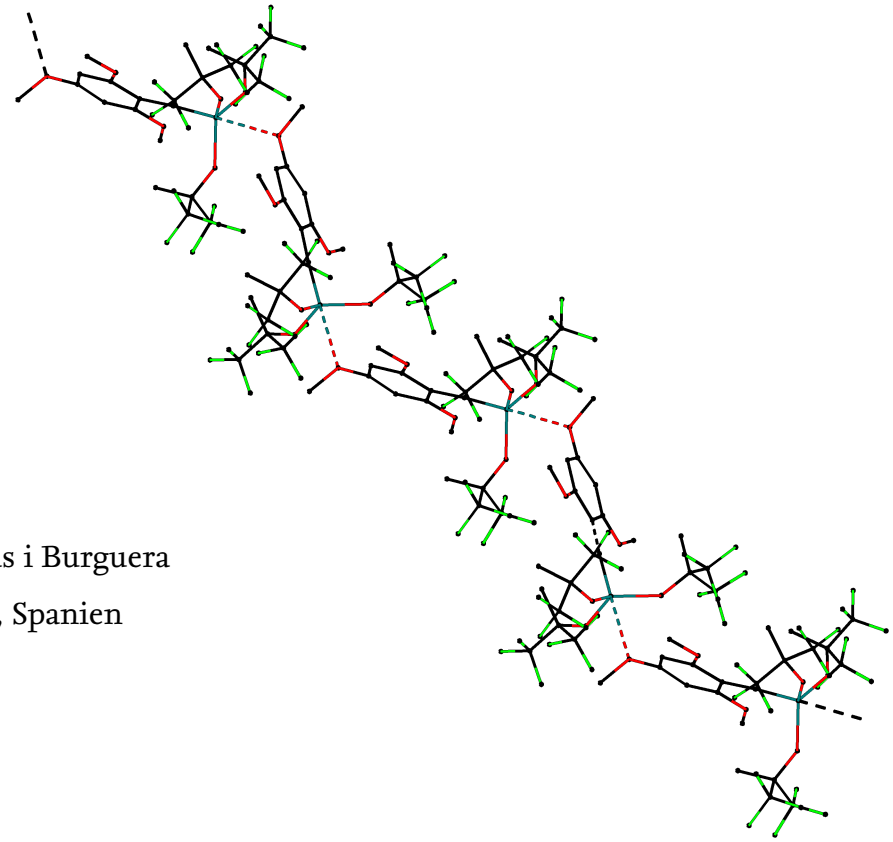

von Òscar Àrias i Burguera

aus Barcelona, Spanien

1. Referent: Prof. Dr. Dr. h.c. Dr. h.c. Matthias Tamm
2. Referent: Prof. Dr. Daniel B. Werz
eingereicht am: 17.06.2019
mündliche Prüfung (Disputation) am: 17.10.2019

Druckjahr 2019

Cover picture: Molecular structure of compound **5**.

Vorveröffentlichungen der Dissertation

Teilergebnisse aus dieser Arbeit wurden mit Genehmigung der Fakultät für Lebenswissenschaften, vertreten durch den Mentor der Arbeit, in folgenden Beiträgen vorab veröffentlicht:

Publikationen

D. P. Estes, C. Bittner, Ò. Àrias, M. Casey, A. Fedorov, M. Tamm, C. Copéret. Alkyne Metathesis with Silica-Supported and Molecular Catalysts at Parts-per-Million Loadings. *Angew. Chem. Int. Ed.* **2016**, *55*, 13960–13964; *Angew. Chem.* **2016**, *128*, 14166–14170.

Ò. Àrias, K. Brandhorst, D. Baabe, M. Freytag, P. G. Jones, M. Tamm. Formation of paramagnetic metallacyclobutadienes by reaction of diaminoacetylenes with molybdenum alkylidyne complexes. *Dalton Trans.* **2017**, *46*, 4737–4748.

Ò. Àrias, H. Ehrhorn, J. Härdter, P. G. Jones, M. Tamm. Synthesis of Ether-Functionalized and Sterically Demanding Molybdenum Alkylidyne Complexes. *Organometallics* **2018**, *37*, 4784–4800.

Tagungsbeiträge

Ò. Àrias, K. Brandhorst, M. Freytag, P. G. Jones, M. Tamm. Challenges in optimizing alkyne metathesis catalysts (**oral presentation**). In: *21st International Symposium in Olefin Metathesis and Related Chemistry* (*ISOM XXI*, Jul 12–16, 2015), Graz (Austria).

Ò. Àrias, K. Brandhorst, M. Freytag, P. G. Jones, M. Tamm. Challenges in optimizing alkyne metathesis catalysts (**oral presentation**). In: *250th ACS National & Exposition: Innovation from Discovery to Application* (Aug 16–20, 2015), Boston, MA (USA), Abstracts of Papers, INOR-470.

Ò. Àrias, D. Melcher, B. Haberlag, M. Tamm. Competing Reactions in Alkyne Metathesis (**poster**). In: *International Symposium in Olefin Metathesis and Related Chemistry XX* (*ISOM XX*, Jul 14–19, 2013), Nara (Japan).

Ò. Àrias, A. R. Petrov, P. G. Jones, U. Rosenthal, M. Tamm. Formation of Unusual 3-, 4-, and 5-Membered Metallacycles (Ti, Zr, Mo) by Reaction with Ynediamines (**poster** including flash poster presentation). In: *7th CaRLa Winter School 2014* (Feb 22–28, 2014), Heidelberg (Germany).

Ò. Àrias, A. R. Petrov, T. Bannenberg, P. Arndt, P. G. Jones, U. Rosenthal, M. Tamm. Formation of Unusual 3-, 4-, and 5-Membered Metallacycles (Ti, Zr, Mo) by Reaction with Ynediamines (**poster**). In: *16th JCF spring symposium 2014* (Mar 26–29, 2014), Universität Jena (Germany).

T. Schnabel, C. Bittner, Ò. Àrias, D. Melcher, M. Tamm. Overview of Recent Developments in Alkyne and Diyne Metathesis (**poster**). In: *5. Braunschweiger Jungchemikertagung* (Apr 15, 2014), Technische Universität Braunschweig (Germany).

Ò. Àrias, P. G. Jones, M. Tamm. Alkynes in stoichiometric reactions with a metathesis catalyst (**poster**). In: *17. Norddeutsches Doktorandenkolloquim 2014* (Sep 11–12, 2014), Leibniz-Institut für Katalyse e.V. an der Universität Rostock (Germany).

Ò. Àrias, K. Brandhorst, M. Freytag, P. G. Jones, M. Tamm. Challenges in optimizing alkyne metathesis catalysts (**poster**). In: *GDCh-Wissenschaftsforum Chemie 2015* (Aug 30–Sep 2, 2015), Dresden (Germany).

Ò. Àrias, J. Härdter, M. Freytag, P. G. Jones, M. Tamm. Ether-functionalised Alkyne Metathesis Catalysts (**poster**). In: *4. Niedersächsisches Katalyse-Symposium 2016* (*NiKaS 2016*, Sep 19–20, 2016), Technische Universität Braunschweig (Germany).

Ò. Àrias, J. Härdter, M. Freytag, P. G. Jones, M. Tamm. Ether-functionalised Alkyne Metathesis Catalysts (**poster**). In: *CaSuS-Workshop* (May 29–30, 2017), Bielefeld (Germany).

Ò. Àrias, M. Freytag, P. G. Jones, M. Tamm. Ligand Variation in Molybdenum Alkylidyne Complexes of the Type [ArC≡Mo{OCMe$(CF_3)_2$}$_3$(L)] (**poster**). In: *5. Niedersächsisches Katalyse-Symposium 2018* (*NiKaS 2018*, Sep 19–20, 2018), Georg-August-Universität Göttingen (Germany).

A les persones que m'han acompanyat

durant tots aquests anys

Fortunately science, like that nature to which it belongs, is neither limited by time nor by space. It belongs to the world, and is of no country and of no age. The more we know, the more we feel our ignorance; the more we feel how much remains unknown; and in philosophy, the sentiment of the Macedonian hero can never apply – there are always new worlds to conquer.

— Sir Humphry Davy, English chemist and physicist (1778–1829)

Contents

1 Introduction 1

1.1. Global relevance of catalysis 1

1.2. Homogeneous catalysis 2

1.2.1. Olefin metathesis 3

1.3. Alkyne metathesis 5

1.3.1. Historical overview 5

1.3.2. The catalytic cycle 7

1.3.3. Alkyne metathesis patterns and selected applications 14

1.3.4. State of the art 15

2 Overview 27

3 Results and discussion 29

3.1. Functionalisation of the alkylidyne moiety 29

3.1.1. Conceptual background and targets 29

3.1.2. Ether-substituted acyl complexes 32

3.1.3. Ether-substituted arylalkylidyne complexes 48

3.2. Coordination of additional ligands 64

3.2.1. Attempted nitrile metathesis: An acetonitrile alkylidyne complex 64

3.2.2. Synthesis of alkylidyne complexes with coordinating ligands 67

3.3. Isolation of intermediates and related species 84

3.3.1. The elusive molybdenacyclobutadiene 85

3.3.2. Species involved in terminal alkyne metathesis 105

3.4. Catalytic studies 116

3.4.1. Determination of calibration curves for gas chromatography analysis 116

3.4.2. Catalytic activity in self-metathesis 116

3.4.3. Identification of air-stable compounds 121

4 Concluding remarks 123

4.1. Summary 123

4.2. Conclusions and Perspectives 128

5 Experimental section 131

5.1. General considerations 131

5.2. Analytical techniques 132

5.2.1. NMR spectroscopy 132

5.2.2. Chromatography techniques 132
5.2.3. X-ray diffraction studies 133
5.2.4. Computational methods 133
5.2.5. Solid-state magnetic susceptibility 134
5.2.6. Other techniques 134
5.3. Experimental procedures 135
5.3.1. Starting materials 135
5.3.2. Potassium alkoxides 136
5.3.3. Organolithium reagents 137
5.3.4. Complexes 139
5.3.5. Alkynes 195
6 Abbreviations and acronyms 201
7 Acknowledgements 205
8 References 207

1 Introduction

Sir Humphrey Davy, who is credited with the invention of the mine safety lamp, discovered around 1816 that a warm platinum gauze would slow down the combustion of fire-damp and other mixtures of vapours, thus preventing ignition and explosion of these gases. Rather than producing a flame, the gauze would just glow. This observation constitutes one of the oldest recorded examples of catalysis,[1] a word adopted by the Swedish chemist Jacob Berzelius during the 1830s. Berzelius himself proposed the platinum body to possess a "catalytic force".[2] The definition of catalysis was refined later by the German chemist and Nobel laureate Wilhelm Ostwald, a definition that is still valid today: "catalytic action consists in the modification, by the acting substance, the catalyst, of the rate at which a chemical reaction occurs, without that substance itself being part of the end-products formed".[3]

1.1. Global Relevance of Catalysis

Two centuries later, catalysis is a phenomenon of great impact in economy, ecology and society, and has become an indispensable tool in the vast majority of industrial processes involving chemical transformations. Production of large-scale and fine chemicals, high-value manufacturing, fossil fuel treatment, and pollution and waste reduction are all processes that are unimaginable nowadays without the use of a catalyst (Figure 1). BASF, which defines itself as "The Global Leader in Catalysis", states that "catalysts play a crucial role in 90% of all commercially produced chemical products".[4] Indeed, with the help of catalysts chemical factories can be operated efficiently under industrially feasible conditions of pressure and temperature.[5] Hence, it is probably fair to affirm that the chemical industry relies on catalysis as much as organisms rely on enzymes, which are the most specific catalysts in the world.[5]

In academia, the study of catalysis and underlying phenomena at a theoretical, physical and experimental level has contributed enormously to the scientific progress in this field. Beyond any doubt, catalysis not only is essential for industrial purposes but

Figure 1. Examples of catalysts as used in industry.[6]

has also become an alternative and efficient synthetic tool for chemistry laboratories developing new molecules or materials, facilitating the preparation of challenging compounds under favourable reactions conditions. Catalyst performance is not limited only to accelerate the reaction (activity), but it is usually characterised by a strict control of the reaction outcome (selectivity). Hence, catalyst design and optimisation are of fundamental interest in this research area.

1.2. Homogeneous Catalysis

Commonly, catalysts are classified into heterogeneous, homogeneous and biocatalysts. In particular, the development of homogeneous (or molecular) catalysts is strongly related to organometallic chemistry. Although they are less stable and more difficult to separate than heterogeneous catalysts, homogeneous catalysis offers several advantageous aspects such as high activity and selectivity, mild reaction conditions, elimination of diffusion problems, and control over reaction mechanism and catalyst properties.[7] Relevant examples of the application of organometallic complexes as homogeneous catalysts in industrial processes include (i) coupling reactions, (ii) hydrocyanation, (iii) hydroformylation, (iv) hydrogenation, (v) carbonylation, (vi) olefin metathesis, (vii) olefin oxidation and (viii) olefin polymerisation. Number vi constitutes the historical cornerstone of this PhD thesis, and will be introduced in more detail in the next section.

1.2.1. Olefin metathesis

The olefin metathesis, first named in 1967,[8,9] is a chemical transformation in which a C–C double bond is broken and regenerated again to form a new olefin by combination of the cleaved carbene fragments (see Scheme 1). As mentioned above, this catalytic reaction has found important industrial applications. Although in almost all processes heterogeneous catalysts are still used, two examples should be highlighted: the olefin recycling strategy in the Shell Higher Olefin Process (SHOP), and the ARCO (Atlantic Richfield Company) process that produces propene from ethylene and 2-butene.[10,11] It is therefore not surprising that the developers of the metathesis method, Richard R. Schrock and Robert H. Grubbs, and also Yves Chauvin, who postulated the mechanism, were awarded the Nobel Prize in Chemistry in 2005.[12]

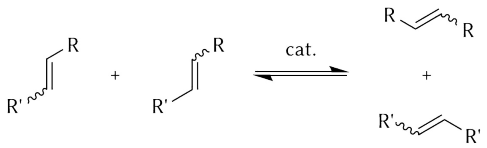

Scheme 1. General equation of the olefin metathesis reaction; cat. = catalyst.

It is beyond the scope of this work to summarise the magnitude of the advances in the field of olefin metathesis, particularly taking into consideration the numerous reviews and monographs written on this subject.[13–17] However, it is important to highlight some transition metal alkylidene complexes largely used as homogeneous catalysts in olefin metathesis. Schrock-type catalysts as well as first- and second-generation Grubbs' catalysts (Figure 2) are archetypical and have inspired the design of countless catalytically active complexes by selective or systematic modification of the ligand environment.[7,18]

Schrock's catalysts (type **A**) are molybdenum and tungsten alkylidene complexes in the highest oxidation state (+VI) and are characterised by their high reactivity and out-

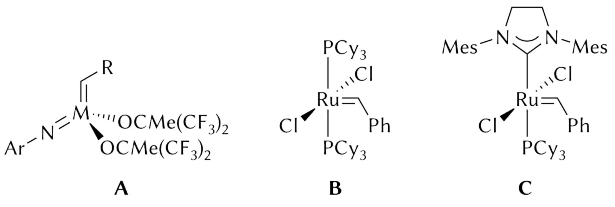

Figure 2. Archetypical homogeneous catalysts for olefin metathesis. **A**, Schrock's catalysts (M = Mo, R = CMe_2Ph; M = W, R = *t*-Bu); **B**, first-generation Grubbs' catalyst; **C**, second-generation Grubbs' catalyst; Cy = cyclohexyl, Mes = 2,4,6-trimethylphenyl.

standing activity, as a result of the electron-withdrawing alkoxide ligands. Despite their inevitable susceptibility towards air or moisture, other decomposition pathways are prevented by the electron-donating and sterically demanding di-*ortho*-substituted arylimido ligand, which increases the stability of the molecules. In fact, the properties of these complexes are based on a balanced push–pull ligand system.

Much more robust yet still remarkable metathesis promoters are Grubbs' 16 VE (valence electrons) ruthenium(II) complexes (**B**, **C**). The catalytically active species is formed upon displacement of one phosphane ligand to generate a 14 VE species. In the second-generation catalyst (**C**) an *N*-heterocyclic carbene ligand replaces one of the phosphane ligands, which furnishes a complex with enhanced stability and a catalytic performance that rivals that of Schrock's catalysts.

Finally, a noteworthy modification introduced by Amir H. Hoveyda in 1999[19] needs to be mentioned here. The essence of the Hoveyda–Grubbs' catalysts (Figure 3, **D**) consists in the chelating *ortho*-isopropxy group attached to the benzylidene moiety,[20,21] which replaces one phosphane ligand. This chelation effect redoubles the stability of the complex, although at the expense of slower initiation rates.

Beyond any doubt, our world has benefited from the development of the olefin metathesis reaction. Not only are several industrially manufactured products and materials a manifest result of this catalytic reaction, but also many research laboratories and facilities around the globe have taken advantage of this synthetic tool to develop new complex molecules such as natural products, pharmaceutical drugs, high-value polymers, or supramolecular structures.[22]

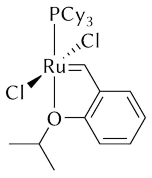

D

Figure 3. First-generation Hoveyda–Grubbs' catalyst (**D**); Cy = cyclohexyl.

1.3. Alkyne Metathesis

Alkyne metathesis, the analogous reaction with alkynes instead of olefins (Scheme 2), has received less attention from the chemical community, and has not yet encountered suitable industrial applications. Nevertheless, as shown by the increasing number of publications, the interest in alkyne metathesis has grown in the past two decades, particularly in the fields of organic and polymer chemistry,[16,23–25] and has been established as a very efficient tool for reorganising C–C triple bonds.

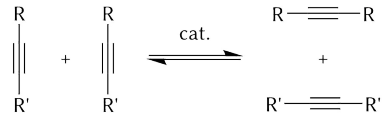

Scheme 2. General equation of the alkyne metathesis reaction; cat. = catalyst.

1.3.1. Historical overview

A short communication by F. Pennella, R. L. Banks and G. C. Bailey[26] a half century ago on the *disproportionation of alkynes* marked the beginning of the alkyne metathesis reaction. This report describes the formation of 2-butyne and 3-hexyne from 2-pentyne at 200–450 °C and atmospheric pressure using a silica-supported tungsten trioxide catalyst precursor. Six years later, in 1974, A. Mortreux and M. Blanchard[27] presented a catalyst system for the metathesis of alkynes at acceptable temperatures based on the combination of molybdenum hexacarbonyl and resorcinol (or other aryl alcohols). Only one year later, T. J. Katz and J. McGinnis[28] suggested a mechanism for the alkyne metathesis reaction (still valid today). This mechanism is analogous to Chauvin's olefin metathesis mechanism, and considers carbyne complexes to be the active catalysts, which combine with one alkyne substrate to generate an intermediate metallacyclobutadiene species (see next section below). This postulation appeared to be in contradiction with the fact that carbyne complexes known at the time (Fischer's carbyne complexes)[29] did not promote the metathesis of acetylenes.

In 1978, however, R. R. Schrock and his team[30] published the preparation and characterisation of a tungsten alkylidyne complex in its highest oxidation state, [M(≡C-*t*-Bu)(CH_2-*t*-Bu)$_3$] (M = W, **E**, Scheme 3), and its molybdenum equivalent (M = Mo). Even if these complexes were not used as alkyne metathesis promoters, they constitute the first examples of group 6 Schrock-type carbynes,[31,32] a family of compounds that later emerged as suitable catalysts for alkyne metathesis.[23,33–35] For example, substitution of

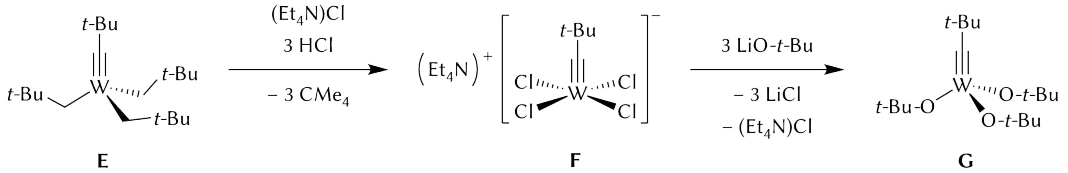

E **F** **G**

Scheme 3. Synthesis of Schrock's catalyst **G** used in alkyne metathesis.

the neopentyl ligands by alkoxides via the tetrachlorido complex $(Et_4N)[W(\equiv C\text{-}t\text{-}Bu)(Cl)_4]$ (**F**) led to alkylidyne complex $[W(\equiv C\text{-}t\text{-}Bu)(O\text{-}t\text{-}Bu)_3]$ (**G**, Scheme 3).[33,36] As stated by the authors, the complex is highly active in alkyne metathesis: "the activities [...] for acetylene metathesis are far greater than those reported for the heterogeneous or $Mo(CO)_6$/phenol catalysts".[33] In addition, isolation of a tungstenacyclobutadiene species by R. R. Schrock and coworkers,[37] and the ability of related systems to perform alkyne metathesis,[38,39] soon confirmed the validity of Katz's mechanism.

Given the success of neopentylidyne catalyst **G**, R. R. Schrock and coworkers explored the variability of the ligands on precursor **F**, and applied the concept to molybdenum-based alkylidyne complexes.[35] Over the following decades, alkyne metathesis received increased attention: improved and alternative synthetic routes were developed by several research groups (particularly the groups of Schrock, Cummins, Fürstner, Moore, Zhang, Johnson, Tamm, Nuckolls, and Fischer), which resulted in a great number of highly efficient, well-defined catalysts and precatalysts for alkyne metathesis.[23,34,40] Some of the most prominent examples and indispensable strategies will be highlighted in Section 1.3.4. In addition, the increasing number of applications and tolerated substrates showcases the importance of alkyne metathesis as a powerful synthetic tool in organic, supramolecular and polymer chemistry.[23–25,41]

For example, one of these applications that had a significant impact in natural product synthesis is the ring-closing alkyne metathesis (RCAM).[42–45] Its early discovered potential in the preparation of functionalised macrocycles is particularly interesting in combination with the Lindlar hydrogenation to stereoselectively afford (*Z*)-configured cycloolefins. Moreover, selective semireduction of cyclic alkynes using a hydrosilylation–protodesilylation approach gives access to the related (*E*)-isomers (Scheme 4).[23]

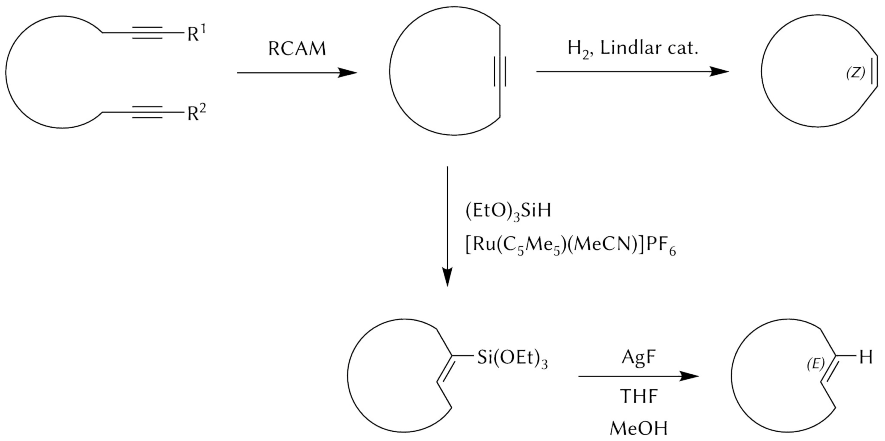

Scheme 4. Tandem ring-closing alkyne metathesis (RCAM) and semireduction reactions give access to cyclic olefins with stereoselectivity (*E*/*Z*) control; cat. = catalyst, THF = tetrahydrofuran.

Despite the admirable advances in this field, the development of the alkyne metathesis reaction lags behind that of its cousin, the olefin metathesis. A number of reasons is responsible for this divergence. One important aspect is the prevalence of olefins compared to alkynes, both as a starting materials or as synthetic targets. A further element to consider is the larger number of studies about the mechanism of the olefin metathesis and the associated modification of reaction conditions. But perhaps the decisive reason for the limited applicability of the alkyne metathesis lies in the lack of appropriate catalysts: most of the complexes are acutely unstable towards oxygen or moisture, so the user is forced to work under an inert atmosphere using glove boxes and vacuum techniques, synthetic protocols are not always convenient, reaction conditions are occasionally adverse, and functional group compatibility depends strongly on the catalysts. All reported alkyne metathesis promoters are intended for some specific applications but still have their own disadvantages or limitations. It is undeniable that the optimal catalyst – highly active, readily prepared, user-friendly, robust and universal – still remains a challenge; even so, the developments of the last five years suggest that this is about to change.

1.3.2. The catalytic cycle

Alkyne metathesis (as well as olefin metathesis) is a catalytic isodesmic reaction[46] that involves the redistribution of triple bonds, and hence requires that the number and type of chemical bonds in the starting materials remain unchanged in the products. For this reason, the reaction is usually thermoneutral ($\Delta H = 0$) and entropy-driven. A direct consequence of this is the reversibility of the metathesis reaction. In addition,

the catalytic character of the reaction implies that it takes place in recurrent cycles. In the following sections, the mechanism of the alkyne metathesis, the nature of reaction intermediates, and some undesired side-reactions will be discussed in more detail.

Reaction mechanism

Following the mechanism described by T. J. Katz,[28] two phases can be distinguished in the catalytic cycle (Scheme 5): the initiation step and the actual cycle. During the – ideally brief – initial period (Scheme 5, left), precatalyst **H** (commonly a metal alkylidyne) combines with the substrate (an alkyne) in a [2+2] cycloaddition reaction to form a metallacyclobutadiene species (**I**). For the sake of simplicity, the substrate is exemplified by a methyl-capped alkyne (RC≡CMe) in Scheme 5. After bond isomerisation and [2+2] cycloreversion, a new alkyne, RC≡CR′, is released and the actual active species **J** is generated. Of course, addition of the alkyne in the reverse orientation (Scheme 5, right) originates a different metallacyclobutadiene intermediate (**I′**) with the methyl group placed in the *β*-position and, subsequently, yields a different alkylidyne complex (**J′**), which acts equally as an active catalyst. Indeed, alkylidyne complexes **J** and **J′** interconvert in each cycle of the catalytic reaction through metallacyclobutadiene intermediates (**K** and **K′**), producing two new alkynes, RC≡CR and 2-butyne in this example, in which the substituents of two substrate molecules have been interchanged *de facto* (see Scheme 2 for the net equation, R′ = Me).

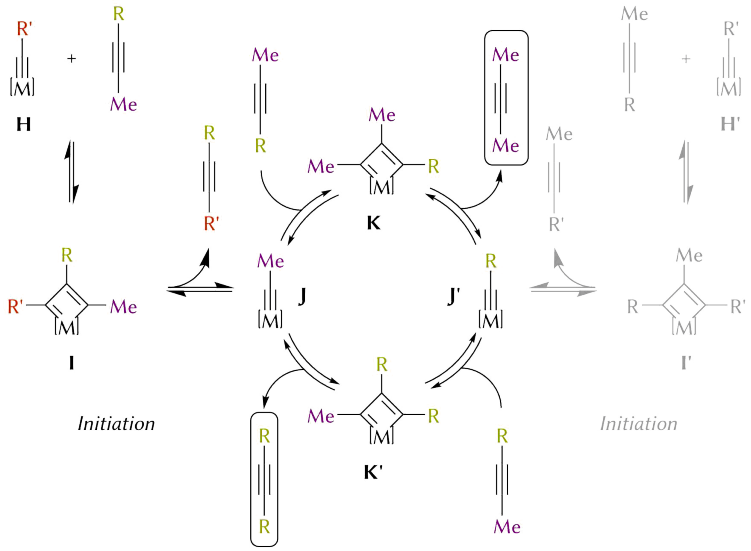

Scheme 5. The alkyne metathesis catalytic cycle based on the self-metathesis of a methyl-capped alkyne (RC≡CMe). The products are enclosed in a rectangular frame. A second possible initiation step is shown in the right side of the scheme in grey. [M] = MX_n (M = Mo, W; X = typically alkoxide, amido or iminato ligands; *n* is ordinarily 3); R′ is predominantly an aryl or a short alkyl chain.

Driving force

Generation of new alkynes is the result of productive metathesis; however, a non-productive metathesis pathway (i.e. if the original alkyne is regenerated) has to be considered as well, because the [2+2] cycloaddition step is not regiospecific and depends on substrate orientation (Scheme 6). Indeed, complete conversion of the substrate is achieved only under the influence of a driving force; otherwise an equilibrium is reached. Moreover, selectivity control (i.e. isolation of a specific target product) is challenging as it is intrinsically associated with isodesmic and reversible reactions.[46] Nevertheless, a few strategies can be adopted to overcome this obstacle, and all are based on the removal of one product in order to shift the equilibrium towards the desired reaction outcome. These are essentially the following:

a) Use of reduced pressure[47] or gas purge.[48] If an alkyne of low molecular weight, such as 2-butyne or acetylene, is generated as the metathesis by-product, the use of gentle vacuum or a constant nitrogen purge during catalysis can be sufficient to remove it from the reaction mixture. For this reason, methyl-capped alkynes (RC≡CMe) are common and convenient substrates in alkyne metathesis.

b) Use of molecular sieves.[49] More effective and less intrusive than the previous method, the use of activated molecular sieves as small alkyne scavengers is the most extended methodology to drive the reaction to completion. First employed for this purpose by A. Fürstner et. al. in 2010, molecular sieves with pore size 5 Å, which are able to adsorb light hydrocarbons effectively, have been proved to increase conversion rates while considerably reducing reaction times. They are advantageous because they do not cause an undesired concentration gradient during the course of the reaction and are easily removed by filtration at the end.

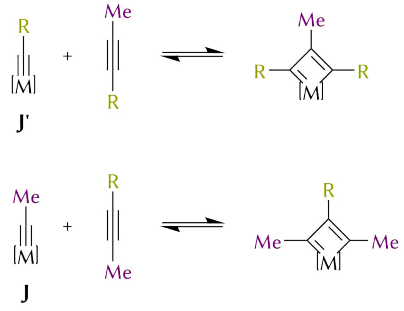

Scheme 6. Two possible pathways of non-productive metathesis (based on the catalytic cycle on Scheme 5).

c) Precipitation-driven strategy. In this approach by W. Zhang and J. S. Moore[50–52] precipitation of a poorly soluble alkyne by-product, which requires the use of large end-substituents, is the driving force of the reaction (see Scheme 7). Although discouraging for the lack of atom economy, this setup can be satisfactorily used also in large-scale procedures.

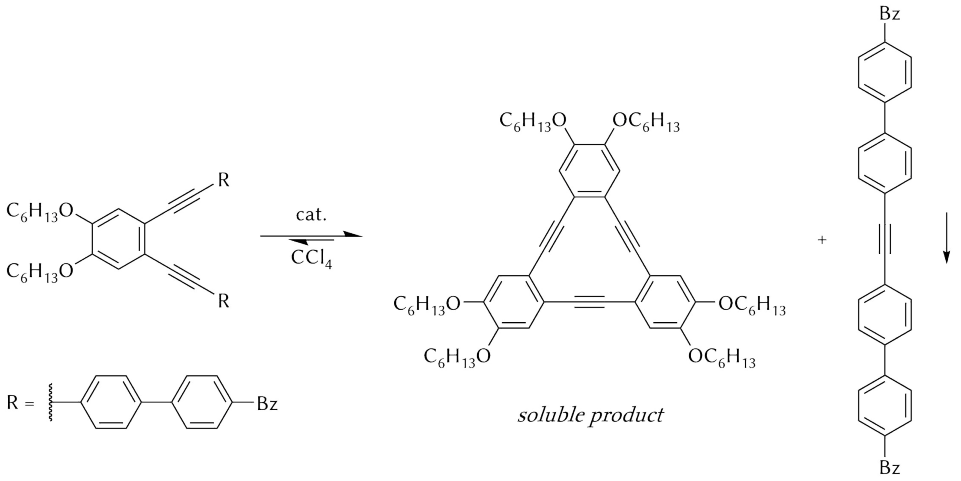

Scheme 7. An example of precipitation-driven alkyne metathesis; Bz = benzoyl (–C(=O)Ph), cat. = catalyst.

Carbyne complexes

According to the reaction mechanism (Scheme 5), the catalytically active species are metal carbyne complexes (**J**/**J′**). By analogy with the metal carbene family, there are two classical types of carbyne complexes, namely, Fischer-type and Schrock-type carbyne complexes,[53] although the latter are preferably called alkylidyne complexes and contain always a substituted methylidyne fragment RC≡. As illustrated in Scheme 8, three major resonance forms (**a–c**) can be used to describe the metal–carbon triple bond. These structures, however, are only theoretical in that carbyne ligands possess an sp-hybridised carbon atom, are nearly always linear, and have a strong preference to form actual M–C triple bonds (**b**).[54]

In Fischer's carbyne complexes the carbyne carbon atom is dominated by an electrophilic character (cf. **J′-c**, Scheme 8), the ligands are generally good π acceptors, and the

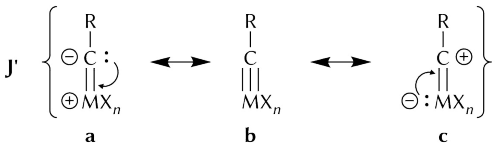

Scheme 8. The metal–carbon triple bond can be described as a resonance hybrid with three major contributing forms.

metal centre is in a low oxidation state. In contrast, Schrock's alkylidyne complexes have a metal atom in a high oxidation state, and the more electronegative carbyne carbon atom is of nucleophilic nature (cf. **J'-a**, Scheme 8). In order to establish a formal oxidation state of the metal atom, the carbyne moiety is considered to be a monocationic fragment (RC^{+}) in Fischer-type complexes and a closed-shell trianionic ligand (RC^{3-}) in the Schrock-type congeners.[11]

Characterisation of intermediates

Since the first isolation of a tungstenacyclobutadiene complex (Figure 4) in 1982,[37] a series of metallacyclobutadiene (MCBD) species have been obtained by cycloaddition of an alkyne to an alkylidyne complex or by reaction of alkynes with complexes containing a W–N or a W–W triple bond.[55] That has illustrated the pertinence of these compounds in the alkyne metathesis cycle and contributed to validate the mechanism proposed by T. J. Katz.[38,39] Even more, several of these species have been structurally characterised by X-ray crystallography.[55]

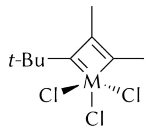

Figure 4. Structure of the first crystallographically characterised tungstenacyclobutadiene complex.

While the bonding situation in metallacyclobutadiene complexes has been the topic of discussion in various computational studies,[55–59] other theoretical calculations have focused on the mechanistic role of these species as reaction intermediates in the alkyne metathesis cycle.[60,61] These computations predict moderate free-energy barriers for the formation of MCBD species, which, in general, are slightly less stable than the reactants. The exact stabilisation of the MCBD intermediates depends on the nature and electronic properties of the supporting ligands, implying that high catalytic activities can be achieved through judicious variation and modulation of those ligands. As will be mentioned below (p 19 f), recent studies from our group have explored this concept by using alkoxide ligands with an increasing degree of fluorination.[62,63] Furthermore, it is important to note that MCBD complexes of more electrophilic metals (e.g. W over Mo) tend to exhibit a higher stability.

Side-reactions and decomposition pathways

The discussion of the catalytic cycle cannot be completed without looking at important side-reactions and undesired decomposition pathways, which are particularly relevant regarding certain substrate classes. Two types of substrates that are prone to cause side-reactions are alkynes with short alkyl chains and terminal acetylenes (RC≡CH). Both types of alkynes usually result in oligomerisation or polymerisation reactions, but the decomposition mechanisms are rather different.

Instead of undergoing metathesis, small alkynes can be processed to cyclic oligomers according to the ring expansion mechanism (Scheme 9).[47,64–67] This mechanism involves insertion of an acetylene molecule to the metallacyclobutadiene species to form metallabenzene (**L**) or even non-planar metallacyclohexatriene intermediates,[68] which rapidly generate a polymer through ring expansion.[69] Alternatively, metallabenzene complex **L** can rearrange to give a substituted cyclopentadienyl complex (**M**).[37,60,64,68]

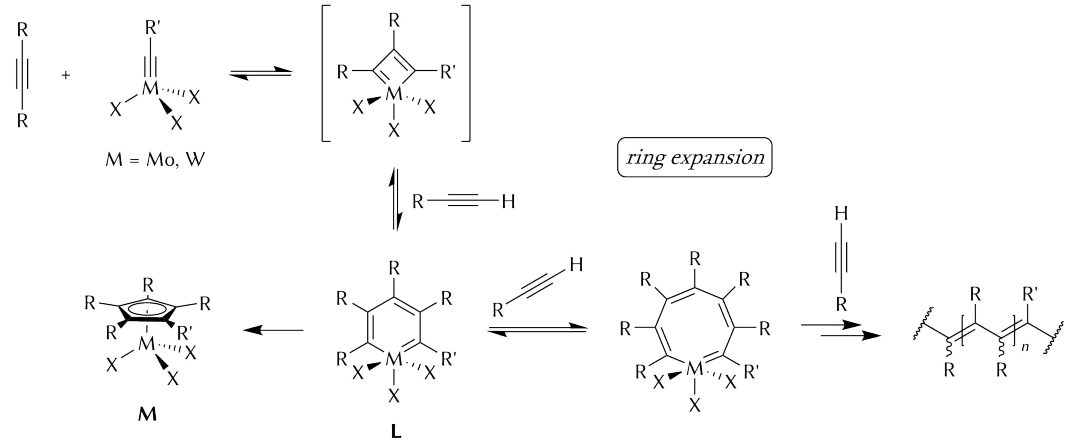

Scheme 9. Decomposition pathways involving small alkynes: Polymerisation via metallabenzene intermediates (**L**) and ring expansion (right), or formation of η^5-cyclopentadienyl complexes (**M**).

Traditionally, terminal alkynes have been unpopular substrates for acetylene metathesis, and until 2012 only a few examples of mostly inefficient terminal alkyne metathesis (TAM) had been communicated (cf. Section 1.3.4. State of the art).[70–73] At least two decomposition pathways (Scheme 10) are responsible for the incompatibility of terminal acetylenes with alkyne metathesis catalysts. In the first case, the metallacyclobutadiene intermediate[74] – formed via cycloaddition of the terminal alkyne with the metal alkylidyne* – can be readily deprotonated, which results in a depro-

* In such a manner that the hydrogen atom occupies the β-position of the four-membered ring. After the initiation step, R′ = R and the pathway is non-productive.

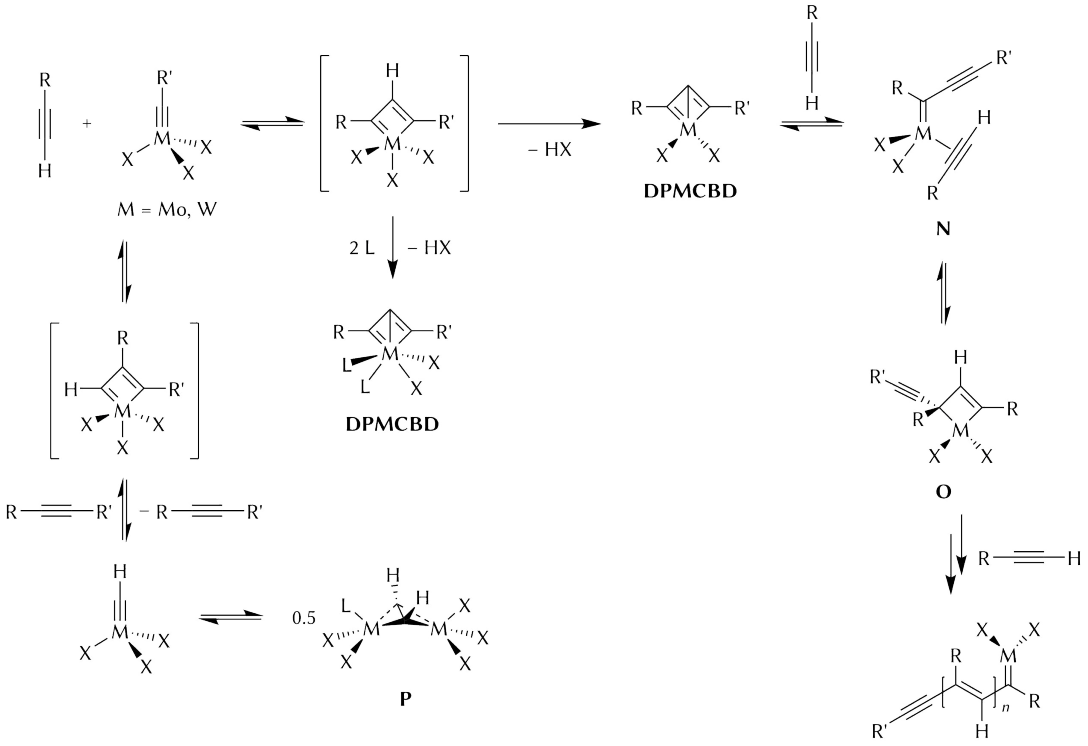

Scheme 10. Undesired decomposition reactions in alkyne metathesis caused by terminal alkynes.

tiometallacyclobutadiene (**DPMCBD**) species.[75] Reasonable candidates for deprotonation (at least under basic conditions) are the ligands (X, usually alkoxide moieties) attached to the metal centre. The DPMCBD can then rearrange to a metallacarbene complex (**N**), which is known to promote acetylene polymerisation via a metallacyclobutene intermediate (**O**) (Scheme 10, right).[76–78] Molybdenum[79,80] and tungsten[70,71,81,82] DPMCBD species have been commonly characterised by NMR spectroscopy. Merely a few DPMCBD complexes could be structurally characterised[81,83] and in general only after addition of strongly coordinating ligands (L, Scheme 10) such as pyridine[79] or 1,10-phenanthroline.[84,85]

The other pathway (which is the productive one) involves dimerisation of methylidyne species, $[M(\equiv CH)X_n]$, which gives acetylene-bridged dimetal compounds of type $[(MX_n)_2(\mu\text{-}\eta^2\text{:}\eta^2\text{-}C_2H_2)]$ (**P**).[70,71] Considering the reversibility of their formation (Scheme 10, bottom left),[71] these dimeric complexes can be best regarded as latent species rather than decomposition products.

In addition, rearrangement of MCBD complexes into metallatetrahedrane (also: η^3-cyclopropenyl) structures has to be considered (Scheme 11),[31,57,68,80,86,87] especially when the coordination number at the metal centre is increased (e.g. by addition of a σ-donor ligand).[54]

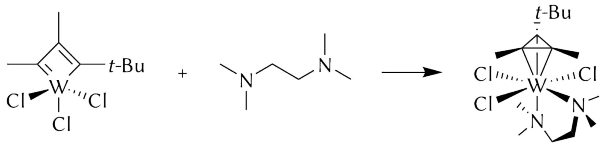

Scheme 11. Example of formation of a metallatetrahedrane complex.

1.3.3. Alkyne metathesis patterns and selected applications

Basically, the alkyne metathesis reaction can be divided into four subclasses,[25,34,88,89] as illustrated in Scheme 12: (i) alkyne cross-metathesis (ACM), (ii) ring-closing alkyne metathesis (RCAM), (iii) ring-opening alkyne metathesis polymerisation (ROAMP), and (iv) acyclic diyne metathesis (ADIMET) polymerisation. ACM, that is, the recombination of two acyclic acetylenes, is the most straightforward yet the least selective reaction pattern, and frequently yields mixtures of reactants and products. This selectivity problem is due to the lack of an inherent driving force (see above); nevertheless, a clever selection of substituents is the road to success. If both alkyne functionalities are part of the same molecule, intramolecular metathesis would result in a cyclic product (RCAM).[90] Formation of dimeric cycloalkynes is also possible through intermolecular reactions† (Scheme 12, top left),[91] and it highly depends on the degree of dilution. ACM and RCAM have been extensively employed in natural product synthesis,[43,92,93] often followed by selective partial reduction reactions (cf. Scheme 4).

α,ω-Diynes that, for geometric reasons, are not able to form cyclic products upon metathesis (e.g. linear molecules) can engage in ADIMET polymerisation.[94,95] Likewise, rigid molecules (bearing two or even more alkyne moieties) can undergo ADIMET reactions to form functionalised 1D-wires, 2D-macrocycles, or even more complex 3D-structures such as molecular cages and networks.[95–98] ADIMET polymerisation initially found application in the synthesis of poly(aryleneethynylene)s,[48,99,100] but also oligomerisation of arylalkynes, leading to shape-persistent macrocycles, has attracted attention in more recent years for its potential use in supramolecular chemistry and materials science.[50,95,97,98]

† Formally, this can be seen as a tandem ACM–RCAM reaction.

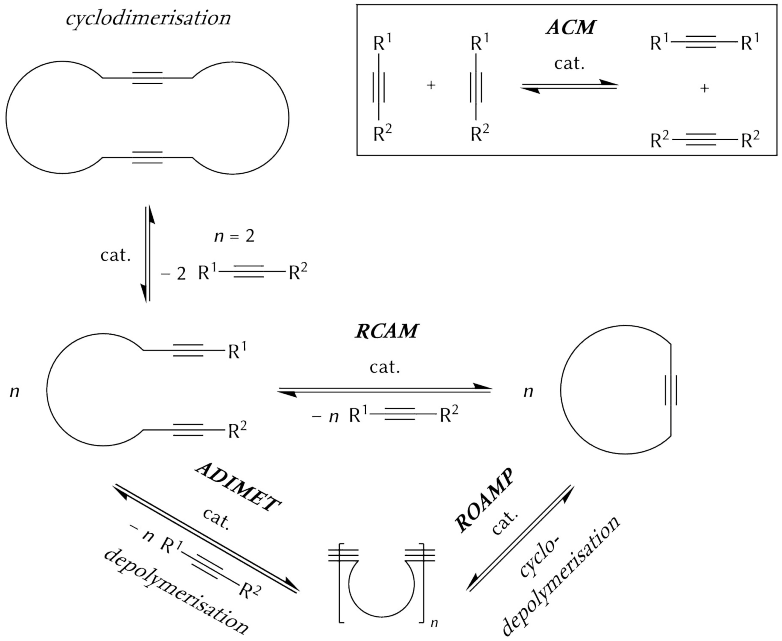

Scheme 12. Reaction types of alkyne metathesis; cat. = catalyst, ACM = alkyne cross-metathesis, ADIMET = acyclic diyne metathesis (polymerisation), RCAM = ring-closing alkyne metathesis, ROAMP = ring-opening alkyne metathesis polymerisation.

Polymeric alkynes can also be produced by ROAMP of strained cyclic alkyne substrates.[95] Both ROAMP and ADIMET polymerisation are an alternative for making functionalised polymeric materials, which otherwise are less convenient to be prepared by other methodologies. By virtue of thermodynamics and as a result of the reversibility of the process,[46] however, (cyclo)depolymerisation is a secondary reaction that cannot be neglected. Particularly under diluted conditions, this reverse reaction has been reported to give soluble (cyclic) oligomers.[95] Therefore, monomer concentration and catalyst selectivity (strained cyclic vs. polymeric acyclic C–C triple bonds) are crucial to control the reaction outcome and resolve the ring–chain dichotomy.

1.3.4. State of the art

Since the original, ill-defined, two-component, Mortreux-type systems ([$Mo(CO)_6$]/phenol derivative), the development of efficient, well-defined catalysts for alkyne metathesis has experienced a dramatic progress (Figure 5). Most of these advances have been highlighted in several reviews, minireviews and book chapters brilliantly written on this topic.[23–25,34,35,40,43,47,101–108] For this reason, only the most prominent examples will be briefly presented herein.

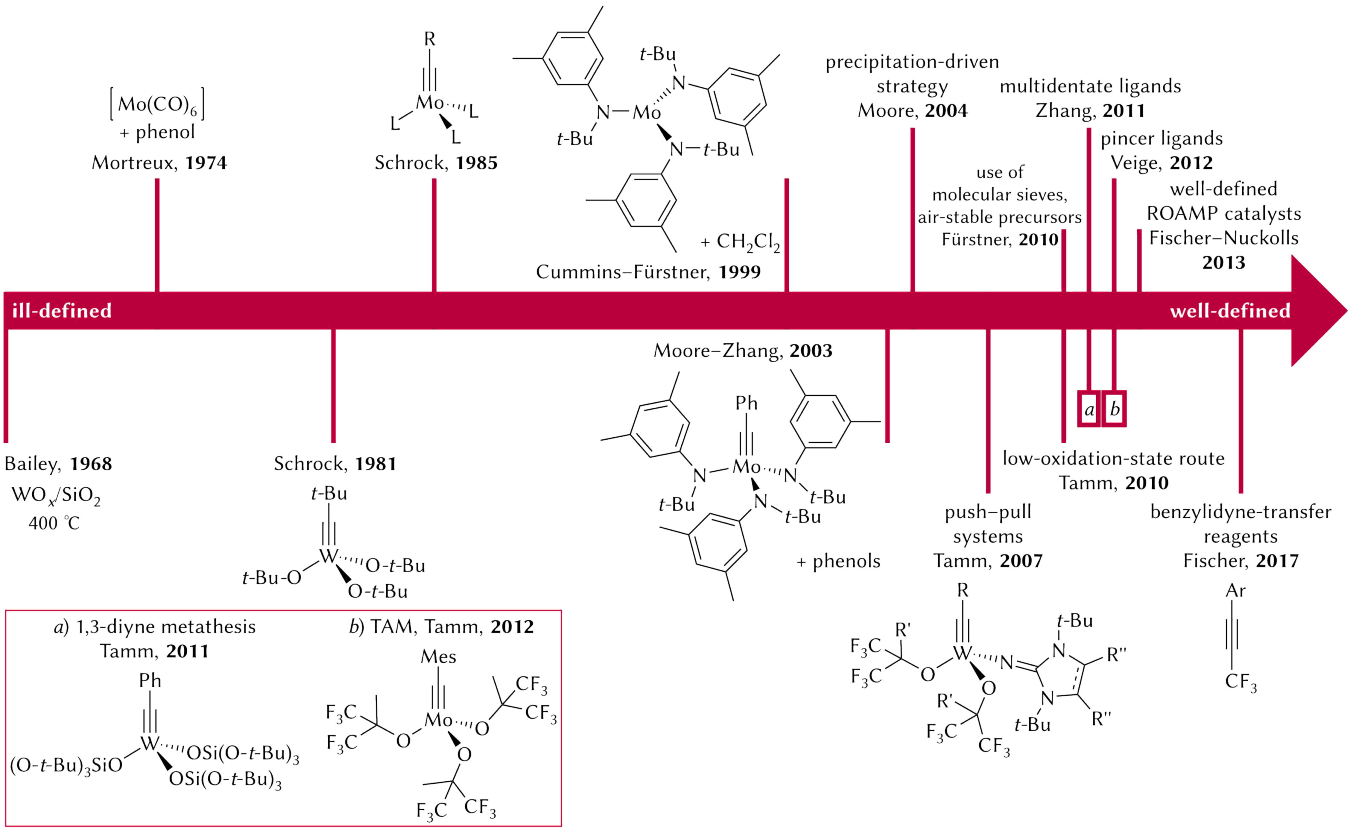

Figure 5. Timeline of the development of catalysts for alkyne metathesis.

Synthetic strategies

Essentially, alkyne metathesis (pre)catalysts with a defined structure are high-oxidation-state tungsten(VI) and molybdenum(VI) alkylidyne complexes of type $[M(\equiv CR)(X)_3]$ (Schrock's alkylidynes; M = Mo, W; R = alkyl, aryl), carrying a wide variety of supporting ligands (X), especially bulky alkoxides (e.g. fluorinated alkoxides, alkoxyaryls, silanolates and multidentate ligands), but also amido and iminato ligands, or combinations thereof.[24,40,101,109]

The synthesis of these complexes can be traced back to the discovery of neopentylidyne complex **E** (Scheme 3) – prepared in two steps from WCl_6 and neopentyl magnesium chloride (t-BuCH_2MgCl) –, which can be treated with HCl and 1,2-dimethoxyethane (DME) in ether to give the versatile precursor *mer*-$[W(\equiv C$-t-Bu$)(Cl)_3(dme)]$ (Scheme 13, top; dme = 1,2-dimethoxyethane).[105] Ligand substitution of the chloride ions through salt metathesis produces an extensive spectrum of tungsten-based catalyst candidates of the type $[W(\equiv CR)(X)_3]$. The preparation of the molybdenum counterparts has suffered from the poor yield (~35%) of the reaction of MoO_2Cl_2 with six equivalents of t-BuCH_2MgCl in tetrahydrofuran (THF) to access extremely air-sensit-

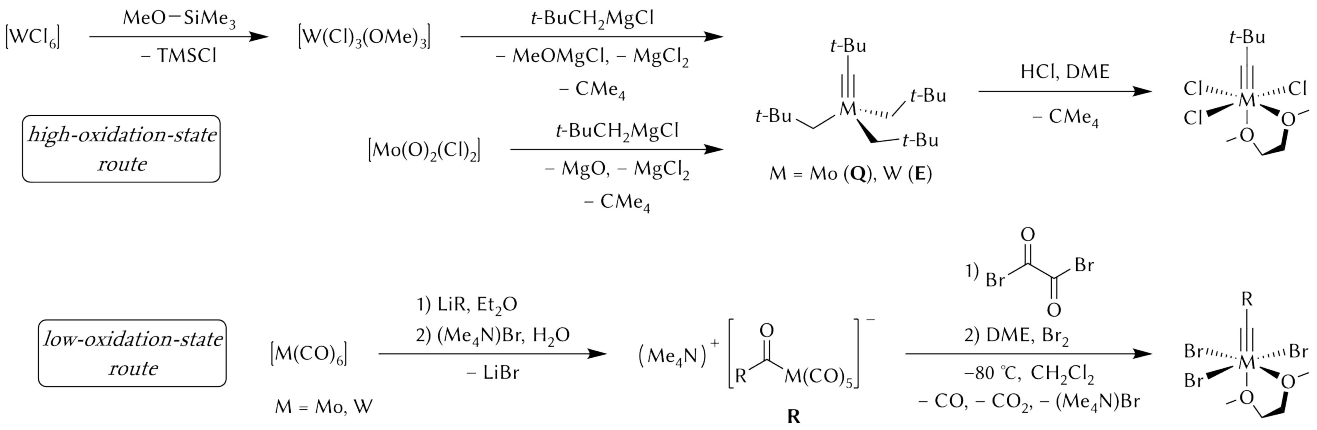

Scheme 13. Comparison of high-oxidation-state (top) and low-oxidation-state (bottom) routes as synthetic pathways to access tungsten and molybdenum alkylidyne complexes for applications in alkyne metathesis; DME = 1,2-dimethoxyethane, TMS = trimethylsilyl ($SiMe_3$).

ive alkylidyne complex [Mo(≡C-*t*-Bu)(CH_2-*t*-Bu)$_3$] (**Q**).[79,105] Even lower yields were obtained by employing $MoCl_5$ or other Mo(VI) sources.[79]

In view of the fact that this synthetic methodology starts with highly oxidised W(VI) and Mo(VI) precursors, it has been termed *high-oxidation-state* route. By contrast, the antonymous *low-oxidation-state* route (Scheme 13, bottom)[34,106,110] is certainly superior in terms of atom economy, operability, and permutation of the alkylidyne substituent, and represented a major improvement in the chemistry of molybdenum and tungsten alkylidyne complexes intended to be used as alkyne metathesis catalysts. Starting from metal hexacarbonyls, this synthetic strategy provides access to *mer*-[M(≡CR)$(Br)_3$(dme)] (M = Mo, W) in essentially two steps:[111,112] nucleophilic attack of a lithium organyl (LiR) at one carbonyl ligand to generate cationic acyl complexes (Me_4N)[M(C(O)R)$(CO)_5$] (**R**) after salt metathesis, followed by oxidation with oxalyl bromide and bromine in the presence of DME at low temperatures. As in the high-oxidation-state case, introduction of, for example, alkoxide ligands (X = OR′) by salt metathesis yields potential alkyne metathesis promoters with the general formula [M(≡CR)$(dme)_n(X)_3$] (n = 0, 1).

Note that acyl complexes **R** are common Fischer-carbene precursors, and the synthesis of an assortment of derivatives has been amply documented.[113–115] In principle, lithium intermediates Li[Mo(C(O)R)$(CO)_5$] could be used directly,[112,116–118] but the tetramethylammonium congeners (**R**) are advantageous because of their higher stability and lower solubility in water, which makes isolation more favourable.

A few alternatives to the high- and low-oxidation-state approaches are also available.[109] Tungsten alkylidyne complexes supported by three alkoxide ligands, [W(≡CR)(OR′)$_3$], are obtained through cross-metathesis of dimeric [(OR′)$_3$W≡W(OR′)$_3$][73,119–121] with alkynes (RC≡CR)[31,121–128] or nitriles (RC≡N).[31,71,122] So far, this route is very limited for molybdenum-based bimetallic species.[121,129,130] Instead, molybdenum alkylidynes are easily generated by cross-metathesis of nitrido complexes, [Mo(≡N)(OR′)$_3$], with substituted ethynes.[23,131–133]

A different strategy, elaborated by the groups of C. C. Cummins, A. Fürstner and J. S. Moore,[23,47,107,134–137] consists in the activation of readily available triamidomolybdenum(III) complexes such as [Mo(N(*t*-Bu)Ar)$_3$] (Ar = 3,5-C$_6$H$_3$Me$_2$) with geminal dichloroalkanes followed by treatment with phenols (Scheme 14).

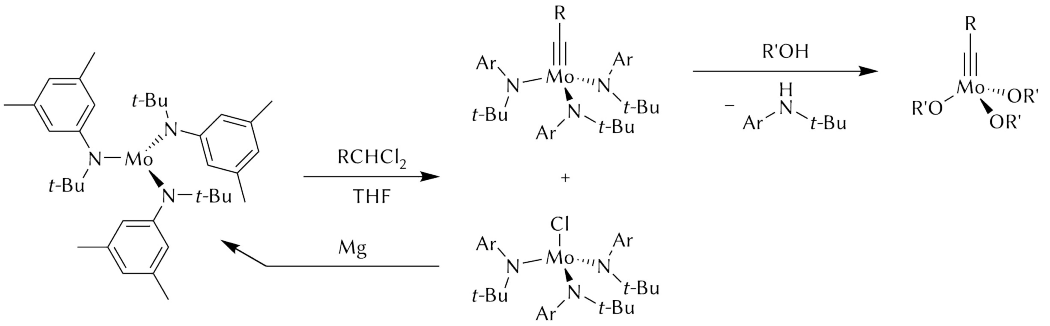

Scheme 14. Formation of alkylidyne species upon activation of triamidomolybdenum(III) complexes.

A more recent method for the synthesis of selectively functionalised molybdenum alkylidyne complexes has been explored by the groups of F. Fischer[138] and R. R. Schrock,[139] and is based in the cross-metathesis reaction of an alkylidyne with a functionalised acetylene. In contrast to the low regioselectivity frequently reported earlier, the revisited protocol takes advantage of 1-aryl-3,3,3-trifluoropropyne (ArC≡CCF$_3$)[138] or aryl(trimethylsilyl)ethyne (ArC≡CSiMe$_3$)[139] derivatives to transfer only the desired aryl moiety. Reaction of these versatile benzylidyne-transfer reagents with [Mo(≡CEt)(dme)(OC(CF$_3$)$_2$Me)$_3$] (Scheme 15) yields the corresponding [Mo(≡CAr)(dme)

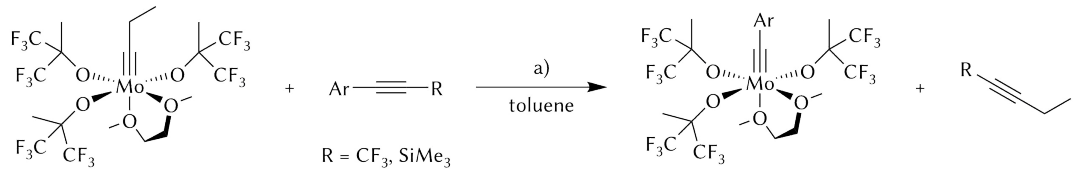

Scheme 15. Use of benzylidyne-transfer reagents in the synthesis of molybdenum alkylidyne complexes. a) Conditions: −60 °C to 24 °C, 0.1 Torr (R = CF$_3$); 30 °C, 0.2 Torr (R = SiMe$_3$).

$(OC(CF_3)_2Me)_3]$ complexes and a highly volatile alkyne (1,1,1-trifluoro-2-pentyne or 1-(trimethylsilyl)-1-butyne, respectively), which can be easily removed under dynamic vacuum. Two potential disadvantages need to be mentioned: (i) the availability of the alkyne reagents is limited, and (ii) alternative starting materials supported by other (alkoxide) ligands or with tungsten as the central atom are yet to be explored.

Catalyst design and scope

The presented synthetic approaches give access to well-defined molecular systems and allow for a rational catalyst design. Functionalisation and tweaking of the alkylidyne complexes are crucial to create the ideal alkyne metathesis initiator. Most desirable features comprise (i) high performance and selectivity, (ii) outstanding functional-group compatibility, and (iii) user-friendliness (including minimal air-sensitivity, convenient preparation, and practicable reaction conditions).[25,102,107]

Typical alkyne metathesis catalysts (see above, p 16) are characterised by the representative formula $[M(\equiv CR)(X)(Y)(Z)(L)_n]$ (where X, Y, and Z are the same or different anionic ligands; L = neutral ligand; M = Mo, W; R = alkyl, aryl; n = 0–2; Figure 6). Consistent with this model, catalyst optimisation essentially comprehends functionalisation of the alkylidyne moiety (R), variation of the ligand sphere (X, Y, Z), and coordination of additional σ- or π-donor ligands (L). Although the alkylidyne unit R contributes significantly to the stability of the complex and determines the synthetic pathway of the catalysts itself, its role during the alkyne metathesis reaction is limited to control the initiation rate. In contrast, the steric and electronic properties of the supporting ligands (X, Y, Z) are decisive in terms of catalytic activity and selectivity, and should be wisely adjusted.[108] Thus, sterically demanding ligands prevent catalyst decomposition (e.g. formation of bimetallic species) or undesired side-reactions (polymerisation), whereas strongly electron-withdrawing substituents increase the electrophilicity of the metal centre, which results in a reactivity increase; ligand overcrowding may be kinetically unfavourable, though.[25]

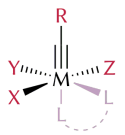

Figure 6. Schematic representation of a typical alkyne metathesis catalyst (M = Mo, W; R = alkyl, aryl; X, Y, Z = anionic ligand; L = coordinating ligand).

In line with this, the alternation of the anionic ligands (X, Y, Z) has been explored methodically, with special emphasis on the degree of fluorination.[24,62,79,109,140] Particular metal and ligand combinations led to remarkably active alkyne metathesis catalysts. Some of the most prominent examples are highlighted in Figure 7.

Alkylidyne complex [W(≡C-*t*-Bu)(NIm$^{t\text{-Bu}}$)(OC(CF$_3$)$_2$Me)$_2$] (**S**, NIm$^{t\text{-Bu}}$ = 1,3-di-*tert*-butylimidazolin-2-iminato) operates at room temperature with low catalyst loadings, and tolerates ethers, esters, and also aryl chloride, thio and nitro functionalities.[141] It combines electron-withdrawing alkoxide ligands with an electron-donating imidazolin-2-iminato moiety, and it was designed by inspiration from related alkylidene imido complexes [M(=CHR)(=NR″)(OR′)$_2$] (M = Mo,[142] W,[143] Figure 7, left), as they are exceptionally active catalysts for olefin metathesis (cf. **A**, p 3). The electronic balance provided by such a push–pull ligand environment seems to be the clue for the outstanding performance and functional group tolerance of these systems.[106]

Alkyne metathesis applications in natural product synthesis are dominated by the triphenylsiloxy-based complexes [Mo(≡CAr)(OSiPh$_3$)$_3$] (primarily **T**, Ar = 4-methoxyphenyl),[49] which are characterised by an excellent compatibility with multiple functional groups.[25]

These qualities arise from the singular electronic properties of silanolate ligands, which were also introduced in tungsten alkylidyne complex [W(≡CPh)(OSi(O-*t*-Bu)$_3$)$_3$] (**U**).[144] Complex **U** catalyses not only the metathesis of isolated alkynes but, for the

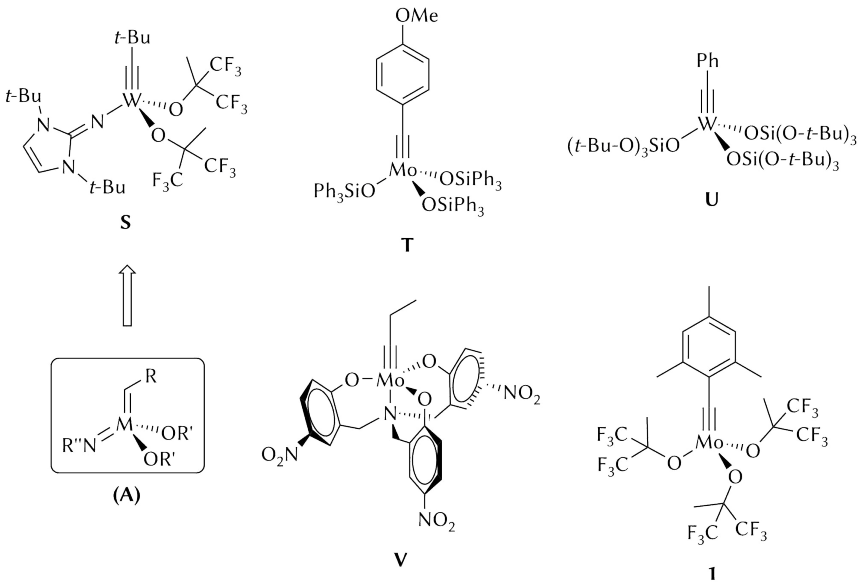

Figure 7. Selection of carefully designed alkyne metathesis catalysts.

first time, also that of conjugated 1,3-diynes, as exemplified by ring-closing diyne metathesis (RCDYM),[145] diyne cross-metathesis (DYCM)[146] and diyne cyclodepolymerisation[147] reactions (Scheme 16). The use of RCDYM in total synthesis was reported subsequently for complex **T**[148] and precatalyst [Mo(≡CEt)(N(*t*-Bu)Ar)$_3$] (Ar = 3,5-$C_6H_3Me_2$, see Scheme 14) in combination with a multidentate trisilanol ligand.[149]

Other multidentate catalysts bearing chelate ligands, such as molybdenum complex **V**[150] and derivatives thereof,[137,151,152] showed improved metathesis activity towards several challenging substrates, inhibition of polymerisation of small alkynes, enhanced robustness and elongated lifetimes.[107] These tripodal systems, which are preferably generated in situ, are leading ADIMET catalysts and have been largely employed in polymer chemistry[95,100] and supramolecular assembly,[98,153–156] giving access to molecular wires (1D) and architectures (2D, 3D).

Finally, highly electrophilic and discreetly encumbered molybdenum 2,4,6-trimethylbenzylidyne complex [Mo(≡CMes)(OC(CF$_3$)$_2$Me)$_3$] (**1**, Mes = mesityl)[157] has emerged as the most active catalyst so far in alkyne metathesis,[63,158] particularly in ACM and RCAM, although complex **1** and related complexes are also excellent ROAMP initiators.[138,159] Moreover, this exquisite catalyst is able to efficiently metathesise even terminal alkynes (Scheme 17).[157,158]

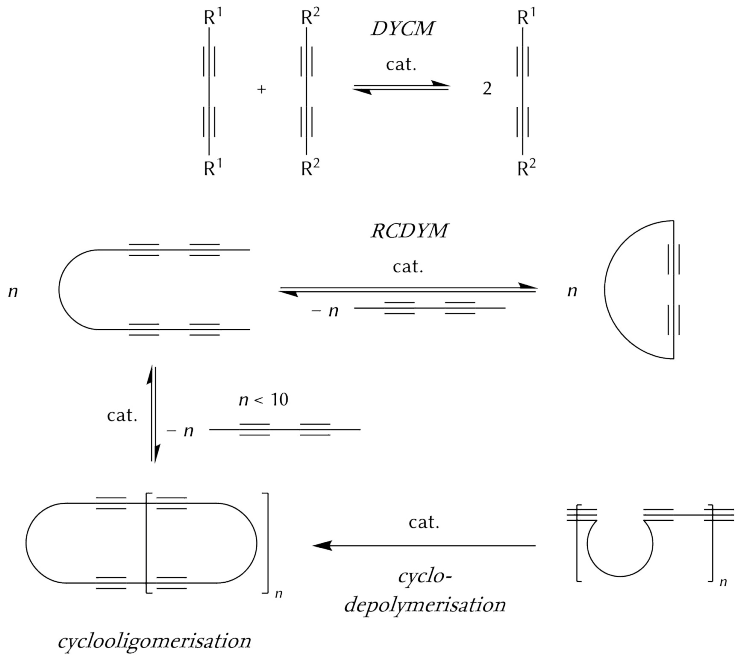

Scheme 16. Diyne metathesis reaction patterns; cat. = catalyst, DYCM = diyne cross-metathesis, RCDYM = ring-closing diyne metathesis.

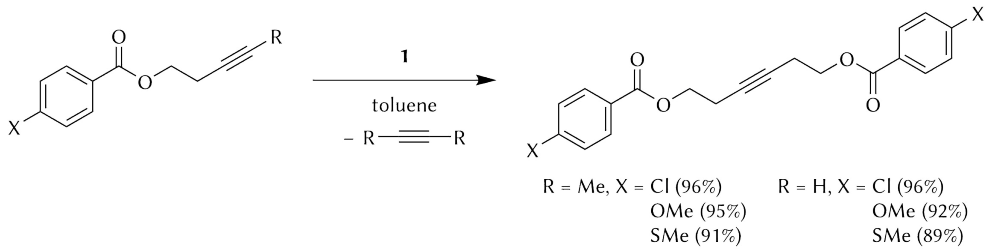

Scheme 17. Examples of ACM of internal (R = Me) and terminal (R = H) alkynes catalysed by **1** (1 mol%, 0.5–1 h, ambient temperature) in the presence of 5 Å molecular sieves; yields are given in parenthesis.

As mentioned above, TAM is a rare phenomenon[70–73] because the catalysts usually suffer from deactivation. Commonly, terminal alkynes undergo side-reactions leading to DPMCBD or acetylene-bridged bimetallic species (see Scheme 10). Complex **1**, however, can deal with terminal alkynes for several reasons: (i) thanks to the lack of coordinating solvents or donor ligands (L), metathesis reactions promoted by **1** are so fast that kinetically less favoured decomposition pathways are mitigated or even suppressed, (ii) the fluorinated alkoxide ligands are weak bases almost incapable of deprotonating the MCBD intermediates, which would form undesired DPMCBD complexes, and (iii) catalysis is performed under sufficient dilution to avoid alkyne polymerisation or catalyst dimerisation.[108] The latter condition is clearly fundamental, as it was lately recognised, and so other systems bearing poorly basic alkoxides have been reported to exhibit activity in TAM using high substrate dilution (for example, **T**,[160,161] [M(≡CMes)(OC(CF$_3$)Me$_2$)$_3$], M = Mo, W,[62] or [Mo(≡CAr)(OC(CF$_3$)$_2$Me)$_3$], Ar = (2,4,6-triisopropyl)phenyl)[162]. In addition, TAM-based natural product syntheses have been communicated.[148,163,164]

Bench-stable precursors

One reason why the scope of the alkyne metathesis reaction is limited compared to the olefin metathesis is the high air-sensitivity of most catalysts and their synthetic precursors, which demands stringently anhydrous and inert reactions conditions.[108] Preclusion of this operability shortcoming is crucial to improve the applicability and the potential of triple-bond metatheses.

All of the above listed catalysts except complex **V** have in common that they are tetracoordinated 12 VE complexes, which grants them sensational reactivity. Saturation of vacant sites by nucleophilic coordinating ligands as in **V** may well increase the stability of the complex yet at the expense of catalytic activity. Notwithstanding, the use

of activators to generate efficient catalysts in situ from suitable 14 VE or 16 VE precursors is a promising strategy that has been reported successful for some bench-stable complexes.

For example, protected precatalysts of the type [Mo(≡CAr)(OSiPh$_3$)$_3$(L)] (L = mono- or bidentate ligand),[24,84] which are 14 VE or 16 VE versions of complex **T** and derivatives, exhibit sufficient stability to be weighed in air (L = pyridine) or are even indefinitely stable towards air and moisture (L = 1,10-phenanthroline, see Scheme 18).[24,107] Under regular conditions, however, the activity of these coordinated compounds is suppressed. To liberate the active catalyst, the phenanthroline adducts must be activated in situ upon dissociation of the coordinated ligand (L) by more electrophilic metal salts (such as $MnCl_2$, $MgCl_2$ and $ZnCl_2$) usually at elevated temperatures.

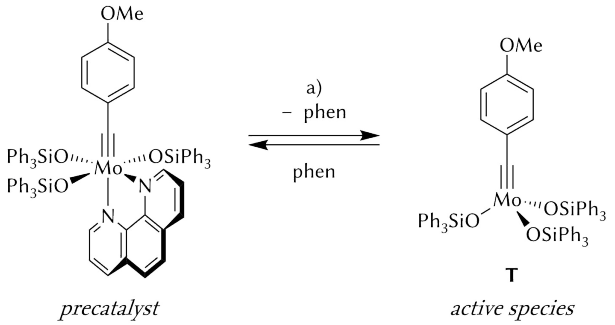

Scheme 18. Activation of a bench-stable precatalyst bearing a 1,10-phenanthroline (phen) ligand to generate active complex **T**. a) Conditions: $MnCl_2$ or $ZnCl_2$ (among other), toluene, 80–100 °C.

Dimeric complex [Mo(≡CEt)(TOBA)]$_2$ (**W**, TOBA = *N,N,N*-tri(2-oxidobenzyl)amine),[165] which is correlated to the previously crystallised phenoxide-bridged dimer [**V**]$_2$,[150] constitutes another example of an air-stable compound that can be activated in situ. Under aprotic conditions, complex **W** is inactive in alkyne metathesis, but addition of methanol generates the active monomeric catalyst (Scheme 19), which is an effective ROAMP initiator.[165]

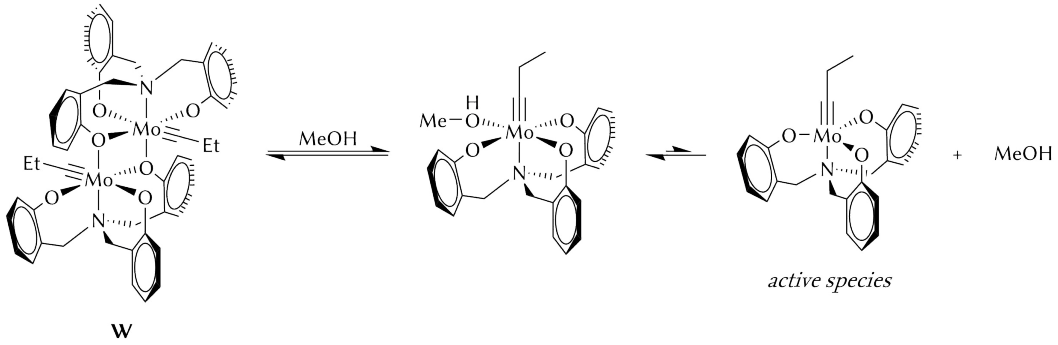

Scheme 19. Treatment with methanol activates bench-stable complex **W**.

An increase in the steric demand around the metal centre can hinder undesirable decomposition reactions and enhance the robustness of the complexes. This concept has been explored in complexes of the type [M(≡CMes)(X)(Y)$_2$] (M = Mo, W; X = Y = OC(CF$_3$)$_2$Me (**1**, M = Mo), OC(CF$_3$)$_3$, OSi(O-*t*-Bu)$_3$, or X = NIm$^{t\text{-Bu}}$, Y = OC(CF$_3$)$_2$Me),[140] in which a mesityl group replaced the unsubstituted, sterically less bulky benzylidyne moiety. In fact, some of the tungsten complexes, namely [W(≡CMes)(NIm$^{t\text{-Bu}}$)(OC(CF$_3$)$_2$Me)$_2$] and [W(≡CMes)(OSi(O-*t*-Bu)$_3$)$_3$] (Figure 8), proved sufficiently robust to be handled in air for at least two or three hours without perceptible loss of their catalytic performance.[140]

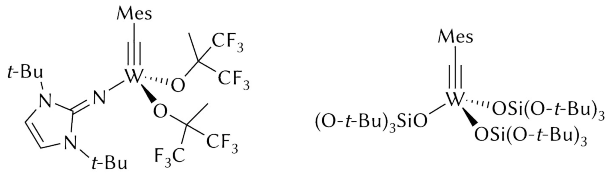

Figure 8. Robust tungsten mesitylidyne complexes; Mes = mesityl (2,4,6-trimethylphenyl).

Aside from these few examples, only the classical yet ill-defined Mortreux-type systems[27,166,167] are user-friendly and robust enough to operate under non-inert conditions.[48,168–170] The catalytic performance of these systems, however, suffers from insufficient efficiency and restricted functional group compatibility.[108] Therefore, further systems need to be explored to find appropriate bench-stable (pre)catalysts; among others, the following molybdenum- and tungsten-based candidates should be considered: stabilised alkylidyne or nitrido complexes, MCBD or DPMCBD species, and bimetallic complexes (Figure 9).

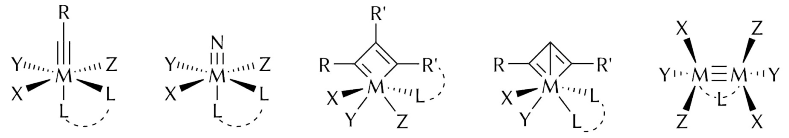

Figure 9. Schematic structures of some potential bench-stable (pre)catalysts.

On the whole, the work published since the beginning of the millennium contributed immensely in deepening the understanding of the role played by the catalyst structure and the reaction intermediates in alkyne metathesis. Both molybdenum and tungsten alkylidyne complexes have been established as admirably metathesis-active catalysts. Advanced catalyst design and clever ligand selection have been crucial for attaining superior catalytic performances and extending the scope of substrates and ap-

plications. Most notably, some robust and user-friendly systems are precious additions to the catalyst toolbox for alkyne metathesis. Although the ideal catalyst remains a challenging goal, the exciting developments in this field offer a promising future for the alkyne metathesis reaction. The present dissertation focuses on functionalising molybdenum alkylidyne complexes, hoping to take this chemistry one step further towards that goal.

2 Overview

Primarily, this research project focuses on the development of potentially bench-stable alkyne metathesis catalysts. As discussed in the Introduction, the availability of user-friendly, air-stable, yet active catalysts and precursors is certainly a decisive milestone in this field in order to extend the applicability and scope of the alkyne metathesis reaction. Although there have been some attempts towards the ideal catalyst, many strategies remain unexplored, which rely necessarily on the fine-tuning of the ligands and the adjustment of the reaction conditions. The modification of the ligand environment must be accompanied by the development of cleverly designed or deliberately modified synthetic routes; in general, a deeper understanding of the catalytic cycle is also required.

On this basis, variation of the ligands to influence the catalysts' features represents a major facet of this project (see Figure 6), in which essentially the alkylidyne moiety (R) will be functionalised, but also the addition of coordinating ligands (L) will be explored. Thus, Chapter 3.1 discusses the synthetic challenges and achievements towards the preparation of molybdenum alkylidyne complexes bearing an ether-functionalised benzylidyne moiety (R = Ar). The introduction of this functionality is intended to stabilise the complexes by intramolecular or even intermolecular contacts with the metal centre (Figure 10), displaying chelating or bridging modes, respectively.

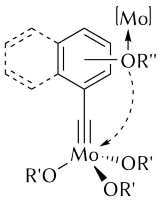

Figure 10. Structural model of functionalised benzylidyne complexes, showing possible binding modes of the ether group attached to the aryl ring.

Chapter 3.2 deals with the addition of coordinating ligands (L), such as amines, carbenes, nitriles or phosphanes, to the highly active molybdenum catalyst **1**. The introduction of nucleophilic ligands can contribute to increase the stability of the mo-

lecules, but can also influence the initiation rates, a question that can be answered with the help of targeted catalytic studies.[151] An exciting aspect of this approach involves the reaction of **1** with nitriles, because these molecules can undergo metathesis under certain conditions (see Section 3.2.1).

Furthermore, to identify and eventually isolate reaction intermediates involved in the catalytic cycle, and to figure out or confirm possible deactivation pathways are essential tasks for gaining a better insight into the reaction mechanism, in particular with regard to challenging or rare substrates. Therefore, alkylidyne complex **1** can be treated stoichiometrically with certain target alkynes, including terminal acetylenes and uncommon alkynes such as electron-rich ynediamines ($R_2NC{\equiv}CNR_2$). Other than the formation of DPMCBD or MCBD species (cf. Scheme 10), these reactions can generate new alkylidyne complexes via cross metathesis. Potentially interesting are aminoalkylidyne complexes (**X**) as a result of this reaction between **1** and ynediamines (Scheme 20). Ultimately, the reactivity studies with ynediamines and other electron-rich acetylenes can extend the substrate scope of alkyne metathesis catalyst **1**. The results of these studies are presented in the third chapter of the Discussion (Chapter 3.3).

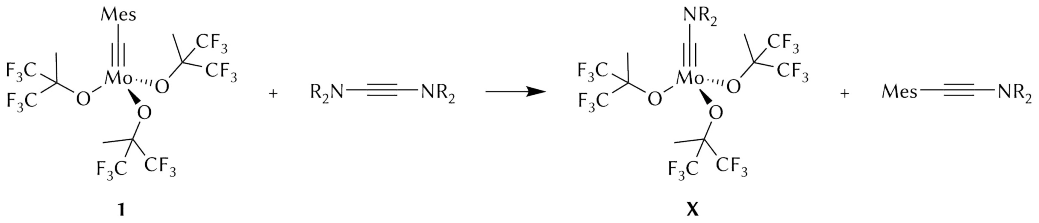

Scheme 20. Proposed cross-metathesis of ynediamines with alkylidyne complexes; Mes = mesityl.

Lastly, Chapter 3.4 analyses the application in alkyne metathesis of the molybdenum alkylidyne complexes reported in the present work. The conducted catalytic studies in ACM and TAM used, respectively, the standard substrates 5-(benzyloxy)-2-pentyne (**Y**-Me) and 4-(benzyloxy)-1-butyne (**Y**-H) as established in our group (Figure 11).[110,157]

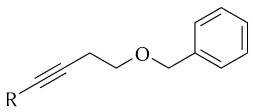

R = Me (**Y**-Me)
H (**Y**-H)

Figure 11. Internal (**Y**-Me) and terminal (**Y**-H) alkynes commonly used in our group as standard substrates for catalytic studies.

3 Results and Discussion

3.1. Functionalisation of the Alkylidyne Moiety

3.1.1. Conceptual background and targets

Robust catalysts for alkyne metathesis, as mentioned in the Introduction (p 22 ff), are scarce. As a compromise, bench-stable precursors introduced by A. Fürstner,[24] which include a chelating ligand (e.g. 1,10-phenanthroline), exhibit permanent stability towards air or moisture; albeit inactive, these precatalysts can be activated with $MnCl_2$ or $ZnCl_2$ (see Scheme 18). There is still room for improvement, however. For example, it would be convenient to achieve stable complexes without the need for additional ligands that have to be removed for activation. One possibility is to promote the formation of intra- or intermolecular interactions with the metal centre. This can be accomplished if proper metal-binding functional groups are introduced at selected positions of the already existing ligands or of the alkylidyne moiety that favour, at least in the solid state, a chelating binding mode or weak covalent interactions with the electrophilic metal atom of a neighbouring molecule.

Blocking of vacant sites to increase stability can hinder substrate attachment and may cause a decrease in the catalytic performance. For this reason, the strength (or weakness) of the interactions is crucial to avoid – perhaps in solution or at elevated reaction temperatures – complete suppression of the activity. In particular, low initiation rates (substitution of the alkylidyne, see Scheme 5, compounds **H–J**) are expected for the metathesis reaction with these complexes. However, if the alkylidyne moiety is involved in chelation, substitution of the alkylidyne during the initiation step would generate the catalytic active species, and complete conversion would presumably be reached, as usual, within a few minutes. Considering that ethers are prone to coordination but are less Lewis basic than amines or phosphanes, this functional group was selected to realise intra- or intermolecular contacts with the molybdenum centres.

Ether-substitution at the benzylidyne moiety (ArC≡) can be executed at different positions. Thus, introduction of a methoxy group in the *para* position, as in target complex [Mo(≡C(4-MeO-C_6H_4))(OC(CF_3)$_2$Me)$_3$] (**2**), aims at stabilisation of the alkylidyne complex through intermolecular contacts with the metal centre (Figure 12). In fact, the *para*-anisole moiety is found in closely related complexes such as [Mo(≡C(4-MeO-C_6H_4))(L)(OC(CF_3)$_2$Me)$_3$] (L = DME or *N*-heterocyclic carbene),[138,171] or in **T**, for which a multi-gram-scale synthesis has been reported.[84] However, complexes [**2**(L)], regardless of their activity in alkyne metathesis, are not capable of forming additional interactions, as the free binding site is already blocked by the coordinating ligand (L).

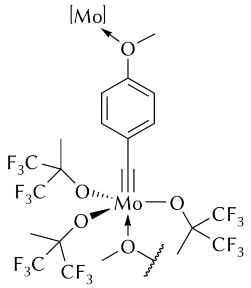

2

Figure 12. Proposed intermolecular coordination of *para*-methoxy benzylidyne complex **2**.

In contrast, *ortho*-functionalised arylalkylidyne complexes such as isopropoxybenzylidyne [Mo(≡C(2-*i*PrO-C_6H_4))(OC(CF_3)$_2$Me)$_3$] (**3**, *i*Pr = 2-propyl) can potentially form *intra*molecular interactions by chelation. Obviously, this is not straightforward in complex **3** because of linearity of the Mo≡C–Ar bond, unless the coordinating ether group is elongated to achieve chelation. Instead, chelation is expected to occur after a small alkyne such as 2-butyne generates an MCBD species upon cycloaddition with the alkylidyne complex (Scheme 21). Remarkably, the structure of these MCBD complexes, which feature a five-membered chelate ring fused to the four-membered metallacycle, is reminiscent of robust and well-established Hoveyda–Grubbs' catalysts for olefin metathesis (e.g. **D**).[19–21,139,172] Hence, an improvement in stability can be postulated also for these complexes, at least in the solid state. Ideally, though, **3** would be in equilibrium with the corresponding MCBD species in solution, allowing for regeneration of the active catalyst via release of the light alkyne. Thus, initiation would be driven by absorption of the liberated alkyne in molecular sieves or by distillation under reduced pressure.

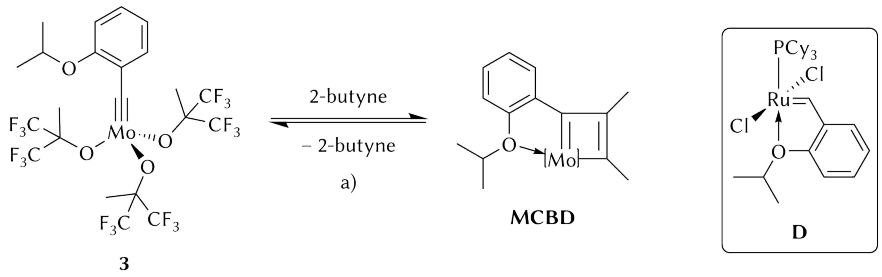

Scheme 21. Representative synthesis of an MCBD complex featuring the envisaged chelation with the isopropoxy group as found in Hoveyda–Grubbs' catalysts of type **D**; a) Exemplary conditions: molecular sieves or reduced pressure; [Mo] = $Mo(OC(CF_3)_2Me)_3$, Cy = cyclohexyl.

It should be mentioned here that a similar strategy (albeit the antagonistic intention) was applied by F. Fischer and coworkers,[173] whereby the addition of functionalised ynamines to a molybdenum alkylidyne catalyst generated stable MCBD complexes chelated intramolecularly by secondary metal-binding sites. As a consequence, the catalytic active centre became irreversibly deactivated. This approach grants control over the termination of a living ROAMP and gives access to telechelic polymers.[173]

Extending the chelating unit by one carbon atom, as in naphthylmethylidyne complex $[Mo(\equiv C(8\text{-MeO-Naph})(OC(CF_3)_2Me)_3]$ (**4**, Naph = 1-naphthyl), would result in an MCBD complex containing a six-membered chelate ring (Scheme 22), which should be even more favoured.

A combination of both strategies (intended formation of intra- and intermolecular contacts) is also possible through substitution at both *ortho* and *para* positions; 2,4,6-trimethoxybenzylidyne complex $[Mo\{\equiv C(2,4,6\text{-}(MeO)_3C_6H_2)\}(OC(CF_3)_2Me)_3]$ (**5**, Scheme 23) would satisfy this condition.

In general, all envisaged complexes are accessible from Schrock-type carbyne complexes *mer*-$[Mo(\equiv CAr)(Br)_3(dme)]$, which in turn can be conveniently prepared

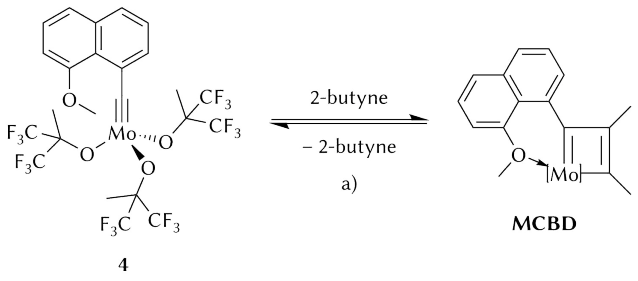

Scheme 22. Complex **4** illustrates the extension of the chelating group by one carbon atom to give an intramolecularly stabilised MCBD species that contains a six-membered ring; a) Exemplary conditions: molecular sieves or reduced pressure; [Mo] = $Mo(OC(CF_3)_2Me)_3$.

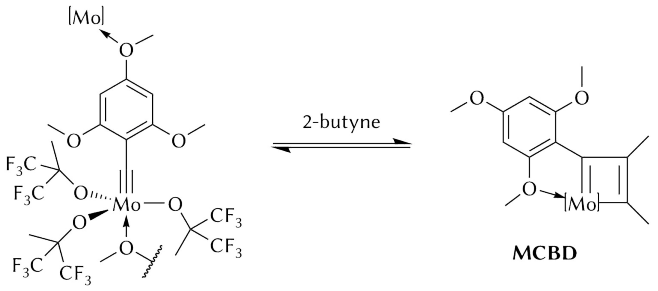

5

Scheme 23. Alkylidyne complex **5** can potentially form both inter- and intramolecular contacts.

through the low-oxidation-state route, as mentioned in the Introduction (Section 1.3.4, p 17). This route involves the use of the corresponding lithium aryls (LiAr) and $[Mo(CO)_6]$ to generate anionic molybdenum acyl complexes. The preparation of these precursors and the corresponding alkylidyne complexes will be discussed in the following subchapters.

3.1.2. Ether-substituted acyl complexes

ortho-Isopropoxyphenyl substituent

The (*ortho*-isopropoxybenzoyl)pentacarbonylmolybdate(0) complex $(Me_4N)[Mo(C(O)(2\text{-}i\text{PrO-}C_6H_4))(CO)_5]$ ((Me_4N)**6**, Scheme 24) was prepared following the traditional protocol for the synthesis of Fischer's carbenes. Reaction of 2-isopropoxyphenyl lithium (generated *in situ* by metal–halogen exchange of 2-bromo-1-isopropoxybenzene and *n*-butyl lithium at –20 °C) with molybdenum hexacarbonyl in diethyl ether yielded the yellow-coloured lithium congener $Li[Mo(C(O)(2\text{-}i\text{PrO-}C_6H_4))(CO)_5]$ (Li-**6**). Regarding their considerable solubility in several solvents and compromised stability, these species are commonly not isolated. Instead, after removal of the solvent under vacuum, salt metathesis with $(Me_4N)Br$ in deoxygenated water resulted in precipitation of (Me_4N)**6** as a vivid yellow solid.

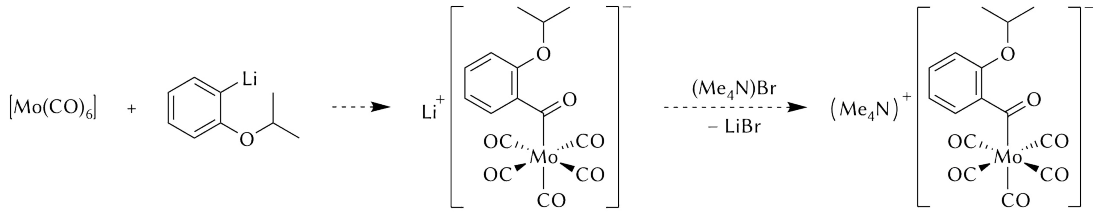

6 6

Scheme 24. Attempted synthesis of (*ortho*-isopropoxybenzoyl)pentacarbonylmolybdate(0) complexes Li-**6** and (Me_4N)**6**.

However, the NMR spectra were not in accordance with the expected product because two distinct sets of resonances were observed for some of the atoms, suggesting the presence of two species in solution. Thus, the ^{1}H NMR spectrum (Figure 13a) revealed a signal duplication for the isopropyl moiety (two doublets at δ_H = 1.28 ppm and δ_H = 1.33 ppm, and two septets at δ_H = 4.46 ppm and δ_H = 4.51 ppm), and also for the aromatic protons (at least seven multiplets). Accordingly, all signals in the ^{13}C{^{1}H} NMR spectrum (Figure 13b) were echoed either downfield or upfield along the spectrum, with the notable exception of the most low-field-shifted signal at about δ_C = 303 ppm, which accounts for the acyl carbon atom (Ar*C*(O)Mo, cf. Table 1, p 36).

Opportunely, colourless prisms precipitated from the NMR solution of the mixture, and its molecular structure (Figure 14) was established by X-ray diffraction analysis,

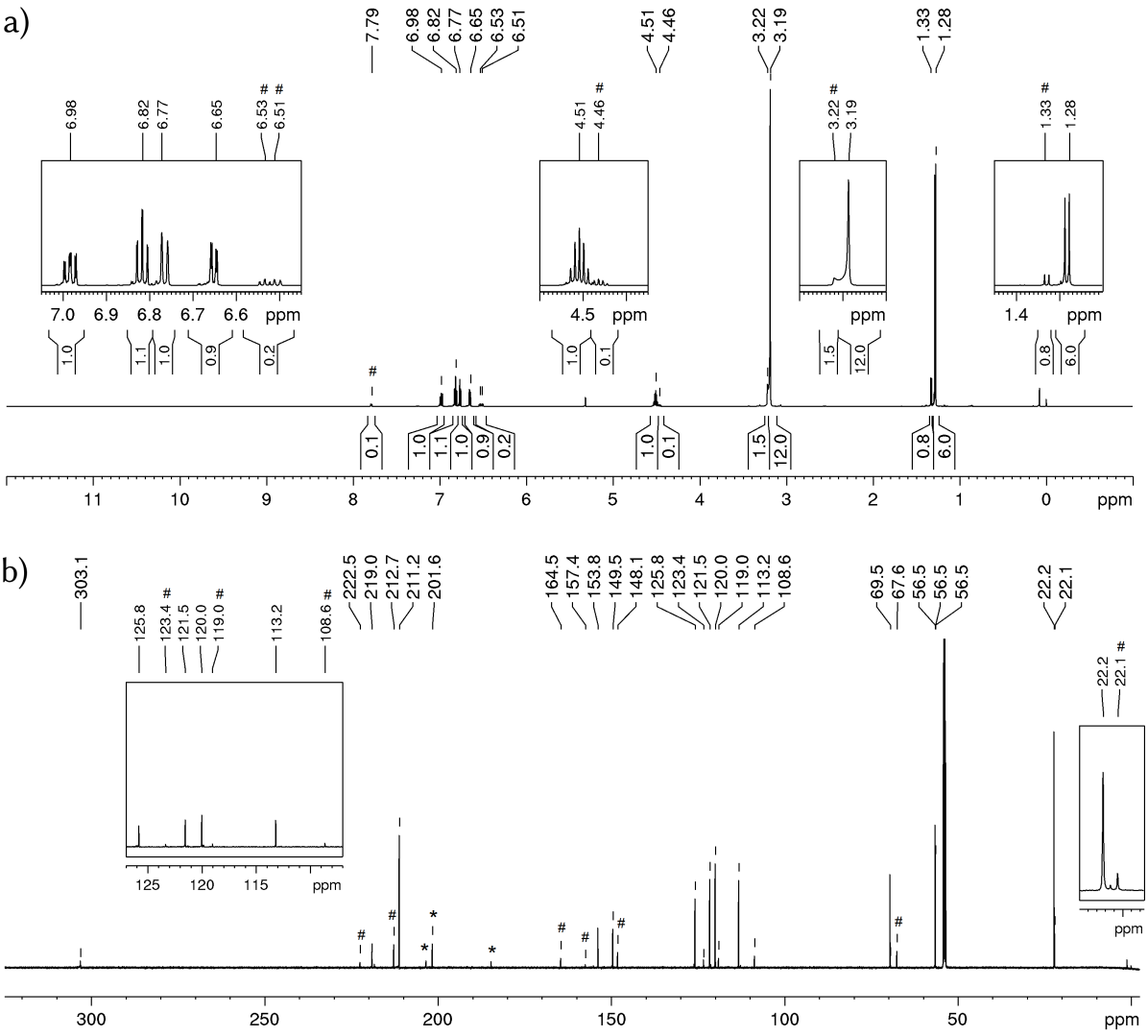

Figure 13. a) ^{1}H NMR spectrum in dichloromethane-d_2 of a mixture of (Me_4N)**6** and its degradation product (Me_4N)**7** (signals labelled with #). b) ^{13}C{^{1}H} NMR spectrum of this mixture in dichloromethane-d_2; * unknown species and $[Mo(CO)_6]$ (δ_C = 201.6 ppm). The insets show expanded regions for clarity.

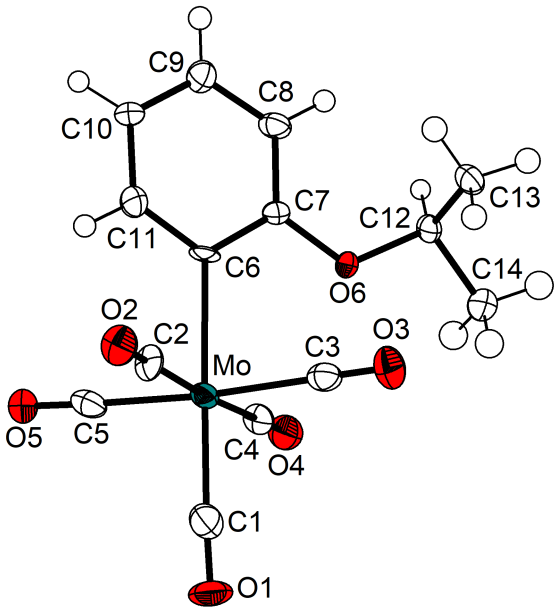

Figure 14. Molecular structure of one anion of (Me_4N)**7** with thermal displacement parameters drawn at the 50% probability level. The second independent anion in the asymmetric unit and the two Me_4N^+ counterions are not displayed. Selected bond lengths (Å) and angles (deg): Mo–C1 1.998(12), Mo–C2 2.076(10), Mo–C3 2.070(10), Mo–C4 2.086(9), Mo–C5 2.019(11), Mo–C6 2.275(9); C1–Mo–C2 93.5(5), C1–Mo–C3 92.2(5), C1–Mo–C4 90.7(4), C1–Mo–C5 92.5(5), C1–Mo–C6 177.7(5), C2–Mo–C3 89.0(4), C2–Mo–C4 175.7(4), C2–Mo–C5 92.1(4), C2–Mo–C6 88.8(4), C3–Mo–C4 91.6(4), C3–Mo–C5 175.1(4), C3–Mo–C6 88.0(4), C4–Mo–C5 86.9(4), C4–Mo–C6 87.0(4), C5–Mo–C6 87.2(4). For additional structural data, see Figure 68, p 144.

which shed light upon this riddle. In contrast to the expected structure for (Me_4N)**6**, the crystallised compound was the anionic (aryl)pentacarbonylmolybdate complex $(Me_4N)[Mo(2\text{-}i\text{PrO-}C_6H_4)(CO)_5]$, (Me_4N)**7**. The formation of (Me_4N)**7** can be rationalised by a common decarbonylation reaction, which involves the successive release of a carbonyl ligand as carbon monoxide followed by deinsertion of the carbonyl group at the acyl moiety. The mechanism and implications of this decarbonylation reaction will be discussed in further detail in the next sections.

Compound (Me_4N)**7** crystallises with two independent molecules per unit cell in the monoclinic, enantiomorphic space group $P2_1$ and adopts essentially an octahedral geometry around the zerovalent molybdenum atom (average angles for each independent molecule, respectively: *trans*, 176.2(4)° and 172.8(5)°; *cis*, 90.0(4)° and 90.1(5)°). The Mo–C_{Ar} bond lengths of 2.275(9) Å and 2.299(9) Å are indicative of a Mo–C single bond and are in the expected range for aryl polycarbonyl molybdenum complexes[174] (for example, complex (PPN)$[Mo(C_6F_5)(CO)_5]$ has a Mo–C_{Ar} bond length of 2.305(3) Å;[175] PPN = bis(triphenylphosphine)iminium). The orientation of the aromatic rings is slightly different in the two independent molecules.

In consequence, the identification of the degradation species satisfactorily explains the additional set of signals observed in the NMR spectra. Unfortunately, because of the similar properties of both compounds, any attempts to separate them were unsuccessful. Moreover, NMR analyses of intermediate Li-**6** revealed the same characteristic patterns as those for the tetramethylammonium equivalent, showing duplicated resonances besides, again, the downfield signal in the $^{13}C\{^1H\}$ NMR spectrum. Hence, the complex must undergo decarbonylation (at least partially) during the course of the first reaction step (Scheme 25).

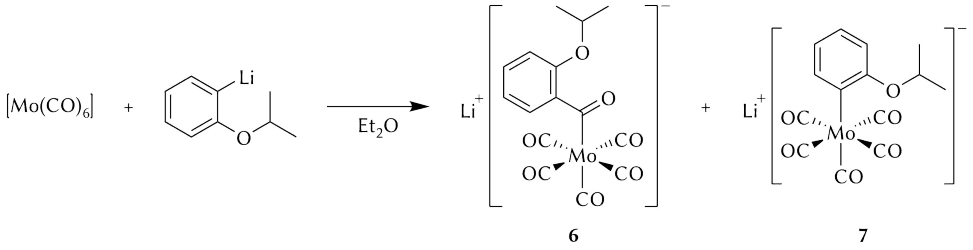

Scheme 25. Reaction of $[Mo(CO)_6]$ and 2-isopropoxyphenyl lithium resulted in a mixture of Li-**6** and Li-**7**.

2,4,6-Trimethoxyphenyl substituent

In a similar manner, the synthesis of $(Me_4N)[Mo\{C(O)(2,4,6\text{-}(MeO)_3C_6H_2)\}(CO)_5]$, (Me_4N)**8**, was unusually challenging. Treatment of molybdenum hexacarbonyl with 2,4,6-trimethoxyphenyl lithium, followed by salt metathesis with $(Me_4N)Br$, produced a mixture of $[Mo(CO)_6]$, 1,3,5-trimethoxybenzene, and the undesired decarbonylated species $(Me_4N)[Mo(2,4,6\text{-}(MeO)_3C_6H_2)(CO)_5]$ ((Me_4N)**9**, Scheme 26). Moreover, as judged by NMR spectroscopy, the attempted isolation of intermediate lithium complex $Li[Mo\{C(O)(2,4,6\text{-}(MeO)_3C_6H_2)\}(CO)_5]$ (Li-**8**) resulted in an intractable mixture of Li-**8**, its decarbonylated counterpart (Li-**9**), and minor amounts of 1,3,5-trimethoxybenzene.

Auspiciously, in an attempt to separate the complexes through fractional crystallisation from Et_2O/*n*-hexane solutions at low temperatures, several yellow to orange crystals were obtained. Inspection under the microscope revealed three different types of

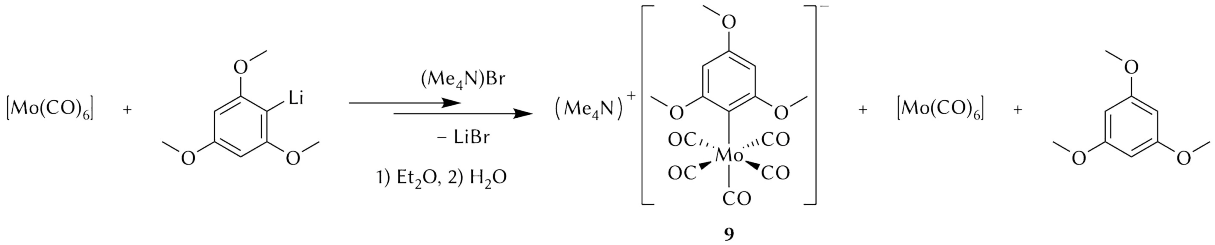

Scheme 26. Reaction of $[Mo(CO)_6]$ with 2,4,6-trimethoxyphenyl lithium, followed by salt metathesis with $(Me_4N)Br$, produced a mixture of decomposition products.

crystals; in all three cases single-crystals suitable for X-ray crystallography were available. Remarkably, the structures unfold the mechanism of the decarbonylation process (Scheme 27), which involves the following three species: (i) the desired acyl complex Li-**8**, (ii) aryl complex Li-**9**, and (iii) intermediate species Li[Mo{C(O)(2,4,6-$(MeO)_3C_6H_2$)}$(CO)_4$] (Li-**10**), an (acyl)tetracarbonyl complex, in which a CO ligand has been released, but the carbonyl group in the acyl moiety has not yet deinserted. The structure of Li-**10** benefits inevitably from chelation of the aryl unit to the metal centre through an *ortho*-methoxy group, which occupies the vacant coordination site and provides additional stability to the unsaturated complex.

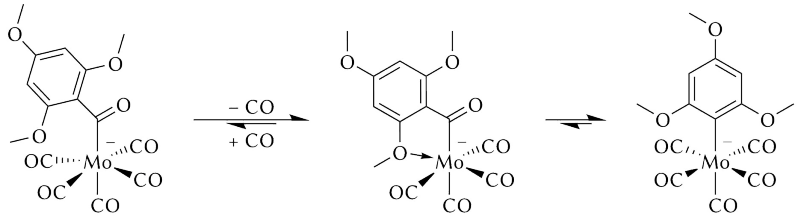

Scheme 27. Decarbonylation pathway of complex Li-**8**. Lithium cations and coordinated solvent molecules are not shown.

Table 1. Selected bond distances (in Å) and characteristic NMR chemical shifts (in ppm) of some acyl molybdenum complexes. Values in brackets indicate the number of resonances.

Compound	Mo–C1	C1–O1	δ_H (Ar-*H*)	δ_C (*ipso*-*C*)	δ_C (Ar–*C*=O)
Li-**6**	nd[a]	nd	6.62–6.96 [4]	154.1	316.3
(Me_4N)**6**	nd	nd	6.65–6.98 [4]	153.8	303.1
$[Li(Et_2O)$**8**$]_2$	2.2470(13)	1.2642(16)	6.05	134.4	313.7
[Li(thf)**8**]$_2$	2.251(2)	1.265(3)	6.01	134.5	313.9
$[Li(Et_2O)$**10**$]_2$, polymorph A	2.196(3)	1.261(4)	nd	nd	nd
$[Li(Et_2O)$**10**$]_2$, polymorph B	2.183(2)	1.261(3)			
[Li(thf)$_3$**11**]	2.2467(19)	1.233(2)	6.69–7.47 [6]	161.3	311.0
Li-**12**	nd	nd	6.81, 7.53	149.8	308.0
(Me_4N)**12**	2.2907(18)	1.238(2)	6.78, 7.57	148.6	289.8
(Me_4N)[Mo(C(O)(2,4,6-$Me_3C_6H_2$))$(CO)_5$]	2.275(4)[b,c]	1.241(4)[b,d]	6.65	159.0	312.3
$[Li_4(Et_2O)_2${Mo(C(O)(2,4,6-(iPr)$_3C_6H_2$))$(CO)_5$}$_4$][e]	2.245(2)[f]	1.266(3)[g]	6.93	155.7	nd
(Me_4N)[Mo(C(O)(2,6-(iPr)$_2C_6H_3$))$(CO)_5$]·CH_2Cl_2[b]	2.2819(14)	1.2407(19)[h]	nd	nd	nd
(Me_4N)[Mo(C(O)Ph)$(CO)_5$][i]	nd	nd	7.23–7.44 [3]	156.1	298.2

[a] nd = no data; [b] See reference [176]; [c] Mo1–C6, as labelled for this structure. The asymmetric unit contains three independent units; the other distances are Mo2–C6′ 2.263(4) Å, and Mo3–C6″ 2.265(3) Å; [d] C6–O6, as labelled for this structure. The asymmetric unit contains three independent units; the other distances are C6′–O6′ 1.247(4) Å, and C6″–O6″ 1.242(4) Å; [e] See references [162,176]; [f] Mo11–C101, as labelled for this structure. The complex is a tetramer; the other distances are Mo21–C201 2.231(2) Å, Mo31–C301 2.236(2) Å, and Mo41–C401 2.238(2) Å; [g] C101–O11, as labelled for this structure. The complex is a tetramer; the other distances are C201–O21 1.247(4) Å, C301–O31 1.272(3) Å, and C401–O41 1.270(3) Å; [h] C1–O6, as labelled for this structure; [i] See reference [84].

Compound Li-**8** crystallises as pale yellow prisms in the triclinic space group $P\bar{1}$ with an additional diethyl ether molecule, and is composed of centrosymmetric dimers of the type $[Li(Et_2O)\mathbf{8}]_2$, in which the lithium atoms bridge the two halves of the molecule (Figure 15). The molybdenum atom resides in a distorted orthogonal environment with average angles of 173.51(6)° (*trans*) and 90.07(6)° (*cis*). The Mo–C1 distance of 2.2470(13) Å (Table 1, p 36) is particularly long and characteristic of a Mo–C single bond, whereas the C1–O1 bond length of 1.2642(16) Å is in the range of a double bond.[177] That underlines the acyl character of the substituent (Mo–C(=O)Ar) rather than having a carbene structure (Mo=C(O)Ar). The lithium cation is tetracoordinated by the carbonyl group of the acyl moieties (O1 and O1#, symmetry operator 1 – *x*, 1 – *y*, 1 – *z*), one *ortho*-methoxy group of the aromatic ring (O2), and one diethyl ether molecule. Calculation of the structural index parameter $\tau_4 = 0.80(19)$[178] indicates a distorted trigonal pyramidal geometry at the lithium atom, in which the apex (O1) is tilted away from O10 (O1···Li···O10, 107.27(13)°).

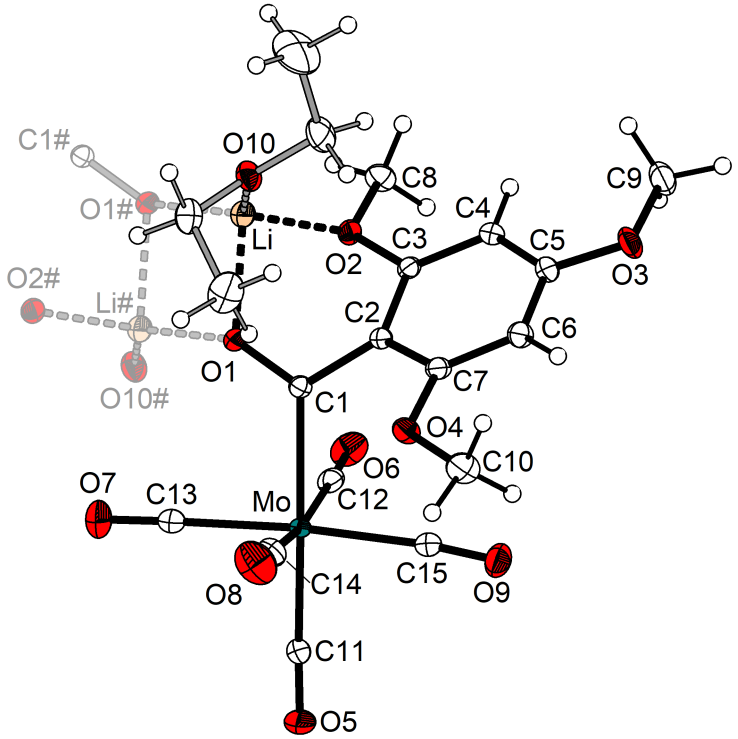

Figure 15. Molecular structure of $[Li(Et_2O)\mathbf{8}]_2$ with thermal displacement parameters drawn at the 50% probability level. Only neighbouring atoms (labelled with #) of the second molecule in the inversion-symmetric dimer are displayed using paler colours. For a representation of the whole dimer, see Figure 70, p 149. Selected bond lengths (Å) and angles (deg): Mo–C1 2.2470(13), Mo–C11 2.0075(14), Mo–C12 2.0497(16), Mo–C13 2.0340(15), Mo–C14 2.0414(17) Mo–C15 2.0511(15), C1–C2 1.5144(18), C1–O1 1.2642(16), Li···O1 1.959(3), Li···O1# 1.908(3), Li···O2 1.969(3), Li···O10 1.910(3); C1–Mo–C11 175.74(6), C12–Mo–C14 169.58(6), C13–Mo–C15 175.20(5), C1–Mo–C12 81.55(5), C1–Mo–C13 89.25(5), C1–Mo–C14 88.08(6), C1–Mo–C15 94.53(5), C11–Mo–C12 94.56(6), C11–Mo–C13 89.23(6), C11–Mo–C14 95.84(6), C11–Mo–C15 87.20(6), C12–Mo–C13 93.31(6), C12–Mo–C15 90.17(6), C13–Mo–C14 87.58(6), C14–Mo–C15 89.59(6), Mo–C1–O1 121.80(9), Mo–C1–C2 122.58(9), O1–C1–C2 114.79(11), C1–O1···Li 121.98(11), C1–O1···Li# 140.72(12), Li···O1···Li# 87.19(11), O1···Li···O1# 92.81(11), O1···Li···O2 85.15(11), O1#···Li···O2 110.36(13), O1···Li···O10 107.27(13), O1#···Li···O10 126.94(14), O2···Li···O10 119.68(13).

The highly air-sensitive, yellow–orange dichroic crystals of complex Li-**10** are triclinic with space group $P\bar{1}$ and, as observed for Li-**8**, reveal a dimeric structure, [Li(Et_2O)**10**]$_2$ (Figure 16), symmetrically bridged by two lithium cations. These atoms are tetracoordinated (to O1, O1#, O4#, and one solvent molecule, symmetry operator 1 – *x*, 1 – *y*, 1 – *z*), and adopt a distorted trigonal pyramidal geometry (τ_4 = 0.80(4))[178] with the apex (O1#) tilted away from O9 (O1#···Li···O9, 110.3(3)°). The molybdenum atom resides in a distorted orthogonal environment with bond angles in the range of 168.81°–174.59° (*trans*) and 72.97°–102.15° (*cis*) and mean angles of 171.09(14)° (*trans*) and 90.12(12)° (*cis*). Notably, the C1–Mo–O2 angle is particularly acute (72.97(9)°) because of the chelating nature of the acyl ligand, which forms a five-membered ring upon coordination of methoxy-O2 to the metal centre. This ring is almost planar, but exhibits a slight envelope conformation in which the Mo atom lies 0.4007(3) Å out of the least-square (l.s.) plane of the other four atoms (C1, C2, C3, O2; r.m.s. deviation 0.004(3) Å). This plane forms a dihedral angle of ϕ = 12.87(16)° with the "closing flap" of the envelope (plane through atoms C1, Mo, O2). The Mo–C1 bond of 2.196(3) Å is 0.051(4) Å shorter than that in complex Li-**8** (Table 1, p 36), but is still in the range of a single bond. Also the C1–O1 bond distance (1.261(4) Å) is slightly shorter (1.2642(16) Å in Li-**8**). A similar structure of a molybdenum tetracarbonyl complex bearing a chelating acyl ligand, [Mo(=C(OMe)(2-Me_2N-C_6H_4))$(CO)_4$], was reported by K. H. Dötz.[179]

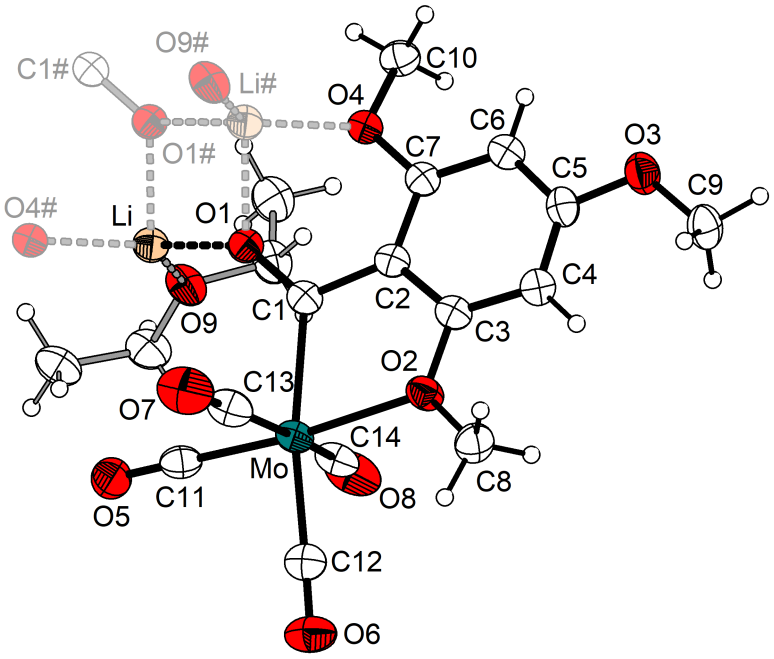

Figure 16. Molecular structure of one polymorph (A) of [Li(Et_2O)**10**]$_2$ with thermal displacement parameters drawn at the 50% probability level. Only neighbouring atoms (labelled with #) of the second molecule in the inversion-symmetric dimer are displayed using paler colours. For a representation of the whole dimer, and selected bond lengths and angles, see Figure 72, p 151.

Interestingly, successive experiments reproduced the concomitant crystallisation of the different species, and on one occasion also produced orange crystals of a second polymorph (B) of [Li(Et_2O_2)**10**], which crystallised in the monoclinic space group $P2_1/n$ (Figure 17). The coordination geometry at both molybdenum and lithium atoms, and relevant structural parameters are very similar to those discussed for polymorph A. Likewise, the acyl unit chelates the molybdenum atom and forms a five-membered ring with a significantly acute angle of 73.28(7)° (C1–Mo–O2). Atoms C1, C2, C3, and O2 are coplanar (r.m.s. deviation 0.007(3) Å), but the ring displays an envelope conformation with a fold angle of $\phi = 13.24(11)°$ between this plane and the plane through atoms C1, Mo, O2. The Mo–C1 bond distance is slightly shorter (1.3 pm) than in polymorph A (Table 1, p 36), but it is still in the range of a typical Mo–C single bond.[180]

Finally, aryl complex Li-**9** crystallises in the monoclinic space group $P2_1/n$ as a diethyl ether disolvate, forming highly air-sensitive, blade-shaped, colourless crystals. In the crystal structure, the complex is a 1D-coordination polymer [Li(Et_2O)$_2$**9**]$_n$ organised in chains parallel to the *b* axis (Figure 18), in which the lithium cations bridge the molybdenum fragments at O2 (*para*-methoxy substituent of the aryl ring) and O4 (carbonyl ligand coordinated *trans* to that ring). The hexacoordinated molybdenum core

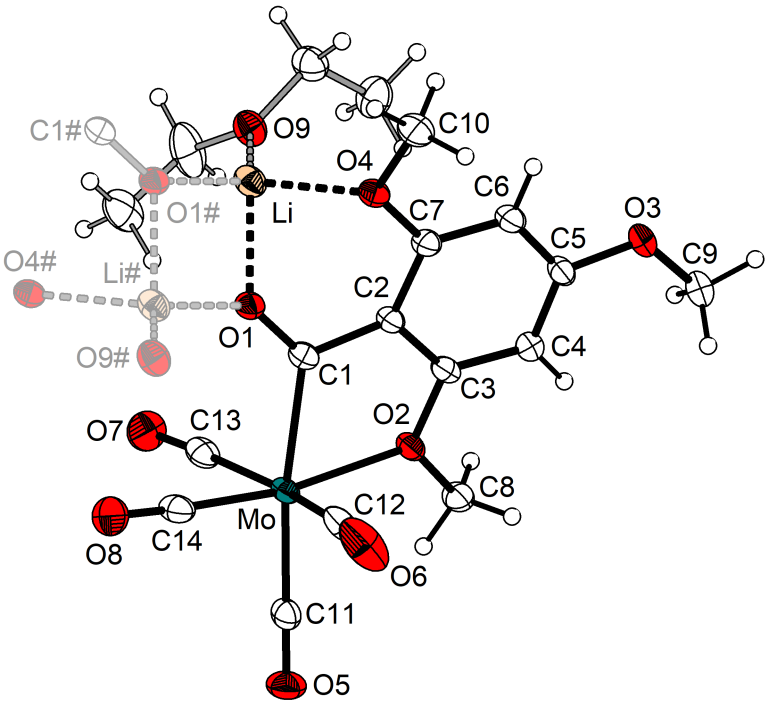

Figure 17. Molecular structure of polymorph B of [Li(**10**)·Et_2O]$_2$ with thermal displacement parameters drawn at the 50% probability level. Only neighbouring atoms (labelled with #) of the second molecule in the inversion-symmetric dimer are displayed using paler colours. For a representation of the whole dimer, and selected bond lengths and angles, see Figure 73, p 152.

resides in an octahedral environment (average angles: *trans*, 177.92(8)°; *cis*, 90.00(8)°), whereas the four-coordinate geometry around the lithium atom is close to tetrahedral (τ_4 = 0.90(3)),[178] with a particularly wide angle of 124.89(19)° for O9···Li···O10. The Mo–C_{Ar} distance (2.312(2) Å) is indicative of a single bond.

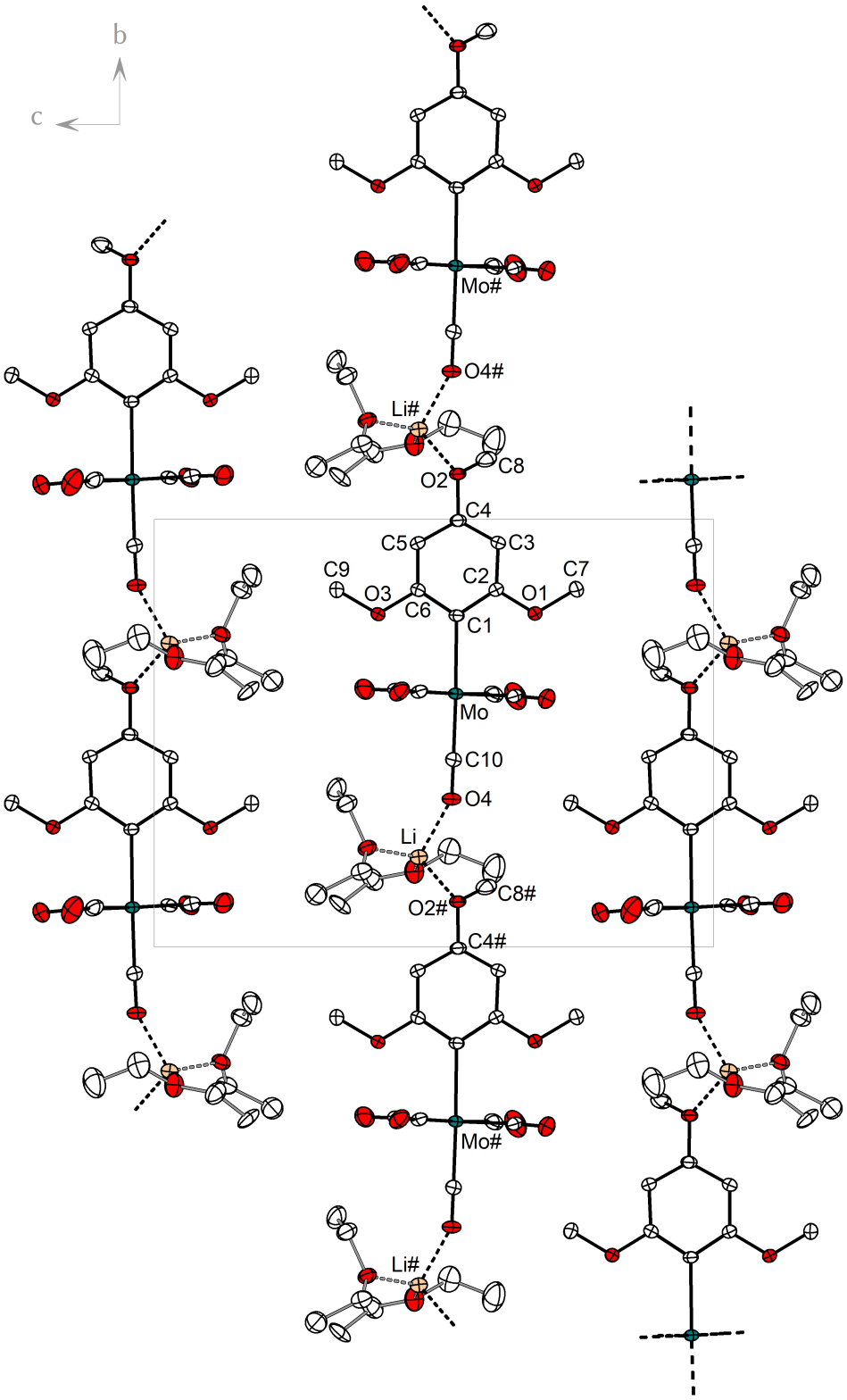

Figure 18. The extended polymeric structure of $[Li(Et_2O)_2\mathbf{9}]_n$ with thermal displacement parameters drawn at the 50% probability level. Hydrogen atoms and the second position of a disordered ethyl group are omitted for clarity. For selected bond lengths and angles, see Figure 71, p 150.

Kinetic study of the carbonyl deinsertion

Decarbonylation processes such as that observed for Li-**8** are a classical type of organometallic reaction and have already been described for Fischer-type carbene complexes of chromium,[181–183] molybdenum[179] and tungsten,[184–187] which resulted in the formation of chelate complexes similar to Li-**10**. In order to obtain some kinetic information on the decarbonylation of Li-**8**, the reaction progress was monitored by NMR spectroscopy. A solution of Li-**8** in tetrahydrofuran-d_8 was thus analysed at specified time intervals. Assuming that the concentration of the intermediate Li-**10** is negligible (it is not observed in the NMR spectra) and the CO deinsertion accordingly occurs rapidly to give Li-**9**, the loss of CO in Li-**8** must be the rate-determining step, and its consumption can be followed by looking at the peak integral of one specific signal (here that of the aromatic protons). The natural logarithm of the peak integral ($\ln A_{\text{Li-}\mathbf{8}}$) against reaction time shows a linear dependence (Figure 19), which suggests that the rate law is first-order in Li-**8** ($r = k[\mathbf{8}]$; k, first-order rate constant). The observed rate constant can be derived from the slope of the regression line and has a value of $k_{293} = 1.26(6)\ 10^{-6}\ s^{-1}$, which corresponds to a half-life of $t_{1/2} = 6.4(3)$ d and a free activation energy of $\Delta G^{\ddagger} = 25.51(19)$ kcal mol^{-1} (106.7(8) kJ mol^{-1}) at $T = 293$ K.

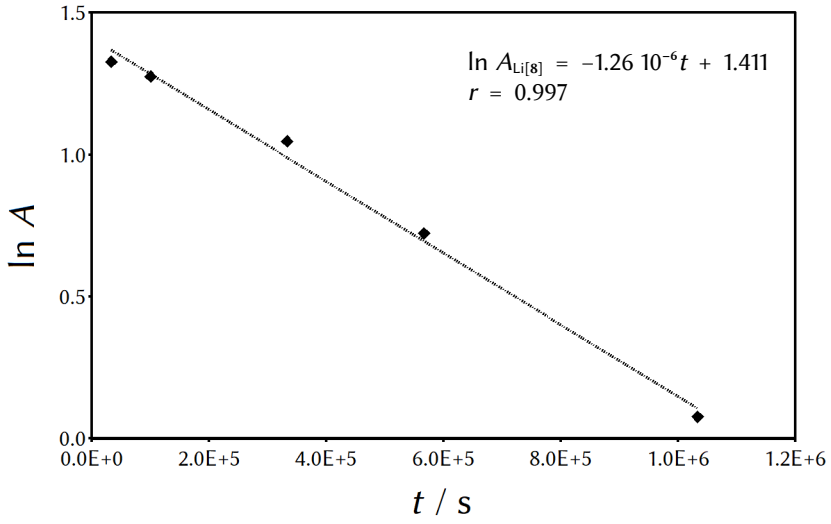

Figure 19. First-order kinetic plot ($\ln A_{\text{Li-}\mathbf{8}}$ vs. t) for the decarbonylation of Li-**8** as followed by NMR spectroscopy in tetrahydrofuran-d_8. The data is based on peak integrals of the aromatic protons at $\delta_H = 6.05$ ppm (calibrated against the solvent signal). Data points were fitted using linear regression.

Isolation of lithium acyl molybdenum complexes bearing ether-substituted aryl moieties

Given the results of the last section, a convenient strategy was needed to circumvent the decarbonylation problem. On the basis of the calculated half-life the deinsertion process can be assumed to be very slow in solution at ambient temperature, which does not justify the obtained mixtures of complexes. Hence, the deinsertion reaction must be accelerated during isolation of the product, probably because of removal of the solvent under dynamic vacuum, which promotes the release of carbon monoxide, and influences the outcome of the reaction. For this reason, alternative experimental conditions were explored to isolate the acyl complex.

Instead of evaporating the solvent, complex Li-**8** was isolated form the reaction mixture by precipitation with *n*-hexane as a yellow powder in moderate yields (Scheme 28). The purity and homogeneity of the product was confirmed by NMR spectroscopy, elemental analysis, and powder X-ray diffraction. It is important to note that the solvent choice was critical to avoid precipitation of by-products or unreacted $[Mo(CO)_6]$. The latter is moderately soluble in several organic solvents, including ethers, alkanes, aromatic and chlorinated solvents. Thus, a mixture of diethyl ether, tetrahydrofuran, and *n*-hexane in a ratio 8:1:14 proved to work well here. Small amounts of tetrahydrofuran are required to ensure complete dissolution of the lithium organyl; excessive use of *n*-hexane would cause precipitation of by-products.

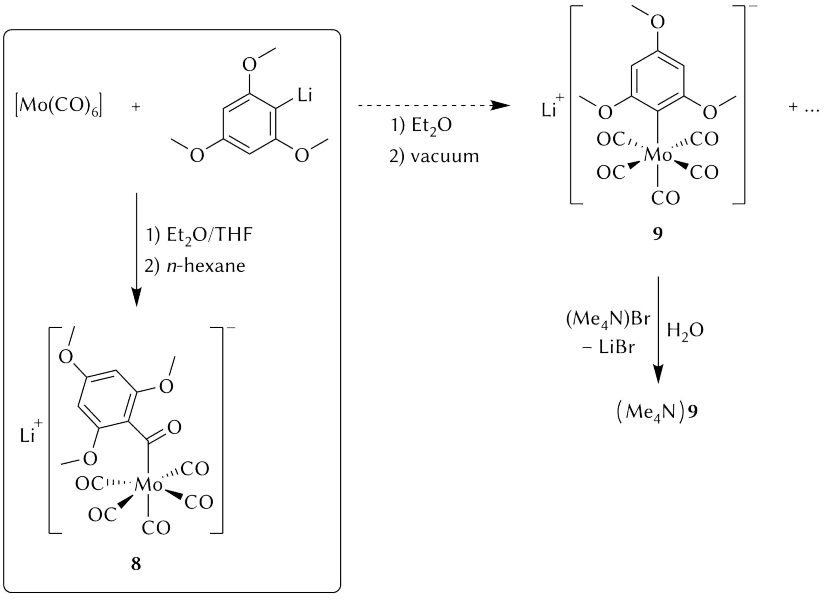

Scheme 28. Synthetic protocol modification of acyl complex **8** using the precipitation approach.

In addition, after filtration, large, block-shaped, orange crystals of [Li(thf)**8**]$_2$ precipitated from the filtrate and were analysed by X-ray diffraction (Figure 20). The compound, which contains a coordinated THF molecule, crystallises in the monoclinic space group $P2_1/n$ as a centrosymmetric dimer with two independent units per unit cell. Structural parameters are similar to those discussed for [Li(Et$_2$O)**8**]$_2$ but the Mo–C1 bond is even longer (2.251(2) Å, Table 1, p 36). Furthermore, there is an additional short contact from one carbonyl group (O6) to the lithium atom (Li···O6 2.739(5) Å), so the alkali metal is pentacoordinated in [Li(thf)**8**]$_2$ and features approximate trigonal-bipyramidal geometry, as indicated by the structural index parameter τ_5 = 0.757(7),[188] with an axial angle (O1#···Li···O6) of 168.4(2)°.

This simple precipitation approach to isolate the acyl complex as a lithium salt is unprecedented and gives access to functionalised Fischer-carbene precursors, which can be used to synthesise alkylidyne complexes. Indeed, this convenient protocol was applied successfully in the preparation of Li-**6** in pure form (Scheme 29). Thus, reaction of molybdenum hexacarbonyl with 2-isopropoxyphenyl lithium in diethyl ether yielded substantial amounts of Li-**6** after precipitation with *n*-hexane at 0 °C.

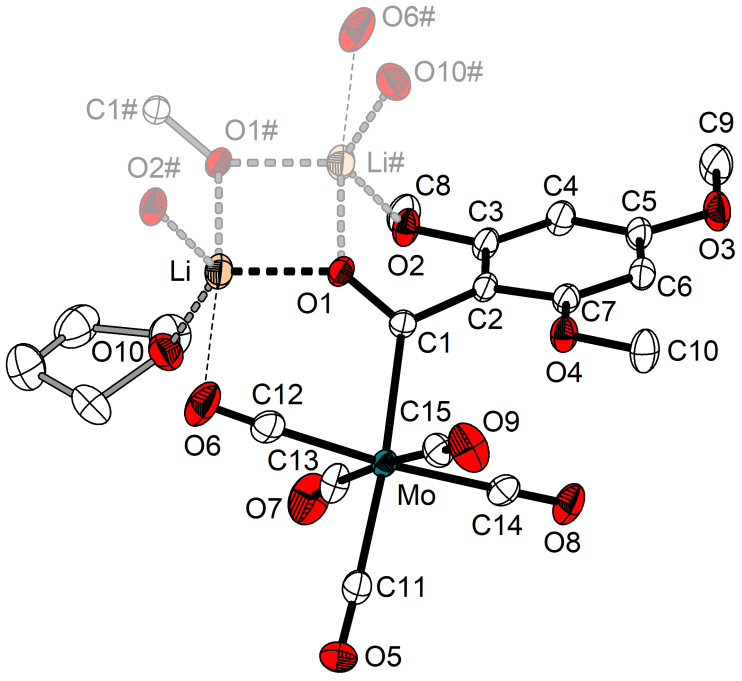

Figure 20. Molecular structure of [Li(thf)**8**]$_2$ with thermal displacement parameters drawn at the 50% probability level. Only neighbouring atoms (labelled with #) of the second molecule in the inversion-symmetric dimer are displayed using paler colours; hydrogen atoms are omitted for clarity. For a representation of the whole dimer, and selected bond lengths and angles, see Figure 74, p 153.

To illustrate the applicability of the method, another still unreported acyl complex was synthesised from $[Mo(CO)_6]$ and 8-methoxynaphthyl lithium in a mixture of diethyl ether and tetrahydrofuran (9:1) at 0 °C. Complex Li[Mo(C(O)(8-MeO-Naph))$(CO)_5$] (Li-**11**, Scheme 29) was obtained in good yield by precipitation with *n*-hexane (10 parts), and its structure was confirmed by NMR spectroscopy (Table 1, p 36) and X-ray diffraction (Figure 21). Complex Li-**11** crystallises as pale yellow needles in the monoclinic, enantiomorphic space group $P2_1$ and contains three coordinated THF solvent moieties per molecule. The molybdenum atom displays a distorted octahedral geometry (*trans* angles, 172.76(9)°–176.15(9)°) and is located 0.0975(2) Å above the l.s. plane formed by the carbonyl groups coordinated *cis* to the acyl unit (C14, C15, C16, C17; r.m.s. deviation 0.029(2) Å). The naphthyl ring is oriented almost perpendicularly to the Mo–C1 bond (torsion angles: Mo–C1–C2–C3 93.8(2)°, Mo–C1–C2–C11 85.5(2)°), and there is no evidence of an additional coordination of the methoxy group of the ring (O7) to the molybdenum core (separation 3.7863(17) Å). As observed for Li-**8**, the Mo–C1 bond distance is considerably long (2.2467(19) Å, Table 1, p 36), and the C1–O1 bond of 1.233(2) Å is consistent with the double-bond character of an acyl fragment.[189] Calculation of the structural index parameter τ_4 = 0.921(3)[178] indicates a distorted tetrahedral coordination at the lithium atom, in which the atom O10 is tilted away from O1 (O1···Li···O10, 119.6(2)°) and forms a narrow angle with O9 (O9···Li···O10, 101.77(19)°).

Additionally, in that particular case, conversion of Li-**11** to (Me_4N)**11** via salt metathesis in deoxygenated water was accomplished successfully, for decarbonylation was not detected.

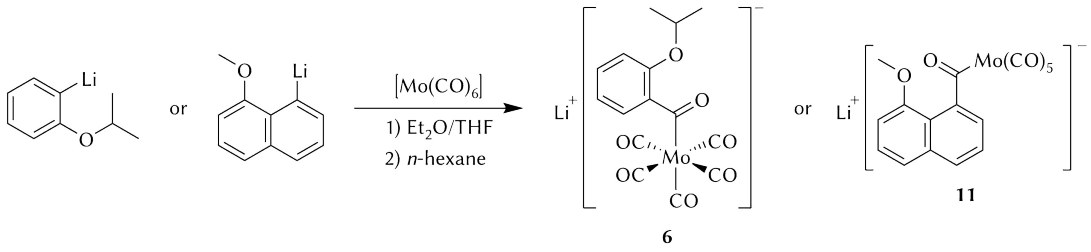

Scheme 29. Synthesis of acyl complexes Li-**6** and Li-**11** applying the precipitation approach.

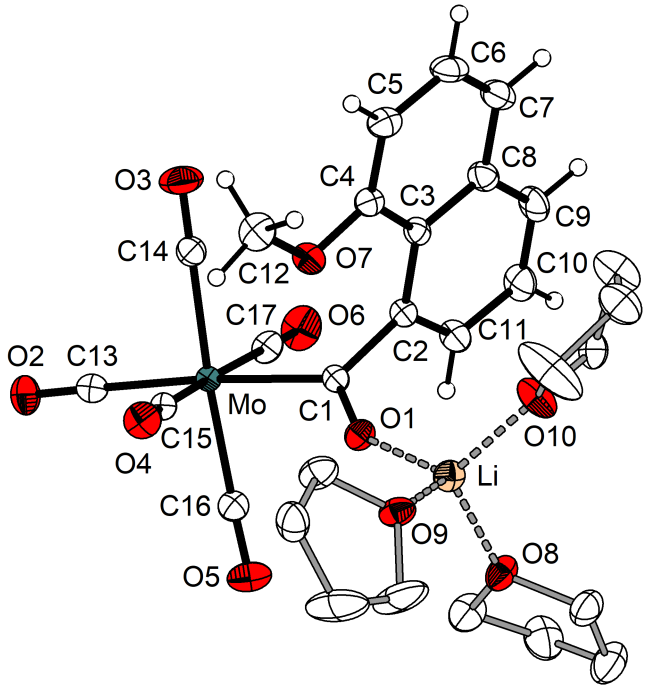

Figure 21. Molecular structure of [Li(thf)$_3$**11**] with thermal displacement parameters drawn at the 50% probability level. Hydrogen atoms of solvent molecules are omitted for clarity. For selected bond lengths and angles, see Figure 69, p 146.

para-Methoxyphenyl substituent[190]

Aiming at the preparation of complex **2**, which bears a *para*-methoxy group at the benzylidyne moiety that can engage in intermolecular interactions intended to stabilise the alkylidyne complex, the synthesis of acyl precursor Li[Mo(C(O)(4-MeO-C$_6$H$_4$))(CO)$_5$] (Li-**12**, Scheme 30) was attempted. Considering that Li-**12** is an intermediate species in the synthesis of Fürstner's acyl complex (Me$_4$N)**12**,[84] it has already been generated *in situ* before; however, it was never isolated to be used as a direct precursor for the preparation of tribrominated alkylidyne complex *mer*-[Mo(≡C(4-MeO-C$_6$H$_4$))(Br)$_3$(dme)] (**13**). Hence, the precipitation approach introduced in the preceding sections was implemented in the reaction of [Mo(CO)$_6$] with 4-methoxyphenyl lithium to yield Li-**12** (Scheme 30, bottom). Addition of *n*-hexane, however, resulted in deposition of only a barely separable, viscous, deep red precipitate. After careful decantation of the supernatant and drying for several hours, a brown solid was obtained. NMR analyses in THF-d_8 revealed a variety of compounds, among which the expected product Li-**12** made up about 75% of the mixture. Characteristic signals in the proton spectrum are a singlet at δ_H = 3.76 ppm (methoxy group) and two doublets at δ_H = 6.81 ppm and δ_H = 7.53 ppm (aromatic protons). In the $^{13}C\{^1H\}$ NMR spectrum the res-

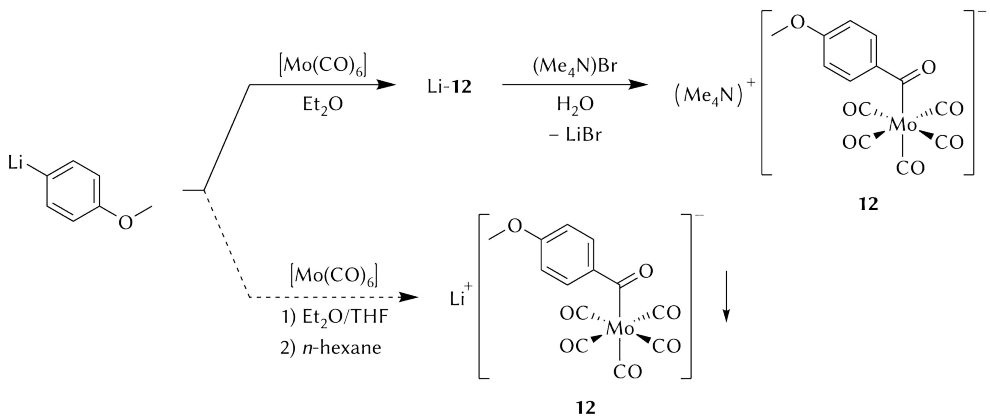

Scheme 30. Synthesis of acyl complex (Me$_4$N)**12** via Li-**12** (top), and attempted isolation of Li-**12** (bottom).

onance for the methoxy group is found at δ_C = 55.4 ppm, the aromatic carbon atoms resonate at δ_C = 112.9 ppm, δ_C = 128.5 ppm, δ_C = 149.8 ppm, and δ_C = 161.6 ppm, and the low-field-shifted signal at δ_C = 308.0 ppm is assigned to the acyl carbon atom.

Unfortunately, any attempts to purify the compound failed; therefore, direct oxidation of Li-**12** omitting salt metathesis to access **13** was not considered further. Instead, the previously published two-step synthesis of (Me$_4$N)**12** (Scheme 30, top)[84] was reproduced with minor changes. Regardless of the literature data, characterisation of (Me$_4$N)**12** deserves some attention here. In their publication, A. Fürstner and coworkers concluded by NMR spectroscopy that two isomers of (Me$_4$N)**12** were present in solution in an approximately 9:1 ratio, but a discussion of the nature and origin of the minor isomer was omitted. Moreover, the reported NMR resonances are inconsistent with two configurational isomers of the same compound (for example, only one downfield signal at δ_C = 294.5 ppm is listed for the acyl carbon atom) and can be better explained if the minor constituent is in fact a degradation product (presumably the decarbonylated derivative analogous to **7** and **9**). In contrast to this observation, the NMR spectroscopic analyses conducted within this thesis revealed one set of signals exclusively, which is indicative of only one species being present in solution. The chemical shifts are very similar to those of the lithium counterpart Li-**12**. Thus, the methoxy group is found at δ_H = 3.75 ppm, and the aromatic protons arise as two doublets at δ_H = 6.78 ppm and δ_H = 7.57 ppm in the ^{1}H NMR spectrum. In addition, a 1:1:1 triplet at δ_H = 3.28 ppm accounts for the twelve hydrogen atoms of the Me_4N^+ cation. An equivalent triplet is also found in the $^{13}C\{^1H\}$ NMR spectrum (Figure 22) at δ_C = 55.7 ppm. The methoxy carbon atom has a chemical shift of δ_C = 55.3 ppm,

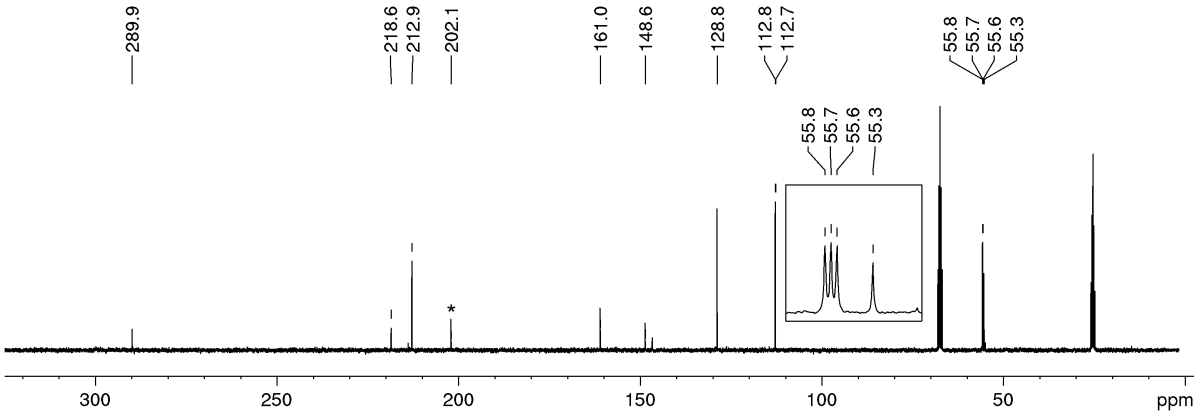

Figure 22. $^{13}C\{^1H\}$ NMR spectrum of (Me_4N)**12** in THF-d_8; * $[Mo(CO)_6]$ (δ_C = 202.1 ppm). The inset shows the expanded region for the observed multiplet.

whereas the aryl carbon atoms resonate in the aromatic region (δ_C = 112.8 ppm, 128.8 ppm, 148.6 ppm, and 161.0 ppm). The acyl carbon atom is significantly shifted to the high field (δ_C = 289.9 ppm) compared to Li-**12** (Table 1, p 36).

In addition, the purity of (Me_4N)**12** was verified by elemental analysis (which is missing in the original publication). Since its solid-state structure has not been reported to date, orange crystals were grown from a concentrated dichloromethane solution at –30 °C, and the molecular structure was established by X-ray crystallography (Figure 23). Compound (Me_4N)**12** crystallises in the monoclinic space group $P2_1/n$. The molybdenum atom resides in a distorted octahedral environment, and is coordinated to five carbonyl ligands (average bond distances: Mo–C 2.0391(18) Å, C–O 1.142(2) Å) and to the acyl carbon atom with a significantly elongated Mo–C1 bond length of 2.2907(18) Å (Table 1, p 36). Indeed, this distance is comparable to the longest Mo–C distance of 2.293(2) Å[191] found in complexes of the type $[Mo(C(O)R)(CO)_5]$.[174] The C1–O1 bond length of 1.238(2) Å is typical for an acyl C–O double bond.[189]

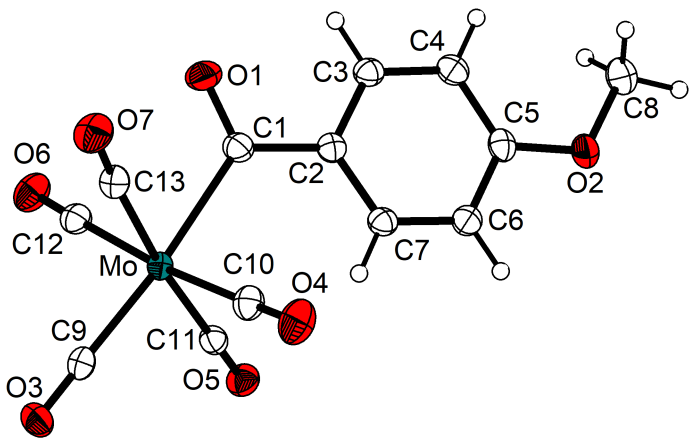

Figure 23. Molecular structure of the anion of (Me_4N)**12** with thermal displacement parameters drawn at the 50% probability level. For selected bond lengths and angles, see Figure 77, p 161.

3.1.3. Ether-substituted arylalkylidyne complexes

Acyl complexes such as those described in Section 3.1.2 (complexes **6**, **8**, **11**, and **12**) are key intermediates to access Schrock's carbyne complexes via the low-oxidation-state route (cf. **R**, Scheme 13, p 17). Oxidation by treatment with oxalyl bromide and bromine in the presence of DME at subambient temperatures (Scheme 31) provides access to the versatile precursor *mer*-[Mo(≡CAr)(Br)$_3$(dme)], which can be further functionalised upon salt metathesis with one to three equivalents of metal alkoxides – K(OC(CF$_3$)$_2$Me), K-**14**, was predominantly used in the present work. Commonly, tetramethylammonium salts of the acyl complexes are used in the oxidation step, but the lithium equivalents might well work instead, as the by-product (LiBr) should also be removable by filtration.

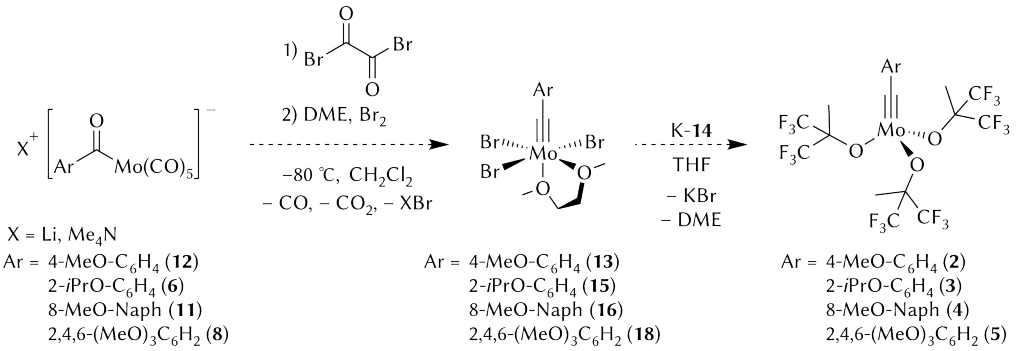

Scheme 31. Envisaged synthesis of ether-substituted arylalkylidyne complexes; DME = 1,2-dimethoxyethane, *i*Pr = 2-propyl, Naph = 1-naphthyl.

Limitations of the low-oxidation-state route

Having developed the modified protocol that allows isolation of the lithium species Li-**6** and Li-**11**, and avoids decomposition of the ether-functionalised acyl complexes, the synthesis of the corresponding carbyne complexes *mer*-[Mo(≡CAr)(Br)$_3$(dme)] (**15**, Ar = 2-*i*PrO-C$_6$H$_4$; **16**, Ar = 8-methoxynaphthyl; see Scheme 31) was attempted. After salt metathesis with K-**14**, alkylidyne complexes **3** and **4**, respectively, may be obtained. As described in the beginning of the chapter, the ultimate target of this functionalisation are MCBD complexes stabilised intramolecularly by chelation with the isopropoxy or methoxy group, respectively (see Schemes 21–22).

Notwithstanding, direct oxidation of acyl complexes Li-**6** and Li-**11** with oxalyl bromide and bromine towards the alkylidyne complexes **15** and **16** was unsuccessful, and repeatedly yielded a mixture of decomposition products (which may include dimeric species similar to [(μ-dme)$_2$(Br)$_3$Mo≡Mo(Br)$_3$]). Even reaction of the commonly used

tetramethylammonium derivative, (Me_4N)**11** in this particular case, did not produce the desired results. These circumstances suggest that the introduced substituents at the acyl moiety – rather than the choice of the counterion – negatively affect the course of the reaction, and it can be assumed that they are incompatible with the harsh conditions of the low-oxidation-state route.

As a matter of fact, treatment of the reaction outcome (crude mixture) with three equivalents of K-**14** in THF also resulted in a complex product mixture. One of these undesired products crystallised at –30 °C and could be identified by X-ray techniques (Figure 24). The structure shows an anionic oxo molybdenum(V) complex carrying a bromido and three alkoxide ligands, $Li(thf)_2[Mo(\equiv O)Br(OC(CF_3)_2Me)_3]$ ($Li(thf)_2$**17**). In addition, the molybdenum atom makes a short contact of 2.531(2) Å to the THF oxygen atom O5, thus completing an irregular octahedral coordination at Mo (*trans* angles: 154.86(8)°, 156.81(6)°, and 167.86(8)°). The four donor atoms O1, O2, O3 and Br are coplanar (r.m.s. deviation 0.0108(17) Å), with the Mo atom lying 0.4286(2) Å out of this plane in the opposite direction to O5. The lithium cation is coordinated by two THF molecules (O4, O5) and two alkoxide ligands (O2, O3), which results in a distorted trigonal-pyramidal configuration (τ_4 = 0.593(4), also described as distorted seesaw struc-

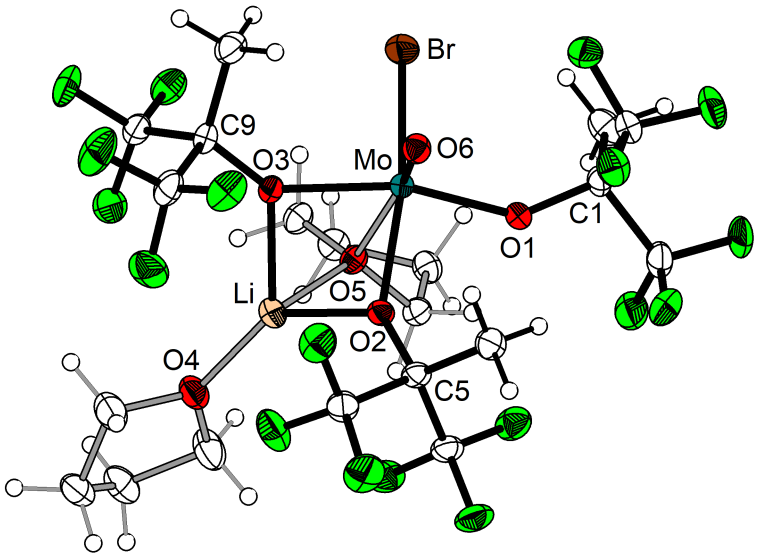

Figure 24. Molecular structure of the side-product $Li(thf)_2$**17** with thermal displacement parameters drawn at the 50% probability level. Selected bond lengths (Å) and angles (deg): Mo–Br 2.4905(4), Mo–O6 1.657(2), Mo–O1 1.9609(19), Mo–O2 2.0396(19), Mo–O3 2.0436(19), Mo–O5 2.531(2), Li–O2 1.960(5), Li–O3 2.005(5), Li–O4 1.900(5), Li–O5 2.126(6); Br–Mo–O6 101.19(7), Br–Mo–O1 92.60(6), Br–Mo–O2 156.81(6), Br–Mo–O3 90.38(6), Br–Mo–O5 86.77(5), O6–Mo–O1 103.48(9), O6–Mo–O2 101.14(9), O6–Mo–O3 100.40(9), O6–Mo–O5 167.86(8), O1–Mo–O2 88.24(8), O1–Mo–O3 154.86(8), O1–Mo–O5 85.13(7), O2–Mo–O3 79.49(8), O2–Mo–O5 70.21(7), O3–Mo–O5 70.13(7), O2–Li–O3 82.4(2), O2–Li–O4 139.5(3), O2–Li–O5 81.06(19), O3–Li–O4 136.9(3), O3–Li–O5 80.0(2), O4–Li–O5 110.7(3).

ture),[178] with the coplanar atoms Li, O2, O3, O4 (r.m.s. deviation 0.057(3) Å) forming the plane of the pyramid and the apex (O5) tilted away from O4 (O4–Li–O5, 110.7(3)°). The O2–Li–O3 bond angle is particularly narrow (82.4(2)°), coming from participation in the bimetallic four-membered ring (Mo, O3, Li, O2), in which the transannular Mo···Li distance is 2.898(5) Å.

Considering the presence of the bromine and lithium atoms, it can be presumed that the cleavage of the alkylidyne group and formation of the oxo species might well have occurred during the oxidation steps of the low-oxidation-state route. As an alternative to this route, the cross-metathesis approach using benzylidyne-transfer reagents ($ArC{\equiv}CCF_3$ or $ArC{\equiv}CSiMe_3$),[138,139] as mentioned in the Introduction (see Scheme 15, p 18), may be suitable to generate the projected alkylidynes **3** and **4**, although in such cases removal of DME may be problematic.

Successful synthesis of 2,4,6-trimethoxybenzylidyne complexes

Better results than for **15** and **16** were obtained in the preparation of the 2,4,6-trimethoxybenzylidyne derivative *mer*-[Mo{≡C(2,4,6-$(MeO)_3C_6H_2$)}$(Br)_3$(dme)] (**18**, Scheme 32). Although the reaction did not proceed as cleanly as usual, treatment of Li-**8** with oxalyl bromide, bromine and DME at –80 °C afforded **18** as a crude product in moderate yields. The alkylidyne complex was unambiguously characterised by NMR spectroscopy. For example, in the ^1H NMR spectrum, the methoxy groups appear as two sharp singlets at δ_H = 3.87 ppm (*para*) and δ_H = 3.91 ppm (*ortho*), whereas the DME ligand exhibits several broad resonances in the range of δ_H = 3.4–4.0 ppm; the peak at δ_H = 6.03 ppm belongs to the aromatic protons. In the $^{13}C\{^1H\}$ NMR spectrum, the DME fragment arises as four resonances (60.0 ppm, 70.0 ppm, 73.4 ppm, and 78.6 ppm), the methoxy moieties resonate at δ_C = 56.0 ppm and δ_C = 56.2 ppm, and the

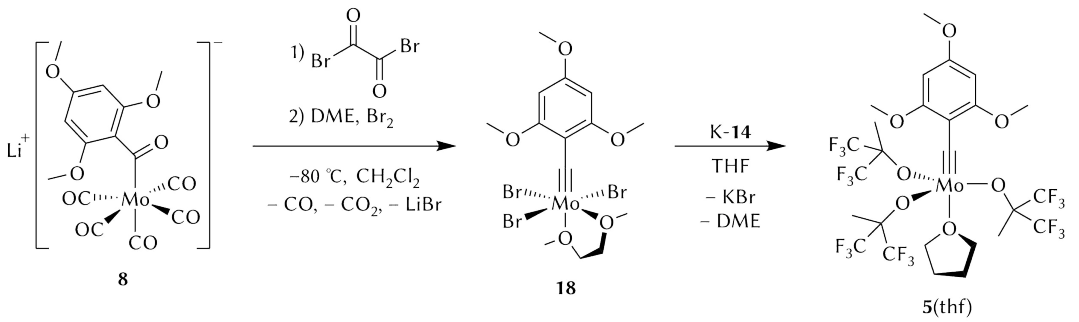

Scheme 32. Synthesis of ether-functionalised benzylidyne complexes **18** and [**5**(thf)]; DME = 1,2-dimethoxyethane.

chemical shifts for the aromatic ring are δ_C = 88.9 ppm (*meta*), δ_C = 117.1 ppm (*ipso*), δ_C = 165.1 ppm (*para*), and δ_C = 168.4 ppm (*ortho*). The characteristic alkylidyne carbon atom is considerably deshielded (δ_C = 331.4 ppm).

Removal of unidentified impurities or degradation products was unsuccessful. These may include, again, the thermodynamically favoured dimer [(μ-dme)$_2$(Br)$_3$Mo≡Mo-(Br)$_3$] or similar species (two additional, broad resonances in the $^{13}C\{^1H\}$ NMR spectrum at δ_C = 62.2 ppm and δ_C = 72.0 ppm evidence the presence of a side-product bearing no organic ligands besides DME). Nevertheless, crude **18** was used without further purification in the next step. Fortunately, reaction with three equivalents of K-**14** in THF (Scheme 32), followed by extraction with *n*-hexane and recrystallisation from *n*-pentane, yielded yellow–orange dichroic plates of pure [**5**(thf)], as determined by X-ray diffraction analysis (Figure 25).

Compound [**5**(thf)] crystallises in the triclinic space group $P\bar{1}$ with two independent molecules in the asymmetric unit; these differ in the orientation of the ligand at O4

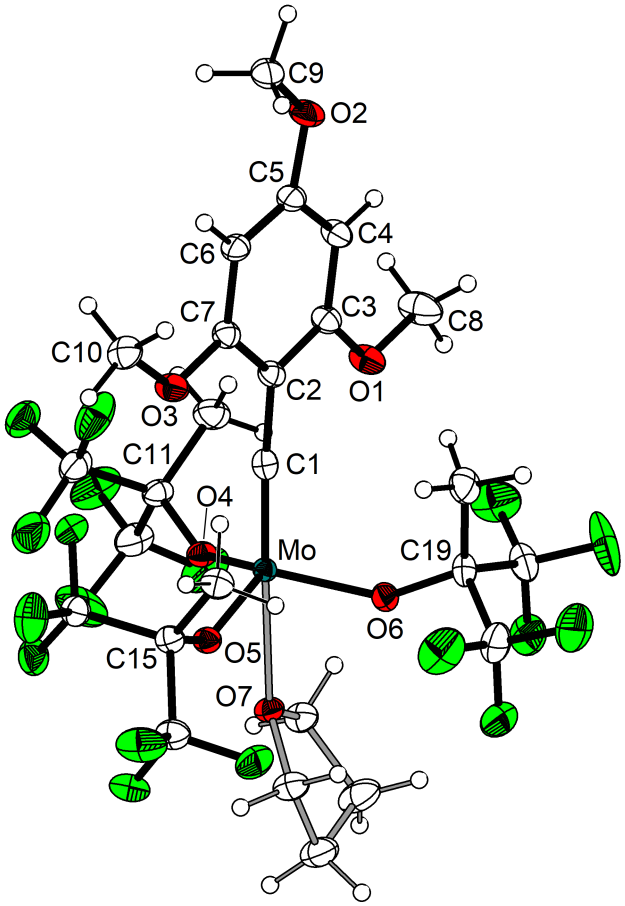

Figure 25. Molecular structure of one independent molecule of [**5**(thf)] with thermal displacement parameters drawn at the 50% probability level. For selected bond lengths and angles, see Figure 75, p 156.

but are otherwise similar. The molybdenum atoms are pentacoordinated and reside in a distorted trigonal-bipyramidal geometry, as indicated by the structural index parameters τ_5 = 0.892(2) and τ_5' = 0.819(2).[188] The alkoxide ligands occupy the equatorial positions, whereas the THF molecule is attached *trans* to the alkylidyne group with axial angles of 174.63(7)° (C1–Mo–O7) and 173.55(7)° (C1′–Mo′–O7′). The Mo–O distances in the alkoxide ligands range from 1.9005(13) Å to 1.9226(13) Å, which is commonly found for covalent bonds; in contrast, the THF molecule suffers from the *trans* effect, as can be concluded by the considerably longer Mo–O bond lengths of 2.4256(13) Å (Mo–O7) and 2.4007(13) Å (Mo′–O7′), and is thus weakly coordinated. The alkylidyne bond (Mo–C1 1.7635(19) Å, Mo′–C1′ 1.7586(19) Å) is in the expected range of a Mo–C triple bond,[192] but the angle deviates significantly from linearity (Mo–C1–C2 171.04(15)°, Mo′–C1′–C2′ 167.28(15)°), presumably originated from steric hindrance between one methoxy group (O3, C10) and the alkoxide group at O5. As a consequence, the opposite methoxy group (O1) approaches the molybdenum centre. The distance of 3.7364(13) Å between them, however, definitely fails to qualify as an intramolecular contact.

In addition, the structure of the compound was confirmed by NMR spectroscopy. The experimental elemental composition, however, indicated a partial loss of THF (~0.5 equivalents, probably caused by thorough drying of the sample), which supports the assumption that the THF ligand is weakly coordinated and can be easily removed.

As expected, a subtle but non-trivial modification of the work-up (extraction of the product with *n*-pentane, then evaporation of the solvent at 50 °C followed by several cycles of dissolution/evaporation) afforded the THF-free complex **5** in modest yields. Complexes [**5**(thf)] and **5** can be distinguished by NMR spectroscopy. For example, all hydrogen atoms are less deshielded in the latter (δ_H = 1.87 ppm, 3.14 ppm, 3.18 ppm, and 5.64 ppm) compared to its THF counterpart (δ_H = 1.94 ppm, 3.17 ppm, 3.21 ppm, and 5.66 ppm). In the $^{19}F\{^1H\}$ NMR spectrum, the fluorine resonance for **5** (δ_F = –78.1 ppm) is slightly high-field-shifted in comparison to that for [**5**(thf)] (δ_F = –77.9 ppm). The most relevant differences in the $^{13}C\{^1H\}$ NMR spectrum (cf. Figure 26) are found for the signals of the alkoxide ligands (δ_C = 18.0 ppm, 84.8 ppm, and 123.9 ppm for [**5**(thf)] vs. δ_C = 18.2 ppm, 84.5 ppm, and 123.6 ppm for **5**) and the alkyli-

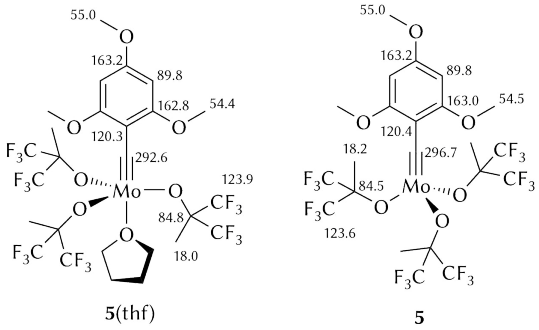

Figure 26. Comparison of the ^{13}C NMR chemical shifts in [**5**(thf)] and **5**.

dyne carbon atom, which resonates at δ_C = 292.6 ppm in [**5**(thf)] and with a higher frequency in **5** (δ_C = 296.7 ppm).

X-ray diffraction analysis of single-crystals obtained from a cold *n*-pentane solution at –35 °C validated the structure of **5** (Figure 27). The yellow–orange dichroic prisms crystallise in the monoclinic space group $P2_1/n$. Importantly, the complex is a 1D-coordination polymer in the solid state (Figure 28), and so it features the envisaged in-

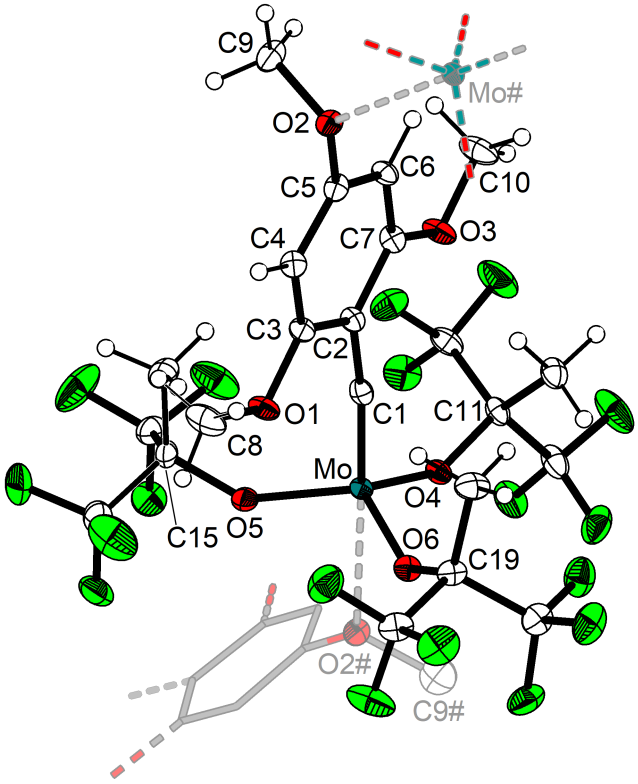

Figure 27. Molecular structure of **5** with thermal displacement parameters drawn at the 50% probability level. Relevant parts of neighbouring molecules are drawn with paler colours. Selected bond lengths (Å) and angles (deg): Mo–C1 1.758(2), Mo–O4 1.9079(15), Mo–O5 1.9018(15), Mo–O6 1.9055(15), Mo···O2# 2.5664(15), C1–C2 1.450(3); C1–Mo–O4 106.26(8), C1–Mo–O5 102.86(8), C1–Mo–O6 102.62(8), C1–Mo···O2# 177.66(7), O4–Mo–O5 113.34(6), O4–Mo–O6 110.67(6), O4–Mo···O2# 76.07(6), O5–Mo–O6 119.29(6), O5–Mo···O2# 75.86(6), O6–Mo···O2# 76.51(6), Mo–C1–C2 170.44(17), C5–O2···Mo# 124.16(12). For the crystal packing, see Figure 76, p 158.

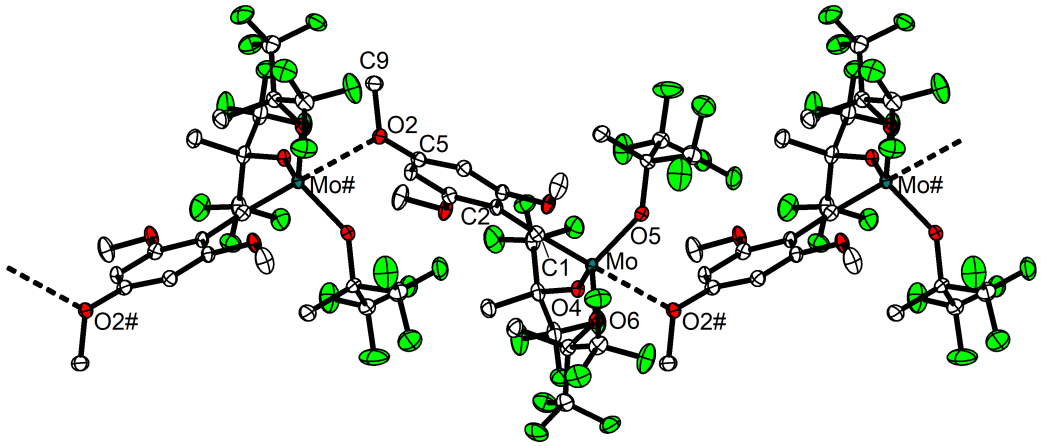

Figure 28. 1D-polymeric chain of **5** viewed along the *a* axis; hydrogen atoms are omitted for clarity.

termolecular contacts. Thus, the *para*-substituent of the alkylidyne moiety is connected via the *n* glide plane to the molybdenum atom of the neighbouring molecule, forming zigzag chains with a bridging angle of 124.16(12)° (C5–O2···Mo#) and overall direction parallel to [101]. The molybdenum centre exhibits a nearly ideal trigonal-bipyramidal geometry (τ_5 = 0.973(2))[188] but is slightly tilted towards C1 out of the equatorial plane formed by the oxygen atoms (O4, O5, O6) of the fluorinated ligands. The molybdenum–carbon triple bond of 1.758(2) Å is in the expected range for alkylidyne complexes,[192] but the Mo–C1–C2 angle deviates significantly from linearity (170.44(17)°), so the aryl ring is inclined away from the fluorinated ligand at O4, again, arising from steric repulsion with the methoxy group at C7. Although the other *ortho*-methoxy substituent (O1) is approaching the metal centre, the separation of 3.6738(15) Å excludes any binding interaction. By contrast, the axial angle C1–Mo···O2# between the alkylidyne unit and the *para*-methoxy group of the next molecule is nearly linear (177.66(7)°). This intermolecular connection is characterised by an elongated Mo···O2# bond of 2.5664(15) Å, which confirms the weak nature of the interaction.

As outlined in Scheme 23, formation of an MCBD species by reacting **5** with a small alkyne such as 3-hexyne is expected to involve a dative bond between one *ortho*-methoxy group and the metal centre. Such intramolecular contacts may contribute to the stability of the complex. Unfortunately, as shown by NMR spectroscopy, reaction of **5** with 3-hexyne delivered a mixture of compounds including the cross-metathesis products: alkylidyne complex [EtC≡Mo(OC(CF$_3$)$_2$Me)$_3$] (**19**) and mixed acetylene

ArC≡CEt (Ar = 2,4,6-trimethoxyphenyl). In addition, precipitation of a colourless solid suggested polymerisation or oligomerisation of the alkyne (cf. Section 3.3.1, pp 85–86).

Attempts to get single crystals from this mixture were unsuccessful, even if the reaction was conducted at low temperature as described for recently isolated MCBD complexes.[62] In one occasion, deep red crystals were obtained from a dichloromethane/*n*-pentane solution at –40 °C. Since the crystals suffered from poor quality and severe disorder, structure refinement was not feasible; however, the data qualitatively shows the formation of a dimolybdenacyclobutadiene(Mo–Mo) species (Figure 29 and Scheme 33) via [2 + 2] cycloaddition of two molecules of **5** after loosing each an alkoxide ligand. In addition, the *para*-methoxy groups coordinate *trans* to a molecule of **19**, implying that **5** underwent cross-metathesis with 3-hexyne. This structure is important for several reasons: (i) it confirms that an MCBD complex with 3-hexyne is thermodynamically unfavoured, (ii) it suggests that reduction of molybdenum and formation of a Mo–Mo bond might be a side-reaction to be considered, (iii) it shows that the

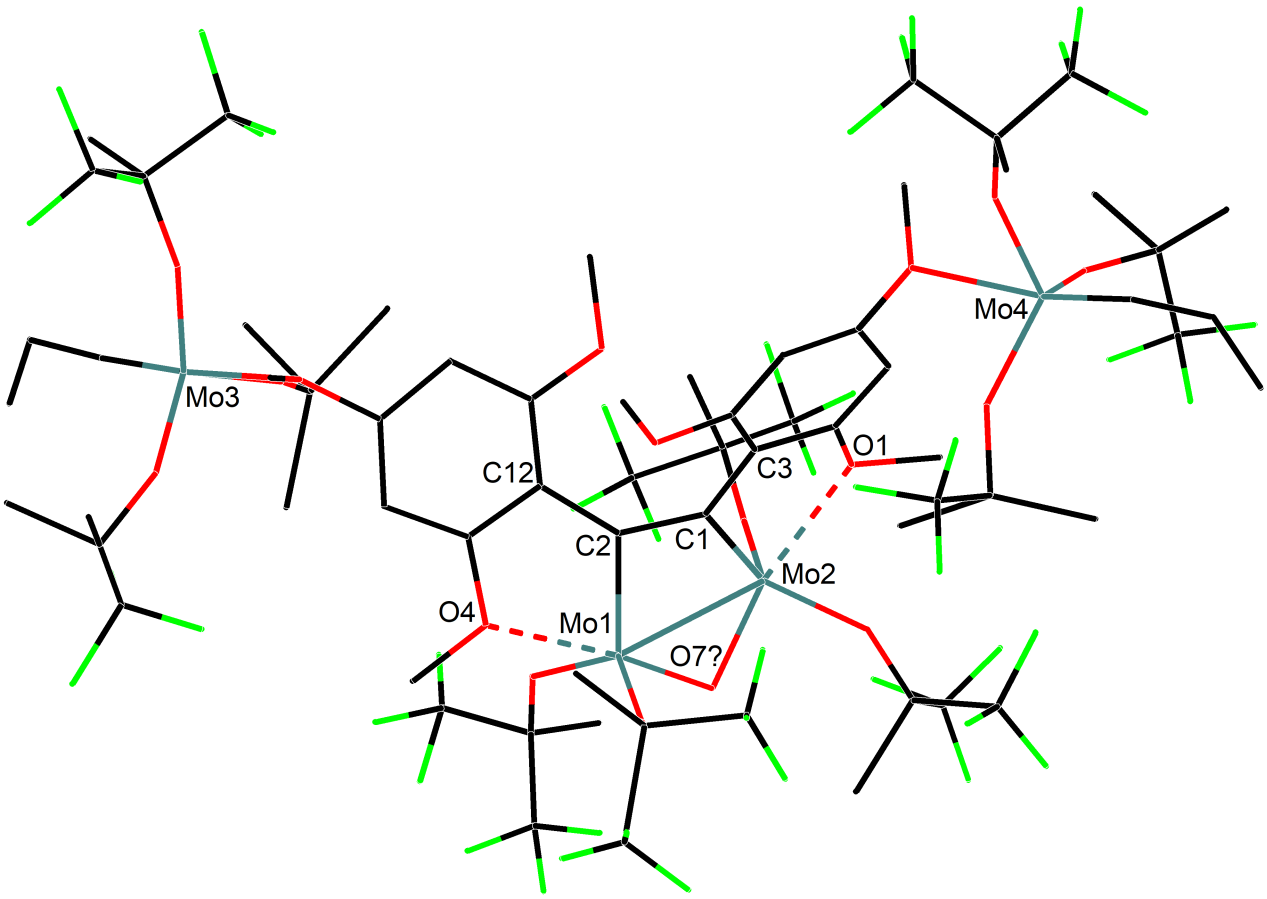

Figure 29. Molecular structure of the identified product from the reaction of **5** with 3-hexyne presented as a wireframe model. Hydrogen atoms and several fluorine atoms were not refined and are missing; co-crystallised CH_2Cl_2 has been omitted. A question mark (?) at O7 indicates that the nature of the atom is uncertain.

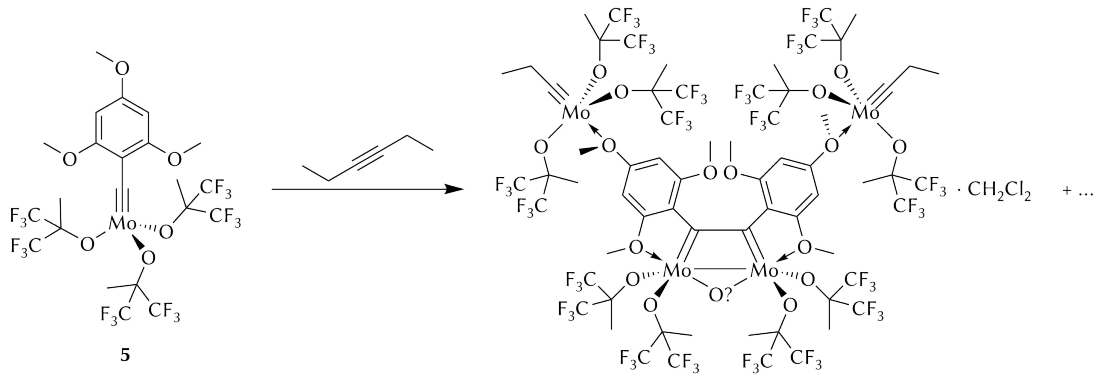

Scheme 33. Identified product from the reaction of **5** and 3-hexyne at −40 °C. The uncertainty about the nature of the bridging group is indicated by a question mark (?).

fluorinated alkoxide is labile and may induce decomposition, and most remarkably, (iv) it evidences that the methoxy group at the *ortho* position of the aryl ring can indeed engage in the hypothesised intramolecular chelation of the molybdenum centre (see Scheme 23).

It has to be noticed that the two molybdenum atoms in the metallacycle are additionally bridged by a light atom. Given the poor quality of the data, it is uncertain if the bridging moiety is an oxo ligand, a hydroxide group, or a fluorine atom. The former is more convincing, assuming that two alkoxide ligands decompose into an ether (R–O–R, R = $C(CF_3)_2Me$) and the oxo moiety, because it affords the same formal oxidation state (i.e. +V) for both molybdenum centres. Otherwise, a proton source such as traces of water may lead to the free alcohol (R–OH) and a bridging hydroxide. In a less thinkable scenario, a fluoride group could arise from complete degradation of the fluorinated ligand.

The unsuccessful attempts to isolate an MCBD species from alkylidyne complex **5** and 3-hexyne by [2 + 2] cycloaddition can be explained by the low energy barriers associated with MCBD intermediates in the alkyne metathesis catalytic cycle.[62] As a consequence, it is extremely difficult to kinetically trap and isolate MCBD complexes, which are often thermally sensitive and readily loose one alkyne molecule. This is particularly true if the complexes perform as highly active catalysts, such as **1** and similar molybdenum alkylidynes bearing the expedient hexafluorinated alkoxide ligands (**14**).

Synthesis of *para*-methoxybenzylidyne complexes[190]

In view of the fact that the lithium salt of acyl complex **12** was not obtained cleanly, *para*-methoxybenzylidyne complex **13** was prepared classically from (Me_4N)**12**.[84] To access target alkylidyne **2**, the tribrominated complex was treated subsequently with three equivalents of K-**14** in tetrahydrofuran, followed by extraction with *n*-pentane. NMR spectroscopic and elemental analyses revealed that the product, [**2**(thf)], contained a coordinated THF molecule (Scheme 34). X-ray diffraction studies of yellow crystals grown from a concentrated *n*-pentane solution at –35 °C confirmed coordination of one solvent molecule *trans* to the alkylidyne moiety (Figure 30), although the structure could not be refined satisfactorily because of twinning and severe disorder. For this reason, discussion of structural parameters will be omitted herein.

In order to obtain better crystals of [**2**(thf)], recrystallisation was attempted from a cold solution of [**2**(thf)] in *n*-pentane, to which a drop of THF was added. In addition to the known yellow crystals, red crystals were obtained and subjected to X-ray diffraction analysis. The molecular structure (Figure 31) shows *cis*,*mer*-[**2**$(thf)_2$],[193] in which two THF molecules are coordinated to the desired compound **2**. The compound crystallises in the monoclinic space group $P2_1/n$, and the molybdenum atom resides in a distorted octahedral environment (the bond angles around the metal centre are in the range of 150.80°–177.79° (*trans*) and 76.51°–102.47° (*cis*)). Indeed, the molybdenum atom

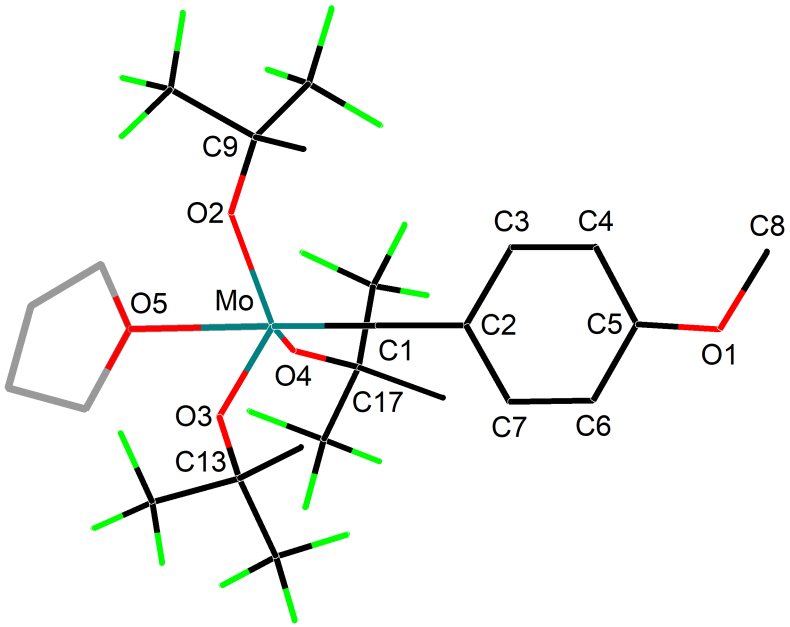

Figure 30. Molecular structure of [**2**(thf)]. Only one of the two independent molecules in the unit cell is shown as a wireframe model; hydrogen atoms are omitted for clarity.

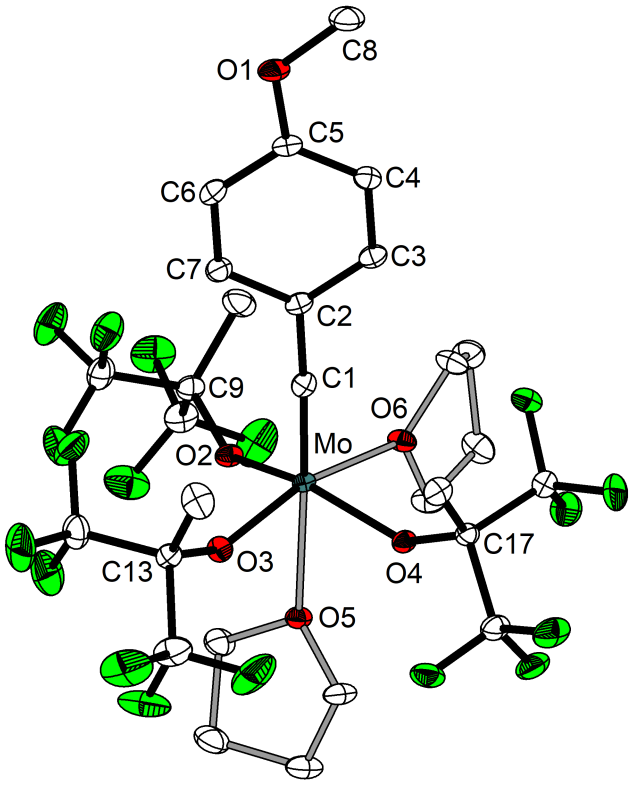

Figure 31. Molecular structure of *cis,mer*-[**2**(thf)$_2$] with thermal displacement parameters drawn at the 50% probability level. Only one position of the disordered THF molecule (at O5) is shown; hydrogen atoms are omitted for clarity. Selected bond lengths (Å) and angles (deg): Mo–C1 1.757(2), Mo–O2 1.9638(14), Mo–O3 1.9340(14), Mo–O4 1.9628(14), Mo–O5 2.4485(14), Mo–O6 2.2352(14), C1–C2 1.448(3); C1–Mo–O2 101.66(8), C1–Mo–O3 102.47(8), C1–Mo–O4 102.37(8), C1–Mo–O5 177.79(7), C1–Mo–O6 94.91(7), O2–Mo–O3 95.48(6), O2–Mo–O4 150.80(6), O2–Mo–O5 76.56(5), O2–Mo–O6 79.82(6), O3–Mo–O4 95.29(6), O3–Mo–O5 76.51(5), O3–Mo–O6 162.59(6), O4–Mo–O5 79.71(5), O4–Mo–O6 81.83(6), O5–Mo–O6 86.09(5), Mo–C1–C2 176.99(17).

is displaced 0.3687(2) Å from the l.s. plane of O2, O3, O4, O6 (r.m.s. deviation 0.0550(14) Å) towards the alkylidyne group, which results in an elongated Mo–O bond of 2.4485(14) Å at the *trans* THF ligand (the *trans* effect is evidenced by the second THF molecule, which displays a shorter Mo–O6 distance of 2.2352(14) Å). Furthermore, the Mo–C1 triple bond length (1.757(2) Å) is comparable to those of similar molybdenum alkylidyne complexes.[174]

In contrast to the closely related DME derivative [**2**(dme)], which was prepared in diethyl ether[171,193] or toluene,[138] the reaction of **13** and K-**14** in tetrahydrofuran afforded THF complex [**2**(thf)]. This distinction is crucial, considering that, as reported previously,[157] THF is much more easily removed than DME to generate the solvent-free alkylidyne complex (cf. **1**). Indeed, recrystallisation of [**2**(thf)] from a cold mixture of toluene and *n*-pentane or, alternatively, repeated dissolution of [**2**(thf)] in toluene followed by evaporation of the solvent at 50 °C and crystallisation from *n*-pentane afforded the desired THF-free complex **2** in moderate yields (Scheme 34).

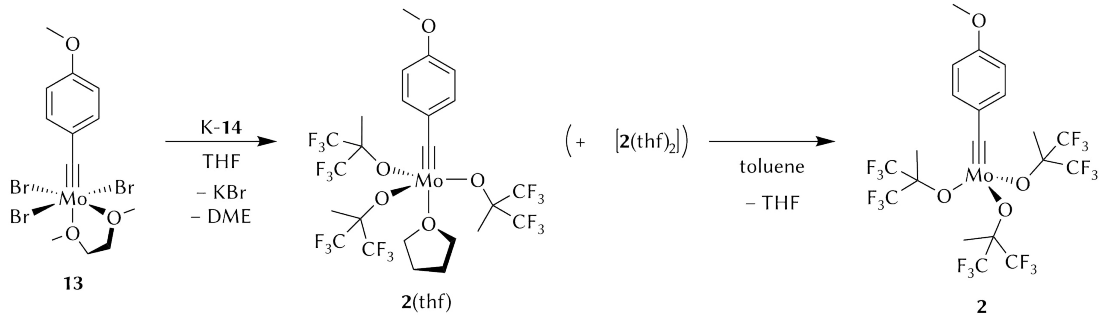

Scheme 34. Synthesis of *p*-methoxybenzylidyne complexes [**2**(thf)$_n$] (n = 0–2); DME = 1,2-dimethoxyethane.

The NMR spectra of **2** show significant differences in comparison with the spectra of [**2**(thf)]. For instance, the methyl groups of the alkoxide ligands are found at δ_H = 1.68 ppm in the former compound and are more deshielded (δ_H = 1.84 ppm) in the latter. Similarly, an increase in the chemical shifts corresponding to the aryl protons (δ_H = 6.41 ppm and δ_H = 7.04 ppm for **2**) is observed for [**2**(thf)] (δ_H = 6.44 ppm and δ_H = 7.16 ppm. In the $^{19}F\{^1H\}$ NMR spectrum, the fluorine atoms give rise to a single peak, which is slightly shifted from δ_F = –77.81 ppm in [**2**(thf)] to δ_F = –77.92 ppm in the THF-free complex. Furthermore, the ^{13}C signals at δ_C = 113.8 ppm and δ_C = 132.6 ppm account for the aromatic atoms at the *ortho* and *meta* positions in [**2**(thf)], whereas the same carbon atoms in **2** resonate at δ_C = 114.1 ppm and δ_C = 131.9 ppm. Finally, the alkylidyne carbon atom is shifted downfield for **2** (δ_C = 299.2 ppm) compared to its THF solvate (δ_C = 294.3 ppm).

The structure of **2** (Figure 32) was confirmed by X-ray diffraction analysis of platy pale yellow crystals; it crystallises in the enantiomorphic, monoclinic space group $P2_1$ with two independent molecules in the asymmetric unit. Analogous to **5**, the complex is a 1D-coordination polymer in the solid state. Hence, each molecule is connected to its neighbour through the *para*-methoxy group at the alkylidyne moiety, forming zigzag polymeric chains (Figure 33) with bridging angles Mo2···O1–C5 128.67(16)°, and Mo1···O5#–C25# 118.41(16)° (symmetry operator $x-1$, y, $z-1$). The overall chain direction is parallel to [101]. The geometry around the pentacoordinated molybdenum atom is trigonal-bipyramidal (τ_5 = 0.940(3) and 1.031(3) for the two independent molecules),[188] with an axial angle of 174.28(10)° (C1–Mo1···O5#) and 179.44(11)° (C21–Mo2···O1) and equatorial mean angles of 114.72(10)° and 115.39(9)°. In both independent units, the molybdenum core is located 0.4433(2) Å (Mo1) or 0.4151(2) Å (Mo2) over the plane formed by the oxygen atoms of the alkoxide ligands (O2, O3, O4 or O6, O7, O8, re-

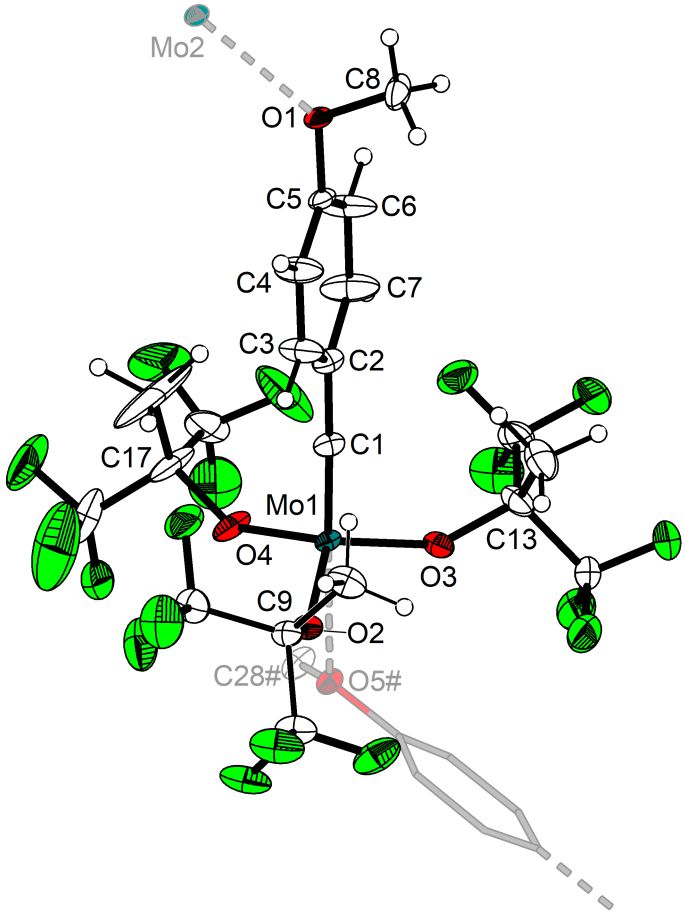

Figure 32. Molecular structure of one of the two independent monomers of **2** with thermal displacement parameters drawn at the 50% probability level. Relevant parts of neighbouring molecules are indicated using paler colours. A second independent molecule in the asymmetric unit and the minor component of a disordered $C(CF_3)_2Me$ group are omitted for clarity. For selected bond lengths and angles, see Figure 79, p 166.

spectively). The alkylidyne bond distances of 1.750(3) Å (Mo1–C1) and 1.753(3) Å (Mo2–C21) are in the expected range for alkylidyne molybdenum complexes,[174] whereas the intermolecular contacts of 2.7241(19) Å (Mo1···O5#) and 2.4723(19) Å (Mo2···O1) are clearly below the sum of the van der Waals radii of molybdenum and oxygen (3.65 Å),[194] although much longer than the covalent Mo–O bonds (1.896(2) Å–1.9052(19) Å and 1.905(2) Å–1.908(2) Å), indicating the weak character of the interactions.

Interestingly, formation of these alkylidyne-based, single-chain coordination polymers is unprecedented and depends strongly on the nature of the supporting ligands. Hence, such intermolecular contacts are not observed, for example, in complex **T**,[84] which bears triphenylsilanolate ligands, certainly more sterically demanding than the fluorinated alkoxides. Another advantage of fluorinated ligands over the Ph_3SiO^- group is that cationic ate-complexes such as $K[Mo(\equiv CR)(X)_4]$ (X = alkoxide ligand)[49]

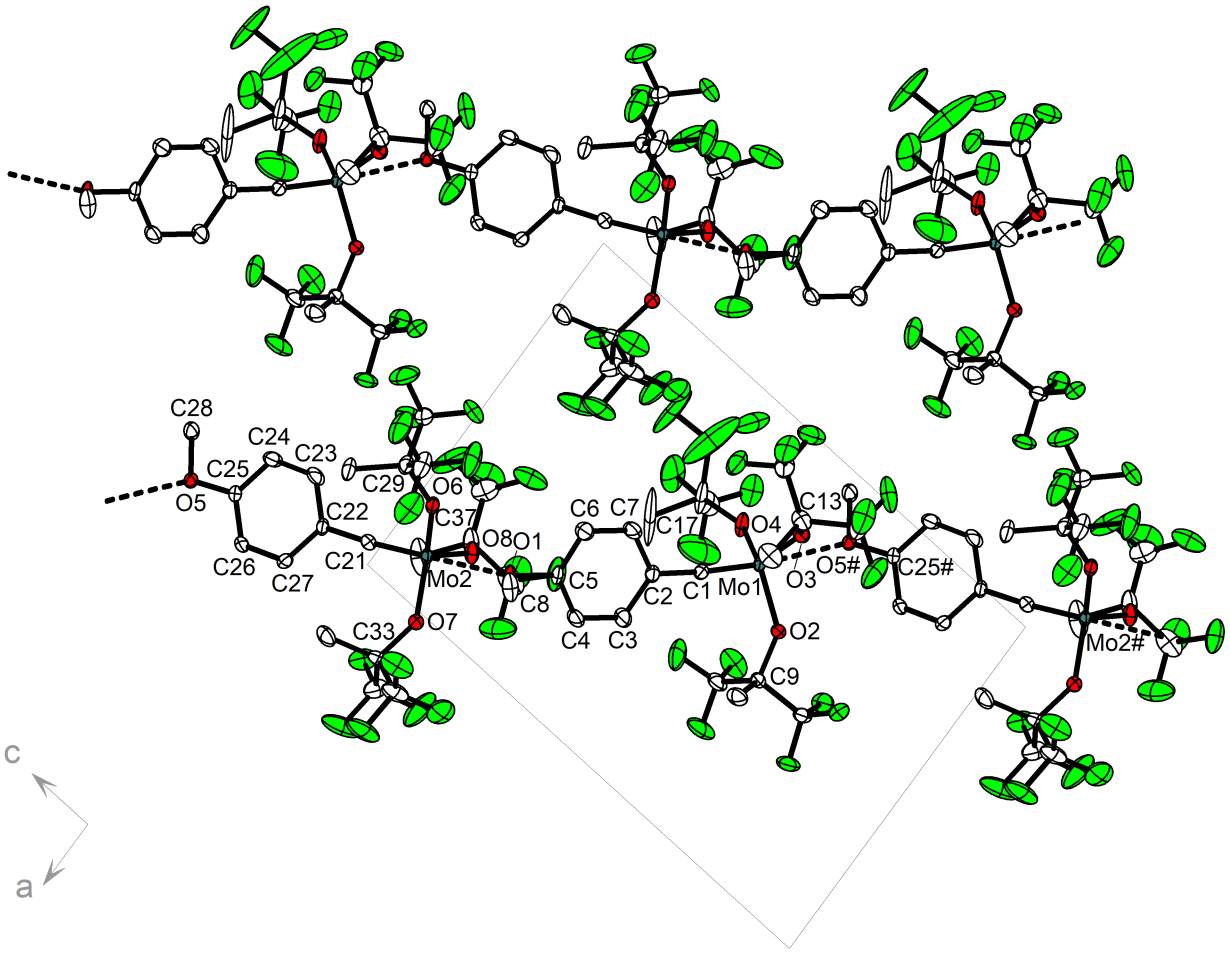

Figure 33. Crystal packing of **2** viewed along the *b* axis with thermal displacement parameters drawn at the 50% probability level. It shows the formation of chain polymers via intermolecular Mo···O contacts (dashed bonds). Hydrogen atoms are omitted for clarity.

are less favoured in the former case, at least in THF. Unfortunately, as will be discussed in Section 3.4.3, the bridging of single molecules in the solid state through the *para*-methoxy fragment did not positively affect the stability of the complexes towards air or moisture.

To further explore the possibilities of these systems, different alkoxide ligands can be employed to adjust the electronic properties of the complexes. For example, an increase in the degree of fluorination would generate alkylidyne complexes with increased electrophilicity. Although the use of perfluorinated ligands (e.g. $(CF_3)_3CO^-$, **20**) has been proved detrimental for catalytic alkyne metathesis,[62,140] the augmented electrophilic character on the metal centre may intensify the affinity to coordinate donating groups intended to stabilise the complex.

Thus, treatment of **13** with three equivalents of K-**20** produced THF complex [Mo(≡C(4-MeO-C_6H_4))(OC$(CF_3)_3)_3$(thf)], [**21**(thf)] (Scheme 35). The ^{1}H NMR spectrum

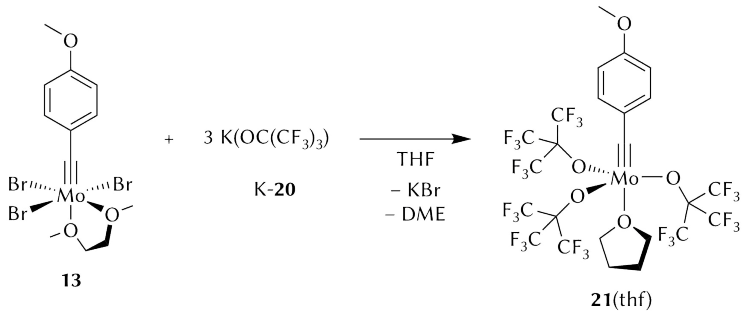

Scheme 35. Reaction of *para*-methoxy benzylidyne complex **13** with 3 equiv of $K(OC(CF_3)_3)$; DME = 1,2-dimethoxyethane.

displays two doublets at δ_H = 6.38 ppm and δ_H = 7.14 ppm for the aryl protons, whereas only one signal at δ_F = –72.34 ppm is observed in the $^{19}F\{^1H\}$ NMR spectrum, which indicates the chemical equivalence of the perfluorinated alkoxide ligands in solution. Accordingly, two multiplets at δ_C = 85.5 ppm and δ_C = 121.6 ppm account for the carbon atoms of these ligands. As expected, the methoxy group is strongly deshielded (δ_C = 54.8 ppm), and the four signals for the aryl carbon atoms are found in the aromatic region from δ_C = 112.8 ppm to δ_C = 161.8 ppm. Finally, the ^{13}C resonance with the highest frequency (δ_C = 315.2 ppm) is characteristic of the alkylidyne carbon atom.

Coordination of one THF molecule was also observed in the NMR spectra (δ_H = 1.32 ppm, δ_H = 3.72 ppm; δ_C = 25.2 ppm, δ_C = 71.2 ppm), and it was confirmed by elemental and X-ray diffraction analyses of red crystals obtained from a cold *n*-pentane solution. Compound [**21**(thf)] crystallises in the monoclinic space group $P2_1/n$, and shows a pentacoordinated molybdenum centre in an approximate trigonal-bipyramidal environment (Figure 34). The structure, however, suffers from severe disorder, and it could not be refined satisfactorily. Although the atom connectivity is qualitatively correct, a discussion of structural parameters would not be appropriate.

Notably, the NMR signals of the coordinated THF moiety are unusually broad, suggesting a dynamic process in solution. It can be assumed, therefore, that the THF molecule is weakly bound and shall be easily displaced to afford a 12 VE complex with an additional free binding site. Unfortunately, removal of THF was not possible, and merely a partial reduction of the THF content was observed by NMR spectroscopy. In consequence, the question whether the desired complex **21** favours intermolecular interactions forming 1D-polymeric chains in the solid state, and whether the stability of the complex is thus improved, remains unanswered.

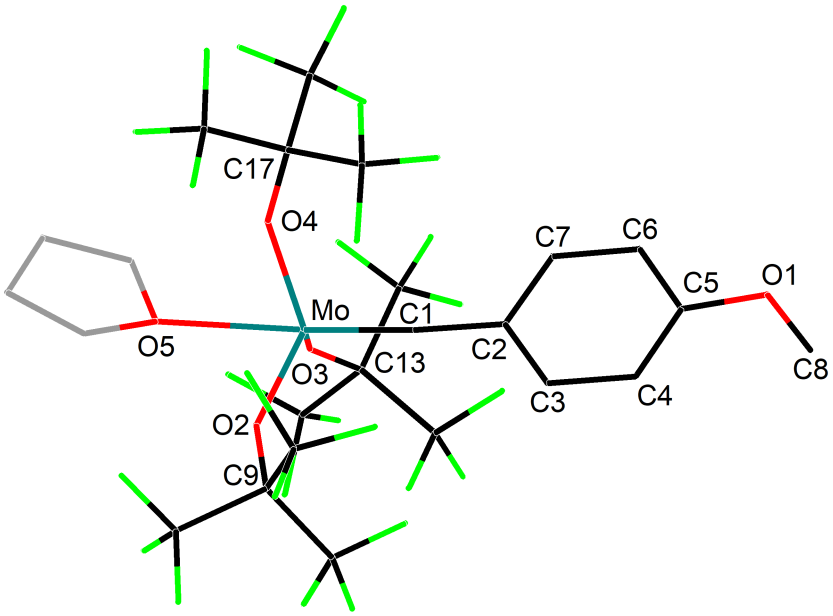

Figure 34. Molecular structure of [**21**(thf)] presented as a wireframe model. Hydrogen atoms are omitted for clarity.

3.2. Coordination of Additional Ligands

3.2.1. Attempted nitrile metathesis: An acetonitrile alkylidyne complex

Nitrile–alkyne cross-metathesis (NACM) and nitrile cross-metathesis (NCM) are attractive variations of the metathesis reaction, which involve the cleavage and re-formation of N–C triple bonds (Scheme 36). In the first case, the reactants and products are an alkyne and one or two nitriles, whereas in the NCM reaction the combination of two nitriles generates an alkyne and dinotrogen. Because the type of bonds is not maintained on both sides of the reaction, the NCM is not an isodesmic reaction and is not thermoneutral; in fact, the formation of N_2 is thermodynamically favoured, and therefore, the nitrile–nitrile metathesis is a desired reaction that has so far escaped the commitment of the chemical community.

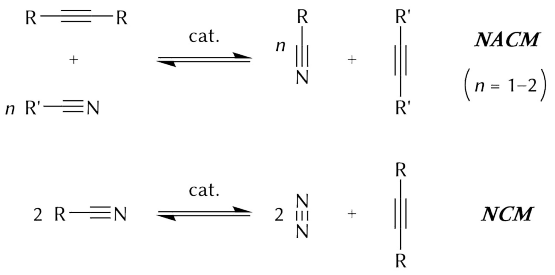

Scheme 36. Nitrile–alkyne cross-metathesis (top) and nitrile cross-metathesis (bottom) reactions.

A number of successful NACM examples has been reported by the group of M. J. A. Johnson,[195,196] who showed that, under certain conditions, tungsten and molybdenum nitrido complexes are able to perform a tandem NACM/ACM reaction, thus involving the use of a sacrificial alkyne. Although these results are promising, more appropriate catalysts need to be developed yet. Given the assumed mechanism of the NACM,[196] one important aspect is the reversible formation of the alkylidyne complexes from the nitrido counterparts upon reaction with alkynes or vice versa (formation of nitrido complexes when the metal alkylidynes are treated with nitriles). This reversibility has been observed in some tungsten complexes.[195] In general, however, tungsten nitrido complexes are thermodynamically favoured over the corresponding alkylidyne complexes, as they are obtained by the reaction of the latter with nitriles, but cannot react back with alkynes to regenerate the alkylidyne moiety (Scheme 37).[197,198] The situation is reversed in molybdenum complexes,[131,199] for which the relative stability of the alkylidyne complexes versus the nitrido complexes can be reasoned by both the higher

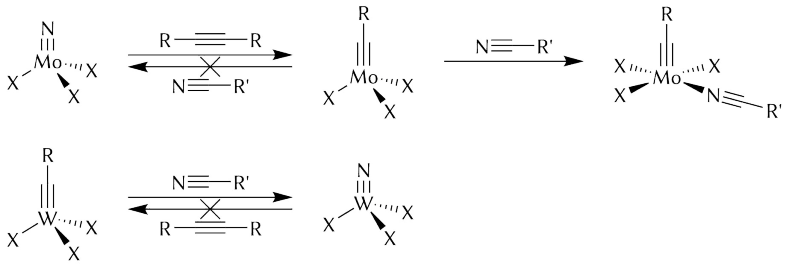

Scheme 37. General behaviour of the interconversion of the nitrido and alkylidyne functionalities in tungsten and molybdenum complexes; X = usually an alkoxide ligand.

electronegativity of the nitrido ligand and the metal centre.[196] Whereas it has been shown that treatment of molybdenum nitrido complexes with alkynes affords readily the alkylidyne complexes,[23,131–133] their interaction with nitriles results only in a (reversible) coordination of the nitrile molecule (Scheme 37).[84,133,171] As a consequence, it is rather unlikely that such compounds are capable of promoting NACM or even NCM. However, because the attachment of the nitrile is reversible, it would be interesting to explore the stability and catalytic activity of these molybdenum alkylidyne complexes.

In line with this and in view of the high activity in alkyne metathesis, the reactivity of mesitylidyne complex **1** with nitriles was investigated under stoichiometric conditions. A solution of **1** in deuterated benzene turned red immediately after addition of an equivalent amount of acetonitrile (Scheme 38), which is the expected colour for a metallacyclobutadiene species.[38,39,69,79,141,200,201] Unfortunately, yet unsurprisingly, the NMR experiment showed the quantitative formation of adduct [**1**(NCMe)] (**22**). Even after heating at 50 °C no further changes were detected in the NMR spectra. Compared to the free solvent,[202] the acetonitrile methyl protons are shifted upfield from δ_H = 0.58 ppm to δ_H = 0.54 ppm suggesting a coordination to the metal centre. The signals for the mesityl moiety are shifted downfield compared to complex **1**, and are found at δ_H = 2.03 ppm (*para*-CH_3), δ_H = 2.59 ppm (*ortho*-CH_3), and δ_H = 6.54 ppm (*meta*-H). In addition, the fluorinated alkoxides resonate at δ_H = 1.71 ppm, and at δ_F = –76.5 ppm in the $^{19}F\{^1H\}$ NMR spectrum. Markedly distinct chemical shifts for the acetonitrile molecule after coordination are also observed in the carbon NMR spectrum (free MeCN, δ_C = 0.2 ppm and δ_C = 116.0 ppm;[202] in **22**, δ_C = –0.2 ppm and δ_C = 124.9 ppm). Last, the signals for the *ipso*-carbon atom and for the alkylidyne carbon atom are slightly shifted, respectively, from δ_C = 143.3 ppm and δ_C = 317.9 ppm (**1**) to

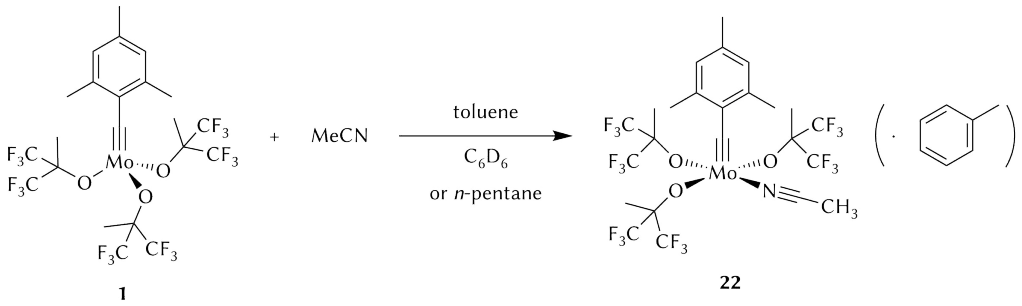

Scheme 38. Synthesis of **22** from **1** and acetonitrile.

δ_C = 141.5 ppm and δ_C = 315.3 ppm (**22**). It is interesting to note that the alkoxide ligands are equivalent in solution, as evidenced by only one observed resonance for the CF_3 groups in both the fluorine and the carbon NMR spectra. This is consistent with a trigonal-bipyramidal structure, in which the alkoxide ligands rest in the equatorial plane, or alternative, a sufficiently fast isomerisation on the NMR timescale by the Berry pseudorotation mechanism.

The new alkylidyne complex **22** was also prepared in a larger scale using *n*-pentane as a solvent, and was isolated in good yields after recrystallisation from an *n*-pentane/toluene mixture at –35 °C. However, application of dynamic vacuum to dry the obtained red crystals induced a loss of crystallinity and discolouration of the solid. This colour change could be explained by the release of the coordinated acetonitrile, which was evidenced by elemental analysis. The coordination is, however, reversible and **22** is re-formed in solution upon addition of more acetonitrile.

Single-crystals of **22** were obtained from a toluene solution at –35 °C, and its solid-state structure was determined by X-ray diffraction analysis (Figure 35). The red–colourless dichroic crystals are monoclinic (space group $P2_1/n$) and contain a solvated toluene molecule per complex unit (**22**·C_7H_8). However, the toluene was released when exposing the crystals to the glove-box atmosphere for several hours, causing also a loss of crystallinity, and, as a result, too low carbon and hydrogen values were obtained in the combustion analysis. The alkylidyne moiety at the pentacoordinated molybdenum atom has a Mo–C1 bond length of 1.7388(15) Å, which is practically equal to that of parent complex **1** (1.7438(16) Å),[157] whereas the Mo–O bond lengths (1.9452(10)–1.9501(10) Å), albeit in the expected range, are slightly longer than in **1** (1.8946(11)–1.9243(11) Å) because of the increase in the coordination number. The Mo–N bond distance of 2.2198(14) Å, however, is larger than expected for a Mo–N single

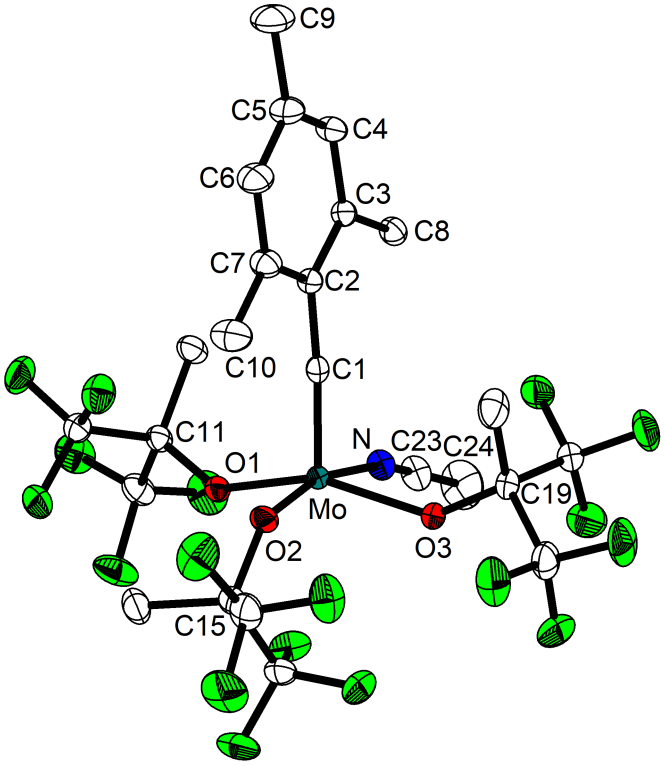

Figure 35. Molecular structure of **22**·C_7H_8 with thermal displacement parameters drawn at the 50% probability level. Hydrogen atoms and two disordered toluene molecules are omitted for clarity. Selected bond lengths (Å) and angles (deg): Mo–C1 1.7388(15), Mo–N 2.2198(14), Mo–O1 1.9452(10), Mo–O2 1.9498(11), Mo–O3 1.9501(10), N–C23 1.135(2), C1–C2 1.444(2); C1–Mo–N 97.84(6), C1–Mo–O1 103.45(6), C1–Mo–O2 96.51(6), C1–Mo–O3 103.94(6), N–Mo–O1 80.87(5), N–Mo–O2 165.62(5), N–Mo–O3 80.45(5), O1–Mo–O2 96.68(5), O1–Mo–O3 148.59(5), O2–Mo–O3 95.20(5), Mo–C1–C2 174.58(12), Mo–N–C23 168.11(14), N–C23–C24 179.0(2).

bond,[180,189] suggesting that the acetonitrile is weakly coordinated to the molybdenum centre. Contrary to the trigonal-bipyramidal structure reasoned from the NMR data, in the solid state the ligands are organised in a square-pyramidal geometry, which was also established for a similar compound (viz. [Mo(≡CEt)(NCEt)(OC(CF_3)$_3$)$_3$]).[133] In this geometry the alkylidyne moiety occupies the apical position, and the base is formed by the remaining ligands with basal angles N–Mo–O2 and O1–Mo–O3 of, respectively, 165.62(5)° and 148.59(5)°. The molybdenum atom is located 0.3723(1) Å above the basal plane (l.s. plane through atoms O1, O2, O3, N, r.m.s. deviation 0.1032(11) Å). Furthermore, the structural index parameter τ_5 = 0.284(2)[188] supports the established coordination geometry.

3.2.2. Synthesis of alkylidyne complexes with coordinating ligands

Despite the increase in the coordination number after the attachment of the nitrile, complex **22** shows excellent activity in alkyne metathesis (see Chapter 3.4). It would be interesting, therefore, to synthesise a series of compounds of the type [**1**(L)] by combination of mesitylidyne complex **1** with several donor ligands (L) (Scheme 39). The

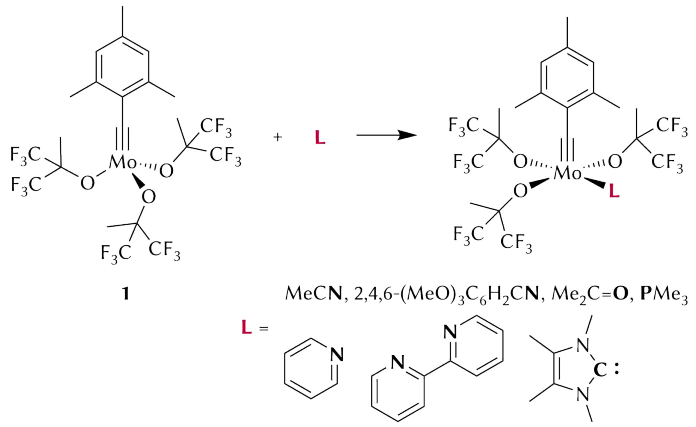

Scheme 39. Projected synthesis of several complexes of the type [**1**(L)].

catalytic activity of the resulting complexes shall be subsequently investigated and compared to that of **22** or that of the parent compound **1**. Moreover, and most interestingly, the coordination of the ligands might supply additional stability to the complexes,[203] or even afford bench-stable precatalysts, as has been shown by A. Fürstner and his team (see Section 1.3.4, p 22 f).[49,84] It is therefore important to explore the coordination of ligands with different steric and electronic properties, such as ketones, nitriles, amines, phosphanes or carbenes.

2,4,6-Trimethoxybenzonitrile

An increase in the steric bulk of the nitrile ligand might contribute to the overall stability of the alkylidyne complex. In addition, the presence of electron-donating groups such as ethers might promote the formation of intermolecular contacts, analogously to the interactions found in complexes **2** and **5**, which feature 1D-polymeric structures in the solid state. For these reasons, 2,4,6-trimethoxybenzonitrile (**23**) was used to generate the next member of the series.

Reaction of the nitrile **23** with alkylidyne complex **1** in toluene or benzene-d_6 (Scheme 40) produced almost instantly a red colouration of the solution. As observed for aceto-

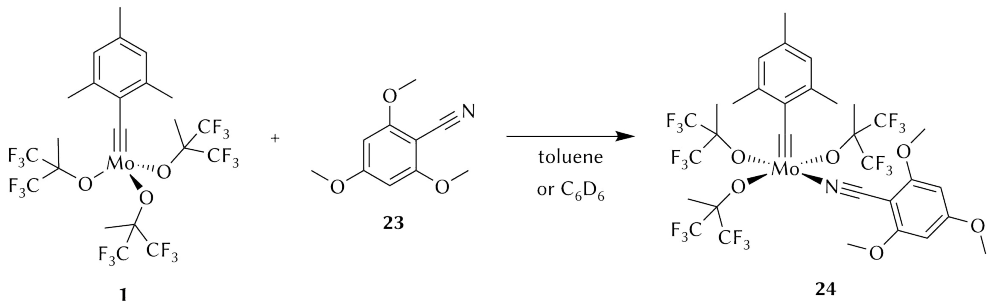

Scheme 40. Synthesis of **24** from alkylidyne complex **1** and 2,4,6-trimethoxybenzonitrile (**23**).

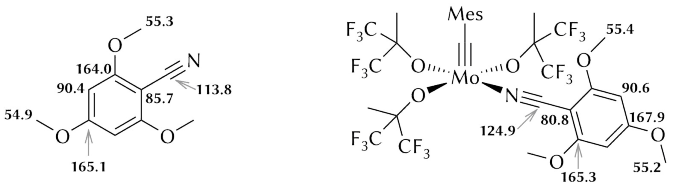

23 24

Figure 36. Comparison of the ^{13}C NMR chemical shifts in the free nitrile **23** and in complex **24**.

nitrile adduct **22**, the colour did not account for the formation of an MCBD species. Instead, quantitative conversion to adduct [**1**(**23**)] (**24**) was evidenced by NMR spectroscopy. The spectra show the expected number of resonances, which differ from those corresponding to the starting materials. For example, compared to the free molecule, the resonances for the nitrile are high-field-shifted in the proton NMR spectrum in toluene-d_8 (δ_H = 3.13 ppm, δ_H = 3.14 ppm, and δ_H = 5.47 ppm versus δ_H = 3.16 ppm, δ_H = 3.22 ppm, and δ_H = 5.66 ppm for the free nitrile), whereas a general shift towards the low field is observed in the carbon NMR spectrum (see Figure 36). An exception is the quaternary *ipso*-carbon atom, which has a chemical shift approx. 5 ppm smaller than before coordination. With regard to alkylidyne complex **1**, not only did the chemical shifts change (see Table 2, p 73, and Table 3, p 76), but the ^1H and ^{13}C methyl resonances of the fluorinated alkoxide ligands are notably broadened. As discussed for complex **22**, the absence of diastereotopic signals for the alkoxide ligands (also in the $^{19}F\{^1H\}$ NMR spectrum) implies the chemical equivalence of these ligands and is indicative of a trigonal-bipyramidal coordination geometry. However, the peak broadening suggests this could be the result of a dynamic process in solution, presumably a geometric isomer interconversion through the Berry pseudorotation mechanism.

Single crystals were obtained from the NMR solution and they were analysed by X-ray diffraction. Compound **24** crystallises in the monoclinic space group $P2_1/n$ as a C_6D_6 solvate, and its molecular structure is shown in Figure 37. The molybdenum atom is pentacoordinated and resides in a distorted square-pyramidal geometry (τ_5 = 0.4292(17)), with the alkylidyne moiety in the apical position. The O1–Mo–O3 angle of 144.51(5)° is particularly small compared to an idealised basal angle of 180°; as a consequence, the plane through atoms O1, O2, and O3 forms an angle of 4.83(4)° with the Mo–N bond. The Mo–C triple bond (1.7423(17) Å) is virtually identical to that of 12 VE complex **1** (1.7438(16) Å).[157] The Mo–O bond lengths (1.9363(11)–1.9517(11) Å) are slightly elongated, but still in the expected range, and the Mo–N bond distance of 2.2066(14) Å

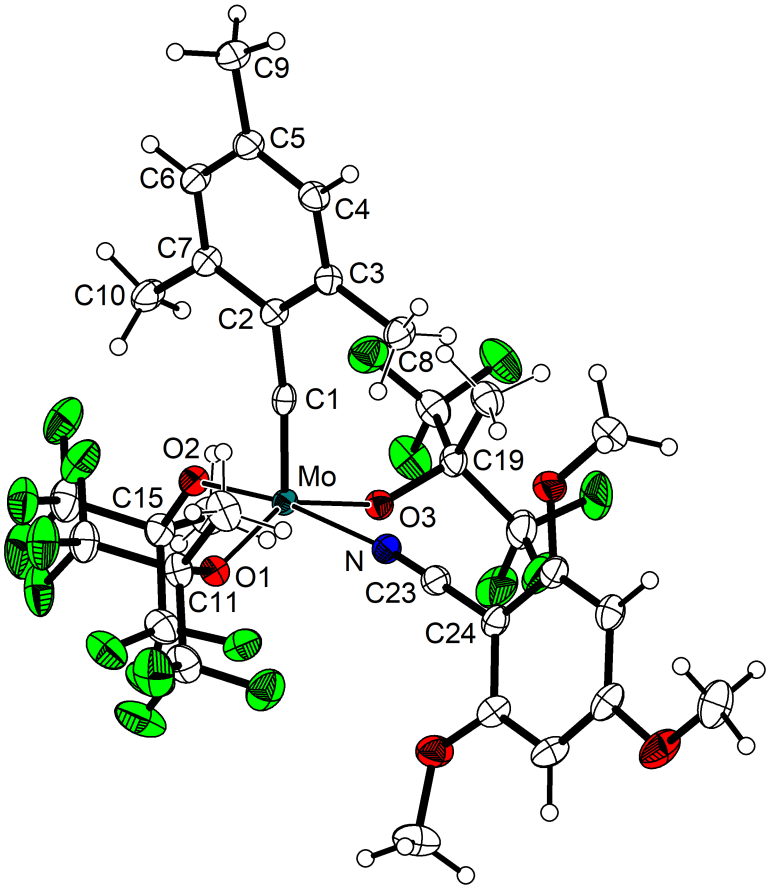

Figure 37. Molecular structure of **24**·C_6D_6 with thermal displacement parameters drawn at the 50% probability level. Solvent molecules were removed using the program *Squeeze*. Selected bond lengths (Å) and angles (deg): Mo–C1 1.7423(17), Mo–N 2.2066(14), Mo–O1 1.9363(11), Mo–O2 1.9459(11), Mo–O3 1.9517(11), N–C23 1.143(2), C1–C2 1.448(2); C1–Mo–N 93.81(6), C1–Mo–O1 105.27(6), C1–Mo–O2 95.89(6), C1–Mo–O3 106.58(6), N–Mo–O1 81.15(5), N–Mo–O2 170.26(5), N–Mo–O3 81.54(5), O1–Mo–O2 95.43(5), O1–Mo–O3 144.51(5), O2–Mo–O3 96.47(5), Mo–C1–C2 173.84(13), Mo–N–C23 173.61(14), N–C23–C24 178.79(18).

is slightly shorter than in acetonitrile complex **22**, but also larger than the calculated distance for a typical Mo–N single bond (2.09 Å),[180] which indicates, again, a weak coordination of the nitrile. The absence of intermolecular contacts between the methoxy groups and the molybdenum centre of neighbouring molecules differs from the situation described for **2** and **5**. This is not surprising, however, because coordination of the ether in the latter complexes results in pentacoordinate 13 VE complexes, whereas **24** *is* already a pentacoordinate 13 VE complex.

Acetone

The tolerance of complex **1** towards ester-functionalised alkynes has been previously established.[157] It is therefore predictable that also ketones do not interfere the catalytic activity of **1**. Acetone complex [**1**(O=CMe_2)] (**25**), if active in alkyne metathesis, should provide some evidence that ketones are compatible functional groups. The reaction of **1** with acetone in *n*-pentane (Scheme 41) resulted in a red solution, from

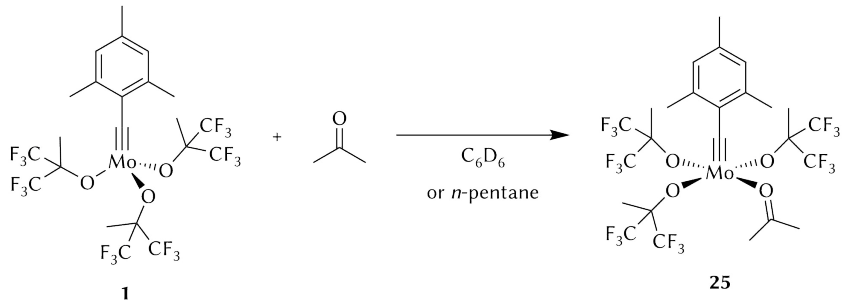

1 25

Scheme 41. Reaction of alkylidyne complex **1** with acetone affords complex **25**.

which red–yellow dichroic crystals of **25** precipitated at –35 °C. Drying of the crystals in high vacuum produced a perceptible loss of crystallinity, and the release of acetone was confirmed by elemental analysis. This behaviour is analogous to that described for **22** and suggests a labile coordination of the acetone. Hence, residual solvent from the reaction was allowed to evaporate at normal conditions, which gave satisfactory values for the elemental composition. The proton and fluorine NMR resonances of complex **25** are clearly shifted downfield compared to the resonances in **1** (see Table 2, p 73). The differences in the carbon NMR spectrum are less obvious (Table 3, p 76), but the signal for the alkylidyne carbon atom at δ_C = 314.2 ppm is significantly shifted towards the high field (δ_C = 317.9 ppm in **1**). The chemical shifts for the methyl groups of the acetone moiety are very close to those of the uncoordinated solvent molecule; however, the signal for the carbonyl carbon atom is substantially shifted from δ_C = 204.4 ppm[202] to δ_C = 218.4 ppm. Similar to nitrile complexes **22** and **24**, the observed chemical equivalence of the alkoxide ligands in all NMR spectra suggests either a trigonal-bipyramidal structure or that a fluxional process is operative in solution.

The solid-state structure of **25** was additionally determined by X-ray diffraction analysis and is presented in Figure 38. Similar to the structures of nitrile adducts **22** and **24**, the complex crystallises in the monoclinic space group $P2_1/n$ and displays a highly distorted square-pyramidal geometry (τ_5 = 0.453(2)) around the pentacoordinated molybdenum centre with the Mo atom lying 0.3398(2) Å out of the basal plane O1, O2, O3, O4 (r.m.s. deviation 0.1810(15) Å). In particular, the O1–Mo–O3 angle of 143.92(6)° is remarkably small compared to an idealised basal angle of 180°. The Mo–C1 triple bond (1.739(2) Å) and the Mo–$O_{alkoxide}$ bond lengths (1.9487(15)–1.9496(15) Å) are all in the expected range, whereas the Mo–O4 bond distance of 2.2166(15) Å is larger than the calculated distance for a typical Mo–O single bond (2.01 Å),[180] which suggests a weak coordination of the acetone molecule.

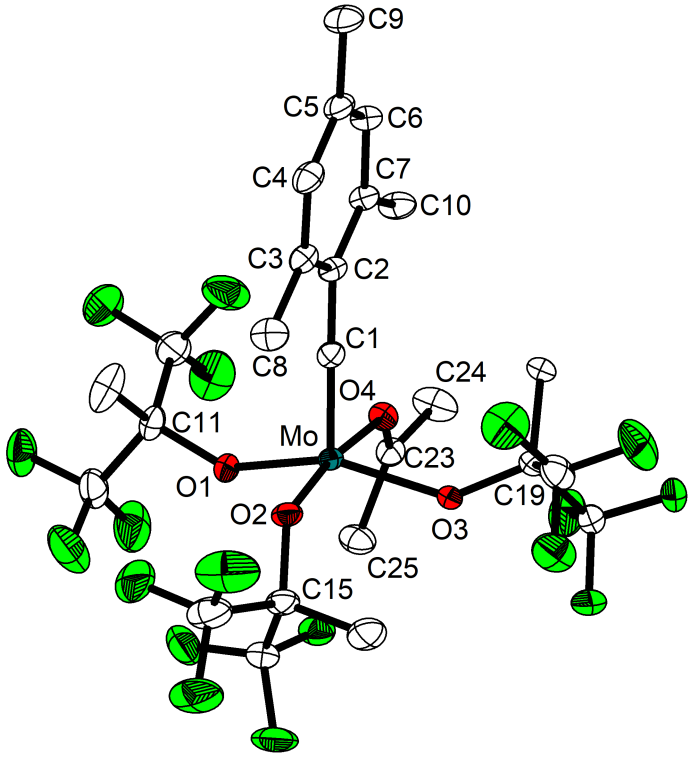

Figure 38. Molecular structure of **25** with thermal displacement parameters drawn at the 50% probability level. Hydrogen atoms are omitted for clarity. For selected bond lengths and angles, see Figure 81, p 173.

Pyridine

As mentioned above, alkylidyne complexes bearing a pyridine ligand have been reported to exhibit limited air-stability.[49] Therefore, molybdenum complex **1** was treated with pyridine (py) to afford the corresponding adduct [**1**(py)] (**26**) in moderate yields after purification (Scheme 42).

For an uncertain reason, the reaction does not proceed cleanly and bis(mesityl)acetylene (**27**) and other unidentified impurities were observed by NMR spectroscopy analysis of the crude product. The NMR resonances of **26** differ from those of the starting materials and are summarised in Table 2 (δ_H) and Table 3 (δ_C, p 76). In particular, the signal for the alkylidyne carbon atom at δ_C = 312.0 ppm is significantly shifted to the

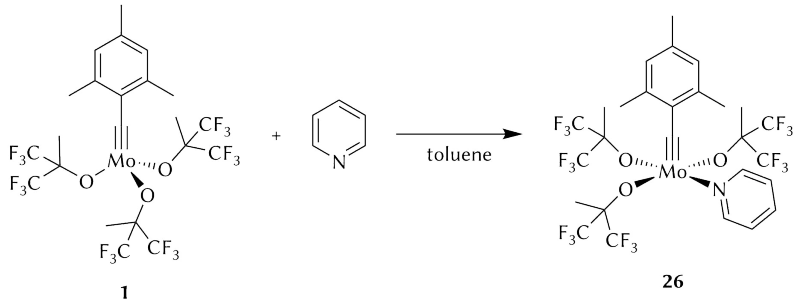

Scheme 42. Reaction of alkylidyne complex **1** with pyridine affords complex **26**.

Table 2. Selected ^{1}H NMR chemical shifts (ppm) of adducts [**1**(L)] compared to parent complex **1**; solvent: benzene-d_6.

Compound	$O(CF_3)_2CH_3$	*para*-CH_3	*ortho*-CH_3	*meta*-H
1	1.57	1.99	2.52	6.48
22	1.71	2.03	2.59	6.54
24	1.95 (br) 1.95 (br)[a]	2.07 2.05[a]	2.78 2.73[a]	6.61 6.57[a]
25	1.70	2.03	2.63	6.55
26	1.70	2,04	2.70	6.56
28	1.49, 2.17	2.12	2.96	6.71
29	1.64 (br), 1.67 (br)	1,96	2,57	6.51
30	1.68, 1.85	2.07	2.79	6.62

[a] Solvent: toluene-d_8.

high field compared to parent compound **1** (δ_C = 317.9 ppm). Crystallisation attempts to structurally characterise complex **26** were unsuccessful; however, colourless crystals were obtained and identified as **27** by X-ray diffraction analysis (cf. Figure 57, p 110), confirming the formation of this side-product.

2,2′-Bipyridine

The use of chelating ligands such as 1,10-phenanthroline (phen) or 2,2′-bipyridine (bipy) is a convenient strategy, as mentioned in the Introduction (p 22), to protect alkylidyne complexes against air and moisture.[24,49] For example, exceptional bench-stability has been reported for complexes such as [**T**(phen)] or [Mo(≡CPh)(OSiPh$_3$)$_3$(bipy)]. Although saturation of the available binding sites suppresses the catalytic activity of these complexes, the coordination of the ligands is reversible upon addition of an electrophilic metal salt.

To prove that **1** can also be stabilised by a chelating ligand, the alkylidyne complex was reacted with bipy in toluene, which yielded the expected product [**1**(bipy)] (**28**, Scheme 43). The NMR spectra in benzene-d_6 showed quantitative formation of **28**, which must have a meridional (*mer*) conformation in solution because all atoms forming the bipy fragment are chemically inequivalent (eight ^{1}H and ten ^{13}C resonances are observable). This is further confirmed by the splitting of the fluorine atoms in three signals of the same integrated area (δ_F = –75.8 ppm, δ_F = –76.3 ppm, δ_F = –76.9 ppm), where the last two resonances emerge as two coupled quartets, which is

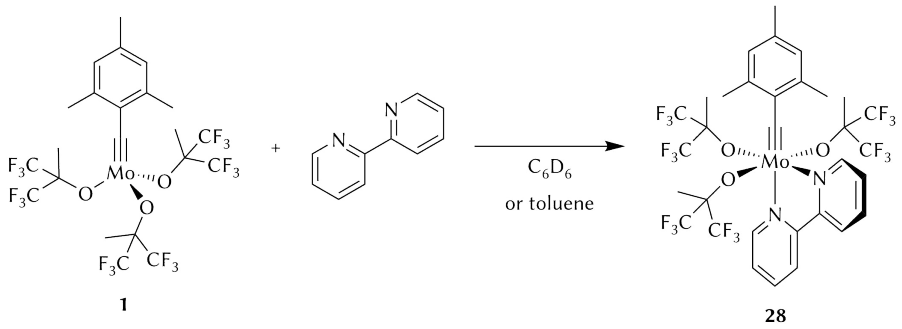

Scheme 43. Reaction of alkylidyne complex **1** with bipy afforded chelated complex **28**.

consistent with a diastereotopic environment in the two alkoxide ligands coordinated *cis* to the bipy ligand.

Compared to parent compound **1** and to the other adducts, the ^{1}H NMR spectrum of **28** revealed that all signals in common are considerably shifted downfield (see Table 2, p 73). The only exception are the methylic protons in the alkoxide ligands coordinated *cis* to the bipy moiety, which are more shielded (δ_H = 1.49 ppm) than in any other complex of this series. The ^{13}C{^{1}H} NMR spectrum presents very few peculiarities in comparison with the other complexes listed in Table 3 (p 76). The most characteristic signal accounts for the alkylidyne carbon atom (δ_C = 306.4 ppm), which is less deshielded than in other complexes. Also the resonance for the alkoxide groups oriented *cis* towards the bipy ligand (δ_C = 17.5 ppm) has a lower chemical shift than those of other complexes and that of the alkoxide group at the *trans* position (δ_C = 18.9 ppm).

The structure was additionally confirmed by X-ray diffraction analysis of purple single-crystals obtained by diffusion of cyclohexane into a benzene solution of **28** (Figure 39). The complex crystallises in the monoclinic, enantiomorphic space group $P2_1$ and adopts a distorted octahedral geometry with a *mer* orientation of the alkoxide ligands, in agreement with the NMR data in solution. The angles around the molybdenum atom range from 158.54(6)° to 164.86(8)° (*trans*), and from 71.20(7)° to 107.60(8)° (*cis*), being the most acute angle (N1–Mo–N2) due to chelation of the bipy molecule. The l.s. plane through the bipy fragment (N1, N2, C23–C32, r.m.s. deviation 0.109(2) Å) forms an angle of 56.60(5)° with the l.s. plane through the aryl ring (C2–C7, r.m.s. deviation 0.0319(17) Å), and is closely parallel to the alkylidyne bond (Mo–C1, deviation 6.92(8)°). Interestingly, the Mo–C1 bond length of 1.781(2) Å is slightly larger than in the other complexes of this series, and the Mo–C1–C2 angle of 166.94(17)° deviates substantially from linearity. Also the Mo–N2 bond, located *trans* to the alkylidyne

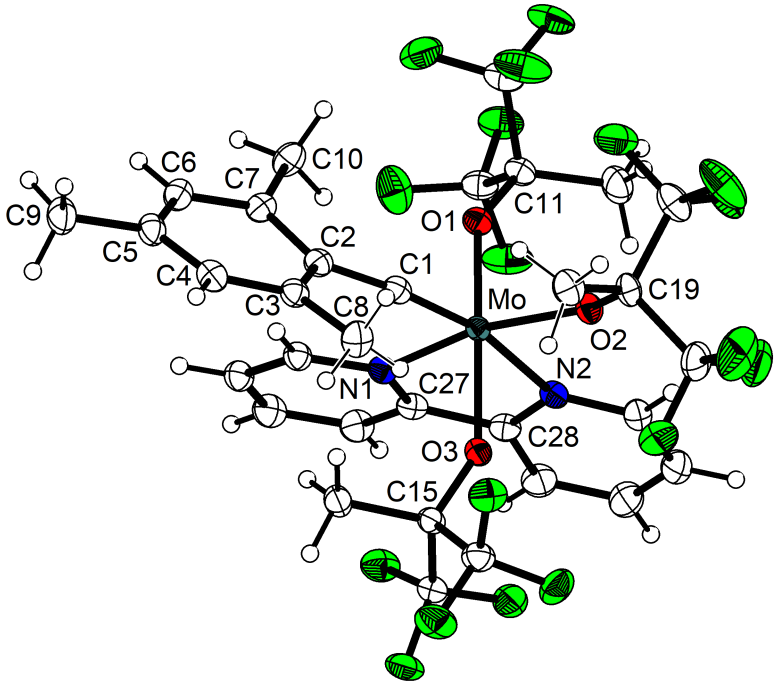

Figure 39. Molecular structure of **28** with thermal displacement parameters drawn at the 50% probability level. Selected bond lengths (Å) and angles (deg): Mo–C1 1.781(2), Mo–N1 2.2656(17), Mo–N2 2.3889(19), Mo–O1 1.9961(17), Mo–O2 1.9488(14), Mo–O3 1.9657(16), N1–C27 1.360(3), N2–C28 1.344(3), C1–C2 1.454(3), C27–C28 1.484(3); C1–Mo–N1 93.85(8), C1–Mo–N2 164.86(8), C1–Mo–O1 93.34(9), C1–Mo–O2 107.60(8), C1–Mo–O3 101.51(9), N1–Mo–N2 71.20(7), N1–Mo–O1 81.65(7), N1–Mo–O2 158.54(6), N1–Mo–O3 82.50(7), N2–Mo–O1 86.98(7), N2–Mo–O2 87.40(6), N2–Mo–O3 74.79(7), O1–Mo–O2 95.95(8), O1–Mo–O3 158.93(7), O2–Mo–O3 93.72(8), Mo–C1–C2 166.94(17), Mo–N1–C27 118.83(15), Mo–N2–C28 115.51(15), N1–C27–C28 117.1(2), N2–C28–C27 116.3(2).

moiety, has a larger bond length (2.3889(19) Å) than what would be expected for a Mo–N single bond.[189]

As presumed, coordination of the bipy ligand increased the stability of complex **1**. Thus, no immediate degradation of the crystals was observed under non-inert conditions, and the elemental composition (C, H, and N) remained stable after exposing the compound to air for 30 min, as determined by combustion microanalysis.

Finally, the catalytic activity of complex **28** will be discussed in Section 3.4. Whether an additional reagent (e.g. a metal salt) is required to generate the active species (cf. Scheme 18, p 23), or the complex by itself is able to promote alkyne metathesis is also an important question that shall be addressed in Section 3.4.

Trimethylphosphane

Phosphane molecules, which possess an electron lone pair, are notable Lewis bases; hence, they are good σ-donor ligands and form dative bonds with metal centres. However, because of the P–R antibonding character of the lowest unoccupied molecular

orbital (LUMO), the σ* orbitals allow for M–P backbonding through dπ → σ* interactions. Therefore, the electron-donating nature of phosphanes is less pronounced than in the lighter homologues, the amine ligands, which are mere σ-donor ligands. Despite this, alkyl phosphanes such as trimethylphosphane (PMe_3) are particularly strong σ-donors and their basicity can be compared to that of some amines. It is therefore expected that coordination of an electron-rich phosphane ligand to the alkylidyne complex produces a positive effect on the overall stability of the complex. Furthermore, phosphanes are typical ligands in markedly robust, olefin metathesis catalysts (cf. **B**, **C**, Section 1.2.1). In these complexes, the phosphane ligand is able to dissociate during metathesis and thus generates a free coordination site for the substrate to bind. This behaviour can also be anticipated for alkylidyne complexes; in such case, the complex might well promote alkyne metathesis, although a decrease in the activity, especially during the initial stage, may be observed. In addition to that, ^{31}P NMR spectroscopy is a standard and fast characterisation technique; therefore, the presence of a phosphorous-containing ligand is useful for mechanistic or structural studies by NMR analyses.

Table 3. Selected $^{13}C\{^1H\}$ NMR chemical shifts (ppm) of adducts [**1**(L)] compared to parent complex **1**; solvent: benzene-d_6.

Compound	*1*[a]	*2*[a]	*3*[a]	*4, 5*	*6*	*7, 8*	*9*	*10*
1	18.4	83.9	123.5	20.3, 21.0	128.5	141.6, 141.2	143.3	317.9
22	18.56	83.77	124.70	19.71, 21.04	128.30	142.31, 140.26	141.48	315.14
24	18.8 (br) 18.8 (br)[b]	83.81 83.82[b]	124.98 124.96[b]	19.98, 21.08 19.98, 21.03[b]	128.35 128.24[b]	142.55, 139.62 142.51, 139.67[b]	141.45 141.46[b]	314.22 314.29[b]
25	18.6	83.6	124.7	19.6, 21.0	128.3	142.7, 140.1	141.8	313.8
26	18.6	84,1	124.7	20.7, 21.0	128.6	143.2, 140.6	141.6	312.0
28	17.5, 18.9	82.6–85.4	124.5, 125.1	21.0, 20.9	128.6	143.3, 139.1	140.3	306.4
29	16.8, 20.7	83.0, 84.1	124.7, 124.8, 125.1	19.1, 21.2	128,6	145.1, 142.0	140,6	323.3
30	18.4, 18.9	83.4	124.4, 124.7, 125.2	21.3, 20.9	128.6	140.6, 138.9	141.8	305.5

[a] Multiple values indicate chemically inequivalent positions; [b] Solvent: toluene-d_8.

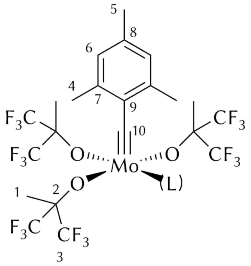

Reaction of PMe_3 with **1** in deuterobenzene resulted in a red solution, in which adduct [**1**(PMe_3)] (**29**, Scheme 44) formed quantitatively. The NMR resonances for the PMe_3 ligand in all three spectra (δ_H = 1.12 ppm, δ_C = 14.4 ppm, δ_P = –0.8 ppm) are clearly shifted compared to the free molecule (δ_H = 0.80 ppm, δ_C = 16.4 ppm, δ_P = –62 ppm), indicating coordination to the metal centre. An increase in the value of the coupling constants is also observed (PMe_3: $^2J_{HP}$ = 2.5 Hz, $^1J_{CP}$ = 13 Hz; **29**: $^2J_{HP}$ = 9.1 Hz, $^1J_{CP}$ = 23 Hz). In addition, the ^{31}P resonance is resolved as a septet and displays a coupling of about 5 Hz with six fluorine atoms of the alkoxide ligands coordinated *cis* to the phosphane. As shown by the signal splitting in the ^1H, $^{13}C\{^1H\}$, and $^{19}F\{^1H\}$ NMR spectra, the alkoxide ligands are diastereotopic in solution, which suggests a square-pyramidal arrangement not (significantly) affected by a fluxional process. While the chemical shifts of the alkoxide ligands in the $^{13}C\{^1H\}$ NMR spectrum are very similar to those of the phosphane-free complex **1** (see Table 3, p 76), the proton signals (at δ_H = 1.64 ppm and δ_H = 1,67 ppm, see Table 2, p 73) and two of the resonances in the $^{19}F\{^1H\}$ NMR spectrum (at δ_F = –75.5 ppm and δ_F = –76.6 ppm; the third resonance is found at δ_F = –78.1 ppm) are appreciably shifted to the low field in comparison with the δ values in **1** (δ_H = 1.57 ppm, δ_F = –78.2 ppm). A considerable downfield shift from δ_C = 317.9 ppm (**1**) to δ_C = 323.3 ppm (**29**) is also observed for the alkylidyne carbon atom. In addition, this atom and all aromatic carbon atoms arise as doublets because of the coupling with the phosphorous atom.

Isolation of the product and recrystallisation in *n*-pentane at –35 °C afforded single crystals, which were analysed by X-ray diffraction. Compound **29** crystallises in the orthorhombic group *P ccn*, and its molecular structure is depicted in Figure 40. The pentacoordinated molybdenum centre exhibits approximate square-pyramidal geo-

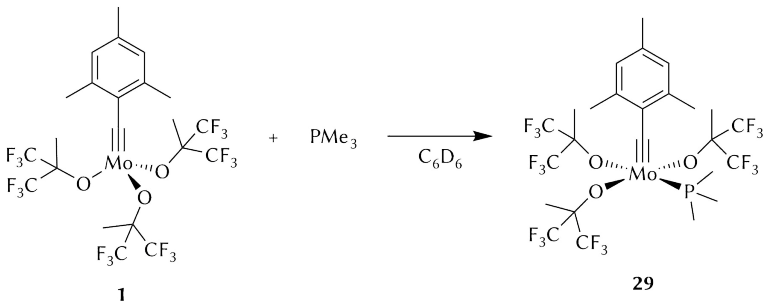

Scheme 44. Trimethylphosphane complex **29** is generated upon reaction of alkylidyne complex **1** with PMe_3.

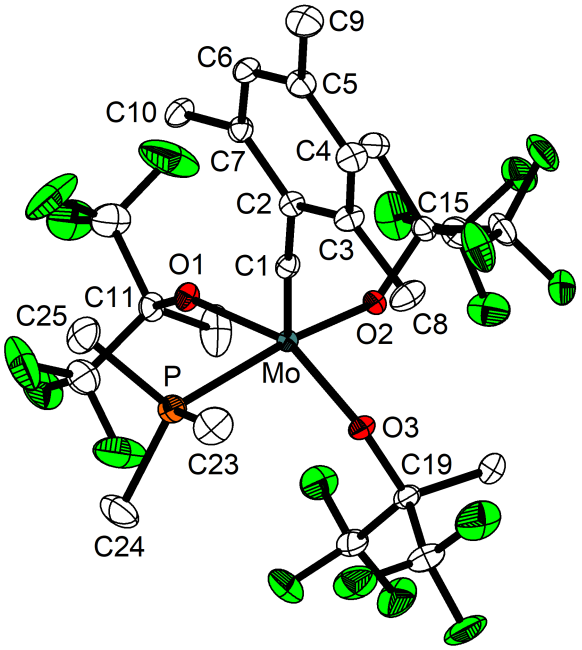

Figure 40. Molecular structure of **29** with thermal displacement parameters drawn at the 50% probability level. Hydrogen atoms are omitted for clarity. Selected bond lengths (Å) and angles (deg): Mo–C1 1.740(2), Mo–O1 1.9742(14), Mo–O2 1.9665(14), Mo–O3 1.9806(14), Mo–P 2.5828(6), C1–C2 1.442(3); C1–Mo–P 80.51(7), C1–Mo–O1 98.12(8), C1–Mo–O2 106.32(8), C1–Mo–O3 97.29(8), P–Mo–O1 83.74(4), P–Mo–O2 173.04(4), P–Mo–O3 82.29(4), O1–Mo–O2 96.40(6), O1–Mo–O3 157.16(6), O2–Mo–O3 95.32(6), Mo–P–C23 111.29(9), Mo–P–C24 124.16(9), Mo–P–C25 111.12(8), C23–P–C24 101.51(13), C23–P–C25 102.64(12), C24–P–C25 103.73(13), Mo–C1–C2 177.22(17).

metry (τ_5 = 0.2647(17)) – which is consistent with the NMR data in solution – with the alkylidyne ligand at the apical position. The molybdenum atom is situated 0.2124(2) Å above the basal plane (l.s. plane through O1, O2, O3, P, r.m.s. deviation 0.1021(12) Å) with O1–Mo–O3 and P–Mo–O2 angles of 157.16(6)° and 173.04(4)°, respectively. The phosphorous atom resides in a distorted tetrahedral environment (τ_4 = 0.8833(12)), with a particular obtuse angle Mo–P–C24 of 124.16(9)°. The molybdenum–phosphorous bond is significantly longer (2.5828(6) Å) than the calculated covalent Mo–P single bond (2.49 Å).[180] This suggests a weakened bond, and hence, the potential reversibility of the phosphane coordination. There is no appreciable difference between the alkylidyne bond length in **29** (Mo–C1, 1.740(2) Å) compared to the phosphane-free complex **1** (Mo–C1, 1.7438(16) Å), whereas the Mo–O distances are slightly elongated (**29**, 1.9665(14) Å–1.9806(14) Å; **1**, 1.8946(11) Å–1.9243(11) Å) but still in the acceptable range of a Mo–O single bond.

Unfortunately, upon exposure to air, slow decomposition of the crystalline material was observed. It can therefore be concluded that the trimethylphosphane ligand does not supply the desired stability to the complex. Nevertheless, it is still interesting to study how the coordination of a phosphane ligand influences the catalytic activity of

the alkylidyne complex in alkyne metathesis (see Section 3.4). Because it is assumed that the phosphane ligand must depart for the alkyne substrate to bind, NMR spectroscopy can be used to investigate if the ligand is prone to dissociate. An exchange spectroscopy (EXSY) experiment conducted on a sample of **29** that contained an excess of PMe_3 showed indeed exchange cross-peaks between the free and the coordinated phosphane (Figure 41), suggesting that the ligand is labile in solution.

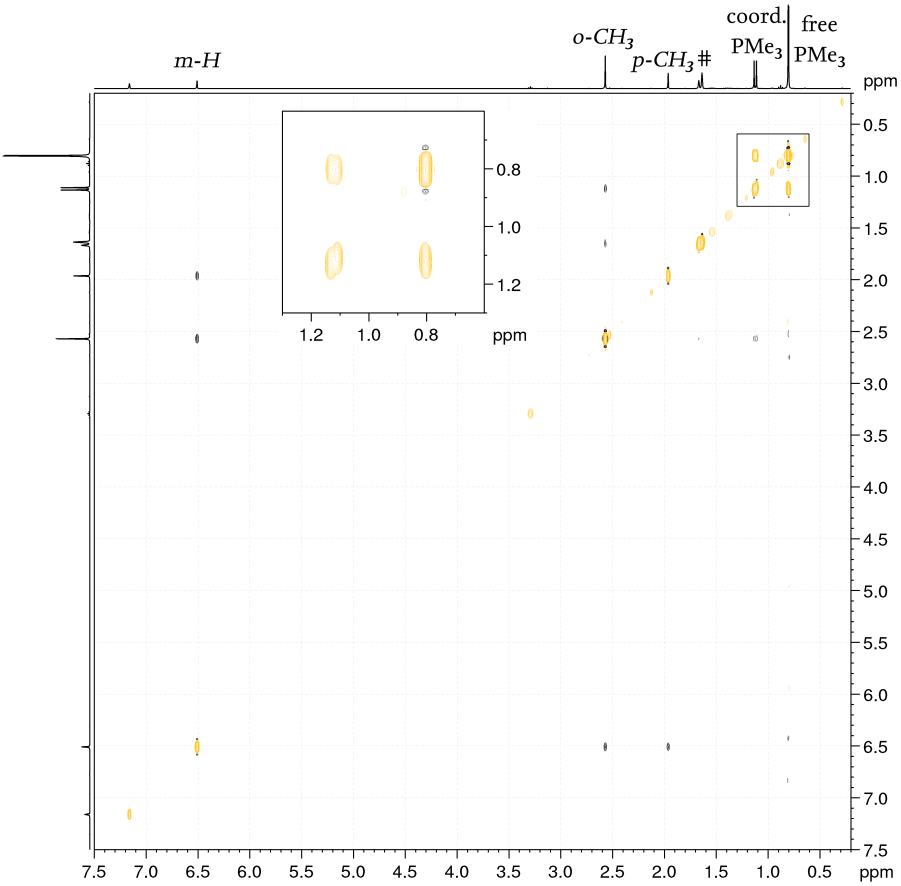

Figure 41. NOESY (nuclear Overhauser effect spectroscopy) spectrum of a mixture of **29** and PMe_3 showing exchange cross-peaks (in yellow) between the signals for the free and the coordinated (coord.) phosphane; # = CH_3 of the alkoxide groups. Inset: Expanded region of the spectrum around the exchange cross-peaks.

1,3,4,5-Tetramethylimidazolin-2-ylidene

N-heterocyclic carbenes (NHC) constitute another ligand class in organometallic chemistry that has been extensively used in olefin metathesis catalysts.[204] Like phosphanes, NHC ligands are strong σ-donor ligands with a relatively weak π-acceptor character, caused by the electron-donating nature of the nitrogen substituents and the heterocyclic π-system. In fact, NHCs are commonly more nucleophilic than alkyl phosphanes and form stronger dative bonds with the metal centre while remaining usually innocent. Moreover, modification of the substituents or alteration of the degree of saturation of the cyclic carbene enables the adjustment of the steric and elec-

tronic properties of the NHC ligands.[11] Hence, coordination of a carbene ligand may help to stabilise the complex, although that can be at the expense of the activity in alkyne metathesis.

It has to be mentioned that a few examples of molybdenum alkylidyne complexes bearing NHC ligands such as 1,3-diisopropylimidazolin-2-ylidene (free[171] and immobilised on silica)[205] or 1,3-dimethyl-4,5-R_2-imidazolin-2-ylidene (R = H, Cl, CN)[171] have been prepared, respectively, upon reaction of the carbenes with [Mo(≡C(4-MeO-C_6H_4))(dme)(OC(CF_3)$_2$Me)$_3$], [**2**(dme)], or by transmetalation of the corresponding NHC silver complexes (Scheme 45). The resulting NHC alkylidyne complexes satisfactorily promote alkyne metathesis reactions with good to excellent conversions using a catalyst loading of 1 mol% or even 0.1 mol%. Three different complexes have been proposed as potential active species: i) the tetracoordinate Schrock-type alkylidyne complexes after dissociation of the NHC ligands, ii) a cationic species formed by alkoxide dissociation, or iii) the neutral, pentacoordinated NHC complexes themselves.[171] Although a minimal degree of carbene or alkoxide dissociation was detected by NMR spectroscopy for some of the compounds after addition of the substrate or in the presence of a proton source, no strong evidence could be provided on the nature of the active species, which remains speculative. Besides this, no air-stability has been reported for these NHC alkylidyne complexes.

In spite of these results, and considering that mesityl-substituted alkylidyne complexes are more robust than other benzylidyne complexes,[140] the preparation of an NHC adduct of molybdenum alkylidyne **1** was attempted. Treatment of complex **1** with the small-sized 1,3,4,5-tetramethylimidazoline carbene (Im^{Me_4}) in toluene at ambient temperature furnished the desired complex [**1**(Im^{Me_4})] (**30**) in excellent yields (Scheme 46).

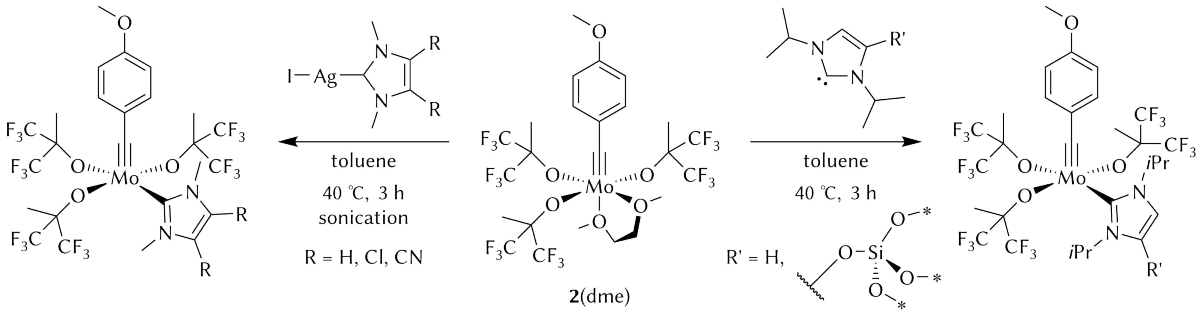

Scheme 45. Synthesis of molybdenum NHC alkylidyne complexes; Si(O–*) = at 650 °C partially dehydroxylated silica 60.

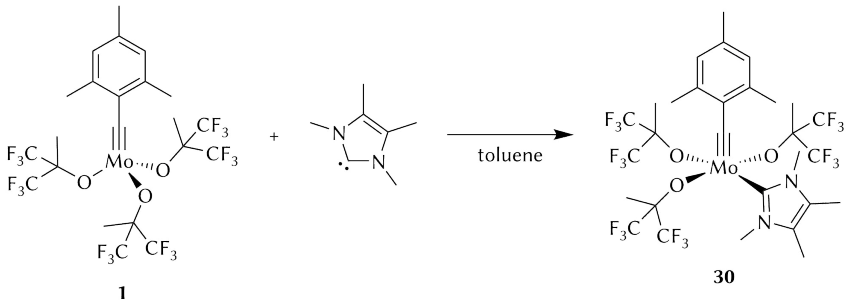

Scheme 46. Synthesis of molybdenum NHC alkylidyne complex **30**.

The coordination of the carbene ligand is evidenced by NMR spectroscopy (see Figure 42). In the ^{1}H NMR spectrum, the methyl groups at the backbond (4- and 5-positions) are shifted to the high field (δ_H = 1.31 ppm) compared with the free carbene (δ_H = 1.59 ppm).[206] The other methyl groups (attached to the nitrogen atoms), which resonate at δ_H = 3.35 ppm in the free carbene, appear as two extremely broad ($\nu_{1/2}$ = 72 Hz) signals at δ_H = 3.06 ppm and δ_H = 3.39 ppm. This phenomenon is indicative of a slow dynamic process in solution, and can be reasoned by a partially hindered rotation of the carbene ligand around the metal–carbon bond. Exchange peaks observed in a NOESY experiment supports this interpretation. The splitting into two resonances and line broadening are also observed in the ^{13}C{^{1}H} NMR spectrum. The methyl substituents at the nitrogen atoms are found at δ_C = 33.3 ppm and δ_C = 36.8 ppm ($\nu_{1/2}$ = 65 Hz), whereas a broad signal ($\nu_{1/2}$ ≈ 110 Hz) at δ_C = 8.1 ppm is assigned to the other methyl groups (for the free NHC, respectively, δ_C = 35.1 ppm and δ_C = 8.8 ppm). In addition, the imidazoline backbond carbon atoms arise also as two broad resonances ($\nu_{1/2}$ ≈ 50 Hz) at δ_C = 123.5 ppm and δ_C = 124.6 ppm; they are shifted downfield compared with the free carbene (δ_C = 122.6 ppm). Most notably, the signal of the carbene carbon atom (δ_C = 186.6 ppm) has a considerably reduced chemical shift in compar-

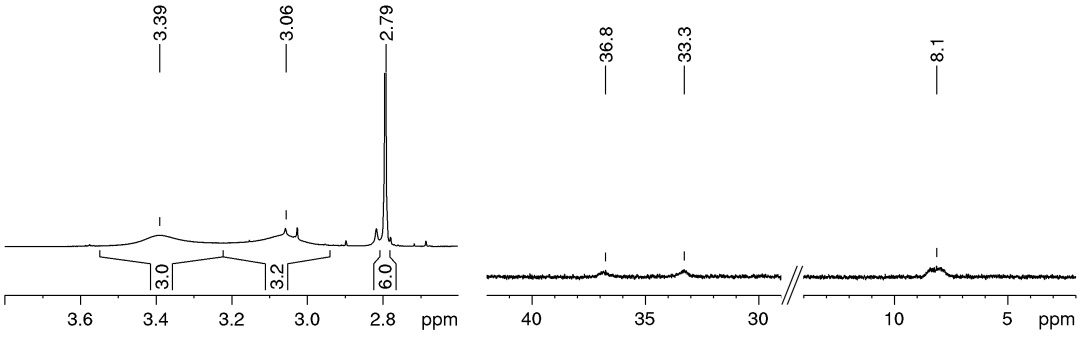

Figure 42. Expanded regions of the ^{1}H NMR (left) and ^{13}C{^{1}H} NMR (right) spectra of **30** showing the broadened signals assigned to the carbene ligand.

ison with the uncoordinated NHC ligand (δ_C = 212.7 ppm), confirming the bonding to the metal centre.

All signals in the ^{1}H NMR spectrum assigned to the mesityl ring (δ_H = 2.07, δ_H = 2.79 and δ_H = 6.62 ppm) or the diastereotopic alkoxide units (δ_H = 1.68 and δ_H = 1.85 ppm) are shifted downfield compared to the carben-free complex **1** (cf. Table 2, p 73). The non-equivalence of the methyl groups in the alkoxide ligands is also observed in the ^{19}F{^{1}H} and the ^{13}C{^{1}H} NMR spectra, and it is in agreement with a square-pyramidal geometry in solution. Comparison of the ^{13}C NMR data reveals no particular differences between the chemical shifts of **30** and the parent complex **1** (Table 3, p 76) except for the resonance of the alkylidyne carbon atom. In the former compound, this signal is found at δ_C = 305.5 ppm (about 12 ppm lower than in the tetrahedrally bonded complex **1**), and represents so far the most shielded alkylidyne carbon atom in the compound series of the type [**1**(L)], although it is in the same range of the shift observed for **28** (δ_C =306.4 ppm).

The square-pyramidal coordination geometry of **30** was verified in the solid-state structure established by X-ray diffraction (Figure 43), as concluded from the structural index parameter τ_5 = 0.2933(15).[188] Analogous to other complexes in this series, **30** crystallises in the monoclinic space group $P2_1/n$. The alkylidyne moiety resides in the apical position and the molybdenum atom is located 0.4712(1) Å above the basal plane (l.s. plane through atoms C23, O1, O2, O3; r.m.s. deviation 0.1302(11) Å). The NHC ligand is coordinated almost parallel to the Mo–C1 triple bond (deviation of 7.04(6)° with the l.s. plane through the imidazoline atoms N1, N2, C23, C24, C25; r.m.s. deviation 0.0013(12) Å), but forms an angle of 44.5(5)° with the mesityl ring, which can be ascribed to steric reasons. In accordance, the Mo–C23 bond is slightly elongated, and the Mo–C1–C2 angle of 167.65(11)° deviates strongly from linearity (otherwise expected for a triple bond) with the aryl unit tilted towards O1. The Mo–C1 bond distance (1.7465(14) Å) is essentially equal to that of parent compound **1** (1.7438(16) Å), whereas the Mo–O bond lengths (1.951(1) Å–1.9835(10) Å) are substantially larger than those in complex **1** (1.8946(11) Å–1.9243(11) Å).

Remarkably, degradation of the crystals was not appreciable upon exposure to air. Indeed, combustion analysis (C, H, and N) showed a stable elemental composition even after the compound had been stored for 24 h under non-inert conditions. This is

quite surprising because no stability improvement was reported for other NHC alkylidyne complexes,[171] but it can be ascribed to the presence of the mesityl fragment, which contributed in the past to stabilise some alkylidyne tungsten complexes.[140]

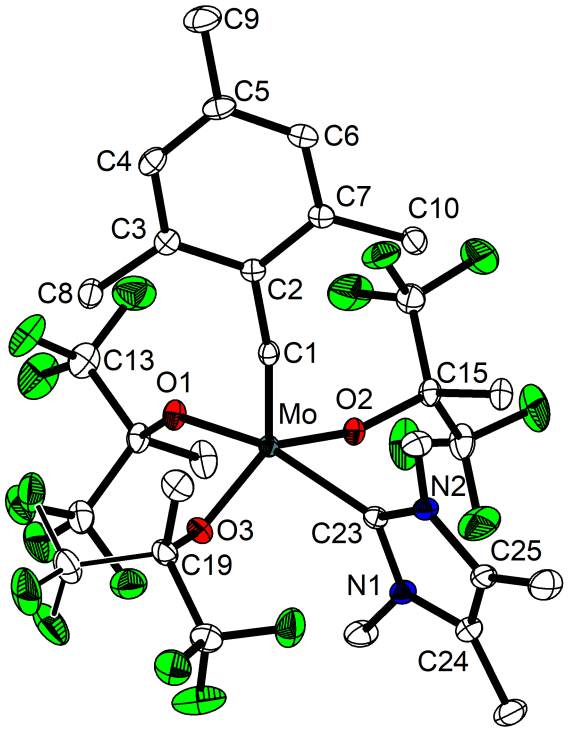

Figure 43. Molecular structure of **30** with thermal displacement parameters drawn at the 50% probability level. Hydrogen atoms are omitted for clarity. Selected bond lengths (Å) and angles (deg): Mo–C1 1.7465(14), Mo–C23 2.2186(14), Mo–O1 1.9835(10), Mo–O2 1.9658(10), Mo–O3 1.951(1), C1–C2 1.4567(19), N1–C23 1.3557(18), N2–C23 1.3518(18); C1–Mo–C23 99.84(6), C1–Mo–O1 98.38(5), C1–Mo–O2 108.14(5), C1–Mo–O3 106.28(5), C23–Mo–O1 161.76(5), C23–Mo–O2 82.61(5), C23–Mo–O3 82.01(5), O1–Mo–O2 90.84(4), O1–Mo–O3 93.81(4), O2–Mo–O3 144.16(4), Mo–C1–C2 167.65(11), Mo–C23–N1 118.56(10), Mo–C23–N2 137.23(10), N1–C23–N2 104.21(12).

3.3. Isolation of Intermediates and Related Species

An important aspect for understanding catalytic reactions is the identification of intermediates, latent species, and deactivation pathways. Although the general mechanism of the alkyne metathesis is well established (cf. Section 1.3.2. The catalytic cycle), and the structure of several metallacyclobutadiene complexes has been determined,[55] relatively fewer molybdenacyclobutadiene complexes have been described than their tungsten analogues. Indeed, crystallographically characterised molybdenacyclobutadiene complexes have not been reported until very recently.[55]

One reason for this divergence is the reduced electrophilicity of molybdenum compared to tungsten.[60,69,79,207] Even though highly Lewis acidic metal centres favour low barriers for MCBD formation, an excessively electrophilic metal environment overstabilises the reaction intermediates, which results in a diminished activity or even suppression of catalytic performance. Assuming that the rate-determining step involves release of the alkyne,[24,38] unstable, not detectable MCBD intermediates combined with an instant cycloreversion process are beneficial if not indispensable features of most efficient alkyne metathesis catalyst.[105]

It has been shown that the catalytic efficiency can be improved and adjusted by a careful selection of the supporting ligands,[106,109] for example through variation of the fluorine content.[62,63,79] Particularly for molybdenum, catalysts bearing hexafluoro-*tert*-butanolate substituents exhibit an activity peak, and perform better than their trifluoro-*tert*-butoxide counterparts, or even much better than related perfluorinated complexes. Hence, metallacycle intermediates derived from these highly active and reactive molybdenum alkylidyne complexes are extremely difficult to trap and study.

Complex **1** is a clear example of a highly active alkyne metathesis promoter, specially distinguished for its ability to perform TAM. It is therefore interesting to investigate the conditions to generate and isolate MCBD complexes and other mechanistically relevant species derived from **1**, such as deactivation products. In this chapter, stoichiometric reactions of **1** with diverse alkynes, including electron-rich acetylenes and 1-alkynes, will be explored. Even if it is not feasible to form or trap the desired species, potential cross-metathesis reactions are also highly attractive. For example,

scarcely known aminoalkylidyne or sulphanylalkylidyne complexes may be obtained upon reaction with diaminoacetylenes[208] or disulphanylacetylenes,[209] respectively.

In addition, the use of terminal alkynes in these experiments can serve to get a better understanding of the TAM reaction and confirm that at least one reason why **1** is able to metathesise these challenging substrates is the disfavoured formation of DPMCBD complexes under common catalytic conditions.

3.3.1. The elusive molybdenacyclobutadiene

Small alkynes and polymerisation

In an analogous fashion as reported for some isolated molybdena- and tungstenacyclobutadiene complexes,[38,39,55,79,141,198,201,207] alkylidyne complex **1** was reacted with an excess of 3-hexyne aiming at the preparation of MCBD complex [Mo(C_3Et_3)($OC(CF_3)_2Me)_3$] (**31**, Scheme 47). Unfortunately, only a yellow solution was obtained (MCBD complexes are typically red),[38,39,69,79,141,200,201] and a colourless polymeric material* (only sparingly soluble in THF, dimethyl sulphoxide or chloroform) precipitated from the mixture. Polymerisation of small alkynes is a known problem that has already been addressed in the Introduction (p 12),[79] and has been observed previously as an undesired alternative to MCBD formation.[69,210]

NMR analyses of the solution revealed the formation of propylidyne complex [Mo(≡CEt)($OC(CF_3)_2Me)_3$] (**19**) and bis(mesityl)acetylene (**27**) as cross-metathesis products of the reaction (Scheme 47). The latter shows three signals in the proton NMR spectrum at δ_H = 2.12 ppm, δ_H = 2.52 ppm, and δ_H = 6.77 ppm, whereas two methyl resonances (δ_C = 21.3 ppm and δ_C = 21.7 ppm), a CH resonance (δ_C = 128.2 ppm), and four quaternary carbon signals (δ_C = 96.0 ppm for the triple bond; δ_C = 121.5 ppm, δ_C = 137.5 ppm, and δ_C = 140.0 ppm for the aryl ring) can be assigned to **27** in the $^{13}C\{^1H\}$ NMR spectrum. Complex **19** is characterised by the alkylidyne carbon atom, which correlates to the downfield signal at δ_C = 313.1 ppm. In addition, the ethyl moiety shows two signals at δ_C = 12.2 ppm and δ_C = 44.9 ppm, and arises as a triplet (δ_H = 0.56 ppm) and a quartet (δ_H = 2.44 ppm) in the ^1H NMR spectrum. Resonances for the alkoxide ligands are found in all three spectra; the groups are chemically equivalent to

* Presumably poly(3-hexyne). However, cyclic oligomeric structures must also be considered. Indeed, as determined by gel permeation chromatography (GPC), the macromolecules were composed of about 10–15 monomeric units. In addition, metal contamination should also be assumed.

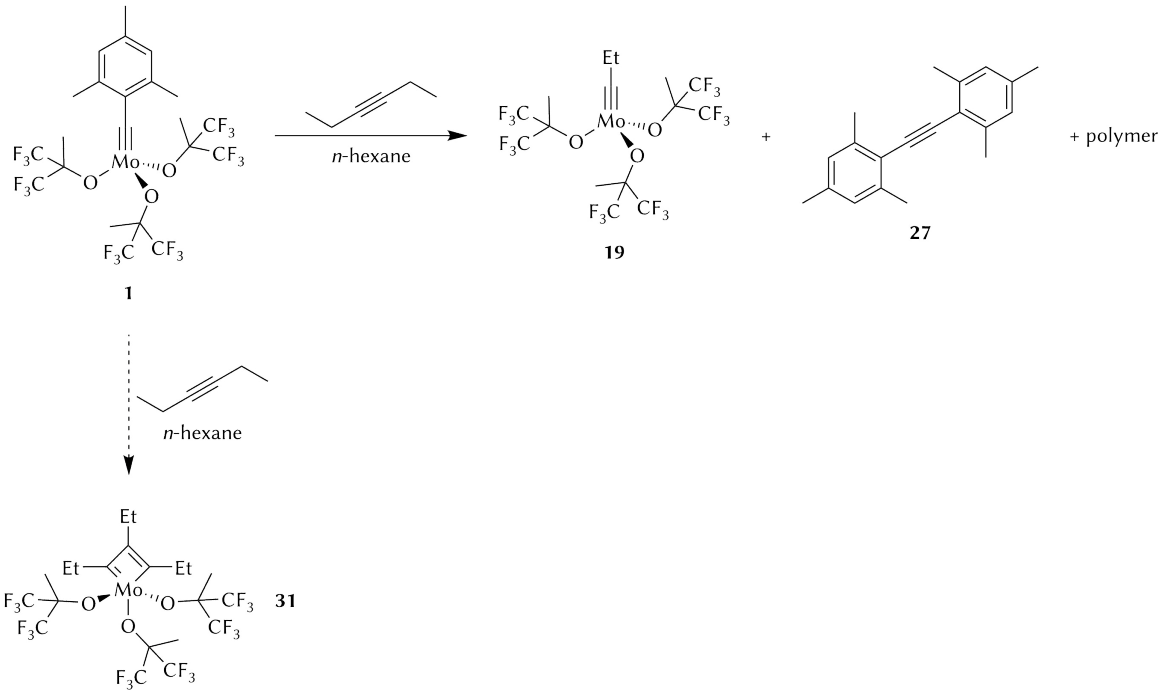

Scheme 47. Reaction of alkylidyne complex **1** with 3-hexyne.

one another and, for example, display only one signal at δ_F = –78.0 ppm in the $^{19}F\{^1H\}$ NMR spectrum. Difficulties in isolating MCBD intermediates and instead identification of new alkylidyne complexes with a replaced alkylidyne moiety have been reported before.[61,79,198] In contrast, latest results from our group show that isolation of MCBD complexes derived from **1** is indeed possible under certain conditions (low temperatures); the MCBD products are, however, highly thermosensitive.[211]

Reaction with tolan and ^{13}C-labelling

In order to avoid polymerisation, isolation of MCBD complexes was attempted with tolan, a larger and aromatic alkyne, which is not prone to undergo the ring-expansion mechanism. Furthermore, the aryl substituents can contribute to stabilise the MCBD system through a positive mesomeric (+M) effect.

In an NMR experiment, complex **1** was treated with diphenylacetylene in benzene-d_6. The NMR spectra, however, did not show any evidence for MCBD formation, but indicated instead the presence of both a C–C triple bond and a new alkylidyne species. 2D NMR spectroscopy revealed a mixture of (phenylethynyl)mesitylene[212] and benzylidyne complex [Mo(≡CPh)(OC(CF$_3$)$_2$Me)$_3$] (**32**), which are the products of the cross-metathesis reaction (Scheme 48). Compound **32** is C_{3v} symmetric in solution (on the NMR timescale), as deduced from the chemical equivalence of the alkoxide groups,

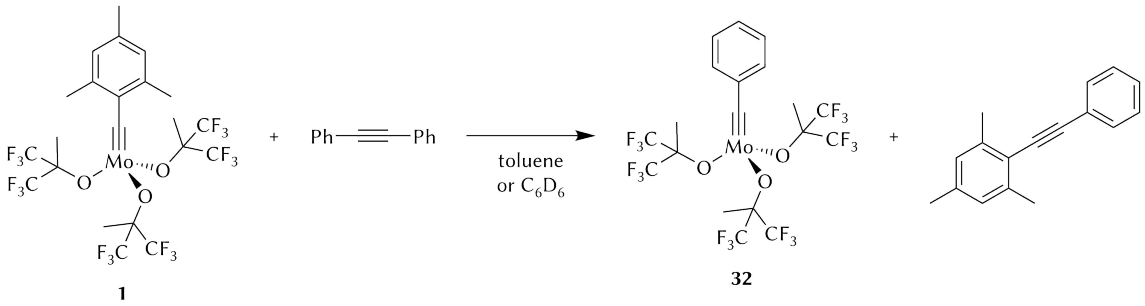

1 32

Scheme 48. Reaction of alkylidyne complex **1** with diphenylacetylene.

which display only one signal in both the ^{1}H (CH_3, δ_H = 1.58 ppm) and the $^{19}F\{^{1}H\}$ NMR spectra (CF_3, δ_F = –78.0 ppm). All other protons belong to the phenyl ring and appear as three multiplets in the aromatic region of the spectrum. In the carbon NMR spectrum four resonances account for the aryl carbon atoms, whereas a singlet, a septet and a quartet with typical chemical shifts are assigned to the fluorinated ligands. The most significant signal is highly deshielded (δ_C = 299.2 ppm) and proves the presence of the alkylidyne carbon atom.

Separation of the products was achieved via fractional crystallisation; after recrystallisation in *n*-pentane **32** was obtained as pale brown needles in 53% isolated yield. X-ray diffraction analysis of a single crystal confirmed the molecular structure of **32** in the solid state (Figure 44). The complex crystallises in the orthorhombic space group *P bca*, and exhibits pseudo-C_s symmetry and a slightly distorted tetrahedral geometry around the metal centre (τ_4 = 0.9403(10)).[178] The Mo–O (average 1.8855(17) Å) and Mo–C (1.743(2) Å) bond distances are very similar to those reported for complex **1**, and the Mo–C1–C2 angle of 177.63(18)° is, as expected, almost linear.

Despite the conjectured positive resonance effect, it is reasonable to assume that steric interactions caused by the three aryl moieties destabilise the formation of the MCBD system.[165] Moreover, the metathetical reaction proceeds quantitatively. Density functional theory (DFT) calculations confirm that the transformation is thermodynamically driven, and the formation of the cross-metathesis products is clearly exergonic ($\Delta G°$ = –17.5 kcal mol^{-1}). Even the combination of *two* equivalents of **1** with *one* equivalent of tolan is energetically favoured with $\Delta G°$ = –16.5 kcal mol^{-1}. Experimentally, this reaction stoichiometry indeed generates complex **32** and bis(mesityl)acetylene (**27**) in a 2:1 ratio (Scheme 49). These reactions are important be-

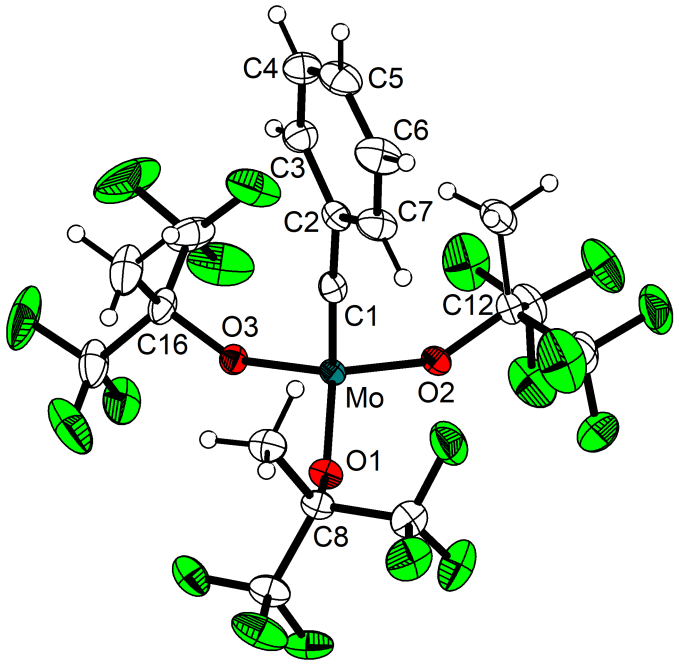

Figure 44. Molecular structure of **32** with thermal displacement parameters drawn at the 50% probability level. Selected bond lengths (Å) and angles (deg): Mo–C1 1.743(2), Mo–O1 1.8846(16), Mo– O2 1.8833(17), Mo–O3 1.8886(17), C1–C2 1.445(3); C1–Mo–O1 106.55(8), C1–Mo–O2 104.97(8), C1–Mo–O3 106.85(9), O1–Mo–O2 113.76(8), O1–Mo–O3 110.41(7), O2–Mo–O3 113.66(6), Mo–C1–C2 177.63(18).

cause benzylidyne complex **32** was previously obtained using various synthetic approaches only with a coordinated solvent, i.e. *mer*-[**32**(dme)],[79,110,133,138] but the DME-free analogue remained elusive. Given that 12 VE complexes without additionally bonded Lewis bases have a beneficial effect on the catalytic performance, it can be anticipated that complex **32** will be highly active in alkyne metathesis, at least as active as complex **1** (cf. Section 3.4.2).

Thermodynamically favoured stoichiometric metathesis reactions, in which the alkylidyne moiety of a complex is replaced by another carbyne group, are a well-known approach for the preparation of new alkylidyne complexes.[54,79,124,130] However, one has to cope with regioselectivity issues if the employed alkyne carries two distinct substituents.

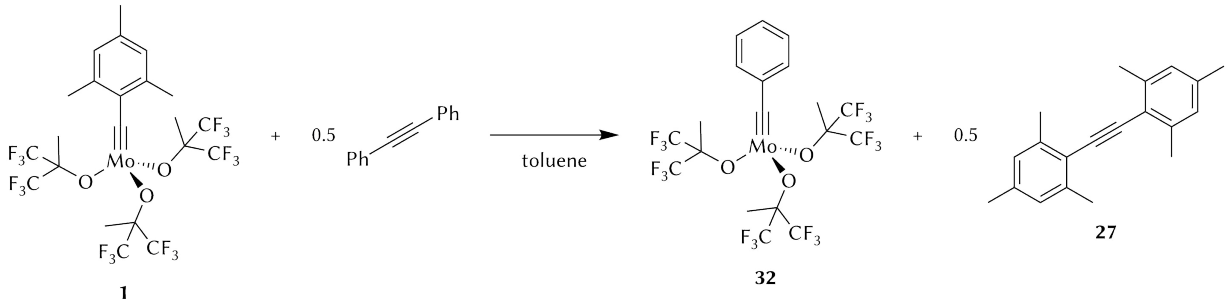

Scheme 49. Same reaction as above with a different stoichiometry (**1**:tolan, 2:1)

A direct application of this reaction involves the use of labelled acetylenes to furnish complexes with a ^{13}C-enriched alkylidyne position. These complexes facilitate solid-state NMR studies of the corresponding silica-supported derivatives. Surface organometallic chemistry (SOMC) is an ongoing research field in molecular catalysis.[213] In this context, grafted catalysts are interesting because compared to classical, ill-defined heterogeneous systems they have local and defined active sites, but in contrast to homogeneous catalysts, they are not dissolved and form a heterogeneous mixture. That enables a facile separation of the catalyst at the end of the process, and frees the product from undesired metal leaching.

There are several examples of alkyne metathesis catalysts immobilised on a silica surface.[205,213–216] In addition to avoiding metal contamination, thanks to surface anchoring, side-reactions such as alkyne polymerisation or bimolecular decomposition are minimised in these systems. In a recent study in cooperation with our group,[158] the highly active complex **1** was coordinated to partially dehydroxylated silica (**1**/$SiO_{2\,(700)}$, Scheme 50), and its activity in alkyne metathesis was compared to that of the homogeneous catalyst. Although the supported complex performed with an unusually high activity, the unprecedented TOFs and TONs reported for **1** were even superior, provided that the alkynes were carefully purified.[158] In order to prove the presence of the alkylidyne functionality after grafting, which was not observed in the NMR spectra because of the low sensitivity of ^{13}C magic angle spinning (MAS) NMR spectroscopy, ^{13}C-labelled complex [*alkylidyne*-^{13}C]**32** ([Mo(≡[^{13}C]Ph)(OC$(CF_3)_2$Me$)_3$], **32′**) was used as a substitute for **1** (Scheme 50). In fact, the alkylidyne resonance was visible in the ^{13}C MAS NMR spectrum after the complex was grafted on silica (**32′**/$SiO_{2\,(700)}$).[158] The syn-

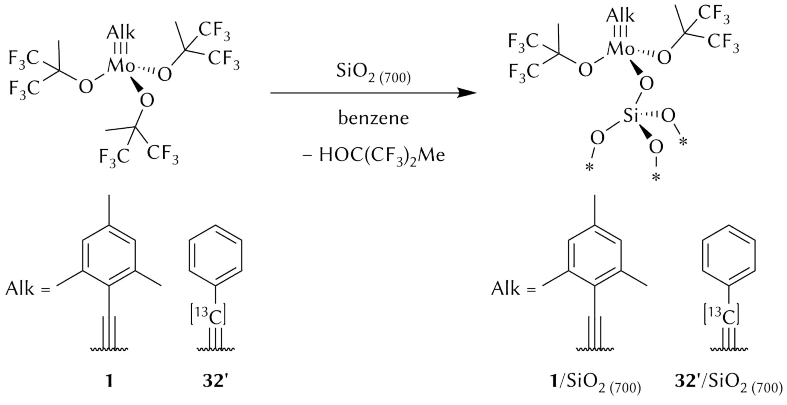

Scheme 50. Grafting of alkylidyne complexes onto partially dehydroxylated silica ($SiO_{2\,(700)}$).

thesis of complex **32′** is outlined in Scheme 51 (bottom), and follows the cross-metathesis strategy by reacting **1** with a mixture of tolan and (1,2-$^{13}C_2$)-tolan. The latter was prepared based on published procedures[217,218] upon bromination of commercially available *trans*-(1,2-$^{13}C_2$)-stilbene followed by dehydrohalogenation (Scheme 51, top).

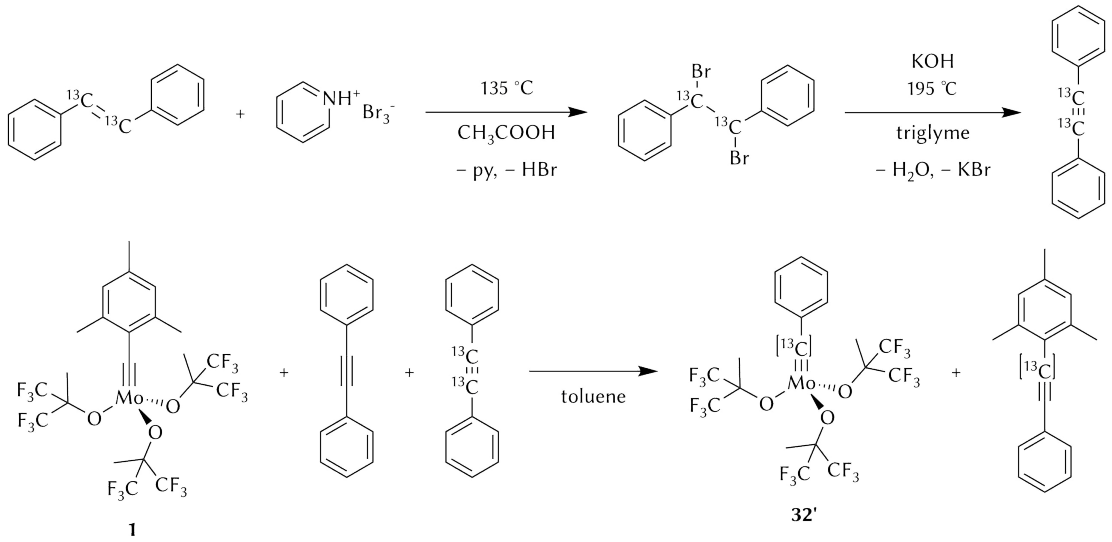

Scheme 51. Synthesis of ^{13}C-substituted tolan (top) and its use in the synthesis of ^{13}C-enriched **32′**. A 1:1 mixture of unmodified tolan and (1,2-$^{13}C_2$)-diphenylacetylene was used to label the alkylidyne complex.

Reaction with ynediamines: formation of paramagnetic metallacyclobutadiene complexes

Challenging substrates such as heterosubstituted acetylenes (XC≡CY, X = SiR_3, SnR_3, NR_2, PR_2, OR, SR, among others; Y = R or X; R = alkyl, aryl)[219] have rarely been reported to undergo catalytic alkyne metathesis; a few examples include alkynyl silanes and phosphanes,[62,147,148,158,160,220–222] although formation of disilylacetylenes from silylated substituents is not favoured.[62,122,150]

Stoichiometric reactions of heteroalkynes with alkylidyne complexes of the type [M(≡CMe)(O-*t*-Bu)$_3$] (M = Mo, W) or with bimetallic complex [W_2(O-*t*-Bu)$_6$] have been documented.[79,124] Cross-metathesis of $Me_3SiC{\equiv}CH$ with the molybdenum complex gave only a mixture of alkylidyne products.[79] In contrast, the reactions with tungsten complexes produced functionalised alkylidyne complexes of the type [W(≡CX)(O-*t*-Bu)$_3$] with silyl- (X = $SiMe_3$), amino- (X = NEt_2), or sulphanylcarbyne (X = S-*t*-Bu) moieties.[124] In particular, the aminoalkylidyne complex [W(≡CNEt_2)(O-*t*-Bu)$_3$(quin)] was formed by reaction of an ynediamine ($Et_2NC{\equiv}CNEt_2$, **33**) with [W(≡CMe)(O-*t*-Bu)$_3$] in the presence of an excess of quinuclidine (quin). This report suggests that even very electron-rich ynediamines are susceptible to alkyne metathesis, and that the observed

alkylidyne exchange should involve formation of intermediate MCBD species bearing uncommon heterosubstituents (X). Indeed, it is known that electron-rich substrates interact better with the electrophilic metal atom than electron-poor acetylenes.[47]

The high reactivity associated with ynediamines and the lack of reliable and adaptable synthetic approaches have limited their use as a ligand in organometallic chemistry.[223–226] Most of this chemistry has been developed in the present decade,[227–235] after our group established an alternative synthetic protocol.[236] This simple, two-step procedure is based on the Fritsch–Buttenberg–Wiechell rearrangement,[237] and grants access to several symmetrically substituted ynediamines (e.g. dipiperidinoacetylene, bis(4-methylpiperidino)acetylene (**34**)) from 1,1-ethenediamines via 1,1-dibromo-2,2-diaminoethenes. In particular, the combination of these alkynes with titanocene and zirconocene complexes gave unusual amino-substituted three- and five-membered metallacyclopropene (MCP) and metallacyclopentadiene (MCPD) structures (Figure 45).[228]

Entirely aminated four-membered MCBD complexes are practically unknown; the only example is a series of ferracyclobutadiene complexes published by A. C. Filippou and P. Vöhringer (Figure 45, centre).[238,239] Hence, it would be interesting to generate similar molybdenacyclobutadiene species by consecutive cycloaddition/cycloreversion reactions between ynediamines and molybdenum alkylidyne complexes such as **1**. Alternatively, as mentioned in the Overview (see Scheme 20), these compounds might engage in a cross-metathesis reaction affording novel aminocarbyne complexes, which are also expected to form as intermediates in the alkyne metathesis of amino-substituted acetylenes.

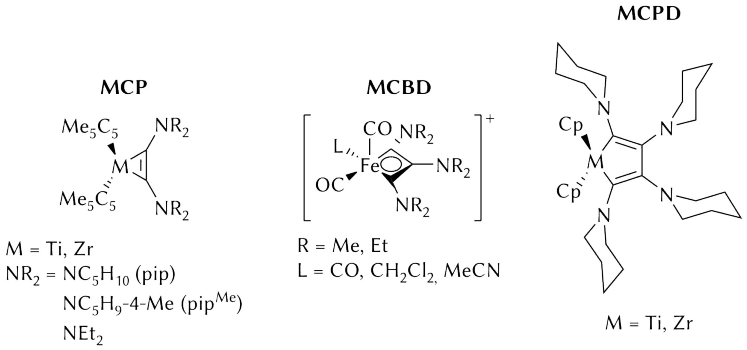

Figure 45. Reported structures of entirely aminated 3-, 4-, and 5-membered metallacycles; pip = piperidin-1-yl, pip^{Me} = 4-methylpiperidin-1-yl.

Preliminary experiments concerning the metathesis of **34**[236] with diphenylacetylene or 5-(benzyloxy)-2-pentyne (**Y**-Me)[110] in the presence of 1 mol% of alkylidyne complex **1** (Scheme 52) showed no conversion at all by NMR spectroscopy, although a colour change to red was observed immediately after addition of **1**. Because this chromatic shift is characteristic of MCBD formation,[38,39,69,79,141,200,201] isolation of the putative MCBD complex was subsequently attempted in a stoichiometric reaction. Thus, treatment of an *n*-pentane solution of complex **1** with ynediamine **34** resulted in an instantaneous colour change from yellow to red, and a crystalline precipitate formed in good yield upon refrigeration at low temperature (–30 °C). After recrystallisation, deep red crystals suitable for X-ray diffraction analysis were obtained, which revealed the formation of a four-membered molybdenacycle, [Mo(C(pip^{Me})C(Mes)C(pip^{Me})-κ^2*C*)(OC(CF$_3$)$_2$Me)$_3$] (**35**, pip^{Me} = 4-methylpiperidin-1-yl, Mes = mesityl; Scheme 53).

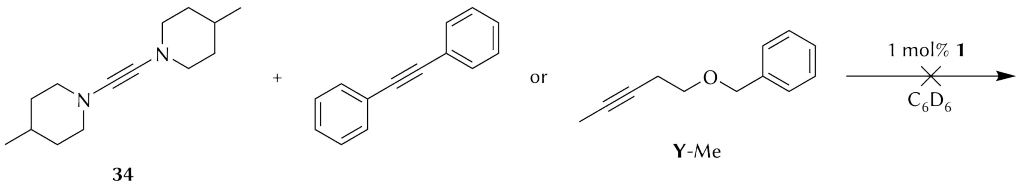

Scheme 52. Attempted ACM of ynediamine **34** with model alkynes in the presence of alkylidyne complex **1**.

In a similar manner, the diethylamino congener **33** was reacted with alkylidyne complex **1** to yield orange–brown dichroic crystals after recrystallisation at low temperature (–30 °C). X-ray crystallography showed an analogous structure to **35**, [Mo(C(NEt$_2$)C(Mes)C(NEt$_2$)-κ^2*C*)(OC(CF$_3$)$_2$Me)$_3$] (**36**, Scheme 53), with diethylamino groups in place of the piperidino rings. It should be mentioned here that both compounds are slightly thermosensitive, but they can be stored in crystalline form at –30 °C for months with no evidence of degradation.

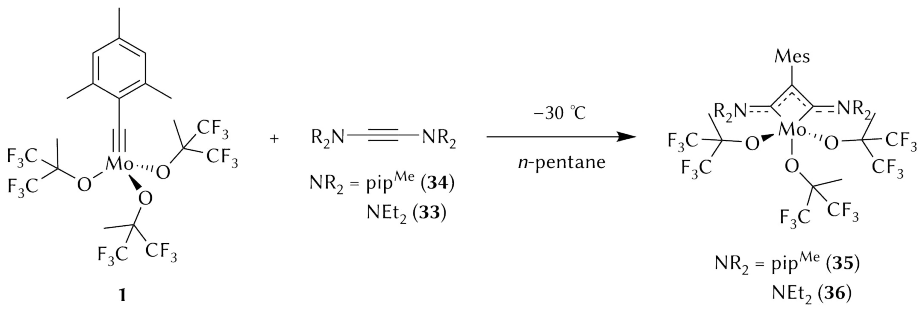

Scheme 53. Formation of MCBD complexes **35** and **36**; Mes = mesityl, pip^{Me} = 4-methylpiperidin-1-yl.

The molecular structures of **35** and **36** are depicted in Figure 46. Both compounds crystallise in the triclinic space group $P\bar{1}$ and exhibit pentacoordinated molybdenum atoms with a coordination geometry between idealised square-pyramidal and trigonal-bipyramidal conformations (τ_5 = 0.484(4) and τ_5 = 0.590(2), respectively).[188] Surprisingly, the molecules could be described as having pseudo-C_s symmetry, because both amino substituents in each compound are attached to the metallacycle systems

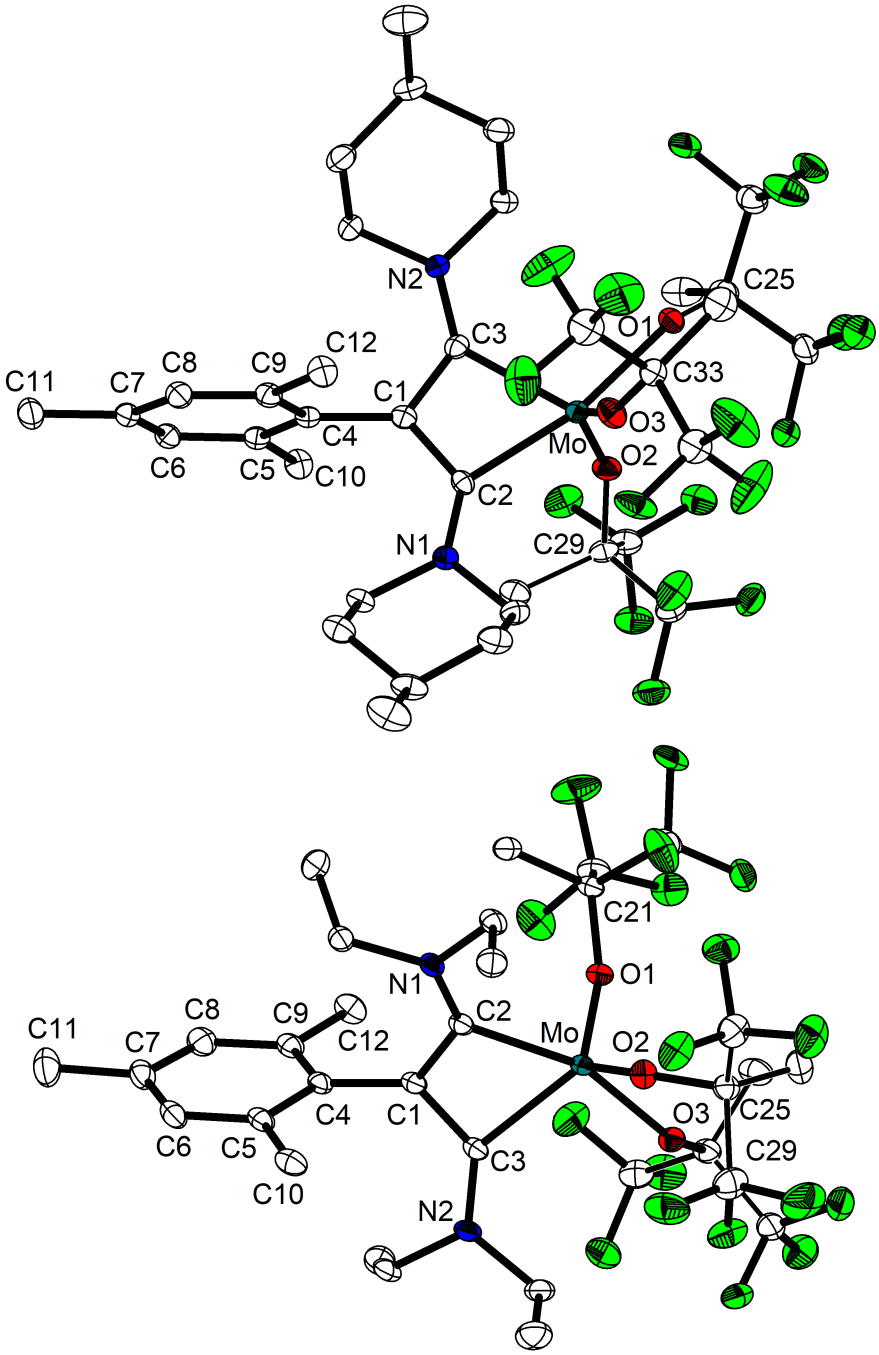

Figure 46. Molecular structures of complexes **35** (top) and **36** (bottom) with thermal displacement parameters drawn at the 30% probability level. Alternative disordered positions of some fluorinated groups and hydrogen atoms are omitted for clarity. For selected bond lengths and angles, see Figures 84 and 85.

in the α positions, while the aryl moiety lies in the β position between these sites. From this it can be surmised that the alkynes were indeed involved in a metathetical transformation prior to the formation of the symmetrical MCBD species.

In accordance with the vast majority of MCBD complexes,[55] the MoC_3 ring in **35** adopts a nearly planar structure with a dihedral angle of ϕ = 172.9(2)° between the C2, Mo, C3 and the C2, C1, C3 planes (the r.m.s. deviation of the l.s. plane through atoms Mo, C2, C1, C3 is 0.037(3) Å). On the contrary, the corresponding dihedral angle in complex **36** is substantially smaller (ϕ = 147.02(11)°), so the metallacycle displays a much less common, puckered conformation. As expected, the C2–Mo–C3 angles in **35** and **36** are inordinately narrow (approx. 62°), but the overall bonding situation in the four-membered ring differs significantly from the structural motif observed in tungstenacyclobutadiene complexes consisting of a WC_3 ring with a clear long–short–long–short alternation of bond lengths.[55] While the Mo–C distances in **35** and **36** (2.120(2) Å–2.166(3) Å) have a single bond character,[180] the C1–C2 and C1–C3 bond lengths of 1.413(4) Å–1.433(3) Å are intermediate between the values expected for C(sp^2)–C(sp^2) single and double bonds,[240] and together with short exocyclic C2–N1 and C3–N2 bonds (1.322(4) Å–1.324(3) Å), they indicate strong π-conjugation and electron delocalisation within the N1–C2–C1–C3–N2 moiety (see Scheme 53). Furthermore, the perpendicular orientation of the mesityl groups† with long C1–C4 bond lengths of approximately 1.50 Å precludes their interaction with the π systems.

Structurally characterised molybdenacyclobutadiene complexes are scarce, and except for very recent examples from the group of F. Fischer[173] and our group[62,63,211] that followed the prior publication of **35** and **36**, no other than the dicationic molybdenum complex [Mo(C(Ph)C(Ph)C(NHXy)-κ²*C*)(η₅-C_5Me_5)(CNXy)₃](BF₄)₂ (**37**(BF₄)₂, Xy = 2,6-dimethylphenyl) was reported before.[241] Compound **37** was formed by an isocyanide–alkyne coupling reaction (Scheme 54), and was described as a Mo(IV) iminium metallacyclobutene complex; compared to **35** and **36**, it exhibits similar, albeit slightly longer, Mo–C bond lengths.

In contrast to the diamagnetic nature of compound **37**, MCBD complexes **35** and **36** are paramagnetic, as reflected by extremely broad, unusually upfield- and downfield-

† The l.s. planes through the aromatic carbon atoms C4–C9 in **35** and **36** (r.m.s. deviations 0.003(4) Å and 0.011(2) Å, respectively) form almost a right angle (86.86(17)° and 89.87(11), respectively) with the corresponding C2, C1, C3 planes.

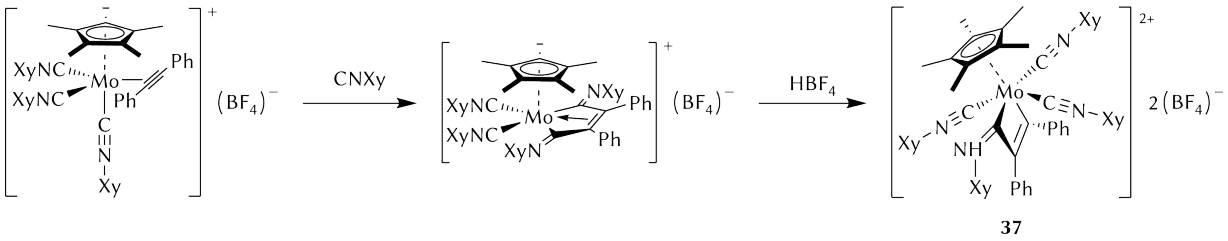

37

Scheme 54. Synthesis of MCBD complex **37**; Xy = 2,6-dimethylphenyl.

shifted resonances in the NMR spectra. Considering this and the thermal instability of the complexes, a detailed variable-temperature (VT) NMR study was required.

NMR analyses of solutions of pure crystalline **35** produced very intricate spectra with extremely broad resonances induced by the low temperatures of the measurements (to avoid decomposition of the sample) and the paramagnetic nature of the molecule. The ^{1}H chemical shifts range from approx. –10 ppm to +50 ppm (Figure 47), and are singularly temperature-dependent. Moreover, two similar sets of paramagnetic signals can be identified in all ^{1}H NMR spectra at different temperatures, suggesting the presence of two isomers in solution in a ratio ~1:0.9. For example, three sets of singlets account for the following methyl groups: (i) two and (ii) three signals for the *para* and *ortho* CH_3 groups, respectively, of the mesityl ring (the major isomer possesses

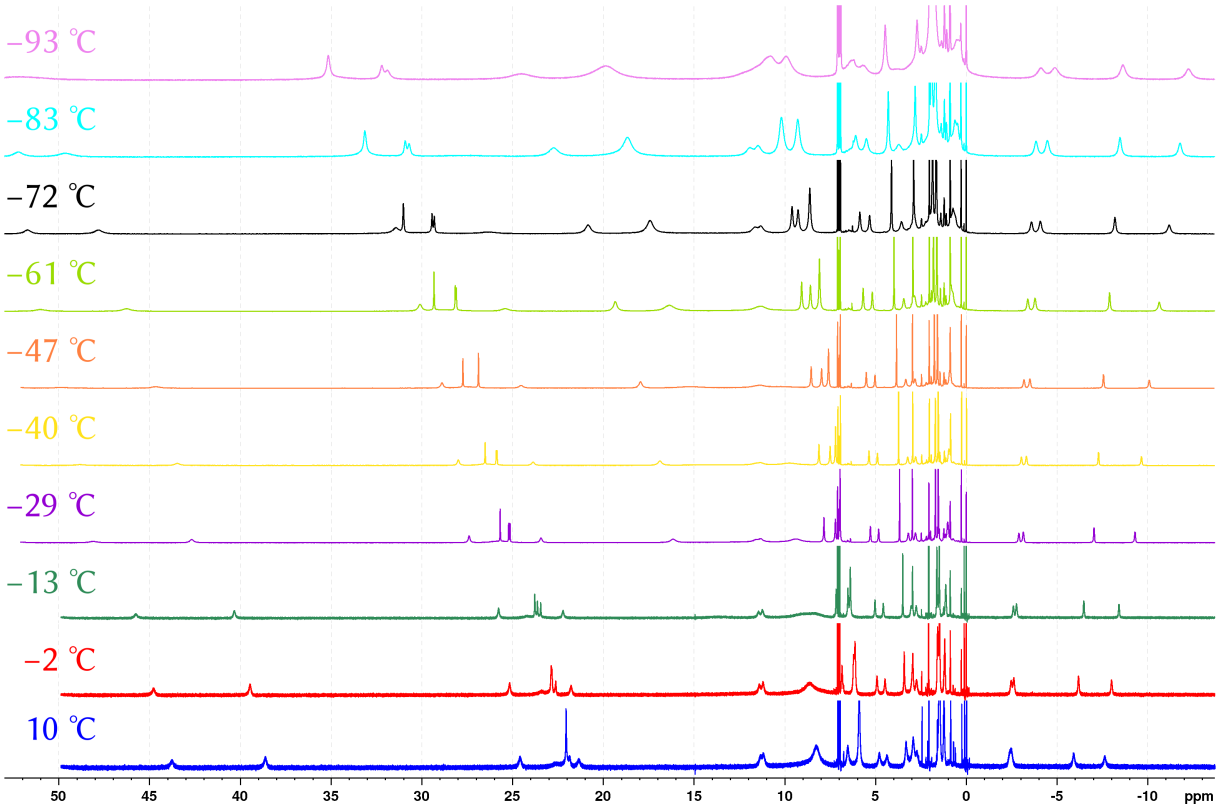

Figure 47. VT ^{1}H NMR of complex **35** in toluene-d_8.

two inequivalent *ortho* positions), and (iii) two signals for the CH_3 group of the piperidinyl moieties. In contrast, an unambiguous assignment of the methyl groups of the fluorinated alkoxides is not possible, since the corresponding resonances are pronouncedly broad and their chemical shifts are dramatically temperature-dependent. Indeed, at least two resonances (a third resonance is observable below –40 °C) can be cautiously assigned to these methyl groups. Furthermore, the CH atoms of the piperidinyl substituents (on the 4-position) are observed as two broad overlapping signals, whereas the aryl hydrogen atoms give rise to three singlets (two inequivalent sites in the major isomer). In addition, 14 signals (of 16 expected) can be tentatively assigned to the diastereotopic hydrogen atoms of the piperidinyl CH_2 groups. The two missing resonances cannot be identified reliably because of overlap. Table 5 and Table 6 (p 184) list all the assignments at different temperatures. Similarly, the $^{13}C\{^1H\}$ and $^{19}F\{^1H\}$ NMR spectra display two sets of signals, but in the latter case the broadness of the resonances and the lack of convenient 2D NMR experiments make the assignment of the fluorine signals virtually impossible. While most of the non-quaternary carbon atoms are observable and can be correlated to one signal in the $^{13}C\{^1H\}$ NMR spectrum (see Experimental section, p 183), nearly all signals corresponding to quaternary carbon atoms are missing, probably because of extreme high frequencies (beyond the measured range) and drastic broadening.

It is important to note that the peak width at half height is directly related to the through-bond distance between the corresponding nuclei and the molybdenum atom. Thus, the broadest signal in the proton NMR spectrum can be assigned to the CH_2 groups at the 2,6-positions of the piperidinyl rings and to the CH_3 groups of the fluorinated alkoxides. This observation is consistent with the fact that the respective ^{13}C NMR signals, and also many quaternary carbon atoms near the paramagnetic centre, could not be detected, and explains further the atypical broadness of the ^{19}F NMR signals.

Assuming a fluxional process that makes the three alkoxide ligands equivalent in solution, there exists only one possible pair of diastereomers, *meso*-**35** and *rac*-**35**, depicted in Figure 48, that is consistent with the NMR data. In both cases, the inversion of the chair conformation of the piperidine rings and also the rotation around the exocyclic N–C bond must be frozen (which is in agreement with a conjugation of the

electron lone pair on the nitrogen atom with the metallacycle). Isomer *meso*-**35** exhibits a *syn* arrangement of the piperidine rings as found in the solid state (Figure 46, top), whereas the rings are oriented *anti* to one another in *rac*-**35**. Nevertheless, the piperidine rings within each compound are equivalent, as a result of either the C_s symmetry (mirror plane) of diastereomer *meso*-**35** or the C_2 symmetry featured by *rac*-**35**. Because of the observed non-equivalence of the *ortho*-CH_3 groups and the *meta*-H atoms in *meso*-**35**, rotation of the mesityl substituent must also be hindered, even though both positions are equivalent through the twofold axis in *rac*-**35**.

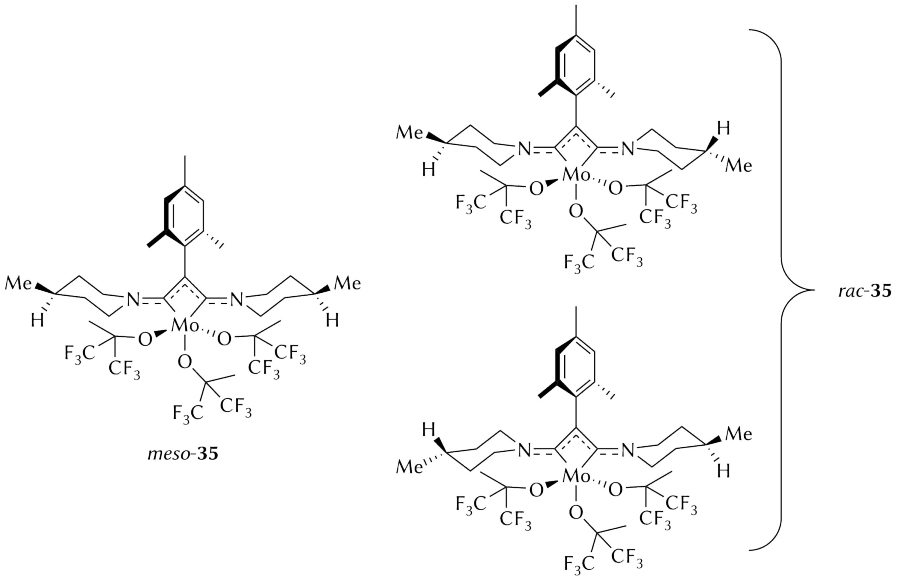

Figure 48. Stereoisomers of complex **35** in solution.

As shall be expected, replacement of the piperidinyl rings in **35** by Et_2N substituents in **36** produced much simpler NMR spectra (Figure 49). Note that VT NMR studies were conducted on a concentrated sample of the reaction mixture, necessitated by the fact that only small amounts of pure, crystalline **36** were available (for details, see the Experimental section, p 186). The ^1H NMR spectrum at 0 °C displays only one set of signals for the paramagnetic compound, thanks to the freely rotating ethyl groups in complex **36**. These groups, however, give rise to two pairs of resonances at $\delta_H = -1.3$ and $\delta_H = 13.1$ ppm ($2 \times CH_3$), and at $\delta_H = 24.1$ ppm and $\delta_H = 26.1$ ppm ($2 \times CH_2$), which reveal that rotation of the amino groups around the C–N bond is also hindered. The *ortho*-CH_3, *meta*-H and *para*-CH_3 hydrogen atoms resonate at $\delta_H = 3.5$ ppm, $\delta_H = 16.9$ ppm, and $\delta_H = 1.9$ ppm, respectively. In addition, the signal at $\delta_H = 10.4$ ppm (9H) is unambiguously assigned to the methyl groups of the fluorinated alkoxides, which

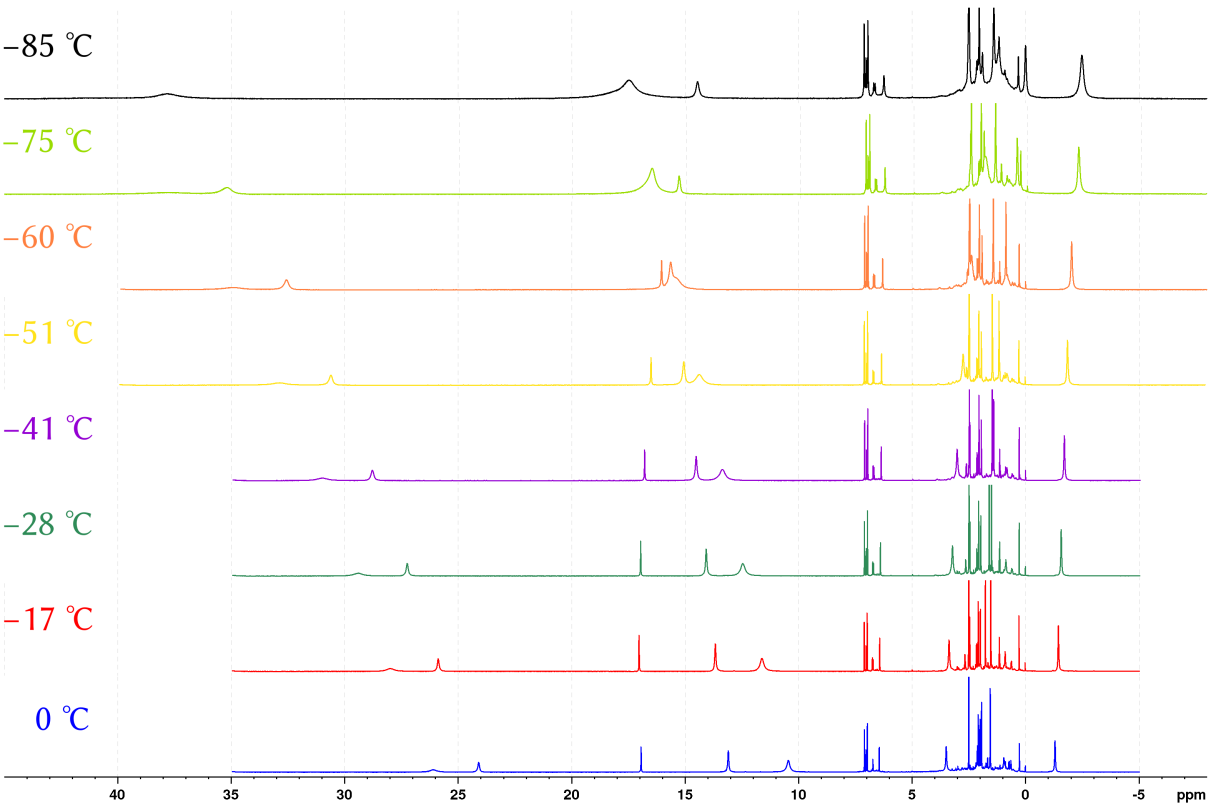

Figure 49. VT ^{1}H NMR of complex **36** in toluene-d_8.

evidences the chemical equivalence of these ligands on the NMR timescale. This is further underlined by the fact that only one paramagnetic resonance is found at δ_F = −2.4 ppm for the corresponding fluorine atoms in the $^{19}F\{^{1}H\}$ NMR spectrum. Furthermore, additional diamagnetic resonances are tentatively assigned to a mixture of compounds, which might include some predicted side-products of the cross-metathesis reaction between alkyne **33** and complex **1** (see Figure 53).

The paramagnetism of MCBD complex **35** was investigated first by electron paramagnetic resonance (EPR) spectroscopy, which showed only small amounts of a Mo(V) d^1 (S = ½) paramagnetic impurity that increased over time (~30 h) at ambient temperature and in solution, indicating decomposition of the complexes. This observation implies that the actual MCBD complexes **35** and **36** are EPR silent, and therefore, must have an integer total spin, most likely S = 1, which conforms to the formal oxidation state +IV (d^2) on the molybdenum atoms. To confirm this hypothesis, magnetic susceptibility measurements of crystalline samples were conducted on a superconducting quantum interference device (SQUID). The effective magnetic moment (μ_{eff}) of **35** and **36** was recorded in the temperature range T = 2.6–300 K; above T = 200 K the magnetic data (**35**, μ_{eff} = 2.46–2.62 μ_B; **36**, μ_{eff} = 2.50–2.61 μ_B) are fully consistent with a

high-spin (S = 1) Mo(IV) d^2 centre. Similar values were reported previously for other pentacoordinate tetravalent high-spin molybdenum complexes.[242] Small deviations from the spin-only value of μ_{eff} = 2.83 μ_B for an S = 1 spin-state might be ascribed to weighing errors or partial decomposition caused by the inherent thermal instability of these compounds. In addition, computational calculations predicted average g values of g_{av} = 1.802 and g_{av} = 1.847 for **35** and **36**, respectively, which are clearly lower than the free electron value ($g \approx 2.002$), and suggests that the reason for the observed reduced effective magnetic moments has a molecular basis. A plot showing the temperature dependence of the effective magnetic moments is presented in Figure 50. At low temperatures (T < 75 K), the decreasing μ_{eff} values are attributable to the presence of zero-field splitting.

Decomposition studies of a sealed sample of complex **35** at T = 310 K gave a paramagnetic degradation product with a half-life of $t_{1/2}$ = 287 min and an S = ½ spin-centre ($\mu_{eff} \approx 2\ \mu_B$, see Figure 51, top), which confirmed the formation of a Mo(V) d^1 species already observed by EPR spectroscopy. Also compound **36** decomposed at T = 300 K with a half-life of $t_{1/2}$ = 138 min (Figure 51, bottom) to give a pentavalent d^1 molybdenum degradation product. The structure of these products, however, has not been elucidated so far.

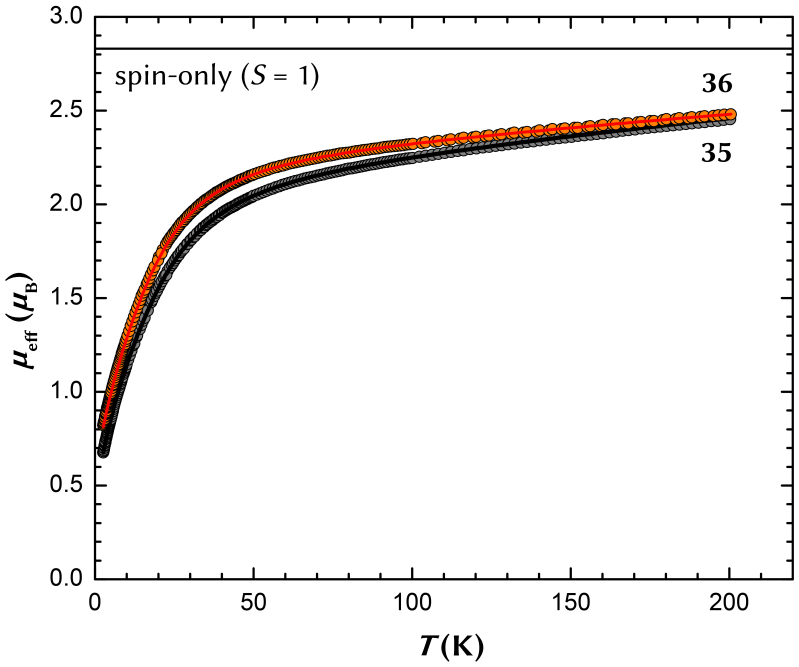

Figure 50. Effective magnetic moment (μ_{eff}) vs. T plots for complexes **35** (grey) and **36** (orange) measured with an externally applied magnetic field of B_{ext} = 0.1 T.

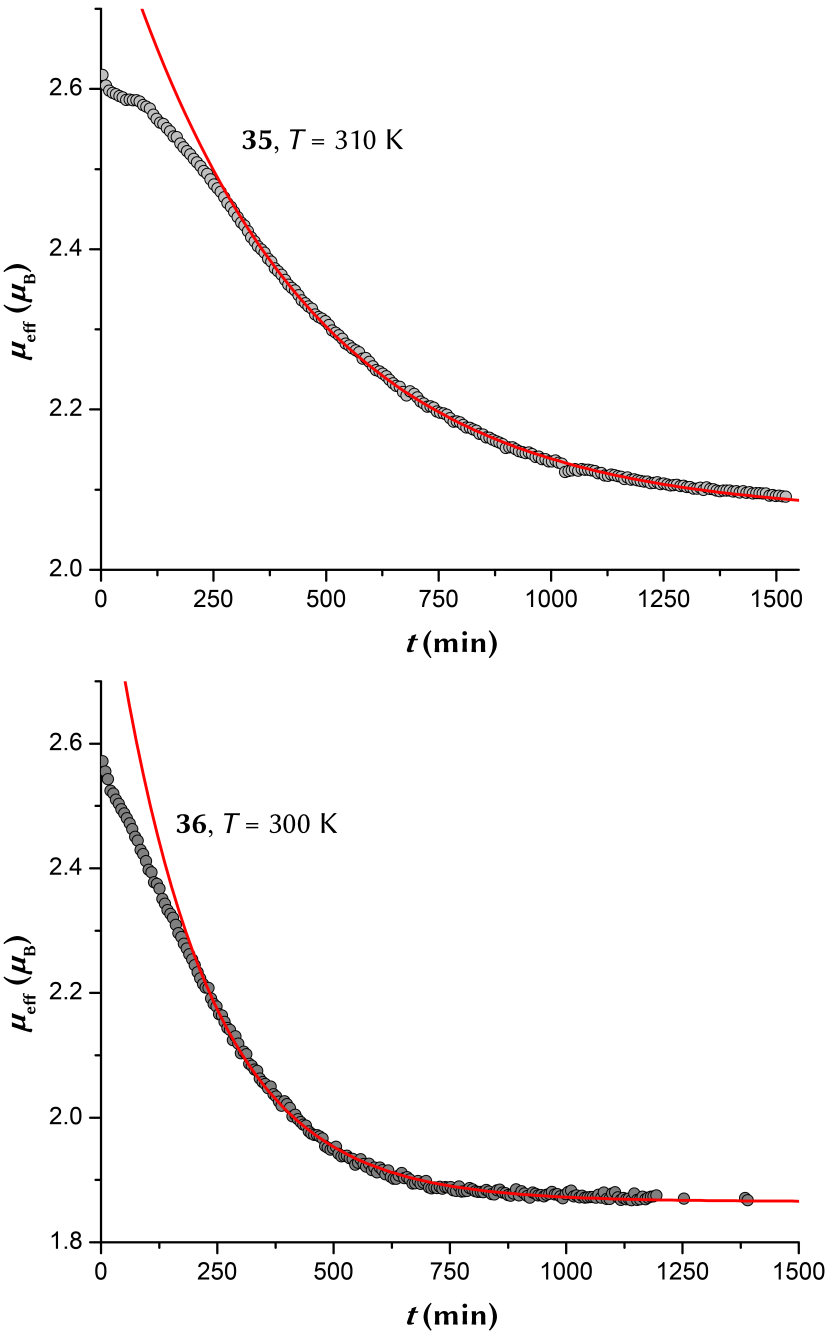

Figure 51. Effective magnetic moment (μ_{eff}) vs. time (t) plots for complexes **35** (top) and **36** (bottom) measured with an externally applied magnetic field of B_{ext} = 0.1 T at indicated temperatures (T). The linear fit is based on an exponential decay model.

Both the magnetic properties and the mechanistic formation of metallacycles **35** and **36** were analysed by DFT methods; numerical results are presented in Table 4. To understand the prevalence of a high-spin configuration the electronic energies of the singlet (S = 0) and triplet (S = 1) states were calculated for both complexes. These calculations predict the stabilisation of the triplet (S = 1) relative to the singlet states (S = 0) by ΔG_{298}(**35**) = –11.46 kcal mol^{-1} and ΔG_{298}(**36**) = –13.07 kcal mol^{-1}, confirming the paramagnetic nature of the MCBD complexes. Structural parameters of the calculated

singlet and triplet states are very similar, and they are consistent with the crystallographic data, which is in agreement with the apparent non-bonding character of the frontier orbitals. Indeed, a biorthogonalisation[243] of the α- and β-orbital space reveals two singly occupied molecular orbitals (SOMOs), which closely resemble the two d orbitals on the molybdenum atom (Figure 52). Therefore, metallacycles **35** and **36** are best described as complexes having a Mo(IV) d^2 centre.

As indicated above, the formation of symmetrically substituted complexes **35** and **36** must have occurred upon cleavage of the acetylenic bond in **34** and **33**, respectively. Therefore, possible reaction intermediates were calculated on the basis of the alkyne metathesis mechanism, which involves MCBD and alkylidyne species generated by consecutive [2 + 2] cycloaddition and cycloreversion reactions (cf. Scheme 5, p 8). A diagram of the proposed reaction pathway is shown in Figure 53. Accordingly, metallacycles **38a** and **38b**, which feature a non-symmetric substitution on the four-membered ring, are initially formed by combination of complex **1** with ynediamines **34** and **33**, respectively. Subsequent release of the ynamines $R_2NC{\equiv}CMes$ (**39a/b**), fol-

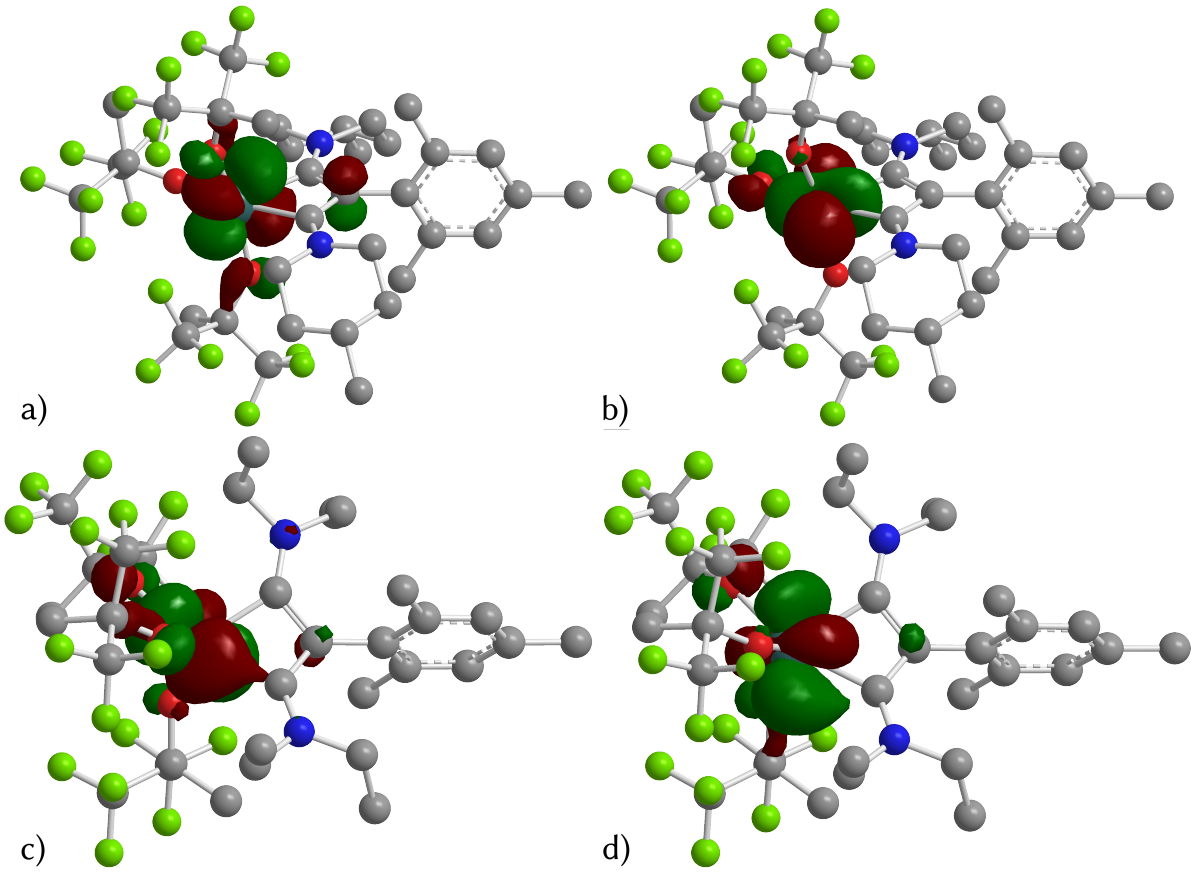

Figure 52. Contour plots (isovalue = 0.40) of the biorthogonalised SOMO (a) and SOMO–1 (b) of complex **35**, and of the biorthogonalised SOMO (c) and SOMO–1 (d) of complex **36**.

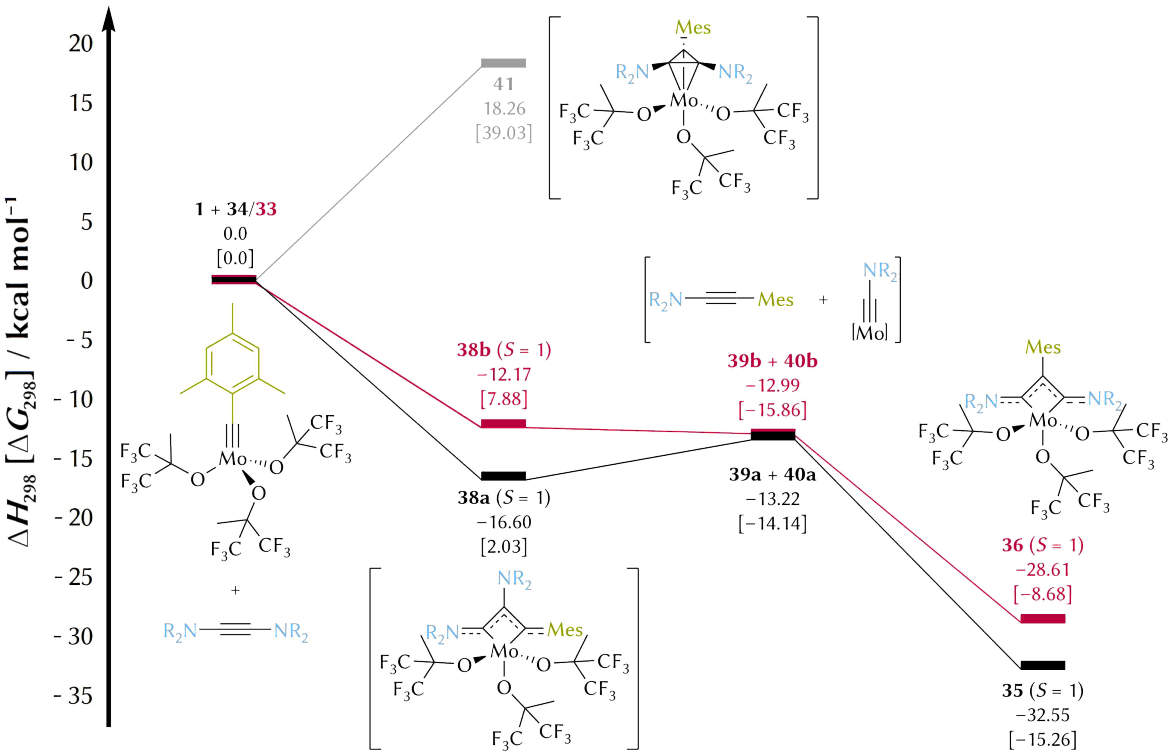

Figure 53. Energy profile for the formation of **35** (black, R_2N = pip^{Me}) and **36** (red, R_2N = Et_2N), and alternative reaction pathway involving the formation of metallatetrahedrane **41** (grey, R_2N = pip^{Me}); Mes = mesityl, pip^{Me} = 4-methylpiperidin-1-yl.

lowed by inverse re-addition to the aminoalkylidyne intermediates [Mo(≡CNR$_2$)(OC(CF$_3$)$_2$Me)$_3$] (**40a/b**), furnishes, respectively, the final products **35** and **36** with both amino groups in α positions as observed experimentally (Figure 46).

Indeed, the computed energies support the favoured formation of the symmetric metallacycles **35** (ΔG_{298} = –15.26 kcal mol^{-1}) and **36** (ΔG_{298} = –8.68 kcal mol^{-1}) in their triplet states, which is markedly exergonic, over the non-symmetric intermediates **38a** (ΔG_{298} = 2.03 kcal mol^{-1}) and **38b** (ΔG_{298} = 7.88 kcal mol^{-1}), also in their triplet states, although in this case the singlet–triplet gap is significantly smaller (see Table 4). In addition, the estimated enthalpies (ΔH_{298}, Table 4) indicate the formation of the final products to be strongly exothermic. Moreover, the calculated energy profile suggests the possibility of aminocarbyne formation, namely **40a/b**, which might account for the observation of diamagnetic side-products in the NMR spectra of **36** (cf. Figure 49).

An alternative pathway for the formation of **35** and **36** might proceed in a single step via metallatetrahedrane intermediates (cf. Scheme 11, p 14).[57,80,87,244,245] Such species, however, are predicted to be unstable for the present systems (e.g. ΔG_{298} = 39.03 kcal mol^{-1} for the formation of **41**, R_2N = pip^{Me}; see Figure 53), and therefore, this mechanism was not considered further.

Table 4. Relative electronic and thermodynamic data computed at the B3LYP/6-311G(d,p) level of theory. All values are given in kcal mol^{-1}.

Compound or reaction	S	ΔE_0	ΔE_{298}	ΔH_{298}	ΔG_{298}
1 + **34**/**33**	0	0.00	0.00	0.00	0.00
38a	0	−13.07	−13.25	−13.84	5.89
	1	−15.79	−16.01	−16.60	2.03
39a + **40a**	0	−13.18	−13.22	−13.22	−14.14
35	0	−22.11	−22.17	−22.76	−3.81
	1	−32.10	−31.96	−32.55	−15.26
38b	0	−7.26	−8.03	−8.62	13.66
	1	−11.16	−11.58	−12.17	7.88
39b + **40b**	0	−13.12	−12.99	−12.99	−15.86
36	0	−14.34	−14.76	−15.36	4.39
	1	−27.64	−28.02	−28.61	−8.68
41	0[a]	18.91	18.85	18.26	39.03

[a] The optimisation of the structure of **41** in the triplet state (S = 1) was attempted, but no reasonable minimum structure was found.

The bonding situation in the tetravalent complexes **35** and **36** can be rationalised by fragmentation into cationic $[Mo(OC(CF_3)_2Me)_3]^+$ and anionic $((R_2N)CC(Mes)C(NR_2))^-$ moieties (Scheme 55). In this representation, the NC_3N ligand can be regarded as a di-carbene ligand (for a carbenoid depiction, see canonical forms, Scheme 55, top), which can be formally derived from vinamidinium salts $(R_2NC(H)C(R')C(H)NR_2)^+$ by twofold deprotonation at the 1,3-positions.[246–248]

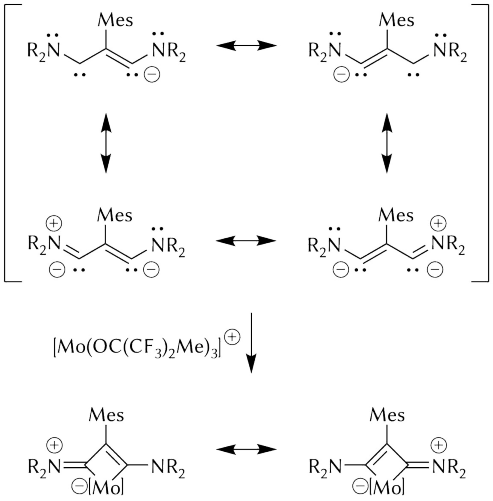

Scheme 55. Resonance structures of the dicarbene NC_3N ligand (top) and of complexes **35** (R_2N = pip^{Me}) and **36** (R_2N = Et_2N) (bottom); Mes = mesityl, pip^{Me} = 4-methylpiperidin-1-yl, [Mo] = $Mo(OC(CF_3)_2Me)_3$.

In addition, DFT calculations were carried out for the free anionic dicarbene ligand in **35** (R_2N = pip^{Me}). The unconstrained optimisation of the dicarbene fragment gave structural parameters similar to those in **35**, indicating strong π-conjugation and electron-delocalisation within the NC_3N unit, as best illustrated by the corresponding resonance structures (Scheme 55, centre). The two highest occupied molecular orbitals (HOMO and HOMO–1, Figure 54) of the carbene ligand represent two doubly occupied σ orbitals (lone pairs) located at the carbon atoms in the 1,3-positions. These two σ orbitals can donate electron density to the metal atom, forming two Mo–C σ bonds in the complex. HOMO–2, HOMO–5, and HOMO–6 (Figure 54) are three doubly occupied orbitals of the orthogonal 6-electron NC_3N π system; however, this is expected to consist of five molecular orbitals, but the two remaining unoccupied π* orbitals could not be identified unambiguously in the virtual space.

According to these results, the ligand can be regarded as a 4-electron σ donor through HOMO and HOMO–1 and potentially also as a 2-electron π donor through HOMO–2 towards the Mo(IV) atom. Essentially, these patterns are recognisable in some molecular orbitals of complex **35** (viz. HOMO–2, HOMO–5, and HOMO–7, not shown). In contrast, backbonding through dπ → π* interactions, which play a significant role in the overall binding in conventional MCBD complexes, is negligible. As a consequence, the resonance structures in Scheme 55 (bottom) characterise much better the bonding situation in the metallacyclic systems **35** and **36** rather than the most commonly encountered MCBD description.

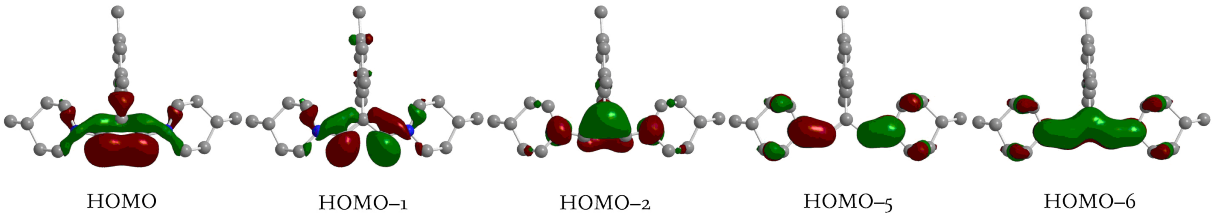

Figure 54. Contour plots (isovalue = 0.40) of selected molecular orbitals of the NC_3N dicarbene ligand; HOMO–3, HOMO–4 and HOMO–7 (not shown) represent the π system of the mesityl group.

3.3.2. Species involved in terminal alkyne metathesis

Complex **1** is an effective alkyne metathesis promoter for a wide range of substrates, including even terminal alkynes. The reasons why the catalyst does not deactivate in the presence of 1-alkynes or switches its catalytic reactivity to produce poly(acetylene)s have been exposed in the Introduction (see p 22). Both an exceptional activity and the poor basicity of the hexafluoro-*tert*-butanolate ligands, are evident prerequisites to succeed in the metathesis of terminal alkynes and to avoid decomposition pathways (cf. Scheme 10, p 13); sufficient dilution is another important condition.

On this basis, and given the short lifetimes of such species, isolation of MCBD or DPMCBD intermediates is expectably challenging. Indeed, it has been shown in the preceding section that complex **1** forms isolable MCBD complexes only under very specific circumstances. Otherwise, cross-metathesis products (e.g. **19**, **32**) are usually obtained. Nonetheless, DPMCBD stabilisation, if not inherently favoured for **1**,‡ can be induced under certain conditions. Addition of a Lewis base or a coordinating agent (L, e.g. 2,2′-bipyridine) as found in several documented examples[70,71,79–82,84,85,207] is a valid approach to trap DPMCBD species (Scheme 56). Some bases such as Et_3N, besides their coordination potential, can assist in the elimination of the ring proton by the alkoxide ligands as tertiary ammonium salts.[55,82,83]

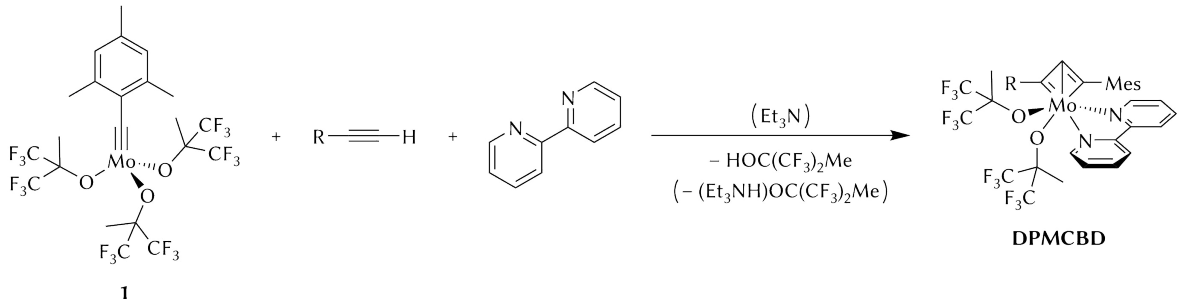

Scheme 56. Proposed stabilisation of a DPMCBD species derived from alkylidyne complex **1**.

For this purpose, alkylidyne complex **1** was reacted with stoichiometric amounts of phenylacetylene, PhC≡CH, in the presence of 2,2′-bipyridine (bipy). At room temperature, however, the reaction is too fast, and after filtration of some polymeric material and precipitation at –30 °C only the cross-metathesis alkylidyne product was obtained from the filtrate. Analysis by NMR spectroscopy indicated coordination of one bipy

‡ Isolation of "naked" DPMCBD complexes (without donor ligands) is possible for particular combinations of some anionic ligands with certain molybdenum or tungsten alkylidyne fragments.[71,79,81–83,211]

ligand to the metal complex, which gives a compound of the formula [**32**(bipy)] (**42**, Scheme 57). Interestingly, eight multiplets in the ^{1}H NMR spectrum and ten signals in the ^{13}C{^{1}H} NMR spectrum can be assigned to the chelating ligand, which evidences an inequivalent chemical environment. As already discussed for **28**, this circumstance can be reasoned by a meridional (*mer*) distribution of the alkoxide ligands. Indeed, two resonances at δ_H = 1.81 ppm and δ_H = 2.09 ppm with an integral ratio 6:3 account for the methyl groups of the alkoxides, and in the fluorine spectrum three equally integrating multiplets are observed for the corresponding CF_3 groups (δ_F = –78.3 ppm, –76.7 ppm, and –76.6 ppm). Together with the resonances in the carbon NMR spectrum (two signals at δ_C = 18.4 ppm and δ_C = 19.7 ppm for the CH_3 groups, two septets at δ_C = 83.65 ppm and δ_C = 83.67 ppm for the quaternary carbon atoms in $C(CF_3)_2Me$, and three quartets at δ_C = 124.61 ppm, δ_C = 124.63 ppm, and δ_C = 125.0 ppm for the CF_3 groups), these data clearly support the *mer*-structure. Compared to the bipy-free complex **32**, all related chemical shifts in **42** are shifted downfield in the proton NMR spectrum, although such a clear pattern is not recognisable for the carbon signals. For example, three aromatic signals (δ_C = 128.6 ppm, δ_C = 128.9 ppm, δ_C = 143.9 ppm) and the alkylidyne carbon atom (δ_C = 292.4 ppm) are shifted upfield, whereas the carbon atoms at the *ortho*-positions (δ_C = 130.7 ppm) and in the CF_3 groups are slightly more deshielded.

In addition, the molecular structure of **42** was established by X-ray diffraction analysis and is presented in Figure 55. The complex crystallises in the triclinic space group $P\bar{1}$ and displays a highly distorted octahedral geometry around the molybdenum centre (*cis*, 71.78(6)°–104.68(7)°; *trans*, 153.78(6)°–170.31(7)°), with the Mo atom located 0.3953(1) Å above the l.s. plane N1, O1, O2, O3 (r.m.s. deviation 0.0237(14) Å). As rationalised from the NMR data in solution, the alkoxide ligands are arranged in a *mer* conformation

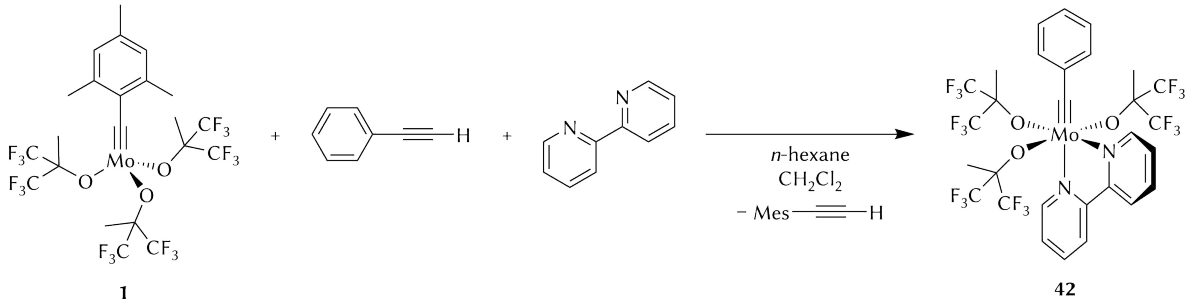

Scheme 57. Reaction of alkylidyne complex **1** with phenylacetylene in the presence of 2,2′-bipyridine.

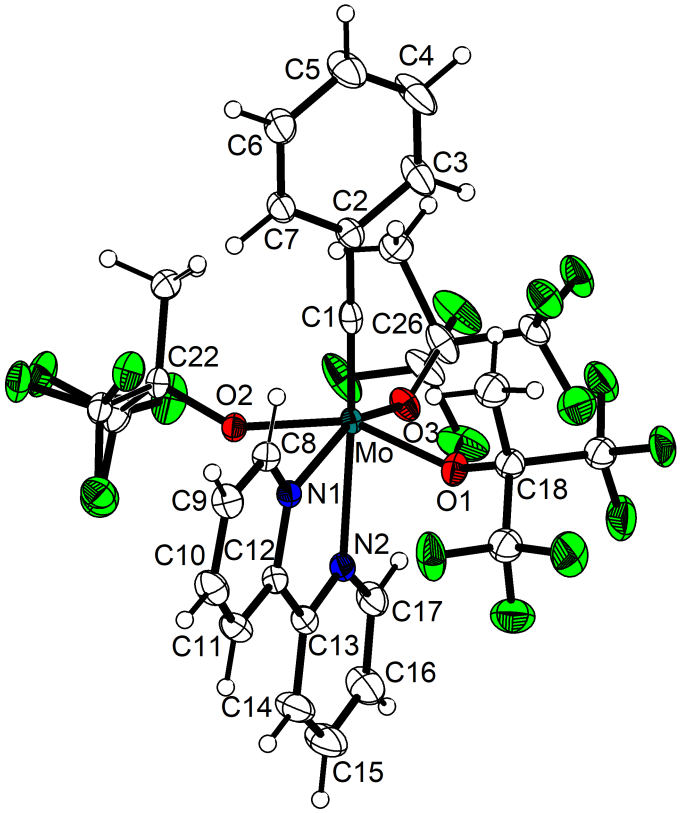

Figure 55. Molecular structure of **42** with thermal displacement parameters drawn at the 50% probability level. Disordered $C(CF_3)_2Me$ ligands (at O1 and O3) are omitted for clarity. Selected bond lengths (Å) and angles (deg): Mo–C1 1.771(2), Mo–N1 2.2530(15), Mo–N2 2.3614(16), Mo–O1 1.9647(14), Mo–O2 1.9666(13), Mo–O3 1.9482(14), N1–C12 1.353(2), N2–C13 1.344(3), C1–C2 1.448(3), C12–C13 1.490(3); C1–Mo–N1 98.54(7), C1–Mo–N2 170.31(7), C1–Mo–O1 100.14(7), C1–Mo–O2 101.18(7), C1–Mo–O3 104.68(7), N1–Mo–N2 71.78(6), N1–Mo–O1 80.70(6), N1–Mo–O2 81.21(6), N1–Mo–O3 156.78(6), N2–Mo–O1 78.19(6), N2–Mo–O2 78.22(5), N2–Mo–O3 84.99(6), O1–Mo–O2 153.78(6), O1–Mo–O3 94.96(6), O2–Mo–O3 94.22(6), Mo–C1–C2 178.26(16), Mo–N1–C12 118.56(12), Mo–N2–C13 115.99(12), N1–C12–C13 117.55(17), N2–C13–C12 116.08(17).

also in the solid state. The chelating ligand forms a five-membered ring with a particularly narrow angle of 71.78(6)° (N1–Mo–N2). Both l.s. planes through the bipy ligand (N1, N2, C8–C17, r.m.s. deviation 0.0274(19) Å) and through the phenyl ring (C2–C7, r.m.s. deviation 0.0060(19) Å) are approximately parallel to the alkylidyne bond (Mo–C1; deviation, 0.07(8)° and 0.46(6)°, respectively) and display a dihedral angle of 35.44(6)° between them. The alkylidyne functionality, *trans* to N2, is almost linear (Mo–C1–C2 178.26(16)°) and features a slightly elongated Mo–C1 triple bond (1.771(2) Å).

Conducted at low temperature (–40 °C) to motivate the stabilisation of the deprotiometallacycle, the combination of complex **1** with phenylacetylene and bipy produced only the already known chelated version of **1**, complex **28** (Scheme 58), as judged by NMR spectroscopy. It is also interesting to note that complex **28** was similarly generated from a mixture of **1**, mesitylacetylene (MesC≡CH), and bipy.

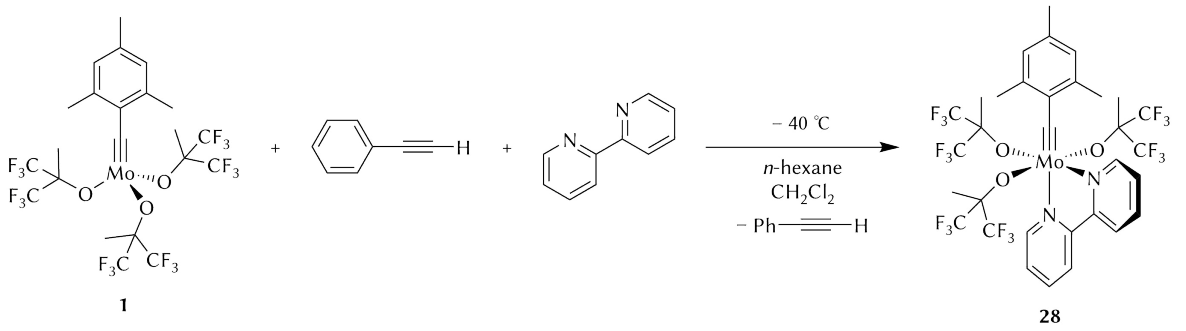

Scheme 58. Reaction of complex **1** with phenylacetylene and 2,2′-bipyridine applying low temperatures.

Even in the presence of Et_3N to promote deprotonation of the MCBD and elimination of the alcohol as an ammonium salt, and maintaining low-temperature conditions, no other than the cross-metathesis products (**42** and MesC≡CH) were identified by NMR analyses. Unexpectedly though, after addition of phenylacetylene at –50 °C, and before the other reactants had been added, the reaction mixture turned green for a few seconds before changing back to brown. The intermediate responsible for this chromatic change is still unknown, but since DPMCBD complexes have been occasionally reported to be green,[79] this should be investigated in the future.

In a similar manner, aliphatic alkynes react with **1** and bipy to generate new chelated alkylidyne complexes. For example, combination of complex **1** with 1-heptyne in the presence of bipy at room temperature afforded the deep red hexylidyne complex *mer*-[Mo(≡C(CH_2)$_4$Me)(bipy)(OC(CF_3)$_2$Me)$_3$] (**43**, Scheme 59, top). The molecular structure (Figure 56) was confirmed by NMR spectroscopy and X-ray diffraction analysis of single-crystals obtained from a cold *n*-hexane/dichloromethane solution. The complex crystallises in the monoclinic space group $P2_1/n$, and is isostructural to the other characterised bipy complexes **28** and **42**, in that the alkoxide ligands are organised in the *mer* conformation and the planar bipy unit (r.m.s. deviation 0.0175(11) Å) is aligned parallel to the Mo–C1 alkylidyne bond (deviation 0.47(3)°). As a consequence, all atoms in the bipy ligand are chemically inequivalent. The molybdenum core possesses a distorted octahedral geometry (*cis*, 71.64(4)°–103.30(5)°; *trans*, 152.35(4)°–171.51(5)°) with the metal atom lying 0.4095(1) Å above the l.s. plane N2, O1, O2, O3 (r.m.s. deviation 0.0097(9) Å). Except for the Mo–N1 bond distance, which is significantly elongated (2.3636(10) Å),[189] the other Mo–X bond lengths (X = C1, N2, O1, O2, O3) are all in the expected range.

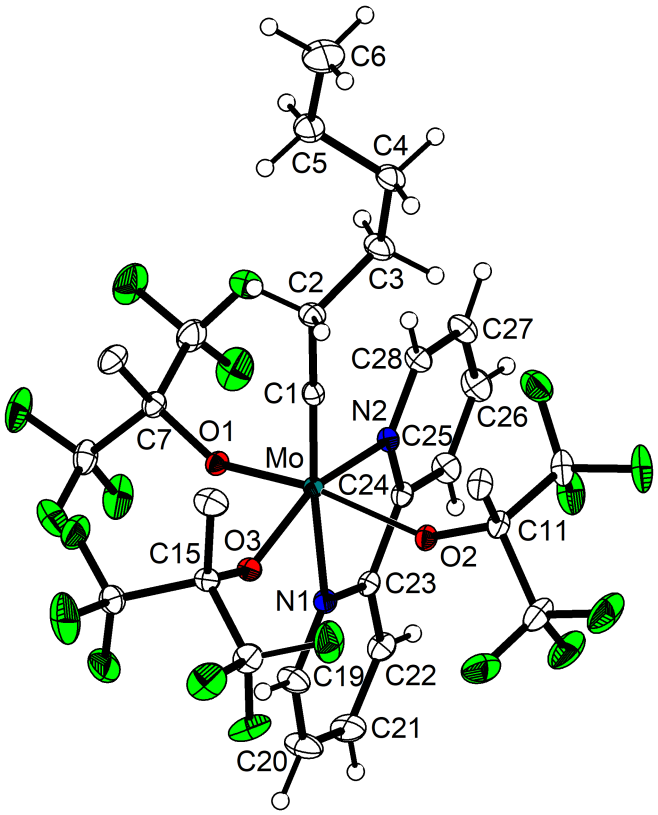

Figure 56. Molecular structure of **43** with thermal displacement parameters drawn at the 50% probability level. Selected bond lengths (Å) and angles (deg): Mo–C1 1.7611(13), Mo–N1 2.3636(10), Mo–N2 2.2560(10), Mo–O1 1.9714(9), Mo–O2 1.9723(9), Mo–O3 1.9492(9), N1–C23 1.3395(16), N2–C24 1.3555(16), C1–C2 1.4837(17), C23–C24 1.4840(18); C1–Mo–N1 171.51(5), C1–Mo–N2 99.87(5), C1–Mo–O1 101.11(5), C1–Mo–O2 102.14(5), C1–Mo–O3 103.30(5), N1–Mo–N2 71.64(4), N1–Mo–O1 77.85(4), N1–Mo–O2 76.94(4), N1–Mo–O3 85.19(4), N2–Mo–O1 80.69(4), N2–Mo–O2 80.77(4), N2–Mo–O3 156.83(4), O1–Mo–O2 152.35(4), O1–Mo–O3 94.77(4), O2–Mo–O3 94.25(4), Mo–C1–C2 179.17(11), Mo–N1–C23 116.04(8), Mo–N2–C24 118.44(8), N1–C23–C24 116.30(11), N2–C24–C23 117.55(11).

Importantly, the by-product of the cross-metathesis reaction was not mesitylethyne (MesC≡CH) but bis(mesityl)acetylene (**27**, Scheme 59), which involves the concomitant formation of acetylene (HC≡CH). Most likely, as discussed above for the synthesis of **32**, formation of **27** over MesC≡CH proceeds under thermodynamic control. Even if the reaction was performed in the absence of bipy, hexylidyne complex $[Mo(\equiv C(CH_2)_4Me)(OC(CF_3)_2Me)_3]$ (**44**) and alkyne **27** were the main products of the reaction, along with some unidentified impurities and variable amounts of an insoluble polymeric or oligomeric solid depending on the number of 1-heptyne equivalents (Scheme 59, bottom). In both cases, not only was the alkyne by-product identified in solution by NMR spectroscopy,[249,250] but it was additionally characterised by X-ray diffraction analysis; the molecular structure of this alkyne has so far not been reported.

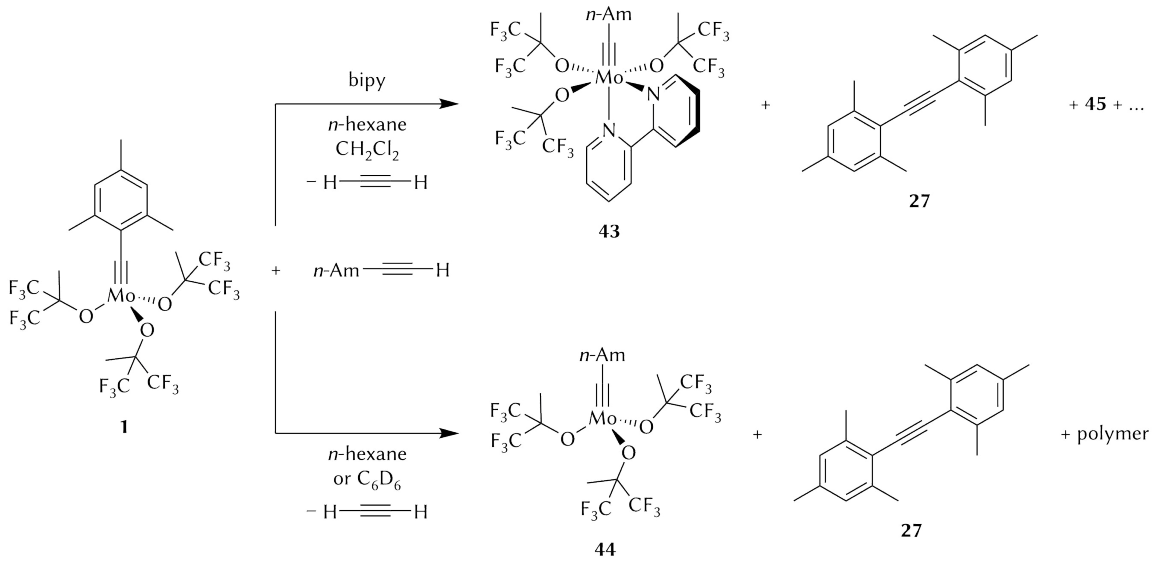

Scheme 59. Cross-metathesis of alkylidyne complex **1** with 1-heptyne in the presence (top) and in the absence (bottom) of 2,2′-bipyridine (bipy). Alkyne **27** is formed as a by-product in both reactions.

Compound **27** crystallises in the monoclinic space group $P2_1/n$, and the structure displays a virtually planar carbon skeleton (r.m.s. deviation 0.0677(12) Å), which results in approximate D_{2h} symmetry (Figure 57). Accordingly, the aryl rings are nearly coplanar, with an angle of 7.06(4)° between the l.s. planes through the six carbon atoms that form them (r.m.s. deviation: ring at C3, 0.0034(12) Å; ring at C12, 0.0071(12) Å). As expected for a triple bond, which connects two sp-hybridised carbon atoms, the central atoms C3, C1, C2, C12 are aligned (r.m.s. deviation 0.0169(16) Å). This carbon chain features almost straight angles (C2–C1–C3, 178.03(12)° and C1–C2–C12, 179.21(13)°) and parallels one of the pseudo-C_2 axis of the molecule. The C1–C2 bond length (1.2058(18) Å) is in the expected range for a C–C triple bond.[192]

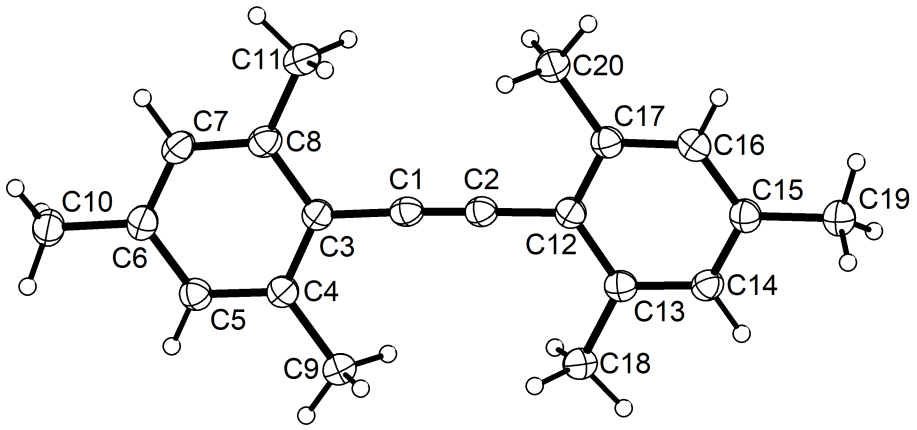

Figure 57. Molecular structure of **27** with thermal displacement parameters drawn at the 50% probability level. Selected bond lengths (Å) and angles (deg): C1–C2 1.2058(18), C1–C3 1.4316(16), C2–C12 1.4323(16); C2–C1–C3 178.03(12), C1–C2–C12 179.21(13).

In addition to all discussed products, a few green crystals of a degradation product co-precipitated along with **43** from the reaction of **1** with 1-heptyne and bipy (Scheme 59, top). The structure was established by X-ray diffraction analysis (Figure 58) and consists of the oxo species *mer*-[Mo(≡O)(bipy)(OC(CF$_3$)$_2$Me)$_3$] (**45**), which crystallises in the triclinic space group $P\bar{1}$ with two independent molecules in the asymmetric unit. The metal centre is in the formal oxidation state +V and displays a distorted octahedral geometry with N1–Mo–N2 and N1′–Mo′–N2′ being the most acute angles (70.27(5)° and 70.81(5)°, respectively) caused by chelation of the bipy ligand. The particularly short Mo–O4 (1.6730(11) Å) and Mo′–O4′ (1.6748(11) Å) bond lengths indicate a Mo–O triple bond,[54,192] and the Mo–N distances are comparable with those of bipy complexes **28**, **42**, and **43**, in which the bond *trans* to the Mo≡X moiety (Mo–N1 and Mo′–N1′ in **45**; X = O for **45**, otherwise X = CR) is substantially longer than the other Mo–N bond. Among other valid explanations, the formation of the undesired compound can be rationalised by hydrolysis with residual water of the solvents employed.

Further attempts to promote DPMCBD formation by using DME to trap and stabilise the deprotonated metallacycle were also unsuccessful. More promising was the use of an aminic base to aid in the proton abstraction. Thus, addition of Et$_3$N and bipy to a cold mixture of **1** and 1-heptyne in diethyl ether (Scheme 60) produced a colour

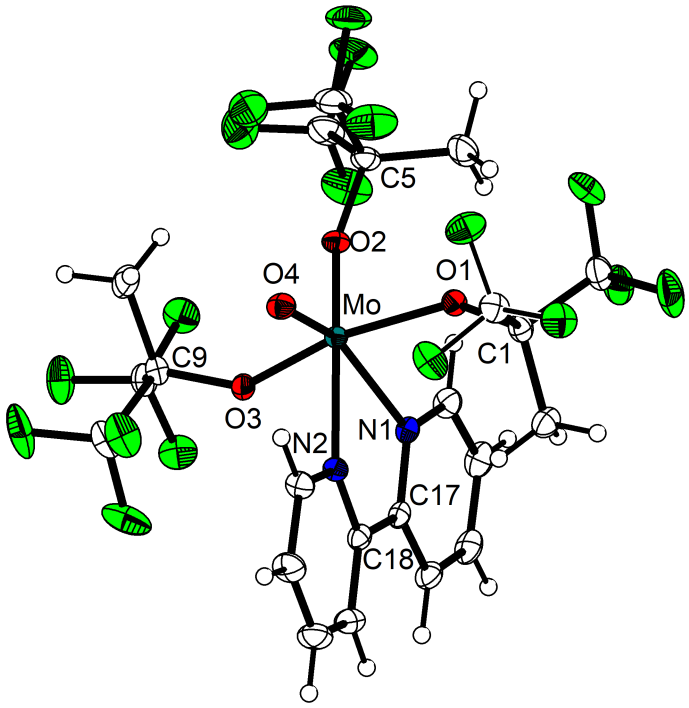

Figure 58. Molecular structure of one independent molecule of **45** with thermal displacement parameters drawn at the 50% probability level. For selected bond lengths and angles, see Figure 87, p 191.

change from red to brownish-violet upon warming up to ambient temperature. After removal of the solvent and a two-step extraction with *n*-pentane and diethyl ether, both extracts were stored separately at –30 °C for crystallisation. Three types of crystals with different shapes and shades precipitated from these solutions (Figure 59); in the *n*-pentane fraction colourless and violet crystals formed, whereas large, deep red crystals were found in the ether solution. The latter were analysed by X-ray diffraction techniques, which revealed indeed the structure of DPMCBD complex **46** (Figure 60).

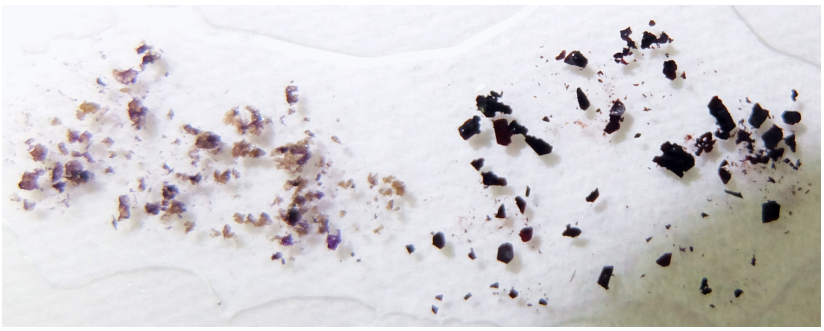

Figure 59. Different types of crystals obtained in the *n*-pentane fraction (violet and colourless, left) and in the diethyl ether fraction (deep red, right).

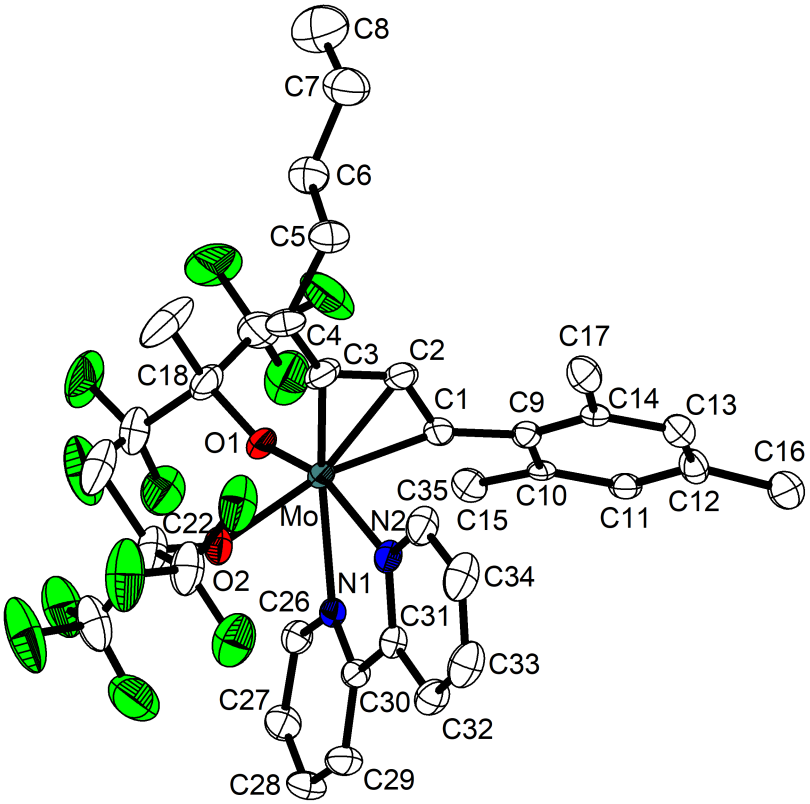

Figure 60. Molecular structure of **46**·Et_2O with thermal displacement parameters drawn at the 50% probability level. Minor components of disordered pentyl chain (at C3) and disordered mesityl group (at C1), a diethyl ether solvate molecule, and hydrogen atoms are omitted for clarity. For selected bond lengths and angles, see Figure 88, p 194.

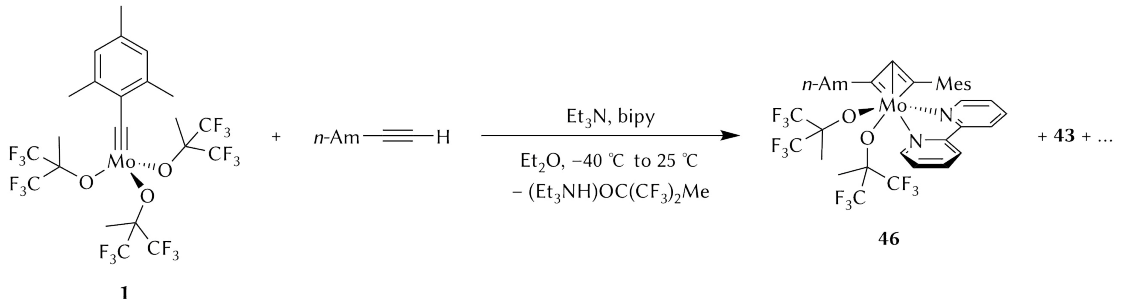

1 46

Scheme 60. Formation of DPMCBD complex **46** upon reaction of **1** with 1-heptyne in the presence of Et_3N and bipy. Other products were also obtained.

Compound **46** crystallises in the monoclinic space group $P2_1/c$ as a diethyl ether solvate, and consists of an asymmetrically substituted deprotiomolybdenacyclobutadiene complex carrying a bipy molecule and two alkoxide ligands coordinated *cis* to each other. Notably, the molecule formed regioselectively concerning the substitution at the DPMCBD ring, so that the alternative isomer with interchanged *n*-amyl and mesityl groups was not observed. Although the hydrocarbon substituents suffer from severe disorder, and had to be refined over several positions, the quality of the final structure is sufficient for an analytical discussion. The structure is best described as a distorted capped octahedron, with the central (β) carbon atom in the DPMCBD occupying the capping position. The four-membered ring is nearly planar (r.m.s. deviation 0.009(3) Å) with the molybdenum atom lying 0.0729(4) Å above the plane through atoms C1, C2, C3. The angle between these atoms (135.2(3)°) is much wider than the opposite angle C1–Mo–C3 of 81.18(13)°; of the three Mo–C bonds the Mo–C3 bond is the shortest (1.925(3) Å), whereas the other two bond lengths are surprisingly similar (2.006(3) Å, 2.020(3) Å). The bipy ligand is nearly planar (r.m.s. deviation 0.090(2) Å), and resides in the same face as the C1–mesityl moiety with an almost perpendicular orientation (89.82(9)°) to the metallacycle fragment. As expected, the N1–Mo–N2 angle is particularly narrow (71.92(7)°), wherein atom N2 is closer to the metal centre (2.251(2) Å) than atom N1 (2.3128(19) Å), which is coordinated *trans* to atom C3.

NMR analyses of the crystals are also consistent with the DPMCBD structure in solution. Interestingly, compared with alkylidyne complexes **28** and **43**, the ^1H resonances for the mesityl and *n*-amyl substituents, and also for the bipy ligand are considerably shifted into the low field. In contrast, the methyl protons on the alkoxide groups are particularly shielded with a low-frequency chemical shift of δ_H = 0.68 ppm. Differences in the $^{13}C\{^1H\}$ NMR spectrum are much less pronounced, yet the fluorinated

ligands display slightly high-field-shifted signals for the methyl group (δ_C = 17.1 ppm) and the central carbon atom (δ_C = 79.8 ppm). In addition, the diastereotopic CF_3 groups are resolved as two quartets in the $^{19}F\{^1H\}$ NMR spectrum (δ_F = –78.3 ppm and δ_F = –77.9 ppm) although this is not the case in the carbon spectrum, in which the two expected quartets overlap at δ_C = 124.3 ppm. Most remarkably, the signals at δ_C = 207.7 ppm, δ_C = 213.9 ppm, and δ_C = 228.0 ppm (Figure 61) are characteristic for the carbon atoms in the DPMCBD ring, where the first peak is assigned to the atom at the β-position and the other two correspond to the α-positions. These values are in the range reported for other DPMCBD complexes of molybdenum[79,211] and tungsten.[71]

It should briefly be mentioned that unreacted bipy as well as minor amounts of unidentified side-products are also observed in the NMR spectra. A careful look into the region of the spectrum depicted in Figure 61, however, reveals additional signals also in this region, which suggest the presence of other DPMCBD species, perhaps the symmetrically substituted bis(*n*-amyl) or bis(mesityl) analogues.

As presented above, two different types of crystals were formed in the *n*-pentane solution from the extraction. Unfortunately, they were not suitable for crystallographic analyses and it can only be speculated about the nature of these products. The colourless crystals are most likely an organic compound, potential candidates include ammonium salt $(Et_3NH)(OC(CF_3)_2Me)$, 2,2′-bipyridine, or bis(mesityl)acetylene (**27**). The violet crystals must contain a metal atom; potentially, complex **46** crystallised there either without solvent molecules, as an *n*-pentane solvate, or in another space group. Otherwise, as discussed for the NMR data, symmetrically substituted DPMCBD complexes may have additionally formed, or even the formation of MCBD species cannot be excluded. From the mother liquor of this mixture, however, additional crystals

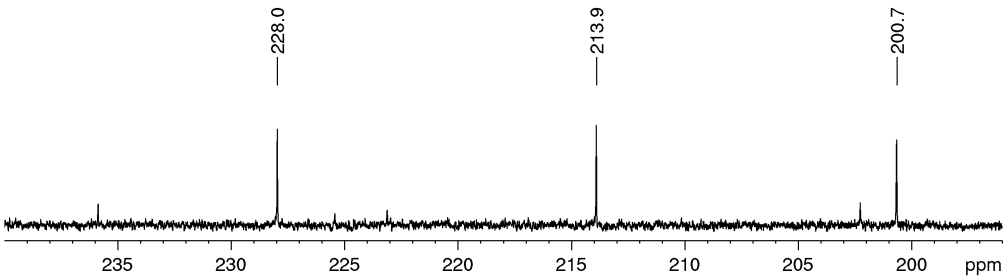

Figure 61. Detail of the $^{13}C\{^1H\}$ NMR spectrum of **46** in benzene-d_6 showing the characteristic carbon resonances for the atoms in the DPMCBD ring. Additional signals indicate the formation of other DPMCBD species.

were obtained, which were identified crystallographically as alkylidyne complex **43** (see Scheme 60). That evidences the formation of cross-metathesis products, and hence, suggests that the deprotonation reaction might not be quantitative.

All the difficulties encountered and discussed in this subchapter concerning the isolation of an DPMCBD complex based on **1**, together with the fact that its formation was neither straightforward nor quantitative, and only attainable under forcing conditions (addition of a base and a strong donor ligand), entirely sustain the conviction that complex **1** is a marvellous TAM catalyst. Because of its remarkable activity and the poor basicity of the fluorinated alkoxide ligands, the metathesis reaction operates under kinetic control, and deactivation pathways are almost prevented. Under regular conditions, the MCBD intermediate with a hydrogen atom at the β-position will be preserved from deprotonation, which is not expected to occur – as demonstrated herein – unless Lewis and Brønsted–Lowry bases are present.

3.4. Catalytic Studies

3.4.1. Determination of calibration curves for gas chromatography analysis

Routinely, the time-dependent conversion of metathesis substrates is followed by gas chromatography (GC) analyses, and it is approximately determined by comparing the area ratio of the alkyne (substrate, *s*) to *n*-decane (reference, *r*) at a given time *t* ($A_{s,t}$ / $A_{r,t}$) with the area ratio at $t = 0$ ($A_{s,0}$ / $A_{r,0}$). The inaccuracy of this method is offset by the determination of isolated yields, which help sustain the conversion values. This procedure is valid and unquestionably useful to study the substrate scope of a particular catalyst. However, it is too laborious and time-consuming for systematic studies, in which the activity in alkyne metathesis is compared for different complexes using the same benchmark substrates. As introduced in Figure 11, the internal and terminal alkynes $BnO(CH_2)_2C{\equiv}CR$ (**Y**-Me, R =Me; **Y**-H, R =H; Bn = benzyl) have been established in our group as standard substrates.

In this regard, an alternative method based on reliable gas chromatographic quantification was implemented, and calibration curves were determined for both **Y**-Me and **Y**-H, and also for the corresponding metathesis product 1,6-bis(benzyloxy)-3-hexyne (**47**). Multiple-point internal calibration was applied in all cases, using *n*-decane as internal standard.

For the preparation of the samples, different amounts of the alkynes precisely weighed in the range of 0–1.5 mg were dissolved with exactly 1 mL of a volumetric solution of *n*-decane in diethyl ether ($c = 1$ g L^{-1}). The samples were then analysed by GC applying standard conditions, and the data were fitted using linear regression. The resulting calibration curves and equations are presented in Figure 62. Hence, given the determined area ratio alkyne/*n*-decane (A_s / A_r; *s* = **Y**-Me, **Y**-H, **47**) for any experimental sample, the amount of alkyne (m_s) present in the sample can be calculated using the corresponding equation.

3.4.2. Catalytic activity in self-metathesis

Employing the calibration parameters, the catalytic performance of all new alkylidyne complexes presented in this dissertation was compared in the self-metathesis of **Y**-Me at ambient temperature (Scheme 61). In a standard setup, the complexes were added

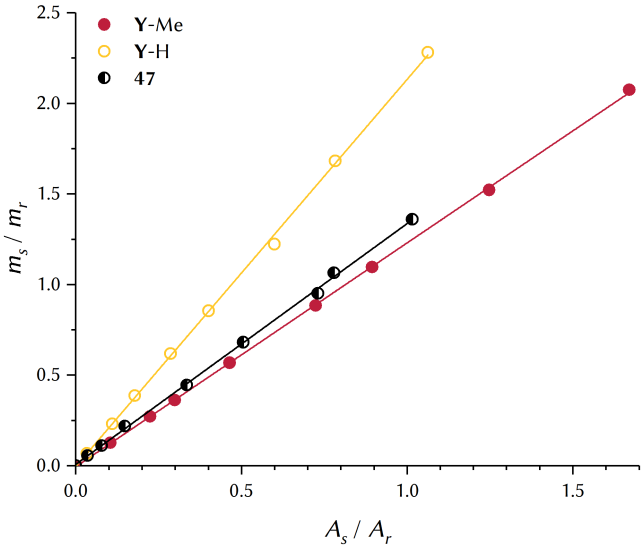

$$\frac{m_{\mathbf{Y}\text{-Me}}}{m_r} = 1.2361\frac{A_{\mathbf{Y}\text{-Me}}}{A_r} - 0.0061 \qquad r = 0.9999$$

$$\frac{m_{\mathbf{Y}\text{-H}}}{m_r} = 2.1371\frac{A_{\mathbf{Y}\text{-H}}}{A_r} - 0.0046 \qquad r = 0.9996$$

$$\frac{m_{\mathbf{47}}}{m_r} = 1.3295\frac{A_{\mathbf{47}}}{A_r} + 0.0070 \qquad r = 0.9996$$

Figure 62. Calibration curves for quantitative GC analysis of **Y**-Me, **Y**-H, and **47** (left); equations of the linear regression including the corresponding correlation coefficients *r* (right).

to a toluene mixture of the substrate and *n*-decane (0.25 mmol both) in the presence of powdered molecular sieves 5 Å, used as 2-butyne scavenger to drive the reaction to completion. In all cases the tests were conducted with 1 mol% (10^4 ppm) catalyst load-

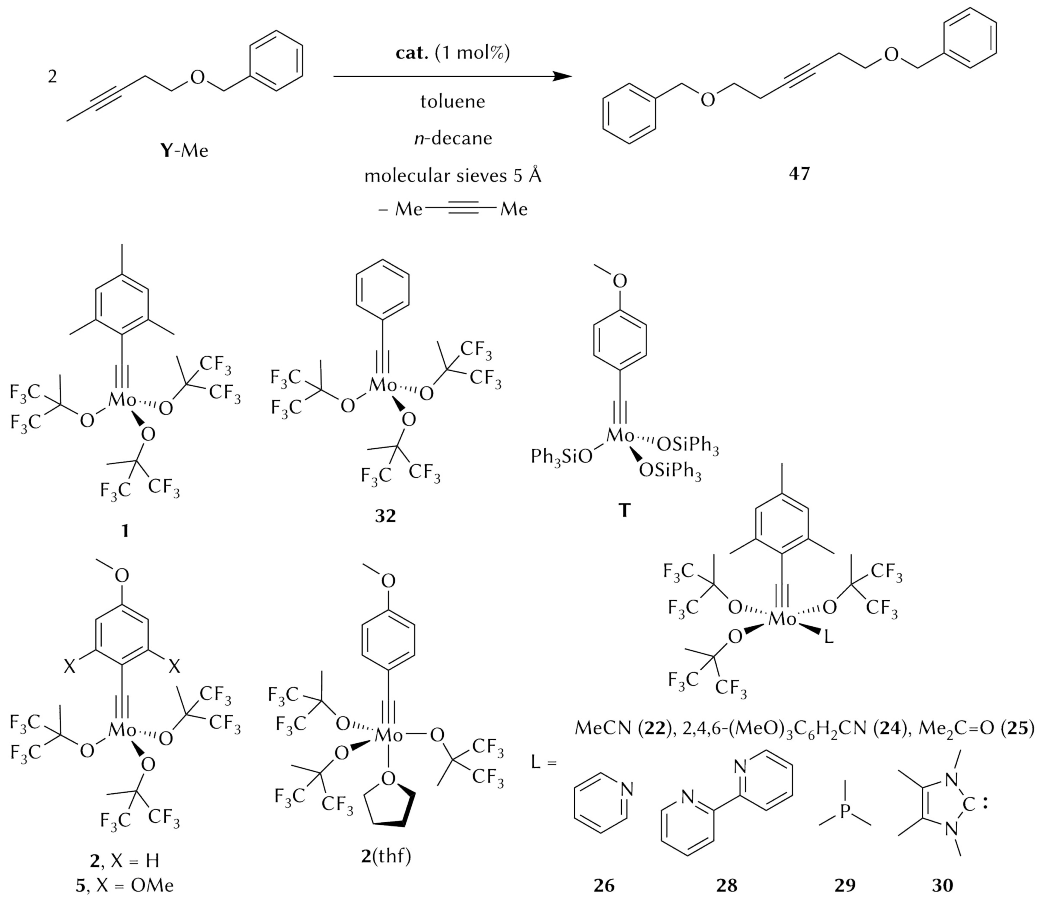

Scheme 61. The ACM (self-metathesis) of **Y**-Me (top) was used to test and compare the catalytic activity of several alkylidyne complexes (bottom); cat. = catalyst.

ings (not optimised), and the conversion was monitored by GC analyses. The results are summarised in Figure 63. To complete data analysis, the turnover numbers (TON) after 1 h and the turnover frequencies (TOF) at t = 2 min and t = 10 min for all tested complexes are presented in Figure 64. For comparison, complexes **1** and **T** have also been included.

Except for a few exceptions that will be discussed below, the studied compounds are highly active and achieved >90% conversion in only 10 min. The TONs after 1 h (92–98) are excellent given the catalyst loading employed, although this parameter was not further optimised. While some complexes initiate faster than others (cf. $TOF_{2\ min}$ values, Figure 64), the TOFs at t = 10 min, except for complexes **28**, **29**, and **30** ($TOF_{10\ min} < 0.12\ s^{-1}$), are rather homogeneous (0.15–0.16 s^{-1}). That can be reasoned by the fact that the active species, once formed, is the same independent of the initiator.

Unsubstituted benzylidyne complex **32** performed almost equally as the extensively used complexes **1** and **T**. Furthermore, coordination of a nitrile molecule (complexes **22** and **24**), acetone (complex **25**), or pyridine (complex **26**) did not seem to affect the

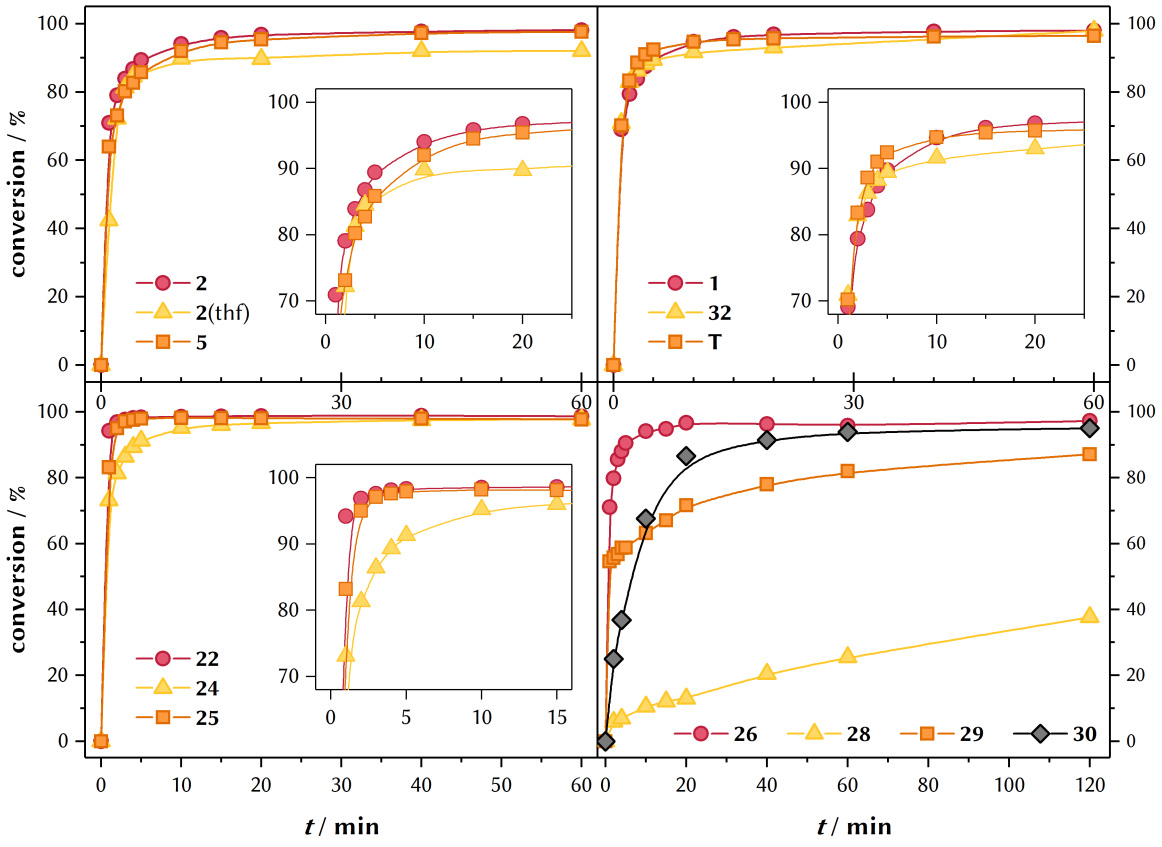

Figure 63. GC conversion–time plots for the ACM of **Y**-Me (0.25 mmol) in toluene (0.2 M) at ambient temperature with 1 mol% catalyst loadings in the presence of molecular sieves 5 Å (250 mg) and *n*-decane (0.25 mmol) as internal standard. The insets show expanded regions for clarity.

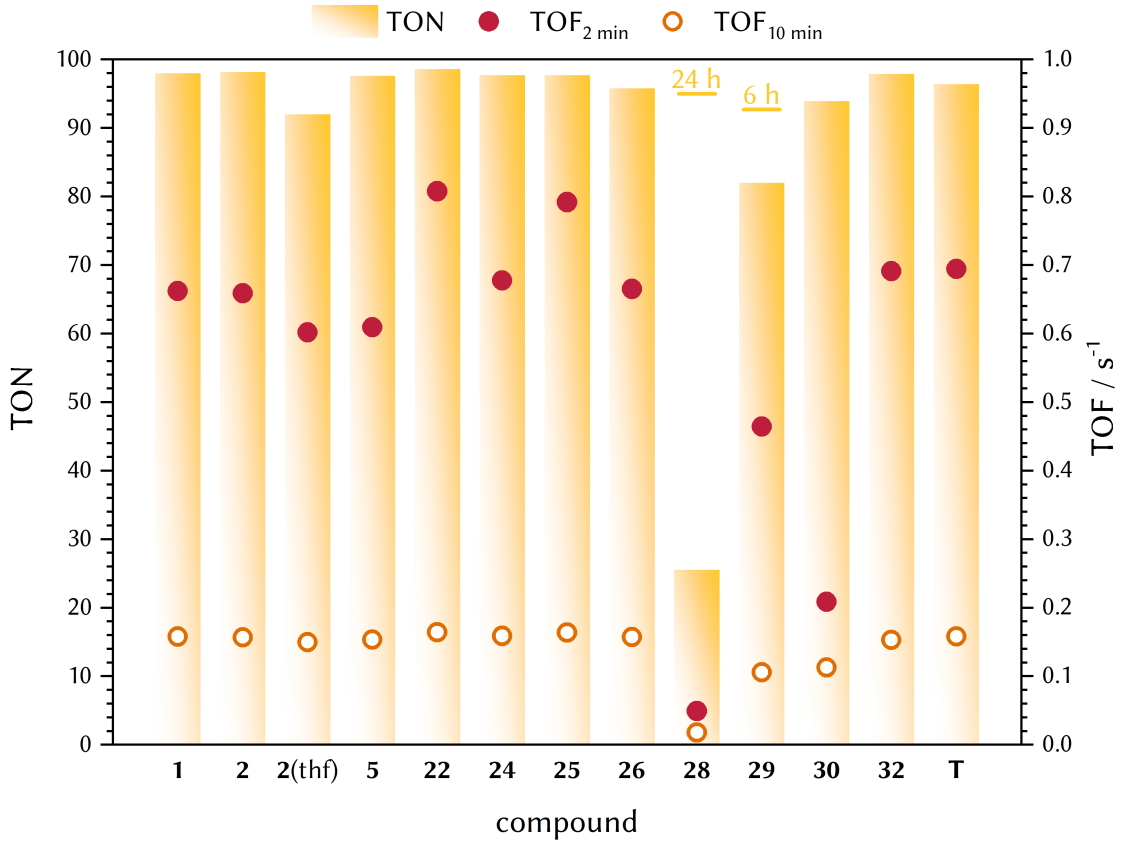

Figure 64. TONs after 1 h and TOFs at t = 2 min ($TOF_{2\ min}$) and at t = 10 min ($TOF_{10\ min}$) for all tested compounds. In addition, the TONs after 24 h and 6 h are also indicated, respectively, for complexes **28** and **29**.

catalytic performance, whereas other coordinated bases, as already mentioned, resulted in more or less significantly decreased activities depending on the ligand (complexes **28**, **29**, and **30**). The lowest activity was found for the bipy derivative **28** (TON = 26). That is reasonable because the bipy moiety, which is a bidentate ligand, saturates all free coordination sites at the metal centre and has to be displaced for the substrate to bind. Remarkably enough, while other reported bipy alkylidyne complexes showed no activity in alkyne metathesis,[84] **28** reached 95% conversion at ambient temperature after 24 h. Similarly, the presence of PMe_3 partially inhibited the catalyst (TON = 82), but after 6 h the substrate had been converted to 93%.

Also the presence of THF in complex **2** did not interfere substantially in the catalytic activity, which was otherwise excellent for the THF-free complexes **2** and **5**. Indeed, the TOFs at t = 10 min ($TOF_{10\ min}$(**2**) = 0.157 s^{-1}, $TOF_{10\ min}$(**5**) = 0.153 s^{-1}) are comparable to those of complexes **1**, **32** or **T** ($TOF_{10\ min}$(**1**) = 0.158 s^{-1}, $TOF_{10\ min}$(**32**) = 0.153 s^{-1}, $TOF_{10\ min}$(**T**) = 0.158 s^{-1}), and the small drop in the performance of [**2**(thf)] ($TOF_{10\ min}$ = 0.150 s^{-1}) is almost negligible.

It can therefore be assumed that some coordinated molecules (nitriles, acetone, py or THF) are easily displaced by the alkyne substrate.[49,84,171] Indeed, dissociation of acetonitrile in complex **22** was confirmed by NMR spectroscopy. Addition of a slight excess (~2 equiv) of **Y**-Me to an NMR sample of **22** showed a complex mixture of products, yet none of the original resonances of **22** was still observed. Two new sets of signals indicated instead the presence of two distinct mesityl moieties, which are supposed to be part of other alkyne molecules (probably **27** and MesC≡C$(CH_2)_2$OBn). Additional signals reflected the formation of alkylidyne complex [Mo(≡C$(CH_2)_2$OBn)(OC$(CF_3)_2$Me)$_3$]. Finally, the signal for the acetonitrile methylic protons, albeit broadened, was in agreement with the chemical shift of the free nitrile. The broadness of the peak was presumably occasioned by a dynamic process, whereby acetonitrile dissociation and association occurred recurrently in the NMR timescale.

In the same way, the intermolecular coordination observed in **2** and **5** in the solid state is believed to disappear upon dissolution or alkyne binding. In contrast, dissociation of more strongly coordinated ligands such as bipy, PMe_3, or Im^{Me_4} (in **28**, **29**, and **30**, respectively) is less favoured and competes directly with substrate binding, which results in relatively lower initiation and conversion rates, as evidenced, respectively, by the TOFs at t = 2 min ($TOF_{2\ min}$(**28**) = 0.05 s^{-1}, $TOF_{2\ min}$(**29**) = 0.46 s^{-1}, $TOF_{2\ min}$(**30**) = 0.21 s^{-1}) and at t = 10 min ($TOF_{10\ min}$(**28**) = 0.018 s^{-1}, $TOF_{10\ min}$(**29**) = 0.105 s^{-1}, $TOF_{10\ min}$(**30**) = 0.113 s^{-1}).

Catalytic activity in TAM

Complexes **5** and **32** were also used in the TAM of substrate **Y**-H. For this reaction, 1 mol% catalyst was added to a diluted toluene solution of the alkyne (0.25 mmol, c = 20 mM) in the presence of *n*-decane and molecular sieves 5 Å (Scheme 62). Although both compounds were less active than in internal alkyne metathesis, the initial rates were still very high ($TOF_{2\ min}$(**5**) = 0.70 s^{-1}, $TOF_{2\ min}$(**32**) = 0.76 s^{-1}), and good TONs of

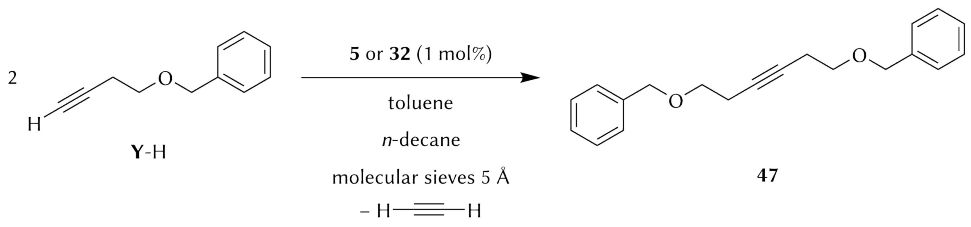

Scheme 62. The catalytic activity of **5** and **32** was tested in the TAM of **Y**-H with 1 mol% catalyst loadings.

86 and 93 were achieved within 1 h. The conversion increment, however, is nearly imperceptible after $t = 5$ min, which suggests that the catalysts deactivated under the applied conditions in the first few minutes.

3.4.3. Identification of air-stable compounds

An important goal of this project was the preparation of bench-stable complexes that are still active catalysts in alkyne metathesis. Functionalised benzylidyne complexes **2** and **5** may exhibit (moderate) air-stability in the solid state based on the hypothesis that the described intermolecular contacts render the molecules robust towards air and moisture. In a preliminary experiment, a sample of compound **5** was exposed for 1 h to air before the ACM of **Y**-Me was repeated under standard conditions. Unfortunately, the catalytic activity decreased dramatically, and after 1 h only a marginal conversion of 4% was determined by GC analysis. In view of these discouraging results no further tests were conducted with the methoxy-substituted benzylidyne complexes.

Other potentially robust candidates are the adducts **22**, **24–26**, and **28–30** because of the additional coordination of a donor ligand, which occupies one vacant site (or two in **28**) and whose basic properties decreases the electrophilicity of the metal centre. In spite of that, degradation of solid samples was observed for most of these compounds after exposure to air. This is not surprising, as, for the most part, they do not exhibit reduced catalytic activities. Only complexes **28–30** are associated with significantly lower activities, and therefore, might feature some air-stability. As already described in Chapter 3.2.2, PMe_3 complex **29** perceptibly decomposed after a short period of time, but crystalline samples of **28** and **30** remained intact for several hours or even days. This was confirmed by elemental analysis, and the elemental composition of both compounds experienced no changes after 1 h of exposure to air.

Most remarkably, the elemental analysis of NHC complex **30** yielded the expected values even after storing the sample for 24 h under non-inert conditions. Aside from its robustness, the catalytic performance of **30** at ambient temperature is not far beyond that of most active catalysts, and activation with external reagents is not required. These two aspects make **30** an interesting precatalyst, for which further air-stability tests, and also catalytic and mechanistic studies shall be conducted in the future.

4 Concluding Remarks

4.1. Summary

In this dissertation, several strategies to functionalise and modify the ligand environment of molybdenum benzylidyne complexes have been examined, with the ultimate goal being the synthesis of bench-stable catalysts for alkyne metathesis. These strategies (Figure 65) included i) the introduction of ether groups on the benzylidyne moiety to achieve inter- or intramolecular contacts under certain conditions, ii) the coordination of donor ligands to increase the coordination number at the metal centre, and iii) the use of alkyne substrates in stoichiometric reactions to either generate the cross-metathesis alkylidyne product or trap important metallacyclic species.

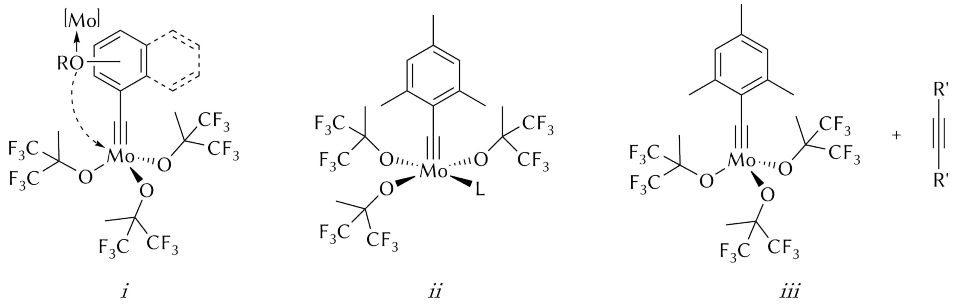

Figure 65. Strategies explored in this work for the functionalisation of molybdenum alkylidyne complexes.

In the first chapter, the preparation of ether-functionalised molybdenum benzylidyne complexes and their precursors has been described; a synthetic overview is presented in Scheme 63. The installation of methoxy groups was successful in *para*-anisole derivative **2** and in trimethoxybenzylidyne complex **5**, whereas the isopropoxybenzylidyne or the methoxynaphthyl versions **3** and **4**, respectively, could not be accessed. In all cases, the synthesis was based on the well-established low-oxidation-state route, which involves oxidation of cationic acyl complexes of the type $[Mo(C(O)Ar)(CO)_5]^+$ into the versatile precursors *mer*-$[Mo(\equiv CAr)(Br)_3(dme)]$. The preparation of these intermediates, however, proved challenging, and therefore, it was crucial to introduce some changes to the standard synthetic protocols.

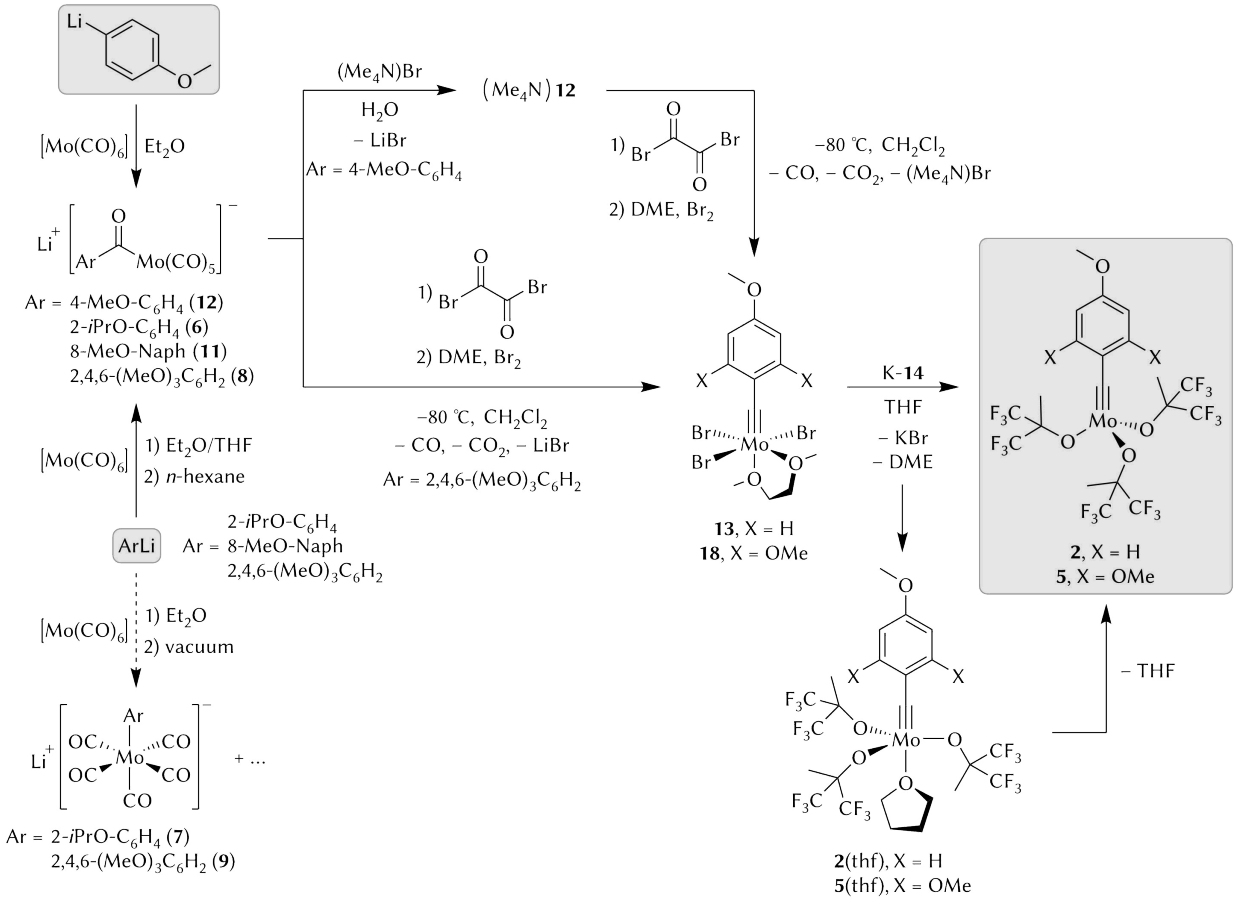

Scheme 63. Synthetic overview of molybdenum benzylidyne and acyl complexes functionalised with ether groups. Lithium reactants and final products are enclosed in a frame. The dashed arrow indicates a decomposition pathway (bottom left). DME = 1,2-dimethoxyethane, Naph = 1-naphthyl.

Undesired decarbonylation of acyl complexes Li-**6** and Li-**8** was the principal problem encountered, which was caused by the use of reduced pressure during solvent evaporation. This step is usually required before performing salt metathesis in water to obtain the tetramethylammonium counterparts. Thus, to avoid carbonyl deinsertion and formation of (aryl)pentacarbonyl complexes **7** and **9**, the lithium acyl complexes were isolated directly by precipitation. This methodology gives a more straightforward access to (acyl)pentacarbonylmolybdate complexes featuring challenging functional groups, and was successfully applied, for example, in the synthesis of naphthyl derivative Li-**11**. Despite this improvement, oxidation and bromination of Li-**6** and Li-**11** towards *mer*-[Mo(≡CAr)(Br)$_3$(dme)] (**15**, Ar = 2-*i*PrO-C$_6$H$_4$; **16**, Ar = 8-methoxynaphthyl) was not feasible under the applied conditions. Only Li-**8** could be transformed to carbyne complex **18**, yet as a crude product.

In addition, isolation of *para*-anisole complex Li-**12** proved to be more difficult than expected, and the corresponding tribrominated alkylidyne complex **13** had to be pre-

pared classically via the ammonium salt (Me_4N)**12**. Both alkylidyne complexes **13** and **18** were subjected to salt metathesis with three equivalents of K-**14**, and target compounds **2** and **5**, or their THF adducts [**2**(thf)] and [**5**(thf)], respectively, were obtained.

Notably, complexes **2** and **5** crystallised as 1D-coordination polymers, in which the methoxy group at the *para*-position was bridged to the neighbouring molecule forming zigzag chains (Figure 66). This constitutes the first example of intermolecularly coordinated metal alkylidynes. Unfortunately, the presence of intermolecular contacts in the solid state did not contribute to stabilise the complexes. Furthermore, the suitability of the *ortho*-methoxy groups in **5** to achieve MCBD species stabilised by intramolecular interactions was not demonstrated.

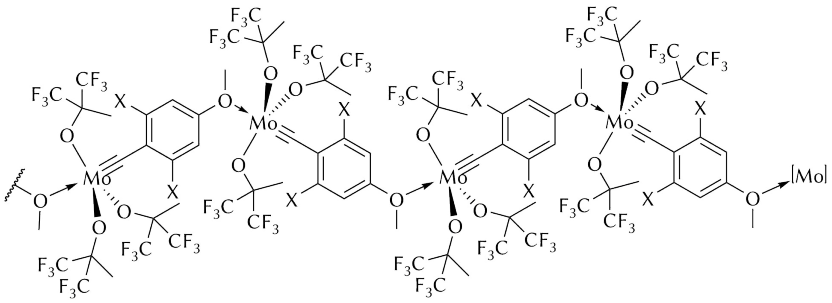

Figure 66. Complexes **2** (X = H) and **5** (X = OMe) form 1D-polymeric structures in the solid state.

Chapter 3.2 addressed the coordination of Lewis bases (L) to alkyne metathesis catalyst **1** in order to protect vacant sites at the metal centre, and hence, induce a stabilising effect (Scheme 64, right). The following ligands were combined with **1**, and yielded pentacoordinate complexes (indicated here in parenthesis): acetonitrile (**22**), 2,4,6-trimethoxybenzonitrile (**24**), acetone (**25**), pyridine (**26**), trimethylphosphane (**29**), and NHC ligand Im^{Me_4} (**30**). All these complexes feature a square-pyramidal geometry in the solid state, but a trigonal-bipyramidal arrangement or a dynamic interconversion between both conformations is generally observed in solution by NMR spectroscopy. In addition, coordination of 2,2′-bipyridine afforded octahedral complex **28**, which is analogous to other stable precatalysts reported in the literature.

Indeed, complexes **28** and **30** are particularly robust, and crystalline samples of these compounds showed no degradation after several hours of storage under non-inert conditions. The integrity of the samples was also supported by elemental analysis.

Beyond that, the reactivity of **1** with nitriles was also interesting because these molecules can undergo NACM or NCM. However, neither could be observed so far.

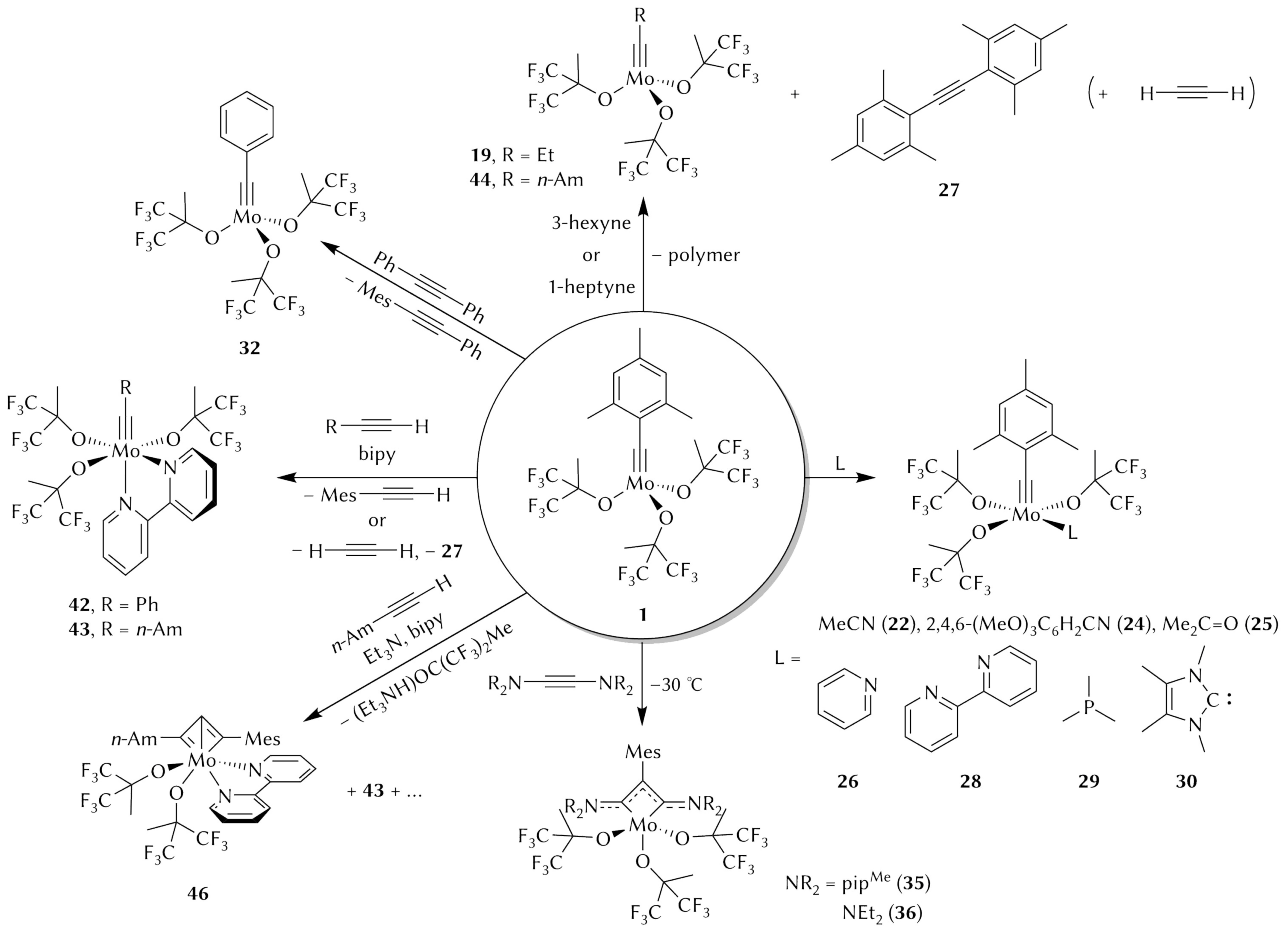

Scheme 64. Stoichiometric reactions of alkylidyne complex **1** with donor ligands (L, right), and with several acetylenes; bipy = 2,2′-bipyridine, Mes = mesityl, pip^{Me} = 4-methylpieridin-1-yl.

The attempted isolation of reaction intermediates involved in ACM or TAM has been discussed in Chapter 3.3. Thus, complex **1** was reacted with stoichiometric amounts of 3-hexyne, tolan, bis(diethylamino)acetylene (**33**), bis(4-methylpiperidino)acetylene (**34**), phenylacetylene, and 1-heptyne (see Scheme 64). Many attempts to trap MCBD species were unproductive, and mostly cross-metathesis products such as alkylidyne complexes **19**, **32**, or **44**, and also bis(aryl)alkynes (e.g. **27**) were obtained. Nevertheless, the use of ynediamines **34** and **33** produced, respectively, paramagnetic MCBD complexes **35** and **36**. Indeed, DFT calculations predicted considerably negative energies for the formation of **35** and **36** in the spin state $S = 1$, which explains the successful isolation of these metallacyclic systems. Thus, a further [2 + 2] cycloreversion step, required in catalytic alkyne metathesis, is disfavoured, and the metal remained sequestered in the form of a molybdenacyclobutadiene complex. In addition, the unusual paramagnetism of these systems was investigated with solid-state magnetic susceptibility techniques.

Although the reaction with tolan did not produce the desired MCBD species, the quantitative formation of benzylidyne complex **32** was of particular relevance because this complex does not carry an additional solvent molecule, as otherwise documented in the literature. Therefore, in analogy to **1**, a higher reactivity and catalytic activity was expected for this molecule. A direct application of this cross-metathesis reaction was the preparation of a ^{13}C-labelled benzylidyne complex from (1,2-$^{13}C_2$)-tolan (Scheme 65). In a cooperation project, complex **32′** was immobilised on partially dehydroxylated silica ($SiO_{2\,(700)}$) and employed in catalytic studies. Because it was isotopically enriched at the alkylidyne position, the conducted MAS NMR experiments were less time-consuming and more reliable.

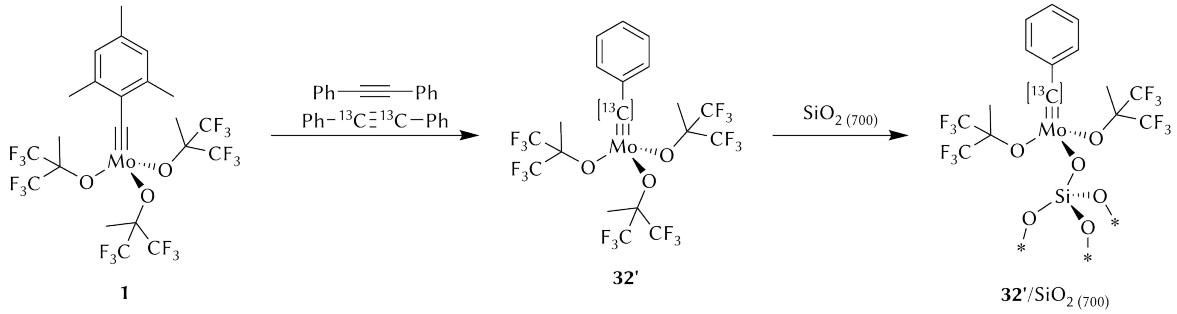

Scheme 65. Synthesis of ^{13}C-enriched complex **32′** and grafting on silica ($SiO_{2\,(700)}$).

Formation of DPMCBD complexes was another interesting target because these species are known to cause decomposition in TAM. For this purpose, aromatic and aliphatic terminal alkynes (i.e. phenylacetylene and 1-heptyne) were added to complex **1** in the presence of bipy, but merely chelated versions of the cross-metathesis products **32** and **44** could be isolated (**42** and **43**, respectively). Only after addition of an aminic base (Et_3N) to a mixture of **1**, 1-heptyne, and bipy, the DPMCBD complex **46** was generated (Scheme 64, bottom left).

Finally, it has been shown in Chapter 3.4 that all investigated alkylidyne complexes were able to promote the ACM of **Y**-Me, but diverse TON and TOF values were determined. Thus, while complexes **2**, **5**, and **32** are excellent initiators, the activities of penta- and hexacoordinated complexes [**1**(L)] presented significant differences. For example, nitrile adducts **22** and **24** performed similarly to the parent compound **1**, whereas coordination of some ligands such as Im^{Me_4}, PMe_3, or bipy resulted in low activities and reached good conversions only after, respectively, 2 h, 6 h, or 24 h.

4.2. Conclusions and Perspectives

Molybdenum benzylidyne complexes bearing fluorinated alkoxides are phenomenal catalysts for alkyne metathesis. In this dissertation, the portfolio of eligible complexes has been extended either by installation of ether substituents on the benzylidyne moiety or by coordination of a nucleophilic ligand to the metal centre. These modifications were intended to increase the robustness of the complexes without suppressing the catalytic performance.

In the first case, the synthesis of methoxy-substituted complexes **2** and **5** was successful, but the preparation of other benzylidyne derivatives (**3**, **4**) was not feasible under the applied conditions. Although alkylidyne complexes **2** and **5** were bridged intermolecularly in the solid state forming 1D-polymeric chains, that circumstance did not suffice to render the complexes stable towards air or moisture. Nevertheless, the formation of intermolecular interactions is unprecedented in metal alkylidyne complexes, and this strategy should be exploited using better donating functional groups (D) such as amines or phosphanes (Figure 67). Also the formation of chelated MCBD complexes (projected for complexes **3**, **4**, and **5**) remains challenging, but the use of chelating fragments containing other heteroatoms in place of the ether oxygen should also be examined (see Figure 67). As a matter of fact, this ligand variation has been already introduced in analogues of Hoveyda–Grubbs' catalysts with chelated nitrogen, phosphorous, sulphur, selenium, and halogens.[20] Moreover, (alkylidene)tetracarbonylmolybdenum complexes bearing ammine, sulphanyl, or phosphane chelating groups are known.[179,181] These complexes may provide inspiration or serve as the basis for the creation of new benzylidyne modified complexes. Besides, other heteroatoms can also replace the oxygen on the alkoxide ligands; for instance, alkylidyne thiolate complexes have already been reported.[251]

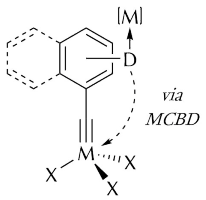

Figure 67. Proposed extension of the strategy that involves formation of inter- or intramolecular contacts in order to stabilise the complex; D = donor group, X = preferably a fluorinated alkoxide ligand, M = Mo, W.

In addition, in view of the fact that a larger number of tungstenacyclobutadiene compounds have been isolated, substituted benzylidyne complexes of the more electrophilic metal tungsten constitute a promising alternative that need to be investigated. To complete the triad, synthesis of chromium complexes might also be attempted.

To overcome the difficulties related to the synthetic protocol, in particular regarding the synthesis of key complexes *mer*-[Mo(≡CAr)(Br)$_3$(dme)], there are a few alternative routes, presented in the Introduction (p 16 ff), that can be useful to generate the desired products (Scheme 66). For example, cross-metathesis reactions involving the use of benzylidyne transfer reagents turned out to be successful in several occasions.[138,139] Also the metathetical combination of a functionalised alkyne or nitrile with bimetallic species of the type [X$_3$M≡MX$_3$] should be taken into consideration.

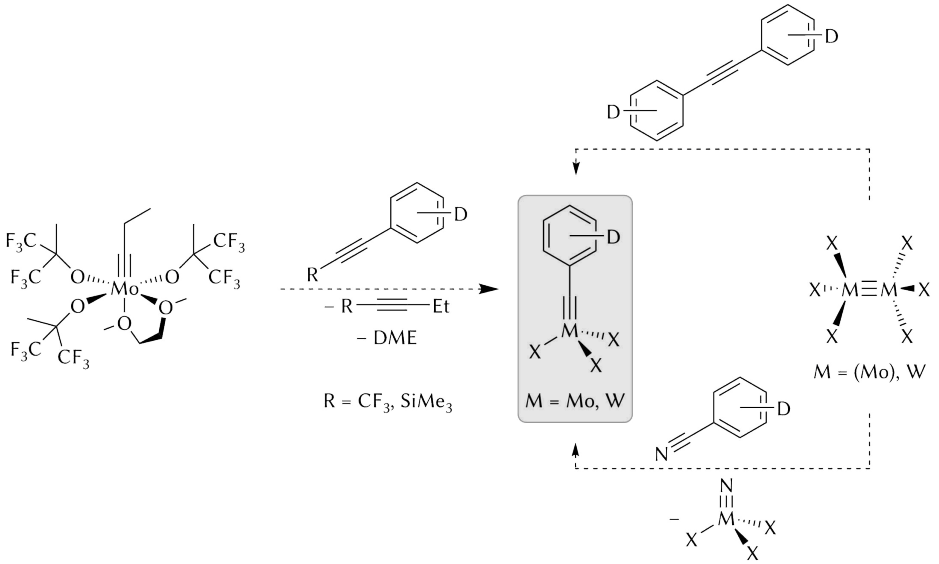

Scheme 66. Proposed alternative syntheses of benzylidyne complexes functionalised with nucleophilic groups; D = donor group, X = preferably a fluorinated alkoxide ligand; DME = 1,2-dimethoxyethane.

Regardless of that, it may be desirable to adjust the conditions of the low-oxidation-state route in order to obtain *mer*-[Mo(≡CAr)(Br)$_3$(dme)] in a more reliable manner. Thus, based on published examples,[112,117,118,252,253] the acyl precursors can be generated in situ, followed by oxidation and halogenation as usual, except for the preferred use of etheric solvents. As an alternative, other oxidising agents such as thionyl chloride,[117] trifluoroacetic anhydride[118] or phosgene[112,252] can be used. Moreover, this one-pot procedure should also avoid decarbonylation side-reactions.

Notwithstanding, it is remarkable that the procedure for preparing acyl complexes could be adjusted to access Fischer-carbene precursors carrying challenging func-

tional groups, for which otherwise synthetic strategies were missing. In particular, the precipitation approach prevented the undesired formation of decarbonylated products. Hence, functionalisation of the benzoyl complexes with other heteroatoms may also be possible using the protocol discussed in this dissertation.

Finally, the stabilisation of **1** with nucleophilic ligands provided promising results. Thus, bipy complex **28** and NHC adduct **30** qualified as robust compounds, although further tests may be necessary to confirm the long-term stability of the complexes. In addition, these complexes promoted the ACM of **Y**-Me at ambient temperature, and additional reagents were not required for activation. NHC complex **30** was particularly active, and reached almost full conversion in just 2 h. Therefore, the use of coordinating ligands should be explored further. That may include: other amine, NHC, and phosphane ligands; amides, sulphones, and thioethers; and also multidentate versions thereof.

Overall, it can be affirmed that the alkyne metathesis reaction is conceptually well understood, and prediction of catalyst stability and activity is progressively becoming more accurate. However, catalyst design is an undergoing challenge, and the optimal catalyst (highly active, selective, and user-friendly) still remains an ambitious goal.

5 Experimental Section

5.1. General Considerations

Except where indicated otherwise, all operations were performed under an atmosphere of dry argon either in a glove-box or using Schlenk and vacuum techniques. Prior to their use, all flasks and glass equipment were previously dried in a hot oven (130 °C) and were evacuated and refilled with argon three times. Celite (545) diatomaceous earth (D.E.), which was often used for filtrations, was stored at least three days in an oven at 130 °C. For alkyne metathesis reactions, the molecular sieve 5 Å (powder <50 μm) was dried for 24 h at 180 °C under vacuum prior to use.

High temperatures were achieved by using a silicone oil bath or a heating mantle, whereas low temperatures were generated using a cooling bath of ice in water or of an organic solvent (2-propanol, toluene, or diethyl ether) mixed with liquid nitrogen. A refrigerated circulating bath (ethanol) was used for specific reaction setups. For storage and crystallisation at low temperatures, the flasks and vials containing solutions or pure substances where placed in a freezer (temperature between –30 °C and –40 °C).

Solvents (except THF and water) used in air-sensitive reactions were purified and thoroughly dried by an MBraun GmbH solvent purification system and deoxygenated by argon-bubbling for at least 15 min prior to use. THF and deuterated solvents were dried by conventional methods[254] and distilled under argon. All solvents were stored under argon over molecular sieves. Water was deoxygenated by three freeze-pump-thaw cycles prior to use. Solvents that were used under non-inert conditions required no further purification. HPLC grade solvents were used for gas chromatography.

5.2. Analytical Techniques

5.2.1. NMR spectroscopy

NMR spectra were recorded on Bruker DPX-200, AV II-300, AV III-HD-300, AV III-400, DRX-400, AV III-HD-500, or AV II-600 spectrometers. Chemical shifts (δ) are reported in ppm (parts per million) and are referenced relative to internal tetramethylsilane (δ_H 0.00 ppm), to residual solvent ^{1}H signals (tetrahydrofuran-d_8, δ_H 1.72 ppm; toluene-d_8, δ_H 2.08 ppm; dichloromethane-d_2, δ_H 5.32 ppm; benzene-d_6, δ_H 7.16 ppm; chloroform-d_3, δ_H 7.26 ppm; dimethyl sulphoxide-d_6, δ_H 2.50 ppm),[202] to the ^{13}C resonance of the solvents (toluene-d_8, δ_C 20.43 ppm; tetrahydrofuran-d_8, δ_C 25.31 ppm; dichloromethane-d_2, δ_C 53.84 ppm; chloroform-d_3, δ_C 77.16 ppm; benzene-d_6, δ_C 128.06 ppm; dimethyl sulphoxide-d_6, δ_C 39.50 ppm),[202] to virtual external $CFCl_3$ (δ_F 0.00 ppm), or to virtual external 85% aqueous phosphoric acid (δ_P 0.00 ppm). The number of protons (n) for a given resonance is indicated by nH. All ^{13}C, ^{19}F and ^{31}P NMR spectra are proton-decoupled, {^{1}H}. Where possible, the number of protons attached to each carbon atom was determined either by ^{13}C-DEPT135 experiments or by multiplicity-edited ^{1}H–^{13}C HSQC NMR experiments. If required, signals were assigned by two-dimensional ^{1}H–^{1}H COSY, ^{1}H–^{1}H NOESY, ^{1}H–^{1}H ROESY, ^{1}H–^{13}C HSQC, and ^{1}H–^{13}C HMBC NMR experiments. The following abbreviations are used for spin multiplicity: s, singlet; d, doublet; t, triplet; q, quartet; sep, septet; dec, dectet; m, multiplet; app, apparent; br, broad. In low-temperature measurements, the temperature display of the spectrometer was calibrated against the methanol standard (4% methanol in methanol-d_4).

5.2.2. Chromatography techniques

Gas chromatography (GC) was executed on a Hewlett-Packard 5890 SERIES II instrument using a DB5-HT column (30 × 0.25 × 0.1) and FID detection (T = 310 °C). In a standard configuration, samples (1 µL) were injected at T = 250 °C (split ratio 10:1), and were passed through the column using a synthetic air/hydrogen mixture as carrier gas (flow rate 1.0 mL min^{-1}) with a temperature program of T = 50 °C (3 min) → ΔT = 10 °C min^{-1} → T = 300 °C (5 min). For calibration, n-decane was used as an internal standard.

Gel permeation chromatography (GPC) was executed on an Agilent Series 1200 device using PSS SDV (Lux) columns (5 µm, 100 Å and 1000 Å) and ELSD detection. Dissolved

samples (100 µL) were injected with a diaphragm valve and were analysed at T = 35 °C with a flow rate of 1 mL min^{-1} using an isocratic pump. Polystyrene standards were used for calibration.

5.2.3. X-ray diffraction studies

Single crystals were examined and mounted in perfluorinated inert oil, and transferred to the cold gas stream of the diffractometer. Data were recorded on an Oxford Diffraction Nova Atlas diffractometer, using mirror-focused Cu K–$L_{2,3}$ radiation (1.54184 Å), or on an Oxford Diffraction Xcalibur Eos diffractometer, using graphite-monochromated Mo K–$L_{2,3}$ radiation (0.71073 Å). Absorption corrections were performed on the basis of multi-scans. All structures were solved by direct methods (SHELXS-97[255] or SHELXT-14)[256] and refined anisotropically by full-matrix least-squares procedures on F^2 using the SHELXL-97 or SHELXL-18 programs.[257] Hydrogen atoms were included as idealised methyl groups allowed to rotate but not tip (all methyls, with the exception of disordered methyl groups in **2** and $[Li(Et_2O)_2\mathbf{9}]_n$), or placed geometrically and allowed to ride on their attached carbon atoms (all other H atoms). If possible, disordered groups were refined on two or more positions; appropriate restraints were employed to improve refinement stability, but the dimensions of disordered groups should always be interpreted with caution. For crystallographic parameters and structural details, see the corresponding section under each compound. The program Diamond[258] was used for graphical representations.

5.2.4. Computational methods

All quantum chemical calculations were performed with the Gaussian09 set of programs[259] using the B3LYP hybrid density functional.[260,261] All atoms except molybdenum were described by the standard triple-zeta all electron basis set of Pople, augmented with one set of polarisation functions (6-311G(d,p)). For molybdenum a double-zeta basis set optimised for use with effective core potentials (ECP) in combination with the corresponding Stuttgart ECP[262] was employed. All reported energies, enthalpies and structural parameters correspond to optimised molecular structures that were obtained from geometry optimisations without imposed symmetry or geometrical constraints. All local minima were confirmed by subsequent frequency calculations at the same level of theory as was used for the optimisations. Enthalpic and

entropic contributions were calculated by statistical thermodynamics as implemented in the Gaussian09 set of programs. The reported (isotropic) electronic g values were calculated as the mean of the eigenvalues (mean of trace) of the anisotropic g tensor which was computed using the EPR module of Gaussian09.

5.2.5. Solid-state magnetic susceptibility

Solid-state magnetic susceptibility measurements on polycrystalline samples of complex **35** (9 mg) and **36** (8 mg) were performed on a Cryogenic Ltd. closed-cycle SQUID magnetometer in the range of T = 2.6–300 K with an external applied magnetic field of B_{ext} = 0.1 T. Supplementary measurements were executed at T = 2.1 K or T = 2.6 K with variable external magnetic fields (B_{ext} = 0.05–7 T). All samples were prepared in quartz tubes as previously described.[263] The diamagnetic background signal of a similar quartz tube filled with quartz wool was experimentally determined and subtracted from the magnetisation data. The molecular diamagnetic susceptibility (χ_D(**35**) = -4.97×10^{-4} cm^3 mol^{-1}, χ_D(**36**) = -4.90×10^{-4} cm^3 mol^{-1}) was corrected using tabulated Pascal constants.[264] Before sample assembly, the thermally unstable compounds **35** and **36** were stored in liquid N_2, and the sample chamber of the magnetometer was precooled (T < 100 K). After assembly, the samples were initially cooled to T = 2.6 K in zero applied magnetic field, and the magnetic susceptibility was recorded in a field-warming sequence with temperature steps up to T = 200 K. Above T = 200 K, the measurement was continued with a constant warm-up rate of approx. ΔT = 4 K min^{-1}. Finally, at T = 310 K (complex **35**) or T = 300 K (complex **36**), the temperature was held constant and the magnetisation was continuously recorded for about 20 hours.

5.2.6. Other techniques

Elemental analyses (C, H, N) were determined by combustion and gas chromatographic analysis on a Vario MICRO cube instrument (Elementar) using argon as carrier gas. Unless otherwise stated, values are reported as an average of three runs.

Mass spectrometry (MS) measurements were performed on a Shimadzu GCMS-QP2010SE instrument operating in positive electron ionisation (EI) mode (70 eV, 60–700 *m/z*). High-resolution GC/MS measurements were performed on an Agilent 6890 GC instrument coupled to a JMS-T100GC AccuTOF (JEOL) mass spectrometer operating in positive EI mode (70 eV).

5.3. Experimental Procedures*

5.3.1. Starting materials

2,2′-Bipyridine was sublimed prior to use. *para*-Bromoanisole (Fluka) was distilled under reduced pressure (68 °C/5.2 mbar) before use. 2-bromomesitylene (TCI, Acros), 1,1,1,3,3,3-hexafluoro-2-methyl-2-propanol and 1,1,1,3,3,3-hexafluoro-2-(trifluoromethyl)-2-propanol (Apollo Scientific), and phenylacetylene (Sigma-Aldrich) were deoxygenated prior to use. *n*-Decane and 1,2-dimethoxyethane (Alfa Aesar) were dried over Na/benzophenone and stored under argon over molecular sieves. Dimethylformamide was dried over molecular sieves and stored under argon previous to use. 1-Heptyne and 3-hexyne (Sigma-Aldrich) were distilled and stored under argon over molecular sieves. Potassium hydride (Acros) was washed with *n*-hexane or *n*-pentane to remove mineral oil and then dried in high vacuum. Pyridine (Sigma-Aldrich) was dried over solid KOH, distilled, and stored under argon over molecular sieves. Triethylamine (Acros) was stored over KOH and deoxygenated prior to use. Triethylene glycol was distilled at T = 116 °C under low pressure (p = 0.13 mbar) prior to use. 5-(Benzyloxy)-2-pentyne[110] and 4-(benzyloxy)-1-butyne[157] were prepared by a Williamson ether synthesis from 3-pentyn-1-ol or 3-butyn-1-ol (ABCR), respectively, and benzyl bromide (Sigma-Aldrich) in anhydrous THF according to the literature procedure. 2,2-Dibromo-1,1-bis(4-methylpiperidino)ethene[236] and lithium diethylamide[225] were synthesised according to the literature procedure. Pyridinium tribromide was prepared from pyridine, hydrobromic acid (Sigma-Aldrich) and bromine (Sigma-Aldrich) according to the literature procedure.[217,265]

All other reagents were obtained commercially and used without further purification (Bromine (Acros), *n*-BuLi (Acros), *t*-BuLi (Sigma-Aldrich), 2-isopropoxyphenyl bromide (TCI), KOH (Carl Roth), 1-methoxynaphthalene (TCI), $[Mo(CO)_6]$ (ABCR), oxalyl bromide (Sigma-Aldrich), *trans*-stilbene (Sigma-Aldrich), *trans*-(1,2-$^{13}C_2$)-stilbene (CDN Isotopes), tetramethylammonium bromide (TCI, Sigma-Aldrich), tolan (ABCR), trichloroethylene (Riedel-de Haën), 1,3,5-trimethoxybenzene (Acros), trimethylphosphane (Sigma-Aldrich)) or had been previously synthesised in our group (1,3,4,5-tetramethylimidazolin-2-ylidene, 2,4,6-trimethoxybenzonitrile).

* Some synthetic procedures and experimental data were published in advance (see *Vorveröffentlichungen der Dissertation*), and are reproduced here almost literally for convenience.

5.3.2. Potassium alkoxides

Preparation of potassium 1,1,1,3,3,3-hexafluoro-2-methyl-2-propanolate, K-14

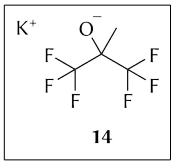

14

The literature procedure[266] was up-scaled and is reproduced here for convenience. A 250 mL Schlenk tube, fitted with a bent adapter, was charged with 1,1,1,3,3,3-hexafluoro-2-methyl-2-propanol (10.695 g, 58.74 mmol, 1.0 equiv) and diethyl ether (90 mL), and was cooled to 0 °C in an ice bath. The solution was stirred vigorously, while potassium hydride (2.356 g, 58.74 mmol, 1.0 equiv), contained in a Schlenk flask, was added carefully in small portions via the bent adapter, resulting in a copious evolution of gas (H_2). The remains in the flask and the bent adapter were rinsed with diethyl ether (2 × 5 mL), and the ice bath was removed. The slightly turbid mixture was stirred over night and then filtered through a frit to remove unreacted potassium hydride. The filtrate was evaporated under reduced pressure to give a white solid after drying in high vacuum. Yield: 94% (12.109 g, 55.00 mmol).

1. NMR spectroscopy

	solvent: tetrahydrofuran-d_8
δ_H (300.3 MHz, 298 K)	1.22 (sep, 3H, $^3J_{HF}$ = 1.1 Hz, CH_3)
δ_C (75.5 MHz, 298 K)	21.9 (C(CH_3)(CF_3)$_2$), 79.3 (sep, $^2J_{CF}$ = 25 Hz, C(CH_3)(CF_3)$_2$), 128.5 (q, $^1J_{CF}$ = 293 Hz, CF_3)
δ_F (282.5 MHz, 298 K)	−80.2

Preparation of potassium 1,1,1,3,3,3-hexafluoro-2-(trifluoromethyl)-2-propanolate, K-20

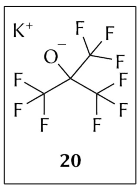

20

The literature procedure[267] was slightly modified as follows. A 100 mL Schlenk tube, fitted with a bent adapter, was charged with 1,1,1,3,3,3-hexafluoro-2-(trifluoromethyl)-2-propanol (6.85 g, 29.0 mmol, 1.0 equiv) and diethyl ether (35 mL). The solution was stirred vigorously, while potassium hydride (1.16 g, 29.0 mmol, 1.0 equiv), contained in a Schlenk flask, was added carefully in small portions via the bent adapter, resulting in a copious evolution of gas (H_2). The remains in the flask and the bent adapter were rinsed with diethyl ether (3 + 2 mL), and the slightly turbid mixture was stirred over night. The mixture was then filtered through a frit to remove unreacted potassium hydride, the flask was rinsed with diethyl ether (2 × 2.5 mL), and the filtrate was evaporated under reduced pressure. The residue was washed with *n*-pentane (20 mL), the solvent was decanted off, and the residual white powder was

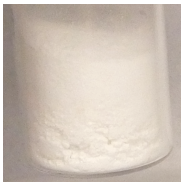

dried under dynamic vacuum. Yield: 85% (6.77 g, 24.7 mmol). Spectroscopic data are in agreement with the literature.[267]

5.3.3. Organolithium reagents

Preparation of 2-isopropoxyphenyl lithium

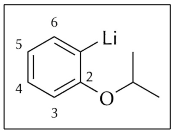

A solution of *n*-BuLi (1.6 M in hexanes, 8.88 mL, 14.2 mmol, 1.0 equiv) was added to a stirred solution of 2-isopropoxyphenyl bromide (3.06 g, 14.2 mmol) in diethyl ether (20 mL) at ambient temperature, which resulted in an exothermic reaction and the formation of a white precipitate. The mixture was stirred at ambient temperature for 12 h, then placed in an ice bath for 30 min, the solid collected by filtration, washed with *n*-hexane (5 × 20 mL) and dried in high vacuum to give the title compound as a colourless solid. Yield: 87% (1.76 g, 12.4 mmol).

1. Elemental analysis

$C_9H_{11}LiO$	C [%]	H [%]
Found	71.38	7.37
Calc.	76.06	7.80

Combustion analysis repeatedly produced low carbon values; the reason is unclear.

2. NMR spectroscopy

	solvent: tetrahydrofuran-d_8
δ_H (600.1 MHz, 303 K)	1.25 (d, 6H, $^3J_{HH}$ = 6.1 Hz, 2 × CH_3), 4.50 (sep, 1H, $^3J_{HH}$ = 6.1 Hz, OCH), 6.55 (app d, 1H, $^{3,app}J_{HH}$ = 8.0 Hz, Ar-H), 6.66 (app tm, 1H, $^{3,app}J_{HH}$ = 6.7 Hz, Ar-H), 6.84 (app tm, 1H, $^{3,app}J_{HH}$ = 7.6 Hz, Ar-H), 7.70 (app dd, 1H, $^{3,app}J_{HH}$ = 6.3 Hz, $^{4,app}J_{HH}$ = 1.7 Hz, Ar-H)
δ_C (150.9 MHz, 303 K)	22.78 (2 × CH$_3$), 69.49 (OCH), 109.94 (3-CH), 121.36 (5-CH), 125.19 (br, $\nu_{½}$ = 19.5 Hz, 6-CH), 143.21 (4-CH), 167.82 (2-C_qO), 169.2 (br, $\nu_{½}$ = 113 Hz, C_qLi)

Preparation of 8-methoxy-1-naphthyl lithium

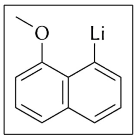

The literature procedure[268] was adapted as follows. To a solution of 1-methoxynaphthalene (2.215 g, 14.00 mmol) in *n*-hexane (10 mL) was added *t*-BuLi (1.7 M in pentane, 8.2 mL, 14 mmol, 1.0 equiv), and the turbid mixture was stirred for 40 h at ambient temperature. The pale yellow precipitate thus formed was filtered off, washed on the frit with *n*-hexane (20 mL, 3 × 10 mL) and dried under dynamic vacuum. Yield: 60% (1.384 g, 8.43 mmol). Spectroscopic data are in agreement with the literature.[268]

Preparation of 2,4,6-trimethoxyphenyl lithium

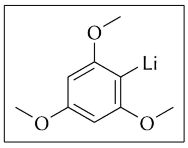

A published procedure[269] was modified as follows. Into a 100 mL Schlenk tube 1,3,5-trimethoxybenzene (5.35 g, 31.8 mmol, 1.0 equiv) in diethyl ether (12 mL) was introduced, followed by addition of *n*-BuLi (1.6 M in hexanes, 20 mL, 32.0 mmol, 1.01 equiv). A reflux condenser was attached, and the reaction mixture was refluxed at 40 °C for 2.5 h, which resulted in the rapid formation of a colourless precipitate. The mixture was allowed to cool down and was then stirred overnight at ambient temperature. The solid was collected on a frit, washed with *n*-hexane (3 × 5 mL) and dried in high vacuum. Yield: 93% (5.13 g, 29.5 mmol).

1. Elemental analysis

$C_9H_{11}LiO_3$	C [%]	H [%]
Found	62.06	6.61
Calc.	62.08	6.37

2. NMR spectroscopy

	solvent: tetrahydrofuran-d_8
δ_H (300.1 MHz, 297 K)	3.68 (s, 3H, *p*-OCH_3), 3.69 (s, 6H, 2 × *o*-OCH_3), 5.98 (s, 2H, 2 × *m*-H)
δ_C (75.5 MHz, 298 K)	54.2 (*o*-OCH_3), 54.8 (*p*-OCH_3), 90.2 (*m*-CH), 136.0 (C_qLi), 161.3 (*p*-C_qO), 169.8 (*o*-C_qO).

Preparation of 4-methoxyphenyl lithium

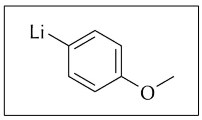

The literature procedure[270] was modified as follows. To a solution of 4-bromoanisole (5.99 g, 4.00 mL, 32 mmol) in *n*-pentane (40 mL) was added *n*-BuLi (2.5 M in hexanes, 15.36 mL, 38.4 mmol, 1.20 equiv), and the mixture was stirred overnight at ambient temperature. The colourless precipitate thus formed was then isolated by filtration, washed on the frit with *n*-pentane (2 × 15 mL) and dried under dynamic vacuum. Yield: 83% (3.04 g, 26.7 mmol).

1. NMR spectroscopy

	solvent: tetrahydrofuran-d_8
δ_H (300.1 MHz, 297 K)	3.61 (s, 3H, OCH_3), 6.52 (d, 2H, $^3J_{HH}$ = 7.8 Hz, 2 × Ar-H), 7.73 (d, 2H, $^3J_{HH}$ = 7.8 Hz, 2 × Ar-H)
δ_C (75.5 MHz, 299 K)	54.4 (OCH_3), 111.4 (*m*-CH), 144.3 (*o*-CH), 157.8 (*p*-C_qO). The C_qLi signal was not observed.

5.3.4. Complexes

Preparation of tetramethylammonium (2,4,6-trimethylbenzoyl)pentacarbonylmolybdate(0)

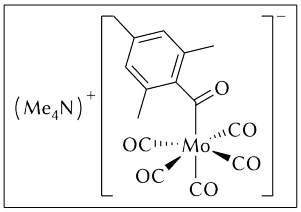

The literature procedures[113,157] were modified as follows. A solution of 2-bromomesitylene (3.78 g, 2.9 mL, 19.0 mmol, 1 equiv) in diethyl ether (80 mL) was treated with *t*-BuLi (20.3 mL, 1.9 M in pentane, 38.6 mmol, 2.03 equiv) in a 250 mL Schlenk flask at a temperature between –20 °C and –30 °C. The resulting suspension (yellow solution, white precipitate) was stirred for 1.5 h at ca. –40 °C, and then it was directly transferred to a precooled solution of $[Mo(CO)_6]$ (5.01 g, 19.0 mmol) in diethyl ether (60 mL) placed in an ice-water bath (0 °C). The deep yellow suspension was stirred for 2 h at ambient temperature, resulting in a clear orange solution. The solvent was removed under reduced pressure, and the residue was dried in high vacuum (it was crushed with a spatula to assist the removing of the solvent). The yellow residue was suspended in deoxygenated water (20 mL), residual $[Mo(CO)_6]$ was filtered off, and the aqueous solution was directly added dropwise to a solution of (Me4N)Br (4.4 g, 29 mmol) in deoxygenated water (15 mL). Meanwhile, the flask and the frit were washed with deoxygenated water (2 × 5 mL). The mixture was stirred for 1 h, and an oily, gold-brown precipitate formed. The mother liquor was removed with a syringe (if the precipitate does not sediment easily, water can be partially removed under reduced pressure), the precipitate was dissolved in diethyl ether (10 mL), and then the volume was reduced to 5 mL under reduced pressure. The ether solution was extracted with dichloromethane (4 × 10 mL), the dichloromethane extracts were combined, and the solvent was removed. After drying in high vacuum, a crystalline yellow solid was obtained. Yield: 81% (7.07 g, 15.5 mmol).

1. NMR spectroscopy

	solvent: C_6D_6
δ_H (300.3 MHz, 298 K)	2.13 (s, 6H, 2 × *o*-CH_3), 2.21 (s, 3H, *p*-CH_3), 3.19 (s, 12H, N(CH_3)$_4$), 6.65 (m, 2H, 2 × *m*-*H*)
δ_C (75.5 MHz, 298 K)	18.4 (*o*-*C*H$_3$), 20.9 (*p*-*C*H$_3$), 56.5 (t, $^1J_{CN}$ = 4 Hz, N(*C*H$_3$)$_4$), 127.4 (*o*-C_qCH$_3$), 128.7 (*m*-*C*H), 133.7 (*p*-C_qCH$_3$), 159.0 (*i*-C_q), 211.2 (4 × *cis*-*C*O), 218.7 (*trans*-*C*O), 312.3 (Ar–*C*=O)

Preparation of *mer*-tris(bromido)(1,2-dimethoxyethane-$\kappa^2 O,O'$)(2,4,6-trimethylbenzylidyne)molybdenum(VI)

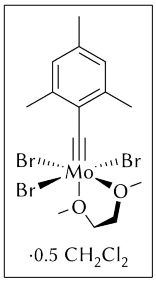

The literature procedure[157] was modified and upscaled as follows. A precooled (–80 °C) solution of oxalyl bromide (7.23 g, 33.50 mmol, 1.20 equiv) in dichloromethane (65 mL) was transferred via cannula to a stirred and precooled (–90 °C) suspension of $(Me_4N)[Mo(C(O)Mes)(CO)_5]$ (12.73 g, 27.83 mmol) in dichloromethane (385 mL). The deep yellow mixture was stirred for 15 min, whereby it darkened gradually, and the resulting brown suspension was then warmed to approx. –10 °C over the course of 2 h (the cooling bath was not removed). The mixture was cooled back to –90 °C and filtered at this temperature through D.E. on a jacketed frit to remove precipitated $(Me_4N)Br$. The stirred yellow filtrate was treated with 1,2-dimethoxyethane (28.9 mL, 25.08 g, 278.3 mmol, 10.0 equiv) at –80 °C, followed by slow addition of a precooled (–70 °C) solution of bromine (1.45 mL, 4.54 g, 28.39 mmol, 1.02 equiv) in dichloromethane (60 mL). The resulting orange-brown solution was stirred for 15 min and allowed then to warm up gradually to 0 °C. The solvent was removed at this temperature under reduced pressure, the residue was dissolved in dichloromethane (110 mL), and the product was precipitated with *n*-pentane (200 mL). The supernatant was decanted off, and the brown precipitate was washed with *n*-pentane (3 × 20 mL). After drying in high vacuum, *mer*-$[Mo(\equiv CMes)(Br)_3(dme)] \cdot 0.5\ CH_2Cl_2$ was obtained as a brown microcrystalline solid. Yield: 72% (12.05 g, 20.10 mmol).

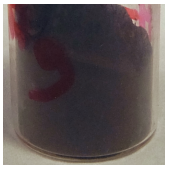

1. NMR spectroscopy

	solvent: dichloromethane-d_2
δ_H (300.3 MHz, 298 K)	2.56 (s, 3H, *p*-CH_3), 3.19 (s, 6H, 2 × *o*-CH_3), 3.85 (s, 3H, DME-CH_3), 3.95 (s, 3H, DME-CH_3), 4.02 (s, 4H, DME-CH_2), 5.33 (CH_2Cl$_2$), 6.89 (s, 2H, 2 × *m*-*H*)
δ_C (75.5 MHz, 298 K)	20.7 (*o*-CH_3), 21.1 (*p*-CH_3), 54.24 (CH_2Cl$_2$), 60.3 (DME-CH_3), 70.1 (DME-CH_2), 73.6 (DME-CH_3), 78.7 (DME-CH_2), 127.5 (*m*-CH), 138.6 (*i*-C_q), 143.3 (*p*-C_qCH$_3$), 146.2 (*o*-C_qCH$_3$), 340.6 (*C*≡Mo)

Preparation of tris((1,1,1,3,3,3-hexafluoro-2-methyl-2-propanyl)oxy)(2,4,6-trimethylbenzylidyne)molybdenum(VI), 1

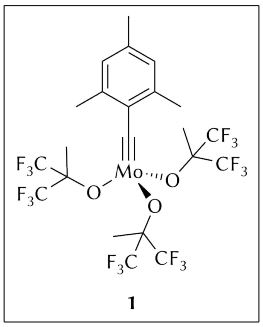

1

The literature procedure[157] was modified as follows. To a stirred solution of K-**14** (960 mg, 4.359 mmol) in THF (11 mL) *mer*-[Mo(≡CMes)(Br)$_3$(dme)]·0.5 CH_2Cl_2 (871 mg, 1.453 mmol) was added in portions through a powder funnel, and the funnel was rinsed with more THF (4 mL). The mixture immediately turned reddish-brown and was stirred over night; on the next day, the colour had changed to ochre. The volatiles were removed under dynamic vacuum, and the residue was dried for 2 h at 50 °C under dynamic vacuum. Then, *n*-pentane (10 mL) was added, the mixture was subjected to a freeze-thaw cycle, and the solvent was removed at 50 °C under dynamic vacuum. The pale brown residue was extracted with *n*-pentane (10 mL, 2 × 5 mL), filtered through D.E., and the frit was washed with more *n*-pentane (2 × 5 mL), leaving a violet solid on the pad of D.E. Finally, the solvent was removed from the yellow filtrate, and the residue was dried under dynamic vacuum. Yield: 84% (940 mg, 1.220 mmol) of an intensely yellow solid.

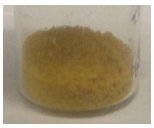

1. NMR spectroscopy

	solvent: C_6D_6
δ_H (300.3 MHz, 298 K)	1.57 (s, 9H, 3 × C(C*H*$_3$)(CF$_3$)$_2$), 1.99 (s, 3H, *p*-C*H*$_3$), 2.52 (s, 6H, 2 × *o*-C*H*$_3$), 6.48 (br m, 2H, 2 × *m*-*H*)
δ_C (75.5 MHz, 298 K)	18.4 (C(*C*H$_3$)(CF$_3$)$_2$), 20.3 (*o*-*C*H$_3$), 21.0 (*p*-*C*H$_3$), 83.9 (sep, $^2J_{CF}$ = 31 Hz, *C*(CH$_3$)(CF$_3$)$_2$), 123.5 (q, $^1J_{CF}$ = 287 Hz, *C*F$_3$), 128.5 (*m*-*C*H), 141.2 (*p*-C_qCH$_3$), 141.6 (*o*-C_qCH$_3$), 143.3 (*i*-C_q), 317.9 (*C*≡Mo)
δ_F (282.5 MHz, 298 K)	–78.2

2. Alkyne metathesis

The catalytic activity was tested according to the general procedure for the metathesis of alkyne **Y**-Me on a 0.250 mmol scale. The isolated yield[157] has been reported before.

Preparation of lithium (2-isopropoxybenzoyl)pentacarbonylmolybdate(0), Li-6

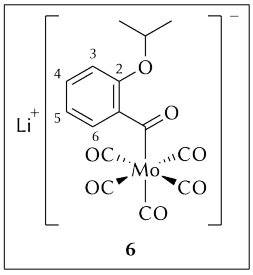

6

A 250 mL Schlenk flask was charged with $[Mo(CO)_6]$ (3.70 g, 14.0 mmol, 1 equiv), 2-isopropoxyphenyl lithium (2.00 g, 14.1 mmol, 1.01 equiv) and diethyl ether (15 mL), and was stirred at ambient temperature for 2 h. After addition of more diethyl ether (20 mL) and *n*-hexane (40 mL) the mixture was allowed to stand in an ice bath for 2 h, which resulted in the formation of a brown precipitate. The supernatant was decanted, the residue was washed with *n*-hexane (3 × 10 mL) and then dried under dynamic vacuum to yield 4.93 g (12.1 mmol, 87%) of an orange solid.

1. Elemental analysis

$C_{15}H_{11}LiMoO_7$	C [%]	H [%]
Found	44.31	2.95
Calc.	44.36	2.73

2. NMR spectroscopy

	solvent: tetrahydrofuran-d_8
δ_H (399.9 MHz, 298 K)	1.29 (d, 6H, $^3J_{HH}$ = 6.1 Hz, 2 × CH_3), 4.53 (sep, 1H, $^3J_{HH}$ = 6.1 Hz, OC*H*), 6.62–6.65 (m, 1H, 6-*H*), 6.73–6.79 (m, 2H, 3-*H*, 5-*H*), 6.91–6.96 (m, 1H, 4-*H*)
δ_C (100.5 MHz, 299 K)	22.4 (2 × *C*H_3), 70.0 (O*C*H), 113.5 (3-*C*H), 120.3 (5-*C*H), 122.1 (6-*C*H), 126.5 (4-*C*H), 150.1 (*C*$_q$O), 154.1 (*i*-*C*$_q$), 210.9 (4 × *cis*-*C*O), 218.2 (*trans*-*C*O), 316.3 (Ar–*C*=O)

Attempted preparation of tetramethylammonium (2-isopropoxybenzoyl)pentacarbonylmolybdate(0), (Me_4N)6

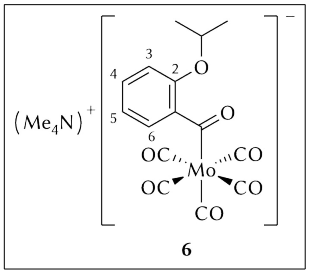

6

To a precooled (–20 °C) and stirred solution of 2-isopropoxy-1-bromobenzene (645 , 3.00 mmol) in diethyl ether (15 mL) was added *n*-butyl lithium (2.5 M in hexanes, 1.22 mL, 3.06 mmol, 1.02 equiv). The colourless suspension was allowed to warm up to 0 °C, was stirred for 1 h, and was transferred slowly to a suspension of $[Mo(CO)_6]$ (792 mg, 3.00 mmol) in diethyl ether (10 mL) placed in an ice bath at 0 °C, which resulted in an immediate colour change to yellow. The cooling bath was removed, the mixture was stirred for 1.5 h, and the solvent was removed under reduced pressure. The deep yellow residue was dried for 1 h under high vacuum and was suspended in deoxygenated water (4 mL). The aqueous suspension was filtered through a frit to remove unreacted $[Mo(CO)_6]$, and the filtrate was added dropwise to a solution of (Me_4N)Br (462 mg, 3.00 mmol, 1.0 equiv) in deoxygenated water (4 mL). A yellow solid precipitated from solution,

which was collected on a frit, washed with diethyl ether (2 × 2 mL + 1 mL) and dried under dynamic vacuum. As judged by NMR spectroscopy, the product was a mixture of (Me_4N)**6** and (Me_4N)**7**. Yield (mixture): ~25% (345 mg, ~0.75 mmol).

1. NMR spectroscopy

(Me_4N)**6**	solvent: dichloromethane-d_2
δ_H (600.1 MHz, 295 K)	1.28 (d, 6H, $^3J_{HH}$ = 6.1 Hz, OCH(CH_3)$_2$), 3.19 (s, 12H, N(CH_3)$_4$), 4.51 (sep, 1H, $^3J_{HH}$ = 6.1 Hz, OC*H*), 6.65 (m, 1H, Ar-*H*), 6.77 (m, 1H, Ar-*H*), 6.82 (m, 1H, Ar-*H*), 6.98 (m, 1H, Ar-*H*)
δ_C (150.9 MHz, 295 K)	22.2 (2 × *C*H$_3$), 56.5 (t, $^1J_{CN}$ = 4 Hz, N(*C*H$_3$)$_4$), 69.5 (O*C*H), 113.2 (Ar-*C*H), 120.0 (Ar-*C*H), 121.5 (Ar-*C*H), 125.8 (Ar-*C*H), 149.5 (*C*$_q$O), 153.8 (*i*-*C*$_q$), 211.2 (4 × *cis*-*C*O), 219.0 (*trans*-*C*O), 303.1 (Ar–*C*=O)

(Me_4N)**7**	solvent: dichloromethane-d_2
δ_H (600.1 MHz, 295 K)	1.33 (d, 6H, $^3J_{HH}$ = 6.1 Hz, OCH(CH_3)$_2$), 3.22 (s, 12H, N(CH_3)$_4$), 4.46 (sep, 1H, $^3J_{HH}$ = 6.1 Hz, OC*H*), 6.51 (m, 1H, Ar-*H*), 6.53 (m, 1H, Ar-*H*), 6.83 (m, 1H, Ar-*H*), 7.79 (m, 1H, Ar-*H*), 6.98 (m, 1H, Ar-*H*)
δ_C (150.9 MHz, 295 K)	22.1 (2 × *C*H$_3$), 56.5 (t, $^1J_{CN}$ = 4 Hz, N(*C*H$_3$)$_4$), 67.6 (O*C*H), 108.6 (Ar-*C*H), 119.0 (Ar-*C*H), 123.4 (Ar-*C*H), 148.1 (Ar-*C*H), 157.4 (*i*-*C*$_q$Mo), 164.5 (*C*$_q$O), 212.7 (4 × *cis*-*C*O), 222.5 (*trans*-*C*O)

Additional signals belong to an unidentified impurity and $[Mo(CO)_6]$ (δ_C = 201.6 ppm).

2. X-ray crystal structure determination

Acicular colourless single-crystals of (Me_4N)**7** were obtained from the NMR solution at ambient temperature.

Special features: The asymmetric unit contains two independent formula units. The compound crystallises only by chance in an enantiomorphic (Sohncke) space group and is not a pure enantiomer. The structure is doubly twinned; pseudomerohedrally and racemically. Relative component volumes were: by rotation 0.011(15); by inversion, 0.017(16); by inversion and rotation, 0.448(15), whereby the parent structure then makes up the difference to 1. The non-exact overlap of reflections from the twin components causes the structure determination to be less than ideally precise, but it is at least qualitatively reliable. A series of restraints was employed to improve refinement stability. Various checking programs indicate no higher symmetry space group. The two independent molecules differ slightly in the orientation of the aromatic rings (e.g. torsion angles C3–Mo–C6–C7 47.3°, 54.6°), a least-squares fit of the two molecules (without H atoms) gives an r.m.s. deviation of 0.28 Å.

empirical formula	$C_{18}H_{23}MoNO_6$
M_w	445.31
wavelength/Å	1.54184
T/K	100(2)
cryst. size/mm³	0.18 × 0.10 × 0.08
cryst. system	monoclinic
space group	$P2_1$
a/Å	9.2023(3)
b/Å	14.4463(5)
c/Å	15.1220(6)
α/°	90
β/°	90.323(4)
γ/°	90
V/Å³	2 010.27(12)

identification code	oscar04
Z	4
ρ_{calc}/(Mg m^{-3})	1.471
μ/mm^{-1}	5.617
F(000)	912
reflections collected	32 243
indep. reflections (R_{int})	7 356 (0.0492)
parameters	482
restraints	235
goodness-of-fit on F^2	1.070
R_1 ($I > 2\sigma(I)$)	0.0504
wR_2 (all reflections)	0.1337
absolute structure parameter	0.448(15)
max and min $\Delta\rho$/(e Å^{-3})	1.160 and −2.591

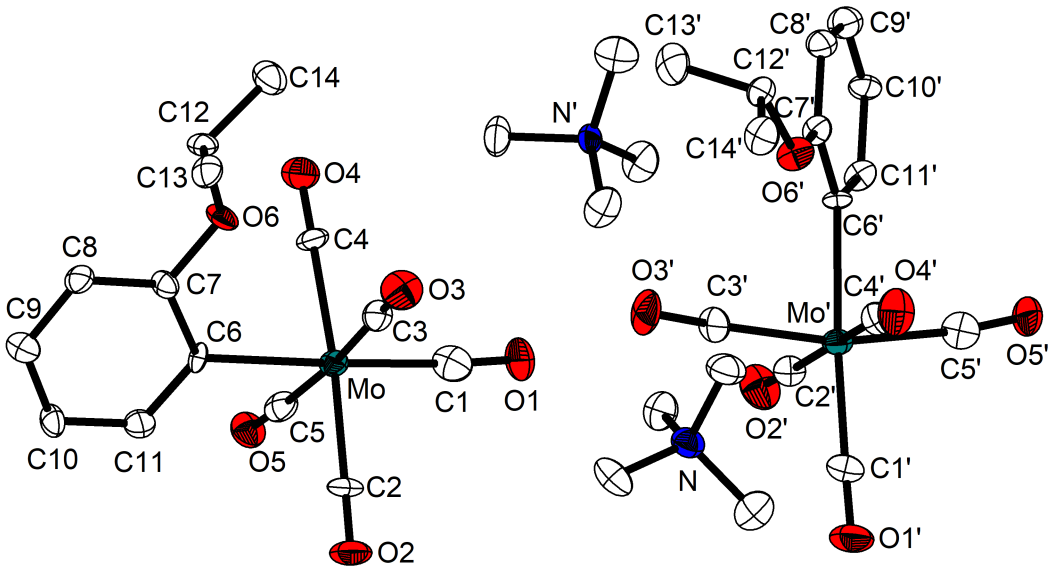

Figure 68. Molecular structure of (Me_4N)**7** with thermal displacement parameters drawn at the 50% probability level. Hydrogen atoms are omitted for clarity. Selected bond lengths (Å) and angles (deg): Mo–C1 1.998(12), Mo′–C1′ 2.028(13), Mo–C2 2.076(10), Mo′–C2′ 2.036(10), Mo–C3 2.070(10), Mo′–C3′ 2.035(11), Mo–C4 2.086(9), Mo′–C4′ 2.057(11), Mo–C5 2.019(11), Mo′–C5′ 2.038(11), Mo–C6 2.275(9), Mo′–C6′ 2.299(9); C1–Mo–C2 93.5(5), C1′–Mo′–C2′ 92.1(5), C1–Mo–C3 92.2(5), C1′–Mo′–C3′ 96.1(5), C1–Mo–C4 90.7(4), C1′–Mo′–C4′ 85.2(5), C1–Mo–C5 92.5(5), C1′–Mo′–C5′ 96.5(5), C1–Mo–C6 177.7(5), C1′–Mo′–C6′ 176.3(5), C2–Mo–C3 89.0(4), C2′–Mo′–C3′ 87.8(5), C2–Mo–C4 175.7(4), C2′–Mo′–C4′ 174.8(5), C2–Mo–C5 92.1(4), C2′–Mo′–C5′ 93.6(4), C2–Mo–C6 88.8(4), C2′–Mo′–C6′ 87.7(4), C3–Mo–C4 91.6(4), C3′–Mo′–C4′ 88.1(5), C3–Mo–C5 175.1(4), C3′–Mo′–C5′ 167.3(5), C3–Mo–C6 88.0(4), C3′–Mo′–C6′ 87.6(4), C4–Mo–C5 86.9(4), C4′–Mo′–C5′ 91.1(4), C4–Mo–C6 87.0(4), C4′–Mo′–C6′ 95.3(4), C5–Mo–C6 87.2(4), C5′–Mo′–C6′ 79.9(4).

Preparation of lithium (8-methoxy-1-naphthoyl)pentacarbonylmolybdate(0), Li-11

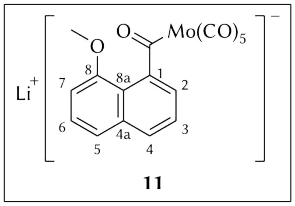

11

A suspension of 8-methoxy-1-naphthyl lithium (0.500 g, 3.05 mmol, 1.01 equiv) in diethyl ether (5 mL) was added to a stirred suspension of [$Mo(CO)_6$] (0.800 g, 3.03 mmol) in diethyl ether (10 mL) placed in an ice bath at 0 °C, which resulted in an immediate colour change to brown. The flask that contained the lithium organyl was rinsed with diethyl ether (4 × 3 mL), and *n*-hexane (30 mL) was added slowly.

After 4 h, the yellowish-brown precipitate was separated by decantation and dried under dynamic vacuum to give [Li(Et_2O)**11**] as a pale fawn solid. A second crop precipitated from the mother liquor overnight. Yield: 70% (1.065 g, 2.12 mmol).

Alternatively, a suspension of 8-methoxy-1-naphthyl lithium (0.980 g, 5.97 mmol) in diethyl ether (10 mL) was added to a suspension of [$Mo(CO)_6$] (1.576 g, 5.97 mmol) in diethyl ether (19 mL) placed in an ice bath at 0 °C, which resulted in an immediate colour change to d yellow. The flask that contained the lithium organyl was rinsed with diethyl ether (3 × 5 mL) and then with THF (5 mL); the fractions were added to the reaction mixture, and *n*-hexane (50 mL) was added slowly. A brown precipitate began depositing from solution. After standing overnight, the brown supernatant was decanted, and the residue was washed with *n*-hexane (7 mL) and dried in high vacuum to give [Li($thf)_2$**11**] as a fawn powder. Yield: 76% (2.60 g, 4.5 mmol).

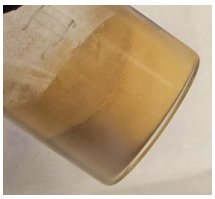

1. Elemental analysis

[Li(Et_2O)**11**]			[Li($thf)_2$**11**]		
$C_{21}H_{19}LiMoO_8$	C [%]	H [%]	$C_{25}H_{25}LiMoO_9$	C [%]	H [%]
Found	49.92	4.04	Found	52.86	4.42
Calc.	50.22	3.81	Calc.	52.46	4.40

2. NMR spectroscopy

[Li(Et_2O)**11**]	solvent: tetrahydrofuran-d_8
δ_H (400.4 MHz, 296 K)	1.11 (t, 6H, Et_2O), 3.38 (q, 4H, Et_2O), 3.86 (s, 3H, OCH_3), 6.70–6.75 (m, 2H, 2-*H*, 7-*H*), 7.22–7.37 (m, 3H, 3-*H*, 5-*H*, 6-*H*), 7.47 (m, 1H, 4-*H*)
δ_C (100.7 MHz, 298 K)	15.7 (Et_2O), 55.3 (OCH_3), 66.3 (Et_2O), 104.6 (7-*C*H), 117.7 (2-*C*H), 119.7 (8a-C_q), 120.9 (5-*C*H), 125.0 (4-*C*H), 126.2 (3-*C*H), 126.3 (6-*C*H), 136.6 (4a-C_q), 157.1 (8-C_q), 161.3 (1-C_q), 211.1 (4 × *cis*-*C*O), 218.4 (*trans*-*C*O), 310.9 (Ar–*C*=O)

[Li($thf)_2$**11**]	solvent: tetrahydrofuran-d_8
δ_H (300.1 MHz, 298 K)	1.76 (m, 2 × 4H, 2 × THF), 3.61 (m, 2 × 4H, 2 × THF), 3.86 (s, 3H, OCH_3), 6.69–6.76 (m, 2H, 2-*H*, 7-*H*), 7.20–7.40 (m, 3H, 3-*H*, 5-*H*, 6-*H*), 7.47 (m, 1H, 4-*H*)
δ_C (75.5 MHz, 299 K)	26.4 (THF), 55.3 (OCH_3), 68.2 (THF), 104.6 (7-*C*H), 117.7 (2-*C*H), 119.7 (8a-C_q), 120.9 (5-*C*H), 125.0 (4-*C*H), 126.2 (3-*C*H), 126.3 (6-*C*H), 136.6 (4a-C_q), 157.1 (8-C_q), 161.3 (1-C_q), 211.1 (4 × *cis*-*C*O), 218.4 (*trans*-*C*O), 311.0 (Ar–*C*=O)

3. X-ray crystal structure determination

Pale yellow needles of [Li(thf)$_3$**11**] were obtained from a THF solution at –35 °C.

Special features: The compound crystallises only by chance in an enantiomorphic (Sohncke) space group and is not a pure enantiomer.

empirical formula	$C_{29}H_{33}LiMoO_{10}$	identification code	oscar35
M_w	644.43	Z	2
wavelength/Å	0.71073	ρ_{calc}/(Mg m^{-3})	1.403
T/K	100(2)	μ/mm^{-1}	0.483
cryst. size/mm^3	0.40 × 0.35 × 0.30	F(000)	664
cryst. system	monoclinic	reflections collected	40 925
space group	$P2_1$	indep. reflections (R_{int})	8 934 (0.0369)
a/Å	9.9569(4)	parameters	371
b/Å	16.6522(4)	restraints	1
c/Å	10.3643(4)	goodness-of-fit on F^2	1.045
α/°	90	R_1 ($I > 2\sigma(I)$)	0.0288
β/°	117.443(5)	wR_2 (all reflections)	0.0651
γ/°	90	absolute structure parameter	–0.043(19)
V/Å^3	1525.07(9)	max and min $\Delta\rho$/(e Å^{-3})	0.667 and –0.519

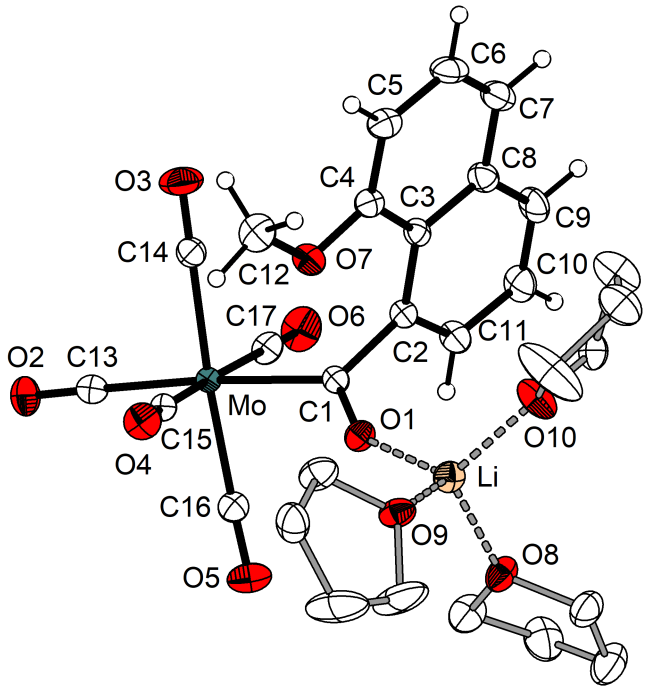

Figure 69. Molecular structure of [Li(thf)$_3$**11**] with thermal displacement parameters drawn at the 50% probability level. Hydrogen atoms of solvent molecules are omitted for clarity. Selected bond lengths (Å) and angles (deg): Mo–C1 2.2467(19), Mo–C13 2.017(2), Mo–C14 2.040(2), Mo–C15 2.044(2), Mo–C16 2.039(2) Mo–C17 2.038(2), C1–C2 1.526(3), C1–O1 1.233(2), Li···O1 1.881(4), Li···O8 1.936(4), Li···O9 1.955(4), Li···O10 1.921(4); C1–Mo–C13 175.29(8), C14–Mo–C16 176.15(9), C15–Mo–C17 172.76(9), C1–Mo–C14 91.52(8), C1–Mo–C15 82.31(7), C1–Mo–C16 84.63(8), C1–Mo–C17 90.68(8), C13–Mo–C14 92.02(8), C13–Mo–C15 94.62(8), C13–Mo–C16 91.83(8), C13–Mo–C17 92.49(8), C14–Mo–C15 89.31(8), C14–Mo–C17 89.07(9), C15–Mo–C16 90.25(8), C16–Mo–C17 90.89(9), Mo–C1–O1 124.79(14), Mo–C1–C2 119.53(13), O1–C1–C2 115.13(17), C1–O1···Li 146.69(18), O1···Li···O8 107.86(19), O1···Li···O9 107.01(19), O1···Li···O10 119.6(2), O8···Li···O9 110.53(19), O8···Li···O10 109.82(19), O9···Li···O10 101.77(19).

Preparation of tetramethylammonium (8-methoxy-1-naphthoyl)pentacarbonylmolybdate(0), (Me_4N)**11**

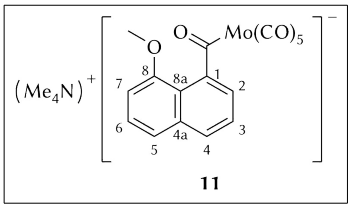

11

To a solution of tetramethylammonium bromide (0.69 g, 4.50 mmol, 1.5 equiv) in deoxygenated water (4 mL) was added dropwise a solution of Li-**11** (1.50 g, 3.00 mmol) in deoxygenated water (2.5 mL), which gave a brown precipitate. The mixture was stirred for 1 h, and the supernatant was decanted off. The solid was washed with diethyl ether (2 mL), but agglomeration hindered the washing process. Thus, *n*-hexane was added, the mixture was frozen, warmed back to ambient temperature, and the solid was dispersed by crushing with a spatula. Removal of the solvent and drying under dynamic vacuum gave the product as a yellowish brown solid. Yield (crude): 62% (0.92 g, 1.86 mmol).

1. Elemental analysis

$C_{21}H_{21}MoNO_7$	C [%]	H [%]	N [%]
Found	47.67	4.89	3.35
Calc.	50.92	4.27	2.83

The elemental composition suggests the presence of one or more impurities.

2. NMR spectroscopy

	solvent: dichloromethane-d_2
δ_H (500.3 MHz, 298 K)	3.03 (s, 12H, N(CH_3)$_4$), 3.86 (s, 3H, OCH_3), 6.72 (app dd, 1H, $^{3,app}J_{HH}$ = 7.3 Hz, $^{4,app}J_{HH}$ = 1.5 Hz, 7-*H*), 6.74 (app dd, 1H, $^{3,app}J_{HH}$ = 7.0 Hz, $^{4,app}J_{HH}$ = 1.3 Hz, 2-*H*), 7.31 (app dd, 1H, $^{3,app}J_{HH}$ = 8.3 Hz, $^{3,app}J_{HH}$ = 7.3 Hz, 6-*H*), 7.34 (app dd, 1H, $^{3,app}J_{HH}$ = 8.3 Hz, $^{4,app}J_{HH}$ = 1.5 Hz, 5-*H*), 7.41 (app dd, 1H, $^{3,app}J_{HH}$ = 8.2 Hz, $^{3,app}J_{HH}$ = 7.0 Hz, 3-*H*), 7.51 (app dd, 1H, $^{3,app}J_{HH}$ = 8.1 Hz, $^{4,app}J_{HH}$ = 1.3 Hz, 4-*H*)
δ_C (125.8 MHz, 298 K)	55.4 (O*C*H$_3$), 56.4 (t, $^1J_{CN}$ = 4 Hz, N(*C*H$_3$)$_4$), 104.4 (7-*C*H), 117.7 (2-*C*H), 119.0 (8a-C_q), 120.5 (Ar-*C*H), 124.3 (Ar-*C*H), 126.1 (Ar-*C*H), 126.3 (Ar-*C*H), 135.8 (4a-C_q), 156.6 (8-C_q), 161.0 (1-C_q), 211.4 (4 × *cis*-*C*O), 219.3 (*trans*-*C*O), 297.1 (Ar–*C*=O)

Additional signals belong to an unidentified impurity.

Preparation of lithium (2,4,6-trimethoxybenzoyl)pentacarbonylmolybdate(0), Li-8

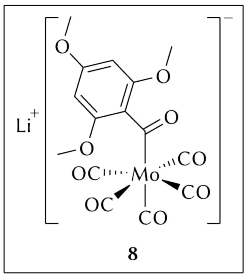

8

A suspension of 2,4,6-trimethoxyphenyl lithium (1.60 g, 9.20 mmol, 1.0 equiv) in diethyl ether (15 mL) was added to a 250 mL Schlenk flask charged with a suspension of $[Mo(CO)_6]$ (2.43 g, 9.20 mmol, 1.0 equiv) in diethyl ether (25 mL), and residual 2,4,6-trimethoxyphenyl lithium in the first flask was rinsed with THF (2 × 2.5 mL) and added to the reaction flask. The mixture immediately turned yellow, and stirring for 15 min at ambient temperature resulted in a clear or-

ange solution. Then, *n*-hexane (70 mL) was added, precipitating a yellow powder that remained in suspension, and a viscid deep orange solid that stuck to the walls of the flask. The suspension was immediately filtered before the yellow powder started to settle; the yellow solid was then dried on the frit under dynamic vacuum to give 1.16 g of product. A second crop of product precipitated from the filtrate as large block-shaped orange crystals (0.91 g). Total yield for $[Li(thf)\mathbf{8}]_2$: 44% (2.07 g, 4.06 mmol).

1. Elemental analysis

$C_{19}H_{19}LiMoO_{10}$	C [%]	H [%]
Found	44.45	4.07
Calc.	44.72	3.75

2. NMR spectroscopy

	solvent: tetrahydrofuran-d_8
δ_H (200.1 MHz, 300 K)	1.73 (m, THF), 3.57 (m, THF), 3.62 (s, 6H, 2 × *o*-OCH_3), 3.67 (s, 3H, *p*-OCH_3), 6.01 (s, 2H, 2 × *m*-*H*)
δ_C (75.5 MHz, 299 K)	26.4 (THF), 55.1 (*o*-O*C*H$_3$), 55.3 (*p*-O*C*H$_3$), 68.2 (THF), 91.0 (*m*-*C*H), 134.5 (*i*-C_q), 153.4 (*o*-C_qO), 159.8 (*p*-C_qO), 211.0 (4 × *cis*-*C*O), 218.6 (*trans*-*C*O), 313.9 (Ar–*C*=O)

3. X-ray crystal structure determination

Before optimising the synthetic protocol, three different types of yellow to orange crystals suitable for X-ray diffraction analysis were obtained from an Et_2O/*n*-hexane solution at –40 °C. Compound $[Li(Et_2O)\mathbf{8}]_2$ crystallised as pale yellow prisms.

empirical formula	$C_{38}H_{42}Li_2Mo_2O_{20}$
M_w	1024.48
wavelength/Å	0.71073
T/K	100(2)
cryst. size/mm³	0.30 × 0.25 × 0.10
cryst. system	triclinic
space group	$P\bar{1}$
a/Å	9.8996(5)
b/Å	11.3257(6)
c/Å	11.7210(4)
α/°	113.249(4)
β/°	95.641(4)
γ/°	108.654(4)
V/Å³	1105.30(9)

identification code	oscar16
Z	1
ρ_{calc}/(Mg m^{-3})	1.539
μ/mm^{-1}	0.644
F(000)	520
reflections collected	102 276
indep. reflections (R_{int})	6 509 (0.0530)
parameters	285
restraints	0
goodness-of-fit on F^2	1.075
R_1 ($I > 2\sigma(I)$)	0.0259
wR_2 (all reflections)	0.0602
max and min $\Delta\rho$/(e Å^{-3})	0.908 and –0.713

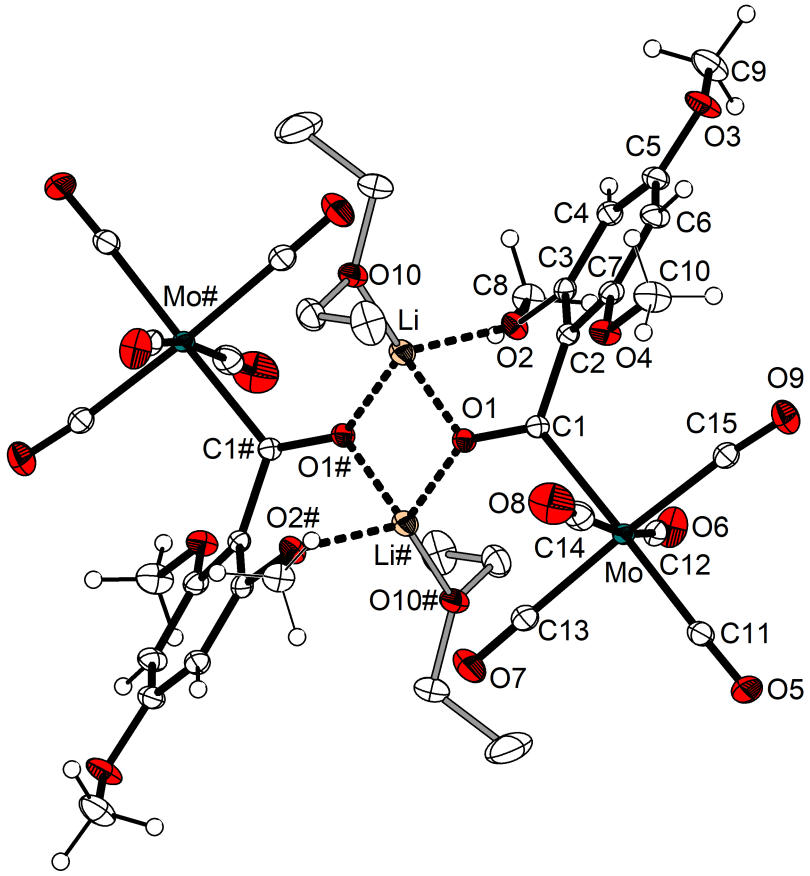

Figure 70. Molecular structure of dimeric $[Li(Et_2O)\mathbf{8}]_2$ with thermal displacement parameters drawn at the 50% probability level. Only the asymmetric unit is numbered entirely. Hydrogen atoms of solvent molecules are omitted for clarity. For selected bond lengths and angles, see Figure 15, p 37.

Compound $[Li(Et_2O)_2\mathbf{9}]_n$ formed highly air-sensitive, blade-shaped, colourless crystals.

Special features: One ethyl group (C21, C22) is disordered over two positions with occupation factors 0.54, 0.46. The monomers are linked to form a chain polymer.

empirical formula	$C_{22}H_{31}LiMoO_{10}$
M_w	558.35
wavelength/Å	1.54184
T/K	100(2)
cryst. size/mm³	0.15 × 0.10 × 0.05
cryst. system	monoclinic
space group	$P2_1/n$
a/Å	12.3623(2)
b/Å	12.6662(2)
c/Å	17.5445(3)
α/°	90
β/°	109.207(2)
γ/°	90
V/Å³	2 594.25(7)

identification code	oscar15
Z	4
ρ_{calc}/(Mg m^{-3})	1.430
μ/mm^{-1}	4.571
$F(000)$	1152
reflections collected	100 435
indep. reflections (R_{int})	5 385 (0.0446)
parameters	322
restraints	9
goodness-of-fit on F^2	1.081
R_1 ($I > 2\sigma(I)$)	0.0299
wR_2 (all reflections)	0.0807
max and min $\Delta\rho$/(e Å^{-3})	0.590 and −0.919

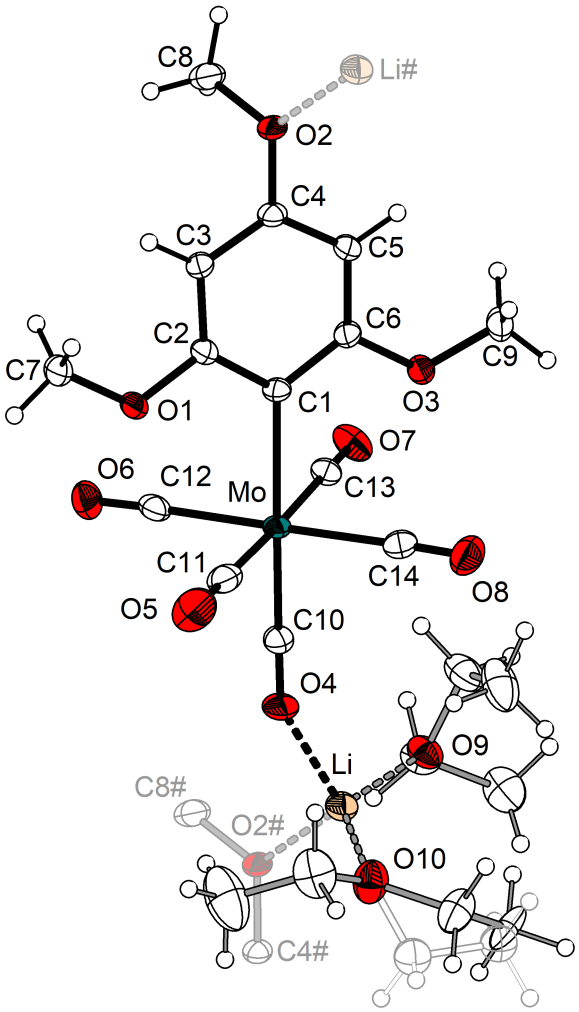

Figure 71. Molecular structure of the monomeric unit of $[Li(Et_2O)_2\mathbf{9}]_n$ with thermal displacement parameters drawn at the 50% probability level. Neighbouring atoms (labelled with #) of the repeating units and the minor component of a disordered ethyl group (at O10) are displayed using paler colours. Selected bond lengths (Å) and angles (deg): Mo–C1 2.312(2), Mo–C10 1.958(2), Mo–C11 2.055(2), Mo–C12 2.046(2), Mo–C13 2.056(2), Mo–C14 2.074(2), Li···O4 1.983(4), Li···O2# 1.944(4); C1–Mo–C10 176.64(7), C11–Mo–C13 178.11(8), C12–Mo–C14 178.97(8), C1–Mo–C11 92.15(7), C1–Mo–C12 89.94(7) C1–Mo–C13 86.50(7) C1–Mo–C14 89.06(7), C10–Mo–C11 91.16(8), C10–Mo–C12 89.53(8), C10–Mo–C13 90.18(8), C10–Mo–C14 91.48(8), C11–Mo–C12 88.62(9), C11–Mo–C14 91.18(9), C12–Mo–C13 90.05(9), C13–Mo–C14 90.13(9), O2#···Li···O4 105.38(17), O2#···Li···O9 107.27(17), O2#···Li···O10 108.33(18), O4···Li···O9 103.12(17), O4···Li···O10 106.25(17), O9···Li···O10 124.89(19), Li···O4···C10 152.67(17).

[Li(Et$_2$O)**10**]$_2$ crystallised as highly air-sensitive, yellow–orange dichroic crystals.

empirical formula	$C_{36}H_{42}Li_2Mo_2O_{18}$
M_w	968.46
wavelength/Å	1.54184
T/K	100(2)
cryst. size/mm³	0.12 × 0.08 × 0.03
cryst. system	triclinic
space group	$P\bar{1}$
a/Å	8.9286(9)
b/Å	11.2383(10)
c/Å	12.5732(9)
α/°	103.667(7)
β/°	102.993(8)
γ/°	113.253(9)
V/Å³	1052.40(16)
identification code	oscar17
Z	1
ρ_{calc}/(Mg m^{-3})	1.528
μ/mm^{-1}	5.506
F(000)	492
reflections collected	23 806
indep. reflections (R_{int})	4 334 (0.0508)
parameters	267
restraints	0
goodness-of-fit on F^2	1.069
R_1 ($I > 2\sigma(I)$)	0.0370
wR_2 (all reflections)	0.0963
max and min $\Delta\rho$/(e Å^{-3})	0.690 and −1.062

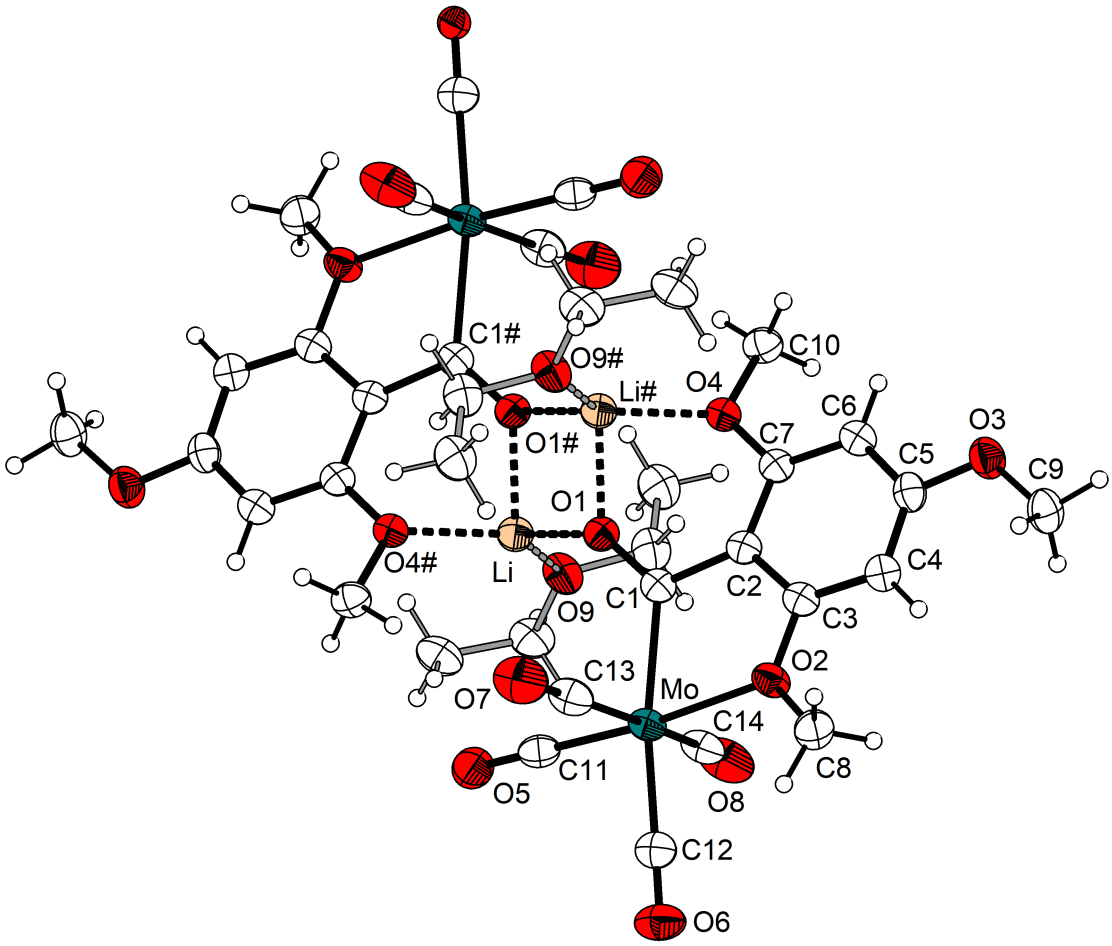

Figure 72. Molecular structure of one polymorph (A) of [Li(Et$_2$O)**10**]$_2$ with thermal displacement parameters drawn at the 50% probability level. Only the asymmetric unit is numbered entirely. Selected bond lengths (Å) and angles (deg): Mo–C1 2.196(3), Mo–C11 1.933(3), Mo–C12 2.019(3), Mo–C13 2.037(3), Mo–C14 2.043(3), Mo–O2 2.294(2), C1–C2 1.496(4), C1–O1 1.261(4), Li···O1 1.897(5), Li···O1# 1.916(5), Li···O4# 1.987(5), Li···O9 1.940(5); C1–Mo–C12 169.86(12), C11–Mo–O2 174.59(10), C13–Mo–C14 168.81(14), C1–Mo–O2 72.97(9), C1–Mo–C11 102.15(12), C1–Mo–C13 87.54(12), C1–Mo–C14 89.83(11), O2–Mo–C12 96.91(11), O2–Mo–C13 93.86(11), O2–Mo–C14 95.77(11), C11–Mo–C12 87.93(14), C11–Mo–C13 83.48(14), C11–Mo–C14 86.45(13), C12–Mo–C13 92.55(13), C12–Mo–C14 91.95(12), Mo–C1–O1 128.4(2), Mo–C1–C2 115.12(19), O1–C1–C2 116.4(3), C1–O1···Li 136.0(2), C1–O1···Li# 130.1(2), Li···O1···Li# 90.2(2), O1···Li···O1# 89.8(2), O1···Li···O4# 122.0(3), O1···Li···O9 110.2(2), O1#···Li···O4# 86.9(2), O1#···Li···O9 110.3(3), O4#···Li···O9 125.1(3).

Orange crystals of a second polymorph of $[Li(Et_2O)\mathbf{10}]_2$ were additionally obtained.

empirical formula	$C_{36}H_{42}Li_2Mo_2O_{18}$	identification code	oa42fr
M_w	968.46	Z	2
wavelength/Å	1.54184	ρ_{calc}/(Mg m^{-3})	1.541
T/K	100(2)	μ/mm^{-1}	5.552
cryst. size/mm^3	0.22 × 0.15 × 0.10	F(000)	984
cryst. system	monoclinic	reflections collected	42 384
space group	$P2_1/n$	indep. reflections (R_{int})	4 364 (0.0592)
a/Å	13.8752(4)	parameters	267
b/Å	10.7698(2)	restraints	0
c/Å	15.1765(5)	goodness-of-fit on F^2	1.024
α/°	90	R_1 ($I > 2\sigma(I)$)	0.0313
β/°	113.016(4)	wR_2 (all reflections)	0.0831
γ/°	90	max and min $\Delta\rho$/(e Å^{-3})	0.373 and −1.011
V/Å^3	2 087.34(10)		

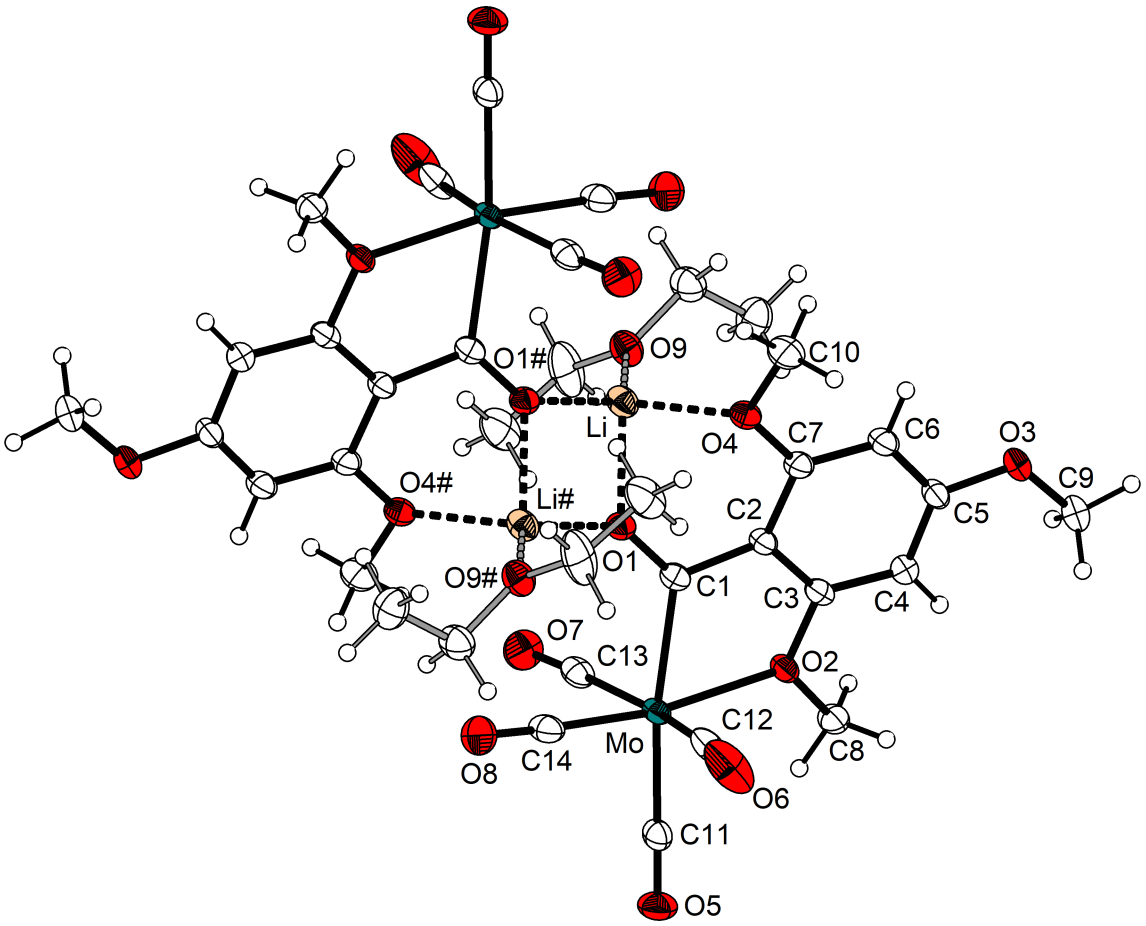

Figure 73. Molecular structure of polymorph B of $[Li(Et_2O)\mathbf{10}]_2$ with thermal displacement parameters drawn at the 50% probability level. Only the asymmetric unit is numbered entirely. Selected bond lengths (Å) and angles (deg): Mo–C1 2.183(2), Mo–C11 2.018(2), Mo–C12 2.041(3), Mo–C13 2.034(3), Mo–C14 1.936(3), Mo–O2 2.2984(16), C1–C2 1.498(3), C1–O1 1.261(3), Li···O1 1.938(5), Li···O1# 1.903(5), Li···O4 2.004(5), Li···O9 1.948(5); C1–Mo–C11 171.45(9), C14–Mo–O2 171.06(8), C12–Mo–C13 165.37(11), C1–Mo–O2 73.28(7), C1–Mo–C12 88.48(10), C1–Mo–C13 89.13(9), C1–Mo–C14 97.88(9), O2–Mo–C11 98.23(8), O2–Mo–C12 95.30(9), O2–Mo–C13 97.83(8), C11–Mo–C12 91.29(11), C11–Mo–C13 93.19(10), C11–Mo–C14 90.62(10), C12–Mo–C14 85.63(12), C13–Mo–C14 80.40(11), Mo–C1–O1 127.63(17), Mo–C1–C2 115.11(16), O1–C1–C2 117.3(2), C1–O1···Li 127.4(2), C1–O1···Li# 141.5(2), Li···O1···Li# 90.8(2), O1···Li···O1# 89.2(2), O1···Li···O4 84.56(19), O1···Li···O9 116.1(2), O1#···Li···O4 126.9(2), O1#···Li···O9 124.1(2), O4···Li···O9 105.5(2).

After optimising the reaction conditions to yield Li-**8** selectively, the compound crystallised as large, block-shaped, orange crystals with coordinated THF, [Li(thf)**8**]$_2$.

empirical formula	$C_{38}H_{38}Li_2Mo_2O_{20}$	identification code	oscar20
M_w	1020.44	Z	2
wavelength/Å	1.54184	ρ_{calc}/(Mg m^{-3})	1.577
T/K	100(2)	μ/mm^{-1}	5.468
cryst. size/mm^3	0.20 × 0.16 × 0.08	F(000)	1032
cryst. system	monoclinic	reflections collected	43641
space group	$P2_1/n$	indep. reflections (R_{int})	4452 (0.0510)
a/Å	9.36672(10)	parameters	283
b/Å	12.67753(15)	restraints	0
c/Å	18.0971(3)	goodness-of-fit on F^2	1.036
α/°	90	R_1 ($I > 2\sigma(I)$)	0.0292
β/°	91.335(2)	wR_2 (all reflections)	0.0763
γ/°	90	max and min $\Delta\rho$/(e Å^{-3})	0.587 and −0.807
V/Å^3	2148.39(5)		

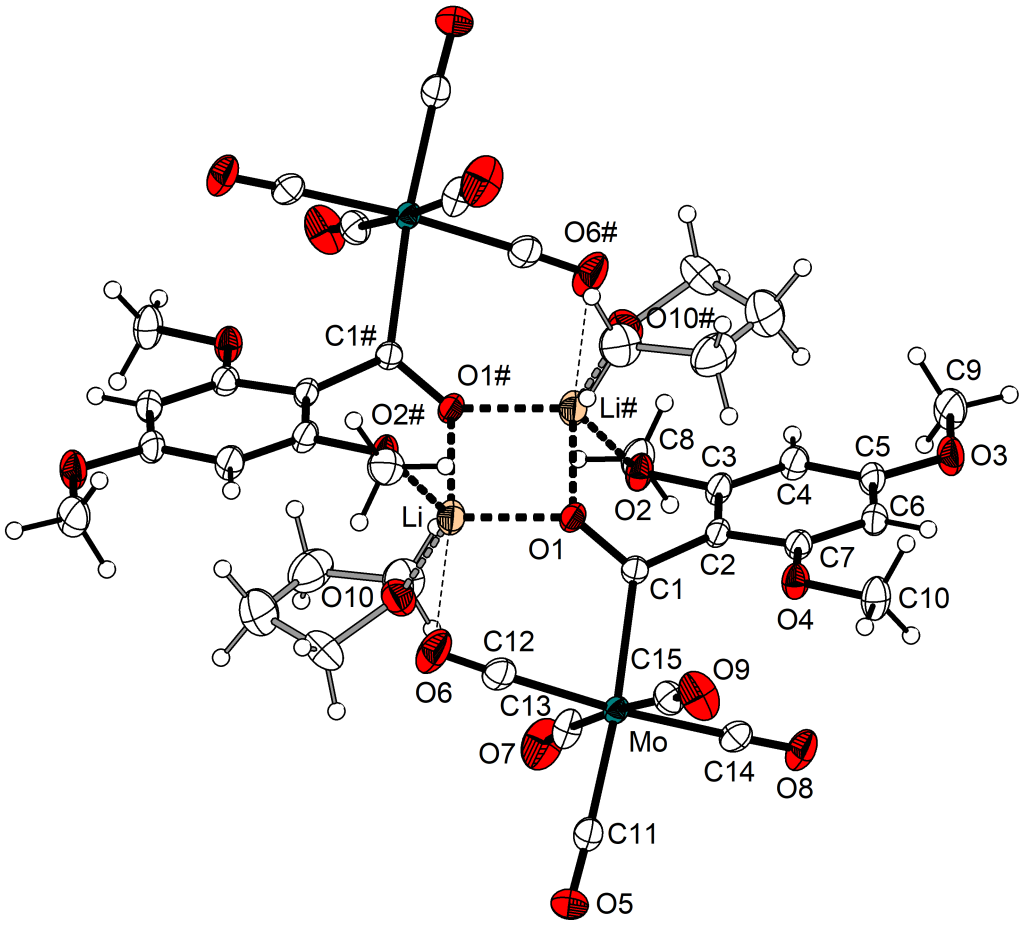

Figure 74. Molecular structure of dimeric [Li(thf)**8**]$_2$ with thermal displacement parameters drawn at the 50% probability level. Only the asymmetric unit is numbered entirely. Selected bond lengths (Å) and angles (deg): Mo–C1 2.251(2), Mo–C11 2.022(3), Mo–C12 2.033(3), Mo–C13 2.034(3), Mo–C14 2.054(3) Mo–C15 2.061(3), C1–C2 1.517(3), C1–O1 1.265(3), Li···O1 1.906(4), Li···O1# 1.962(5), Li···O2# 1.998(5), Li···O6 2.739(5), Li···O10 1.920(5); C1–Mo–C11 174.91(9), C12–Mo–C14 175.46(9), C13–Mo–C15 176.53(10), C1–Mo–C12 85.98(9), C1–Mo–C13 88.79(10), C1–Mo–C14 89.49(8), C1–Mo–C15 93.97(9), C11–Mo–C12 89.96(10), C11–Mo–C13 88.25(11), C11–Mo–C14 94.54(9), C11–Mo–C15 89.15(10), C12–Mo–C13 91.45(10), C12–Mo–C15 90.85(10), C13–Mo–C14 88.08(10), C14–Mo–C15 89.83(10), Mo–C1–O1 121.71(15), Mo–C1–C2 124.23(15), O1–C1–C2 113.50(19), C1–O1···Li 139.4(2), C1–O1···Li# 123.97(18), Li···O1···Li# 87.45(19), O1···Li···O1# 92.55(19), O1···Li···O2# 116.8(2), O1#···Li···O2# 85.31(18), O1···Li···O6 92.24(15), O1#···Li···O6 168.4(2), O2#···Li···O6 83.10(14), O1···Li···O10 118.6(2), O1#···Li···O10 104.2(2), O2#···Li···O10 123.0(2), O6···Li···O10 82.67(16).

Preparation of *mer*-tris(bromido)(1,2-dimethoxyethane-κ^2*O,O'*)(2,4,6-trimethoxybenzylidyne)molybdenum(VI), 18

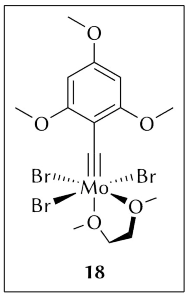

18

To a stirred and precooled (–80 °C) suspension of [Li(thf)**8**] (1.16 g, 2.27 mmol) in dichloromethane (30 mL) was added a precooled (–80 °C) solution of oxalyl bromide (0.59 g, 2.72 mmol, 1.2 equiv) in dichloromethane (5 mL). The brown mixture was allowed to gradually reach –20 °C (the cooling bath was not removed), during which time the colour darkened slightly and evolution of gas was observed. The mixture was cooled back to –80 °C and filtered at this temperature through D.E. on a jacketed frit to separate precipitated LiBr. Then, 1,2-dimethoxyethane (2.35 mL, 2.04 g, 22.60 mmol, 10.0 equiv) was added to the stirred filtrate at –70 °C, followed by slow addition of a precooled (–70 °C) solution of bromine (0.12 mL, 0.37 g, 2.31 mmol, 1.02 equiv) in dichloromethane (5 mL). The resulting orange-brown solution was allowed to warm up gradually to approximately 15 °C, and the volatiles were removed in high vacuum. The deep brown residue was dissolved in dichloromethane (10 mL), and after addition of *n*-pentane (45 mL), a brown solid precipitated. The mother liquor was decanted off, and the solid was dried in high vacuum to give **18** as a crude product as judged by NMR spectroscopy (any attempts to recrystallise or further purify the compound caused additional decomposition). Yield (crude product): 73% (996 mg, 1.65 mmol).

1. NMR spect1ooscopy

	solvent: dichloromethane-d_2
δ_H (300.1 MHz, 297 K)	3.48 (br s, DME), 3.65 (br s, DME), 3.82 (br s, DME), 3.87 (s, 3H, *p*-OCH_3), 3.91 (s, 6H, 2 × *o*-OCH_3), 3.97 (br s, DME), 6.03 (s, 2H, 2 × *m*-*H*)
δ_C (75.5 MHz, 299 K)	56.0 (*p*-O*C*H$_3$), 56.2 (*o*-O*C*H$_3$), 60.0 (DME-*C*H$_3$), 70.0 (DME-*C*H$_2$), 73.4 (DME-*C*H$_3$), 78.6 (DME-*C*H$_2$), 88.9 (*m*-*C*H), 117.1 (*i*-C_q), 165.1 (*p*-C_qO), 168.4 (*o*-C_qO), 331.4 (*C*≡Mo)

Preparation of tris((1,1,1,3,3,3-hexafluoro-2-methyl-2-propanyl)oxy)(tetrahydrofuran-*κO*)(2,4,6-trimethoxybenzylidyne)molybdenum(VI), [5(thf)]

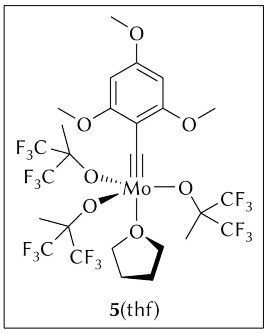

5(thf)

To a stirred solution of K-**14** (132 mg, 600 µmol, 3.3 equiv) in THF (1.5 mL) was added the crude molybdenum complex **18** (111 mg, 183 µmol) in portions through a funnel, and the funnel was rinsed with THF (2 × 0.5 mL). The mixture immediately turned deep brown and was stirred for 16 h at ambient temperature. The volatiles were removed in vacuum, and the deep brown residue was dried for 1 h at 50 °C under dynamic vacuum. The residue was extracted several times with *n*-hexane, filtered through D.E., and the frit was washed with more *n*-hexane, leaving a black residue and a yellow filtrate. Removal of the solvent in high vacuum afforded the product as a yellow solid in 62% yield (101 mg, 113 µmol).

1. Elemental analysis

$C_{26}H_{28}F_{18}MoO_7$	C [%]	H [%]
Found	33.52	2.81
Calc.	35.07	3.17

Combustion analysis repeatedly produced low carbon and hydrogen values, which can be ascribed to partial loss of THF (~0.5 equiv).

2. NMR spectroscopy

	solvent: C_6D_6
δ_H (300.1 MHz, 297 K)	1.43 (m, THF), 1.94 (s, 9H, 3 × C(CH_3)(CF$_3$)$_2$), 3.17 (s, 6H, 2 × *o*-OCH_3), 3.21 (s, 3H, *p*-OCH_3), 3.86 (m, THF), 5.66 (s, 2H, 2 × *m*-*H*)
δ_C (75.5 MHz, 298 K)	18.0 (C(*C*H$_3$)(CF$_3$)$_2$), 25.6 (THF), 54.4 (*o*-OCH$_3$), 55.0 (*p*-OCH$_3$), 68.4 (THF), 84.8 (sep, $^2J_{CF}$ = 30 Hz, *C*(CH$_3$)(CF$_3$)$_2$), 89.8 (*m*-*C*H), 120.3 (*i*-C_q), 123.9 (q, $^1J_{CF}$ = 288 Hz, *C*F$_3$), 162.8 (*o*-C_qO), 163.2 (*p*-C_qO), 292.6 (*C*≡Mo)
δ_F (188.3 MHz, 300 K)	–77.9

3. X-ray crystal structure determination

Single-crystals suitable for X-ray diffraction analysis were obtained by storing a concentrated *n*-pentane solution at –30 °C.

Special features: The asymmetric unit contains two independent molecules, which are related by a pseudo-*C*-centring vector. The THF of the second molecule (singly primed) is disordered over two positions in the ratio 84:16. Figure 75 shows that the two molecules are similar except for the orientation of the ligand at O4.

empirical formula	$C_{26}H_{28}F_{18}MoO_7$
M_w	890.42
wavelength/Å	1.54184
T/K	100(2)
cryst. size/mm³	0.18 × 0.16 × 0.06
cryst. system	triclinic
space group	$P\bar{1}$
a/Å	11.9142(3)
b/Å	16.1715(4)
c/Å	18.2475(4)
α/°	106.467(2)
β/°	90.580(2)
γ/°	90.487(2)
V/Å³	3 371.14(14)

identification code	oscar19
Z	4
ρ_{calc}/(Mg m^{-3})	1.754
μ/mm^{-1}	4.515
$F(000)$	1776
reflections collected	121 665
indep. reflections (R_{int})	13 948 (0.0352)
parameters	958
restraints	26
goodness-of-fit on F^2	1.028
R_1 ($I > 2\sigma(I)$)	0.0308
wR_2 (all reflections)	0.0833
max and min $\Delta\rho$/(e Å^{-3})	0.579 and −1.133

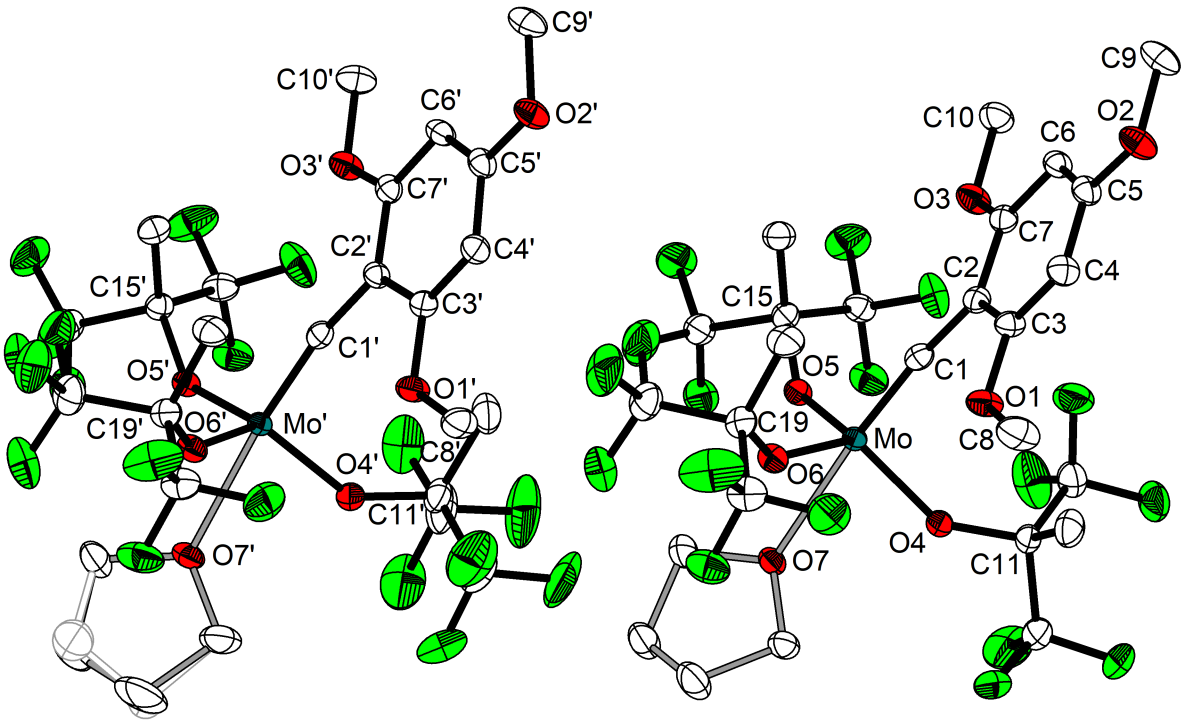

Figure 75. Molecular structure of [**5**(thf)] showing the two independent molecules with thermal displacement parameters drawn at the 50% probability level. Hydrogen atoms are omitted for clarity. A part of the THF molecule coordinated to Mo′ is disordered and was refined on two positions; the minor component is shown here in a paler colour. Selected bond lengths (Å) and angles (deg): Mo–C1 1.7635(19), Mo′–C1′ 1.7586(19), Mo–O4 1.9171(13), Mo′–O4′ 1.9219(13), Mo–O5 1.9020(13), Mo′–O5′ 1.9005(13), Mo–O6 1.9176(13), Mo′–O6′ 1.9226(13), Mo–O7 2.4256(13), Mo′–O7′ 2.4007(13), C1–C2 1.444(3), C1′–C2′ 1.439(2); C1–Mo–O4 101.05(7), C1′–Mo′–O4′ 100.30(7), C1–Mo–O5 107.22(7), C1′–Mo′–O5′ 106.36(7), C1–Mo–O6 102.01(7), C1′–Mo′–O6′ 101.33(7), C1–Mo–O7 174.63(7), C1′–Mo′–O7′ 173.55(7), O4–Mo–O5 113.44(5), O4′–Mo′–O5′ 112.80(6), O4–Mo–O6 121.10(6), O4′–Mo′–O6′ 124.44(6), O4–Mo–O7 75.59(5), O4′–Mo′–O7′ 75.87(5), O5–Mo–O6 109.98(6), O5′–Mo′–O6′ 108.98(6), O5–Mo–O7 78.06(5), O5′–Mo′–O7′ 80.02(5), O6–Mo–O7 76.62(5), O6′–Mo′–O7′ 77.12(5), Mo–C1–C2 171.04(15), Mo′–C1′–C2′ 167.28(15).

Preparation of tris((1,1,1,3,3,3-hexafluoro-2-methyl-2-propanyl)oxy)(2,4,6-trimethoxybenzylidyne)molybdenum(VI), 5

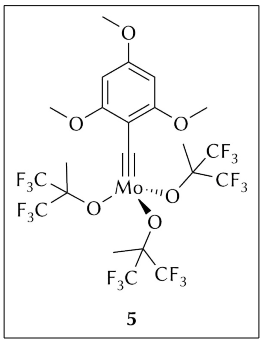

5

K-**14** (228 mg, 1035 µmol, 0.97 equiv) was dissolved in THF (3 mL) and added to a stirred solution of crude **18** (216 mg, 357 µmol) in THF (1 mL), which immediately turned deep brown. The mixture was stirred overnight at ambient temperature. The volatiles were removed under vacuum, and the brown residue was dried for 90 min at 50 °C under dynamic vacuum. It was then extracted several times with *n*-pentane, filtered through D.E., and the frit was washed with more *n*-pentane, leaving a black residue and a yellow filtrate. The solvent was removed under high vacuum, and the residue was dried for 90 min at 40 °C under dynamic vacuum. *n*-Pentane (5 mL) was added and then removed quickly at 40 °C twice. After additional drying for 15 min at 40 °C under dynamic vacuum, the product was isolated as a brown solid in 36% yield (101 mg, 123 µmol).

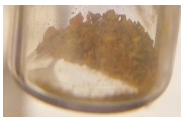

1. Elemental analysis

$C_{22}H_{20}F_{18}MoO_6$	C [%]	H [%]
Found	32.29	2.29
Calc.	32.29	2.46

2. NMR spectroscopy

	solvent: C_6D_6
δ_H (600.1 MHz, 303 K)	1.87 (s, 9H, 3 × C(CH_3)(CF$_3$)$_2$), 3.14 (s, 6H, 2 × *o*-OCH_3), 3.18 (s, 3H, *p*-OCH_3), 5.64 (s, 2H, 2 × *m*-*H*)
δ_C (150.9 MHz, 303 K)	18.19 (C(*C*H$_3$)(CF$_3$)$_2$), 54.54 (*o*-O*C*H$_3$), 55.01 (*p*-O*C*H$_3$), 84.52 (sep, $^2J_{CF}$ = 30.1 Hz, *C*(CH$_3$)(CF$_3$)$_2$), 89.75 (*m*-*C*H), 120.35 (*i*-C_q), 123.62 (q, $^1J_{CF}$ = 286.5 Hz, *C*F$_3$), 163.02 (*o*-C_qO), 163.19 (*p*-C_qO), 296.73 (*C*≡Mo)
δ_F (470.7 MHz, 298 K)	–78.14

3. X-ray crystal structure determination

Single-crystals suitable for X-ray diffraction analysis were obtained from a concentrated *n*-pentane solution at –30 °C.

Special features: Neighbouring molecules are linked by an *n* glide plane to form a linear chain polymer parallel to [101] (see Figure 76).

empirical formula	$C_{22}H_{20}F_{18}MoO_6$
M_w	818.32
wavelength/Å	1.54184
T/K	100(2)
cryst. size/mm³	0.20 × 0.15 × 0.05
cryst. system	monoclinic
space group	$P2_1/n$
a/Å	11.45727(10)
b/Å	16.75394(15)
c/Å	15.91805(15)
α/°	90
β/°	102.3179(10)
γ/°	90
V/Å³	2 985.20(5)

identification code	oscar21
Z	4
ρ_{calc}/(Mg m^{-3})	1.821
μ/mm^{-1}	5.009
F(000)	1616
reflections collected	61140
indep. reflections (R_{int})	6186 (0.0526)
parameters	430
restraints	0
goodness-of-fit on F^2	1.045
R_1 ($I > 2\sigma(I)$)	0.0300
wR_2 (all reflections)	0.0786
max and min $\Delta\rho$/(e Å^{-3})	0.435 and −1.013

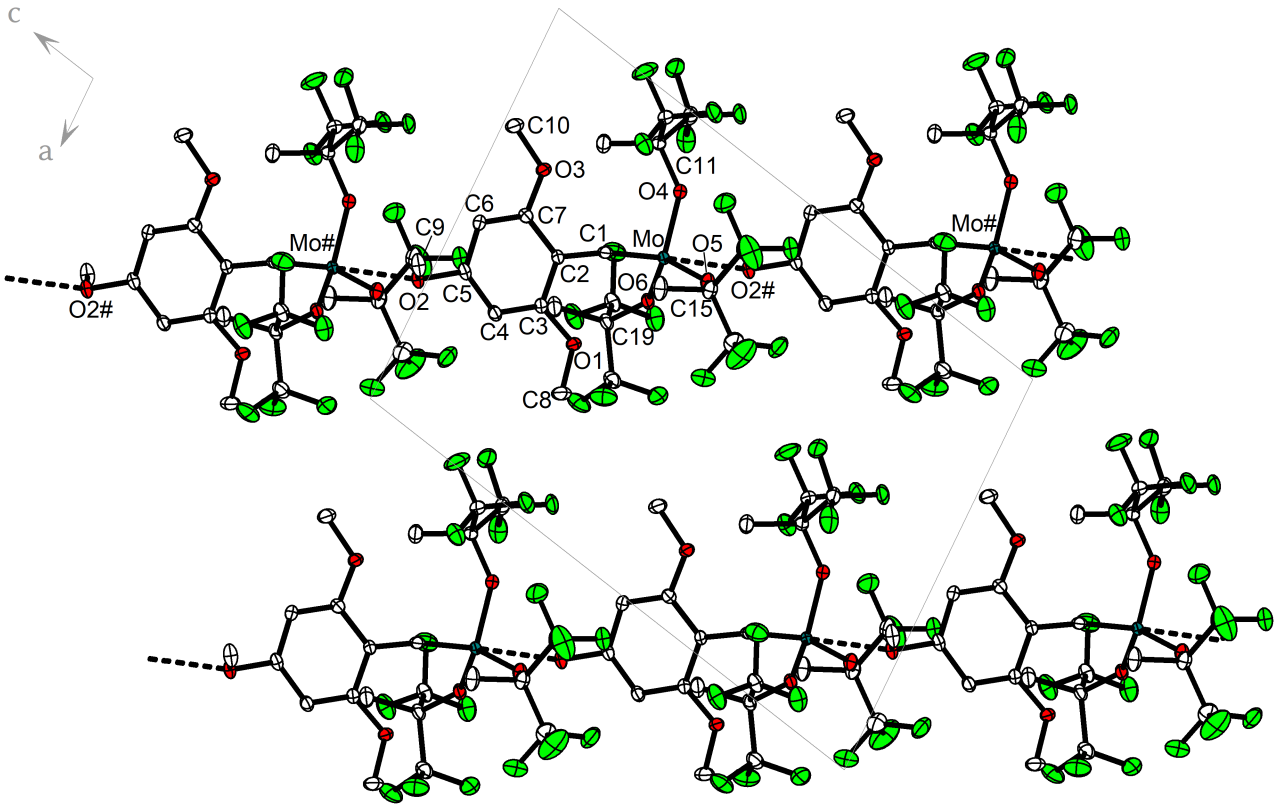

Figure 76. Crystal packing of **5** viewed along the *b* axis with thermal displacement parameters drawn at the 50% probability level. It shows the formation of chain polymers via intermolecular Mo···O contacts (dashed bonds). Hydrogen atoms are omitted for clarity.

4. Alkyne metathesis

The catalytic activity was tested according to the general procedure for the metathesis of internal alkyne **Y**-Me (0.251 mmol) and terminal alkyne **Y**-H (0.250 mmol). In addition, the procedure for **Y**-Me was repeated after exposing the complex to air for 1 h; no samples were measured at t = 2 min and t = 4 min, and the last two samples were measured at t = 120 min and t = 43.5 h.

Attempted preparation of lithium (4-methoxybenzoyl)pentacarbonylmolybdate(0), Li-12

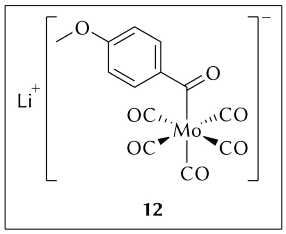

12

A precooled (0 °C) solution of 4-methoxyphenyl lithium (2.73 g, 24.00 mmol) in THF (50 mL) was added to a solution of $[Mo(CO)_6]$ (6.41 g, 24.00 mmol) in THF (120 mL) at 0 °C (exothermic reaction). The mixture, which turned maroon, was stirred for 2 h at ambient temperature; *n*-hexane (140 mL) was then quickly added, and an oily deep red precipitate began depositing from solution. The discoloured supernatant was decanted, and the sticky residue was suspended in *n*-hexane (10 mL); the suspension was then frozen and warmed back to ambient temperature. Removal of *n*-hexane under vacuum gave a brownish solid. The residue was washed with more *n*-hexane (10 mL) and finally dried for several hours under dynamic vacuum to yield 4.53 g (8.70 mmol, 36%) of a crude product as a brown solid. As judged by NMR analyses, compound Li-**12** constitutes approx. 75% of the mixture.

1. NMR spectroscopy

only $[Li(thf)_2$**12**$]$	solvent: tetrahydrofuran-d_8
δ_H (600.1 MHz, 303 K)	1.77 (m, 2 × 4H, 2 × THF), 3.61 (m, 2 × 4H, 2 × THF), 3.76 (s, 3H, *p*-OCH_3), 6.81 (d, 2H, $^3J_{HH}$ = 8.8 Hz, *m*-*H*), 7.53 (d, 2H, $^3J_{HH}$ = 8.8 Hz, *o*-*H*)
δ_C (150.9 MHz, 303 K)	26.37 (THF), 55.44 (OCH_3), 68.27 (THF), 112.94 (2 × *m*-*C*H), 128.52 (2 × *o*-*C*H), 149.77 (*i*-C_q), 161.60 (*p*-C_q), 211.47 (4 × *cis*-*C*O), 217.54 (*trans*-*C*O), 308.01 (Ar–*C*=O)

Preparation of tetramethylammonium (4-methoxybenzoyl)pentacarbonylmolybdate(0), (Me_4N)12

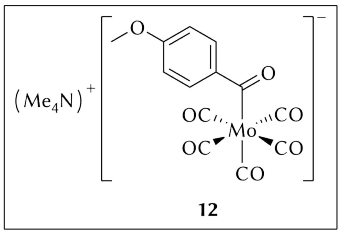

12

The literature procedure[84] was adapted as follows. In a 500 mL Schlenk flask a solution of 4-methoxyphenyllithium (2.587 g, 22.68 mmol) in diethyl ether (90 mL) was added over 20 min to a stirred suspension of $[Mo(CO)_6]$ (5.99 g, 22.69 mmol) in diethyl ether (200 mL), which resulted in a slightly exothermic reaction and an immediate colour change to orange-brown. After addition was complete, the reaction mixture was stirred for 4 h at ambient temperature, and then the solvent was removed under reduced pressure. The brown residue was suspended in *n*-hexane (40 mL) and sonicated for 30 min, the supernatant was decanted, and the residual solid was dried under high vacuum. The deep yellow residue was dissolved in deoxygenated water (30 mL), filtered through a frit to remove unreacted $[Mo(CO)_6]$, and the filtrate was added dropwise to a solution of $(Me_4N)Br$ (5.46 g, 35.44 mmol, ~1.5 equiv) in deoxygenated water (25 mL). Meanwhile, the flask and the frit were rinsed with deoxygenated water (3 × 5 mL), and the mixture was vigorously stirred for 30 min, until precipitation of an orange solid ceased. The precipitate was collected by filtration, washed with diethyl ether (3 × 5 mL) and dried in high vacuum to give (Me_4N)**12** as an orange microcrystalline solid. Yield: 55% (5.57 g, 12.51 mmol).

1. Elemental analysis

$C_{17}H_{19}MoNO_7$	C [%]	H [%]	N [%]
Found	45.90	4.14	3.57
Calc.	45.85	4.30	3.15

2. NMR spectroscopy

	solvent: tetrahydrofuran-d_8
δ_H (300.1 MHz, 298 K)	3.28 (t, 12H, $^2J_{HN}$ = 0.5 Hz, N(CH_3)$_4$), 3.75 (s, 3H, OCH_3), 6.78 (d, 2H, $^3J_{HH}$ = 8.8 Hz, 2 × Ar-*H*), 7.57 (d, 2H, $^3J_{HH}$ = 8.8 Hz, 2 × Ar-*H*)
δ_C (75.5 MHz, 299 K)	55.3 (O*C*H$_3$), 55.7 (t, $^1J_{CN}$ = 4 Hz, N(*C*H$_3$)$_4$), 112.8 (2 × *m*-C_q), 128.8 (2 × *o*-*C*H), 148.6 (*i*-C_q), 161.0 (*p*-C_q), 212.9 (4 × *cis*-*C*O), 218.6 (*trans*-*C*O), 289.8 (Ar–*C*=O)

3. X-ray crystal structure determination

Single-crystals suitable for X-ray diffraction analysis were obtained by storing a dichloromethane solution at –35 °C.

Special features: There are two very short C–H···O contacts between the cation and anion: H14A···O1 2.31 Å and H15C···O1 2.40 Å.

empirical formula	$C_{17}H_{19}MoNO_7$	identification code	oscar26
M_w	445.27	Z	4
wavelength/Å	1.54184	ρ_{calc}/(Mg m^{-3})	1.537
T/K	100(2)	μ/mm^{-1}	5.911
cryst. size/mm^3	0.20 × 0.15 × 0.12	F(000)	904
cryst. system	monoclinic	reflections collected	37 194
space group	$P2_1/n$	indep. reflections (R_{int})	4 012 (0.0405)
a/Å	9.2926(2)	parameters	241
b/Å	12.7946(4)	restraints	0
c/Å	16.3929(4)	goodness-of-fit on F^2	1.042
α/°	90	R_1 ($I > 2\sigma(I)$)	0.0231
β/°	99.097(2)	wR_2 (all reflections)	0.0610
γ/°	90	extinction coefficient	0.00113(8)
V/Å^3	1924.53(9)	max and min $\Delta\rho$/(e Å^{-3})	0.379 and –0.653

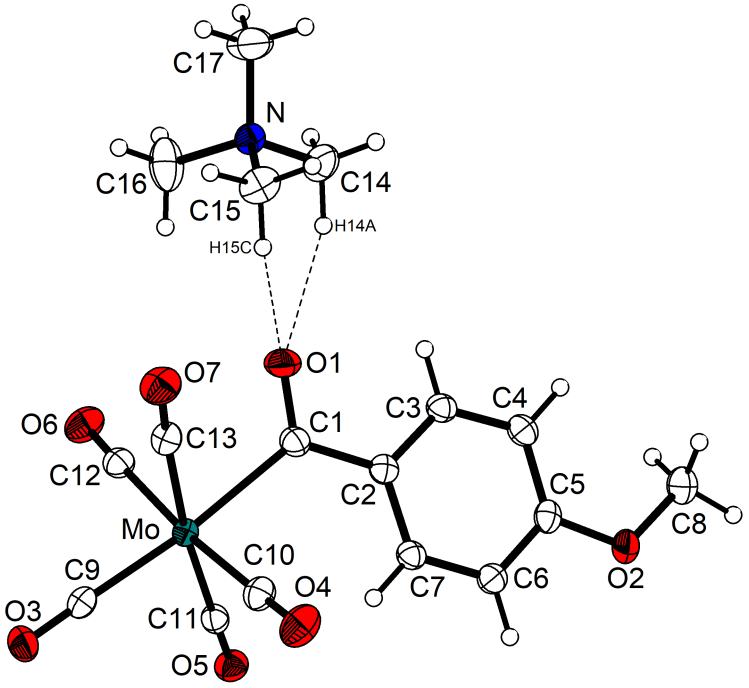

Figure 77. Molecular structure of (Me_4N)**12** with thermal displacement parameters drawn at the 50% probability level. The short contacts H14A···O1 and H15C···O1 are drawn explicitly as dotted bonds. Selected bond lengths (Å) and angles (deg): Mo–C1 2.2907(18), Mo–C9 2.0048(18), Mo–C10 2.0324(19), Mo–C11 2.0364(18), Mo–C12 2.0658(18), Mo–C13 2.0559(18), C1–O1 1.238(2), C1–C2 1.523(2); C1–Mo–C9 174.49(7), C10–Mo–C12 175.03(7), C11–Mo–C13 174.18(7), C1–Mo–C10 92.51(7), C1–Mo–C11 92.98(6), C1–Mo–C12 82.58(7), C1–Mo–C13 81.22(7), C9–Mo–C10 91.83(7), C9–Mo–C11 90.18(7), C9–Mo–C12 93.03(7), C9–Mo–C13 95.64(7), C10–Mo–C11 93.01(7), C10–Mo–C13 86.83(7), C11–Mo–C12 88.02(7), C12–Mo–C13 91.65(7), Mo–C1–O1 119.68(13), Mo–C1–C2 125.57(12), O1–C1–C2 114.72(16).

Preparation of *mer*-tris(bromido)(1,2-dimethoxyethane-κ^2*O,O'*)(4-methoxybenzylidyne)molybdenum(VI), 13

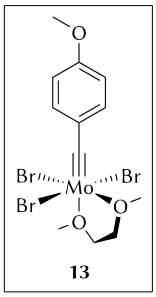

13

The literature procedure[84] was slightly modified as follows. A precooled (–80 °C) solution of oxalyl bromide (2.56 g, 11.86 mmol, 1.09 equiv) in dichloromethane (4 mL) was added over 2 min to a stirred and precooled (–80 °C) suspension of (Me_4N)**12** (4.86 g, 10.91 mmol) in dichloromethane (100 mL). The orange mixture was stirred for 15 min, whereby it darkened gradually and turned violet; a colour change to yellow was then observed as it warmed to approx. –30 °C (the cooling bath was not removed). The mixture was cooled back to –80 °C and filtered at this temperature through D.E. on a jacketed frit to remove precipitated (Me_4N)Br. Then, 1,2-dimethoxyethane (5.67 mL, 4.92 g, 54.57 mmol, 5.0 equiv) was added to the stirred filtrate at –80 °C, followed by slow addition over 3 min of a precooled (–70 °C) solution of bromine (0.57 mL, 1.78 g, 11.13 mmol, 1.02 equiv) in dichloromethane (5 mL). The resulting orange-brown solution was stirred for 15 min and allowed to warm up gradually to ambient temperature. The mixture was concentrated to 50 mL and the product was precipitated with *n*-pentane (130 mL). The supernatant was decanted off; the brown precipitate was washed with *n*-pentane (2 × 10 mL) and dried under high vacuum. Yield: 83% (4.93 g, 9.05 mmol). The spectroscopic data are in agreement with the literature.[84]

Preparation of tris((1,1,1,3,3,3-hexafluoro-2-methyl-2-propanyl)oxy)(tetrahydrofuran-κ*O*)(4-methoxybenzylidyne)molybdenum(VI), [2(thf)]

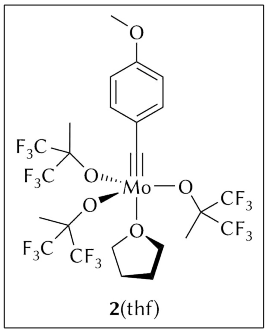

2(thf)

A solution of K-**14** (0.66 g, 3.00 mmol, 3 equiv) in THF (7 mL) was added to a stirred solution of **13** (0.54 g, 1.00 mmol) in THF (3 mL), and the reddish-brown mixture was stirred overnight at ambient temperature. The volatiles were removed under reduced pressure, and the brown residue was dried under dynamic vacuum. It was then extracted repeatedly with *n*-pentane (total amount 10 mL), filtered through D.E., and the frit was washed with more *n*-pentane to give a yellow filtrate. The solvent was removed under high vacuum, and the product was isolated as a pale brown solid. Yield: 70% (0.58 g, 0.70 mmol).

1. Elemental analysis

$C_{24}H_{24}F_{18}MoO_5$	C [%]	H [%]
Found	34.62	3.04
Calc.	34.71	2.91

2. NMR spectroscopy

	solvent: C_6D_6
δ_H (300.1 MHz, 297 K)	1.38 (m, 4H, THF), 1.83 (s, 9H, 3 × C(CH_3)(CF_3)$_2$), 3.17 (s, 3H, OCH_3), 3.82 (m, 4H, THF), 6.44 (d, 2H, $^3J_{HH}$ = 8.9 Hz, 2 × Ar-*H*), 7.16 (d, 2H, $^3J_{HH}$ = 8.9 Hz, 2 × Ar-*H*)
δ_C (75.5 MHz, 299 K)	19.4 (C(*C*H$_3$)(CF$_3$)$_2$), 25.5 (THF), 54.9 (O*C*H$_3$), 68.6 (THF), 84.7 (sep, $^2J_{CF}$ = 29 Hz, *C*(CH$_3$)(CF$_3$)$_2$), 113.8 (*m*-*C*H), 124.1 (q, $^1J_{CF}$ = 288 Hz, *C*F$_3$), 132.6 (*o*-*C*H), 139.2 (*i*-C_q), 160.7 (*p*-C_qO), 294.4 (*C*≡Mo)
δ_F (188.3 MHz, 300 K)	–77.81

3. X-ray crystal structure determination

Crystallisation attempts from concentrated *n*-pentane solutions at –35 °C afforded yellow crystals of [**2**(thf)] (see Figure 30).

Special features/exceptions: First attempts to record data at 100 K led to degradation of the crystals, possibly because of a destructive phase transition. The crystals were pseudomerohedrally twinned, and one of the two independent molecules is badly disordered. It can be concluded that the structure is qualitatively correct, but it could not be refined satisfactorily. For this reason, structural parameters are not included.

empirical formula	$C_{48}H_{48}F_{36}Mo_2O_{10}$
M_w	1660.75
wavelength/Å	1.54184
T/K	150(2)
cryst. size/mm³	0.18 × 0.12 × 0.10
cryst. system	triclinic
space group	$P\bar{1}$
a/Å	10.6657(9)
b/Å	16.9790(9)
c/Å	17.4281(9)
α/°	90.174(5)
β/°	95.412(5)
γ/°	90.361(5)
V/Å³	3142.0(3)
identification code	oscar25
Z	4
ρ_{calc}/(Mg m^{-3})	1.755
μ/mm^{-1}	4.74
F(000)	1648
reflections collected	67087
indep. reflections (R_{int})	13064 (0.0515)
parameters	891
restraints	32
goodness-of-fit on F^2	1.046
R_1 ($I > 2\sigma(I)$)	0.0677
wR_2 (all reflections)	0.2144
max and min $\Delta\rho$/(e Å^{-3})	0.991 and –3.446

Single-crystals of [**2**(thf)$_2$] were obtained from a concentrated *n*-pentane/THF (~20:1) solution of [**2**(thf)] at –35 °C.

Special features/exceptions: The THF at O5 is disordered over two positions with occupation factors 0.83, 0.17.

empirical formula	$C_{28}H_{32}F_{18}MoO_6$	identification code	oscar34
M_w	902.48	Z	4
wavelength/Å	0.71073	ρ_{calc}/(Mg m^{-3})	1.812
T/K	100(2)	μ/mm^{-1}	0.540
cryst. size/mm^3	0.35 × 0.18 × 0.08	F(000)	1808
cryst. system	monoclinic	reflections collected	196 932
space group	$P2_1/n$	indep. reflections (R_{int})	10 261 (0.0631)
a/Å	10.6543(2)	parameters	491
b/Å	19.2597(3)	restraints	21
c/Å	16.1247(3)	goodness-of-fit on F^2	1.050
α/°	90	R_1 ($I > 2\sigma(I)$)	0.0338
β/°	90.420(2)	wR_2 (all reflections)	0.0734
γ/°	90	max and min $\Delta\rho$/(e Å^{-3})	1.097 and –0.690
V/Å^3	3308.69(10)		

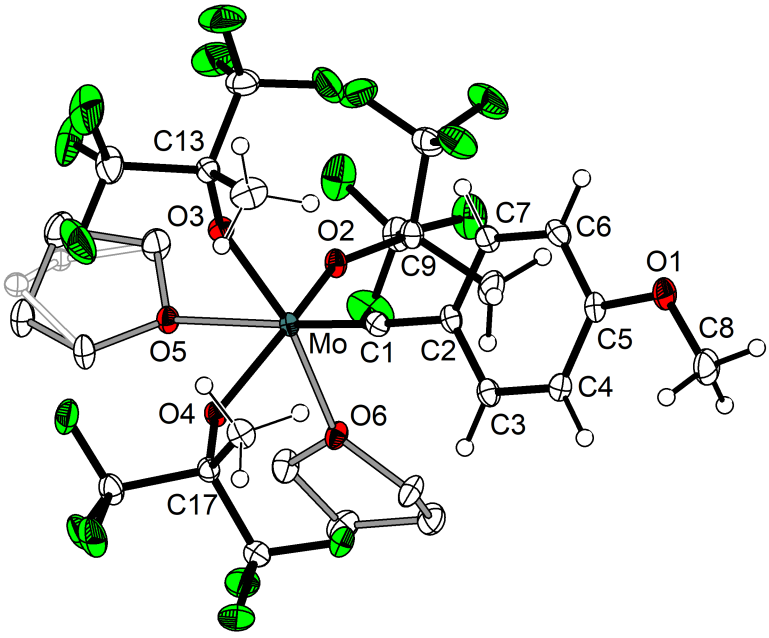

Figure 78. Molecular structure of *cis,mer*-[**2**(thf)$_2$] with thermal displacement parameters drawn at the 50% probability level. Hydrogen atoms of solvent molecules are omitted for clarity. The minor component of the disordered THF (at O5) is drawn in a paler colour. For selected bond lengths and angles, see Figure 31, p 58.

4. Alkyne metathesis

The catalytic activity was tested according to the general procedure for the metathesis of alkyne **Y**-Me on a 0.250 mmol scale. No samples were measured at t = 5 min and t = 15 min. Isolated yield: 96% (from 0.50 mmol).

Preparation of tris((1,1,1,3,3,3-hexafluoro-2-methyl-2-propanyl)oxy) (4-methoxybenzylidyne)molybdenum(VI), 2

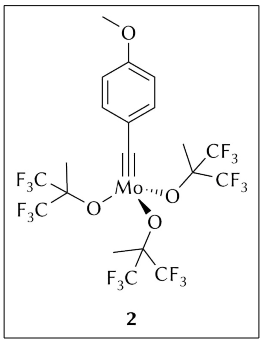

2

A solution of [**2**(thf)] (47 mg, 57 μmol) in toluene (1 mL) and *n*-pentane (1 mL) was stored for 5 d at –35 °C. From that solution pale brown crystals precipitated. After decantation and drying under dynamic vacuum the product was isolated in 43% yield (20 mg, 26 μmol).

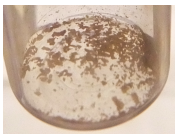

Alternatively, [**2**(thf)] can be repeatedly dissolved in toluene, and the solvent subsequently evaporated at 50 °C to obtain THF-free complex **2**.

1. Elemental analysis

$C_{20}H_{16}F_{18}MoO_4$	C [%]	H [%]
Found	31.70	1.86
Calc.	31.68	2.13

2. NMR spectroscopy

	solvent: C_6D_6
δ_H (300.1 MHz, 298 K)	1.68 (s, 9H, 3 × C(CH_3)(CF_3)$_2$), 3.16 (s, 3H, OCH_3), 6.41 (d, 2H, $^3J_{HH}$ = 9.0 Hz, 2 × Ar-*H*), 7.04 (d, 2H, $^3J_{HH}$ = 9.0 Hz, 2 × Ar-*H*)
δ_C (75.5 MHz, 299 K)	19.6 (C(*C*H$_3$)(CF$_3$)$_2$), 55.2 (O*C*H$_3$), 84.6 (sep, $^2J_{CF}$ = 29 Hz, *C*(CH$_3$)(CF$_3$)$_2$), 114.1 (*m*-*C*H), 123.5 (q, $^1J_{CF}$ = 288 Hz, *C*F$_3$), 131.9 (*o*-*C*H), 139.3 (*i*-C_q), 161.1 (*p*-C_qO), 299.2 (*C*≡Mo)
δ_F (188.3 MHz, 300 K)	–77.92

3. Alkyne metathesis

The catalytic activity was tested according to the general procedure for the metathesis of alkyne **Y**-Me on a 0.252 mmol scale. Isolated yield: 87%.

4. X-ray crystal structure determination

Single-crystals suitable for X-ray diffraction analysis were obtained by precipitation from a solution in a mixture of toluene and *n*-pentane (1:1) after 5 d at –35 °C.

Special features/exceptions: Two of the C(CF$_3$)$_2$Me groups (at O3 and O8) are disordered over two positions. Despite the use of appropriate restraints, the dimensions of these ligands are not entirely satisfactory and should be interpreted with caution. A second position of a third disordered C(CF$_3$)$_2$Me group could not be found. The compound crystallises only by chance in an enantiomorphic (Sohncke) space group and is *not* enantiomerically pure. The asymmetric unit contains two formal monomers. These link to form the extended structure, a chain polymer, as is shown in Figure 33.

empirical formula	$C_{20}H_{16}F_{18}MoO_4$	identification code	oscar30
M_w	758.27	Z	4
wavelength/Å	0.71073	ρ_{calc}/(Mg m^{-3})	1.884
T/K	100(2)	μ/mm^{-1}	0.643
cryst. size/mm^3	0.25 × 0.25 × 0.08	F(000)	1488
cryst. system	monoclinic	reflections collected	122155
space group	$P2_1$	indep. reflections (R_{int})	15296 (0.0587)
a/Å	10.5434(3)	parameters	857
b/Å	16.8971(4)	restraints	271
c/Å	15.0850(3)	goodness-of-fit on F^2	1.052
α/°	90	R_1 ($I > 2\sigma(I)$)	0.0353
β/°	95.937(2)	wR_2 (all reflections)	0.0703
γ/°	90	absolute structure parameter	−0.023(17)
V/Å^3	2673.03(11)	max and min $\Delta\rho$/(e Å^{-3})	0.616 and −0.551

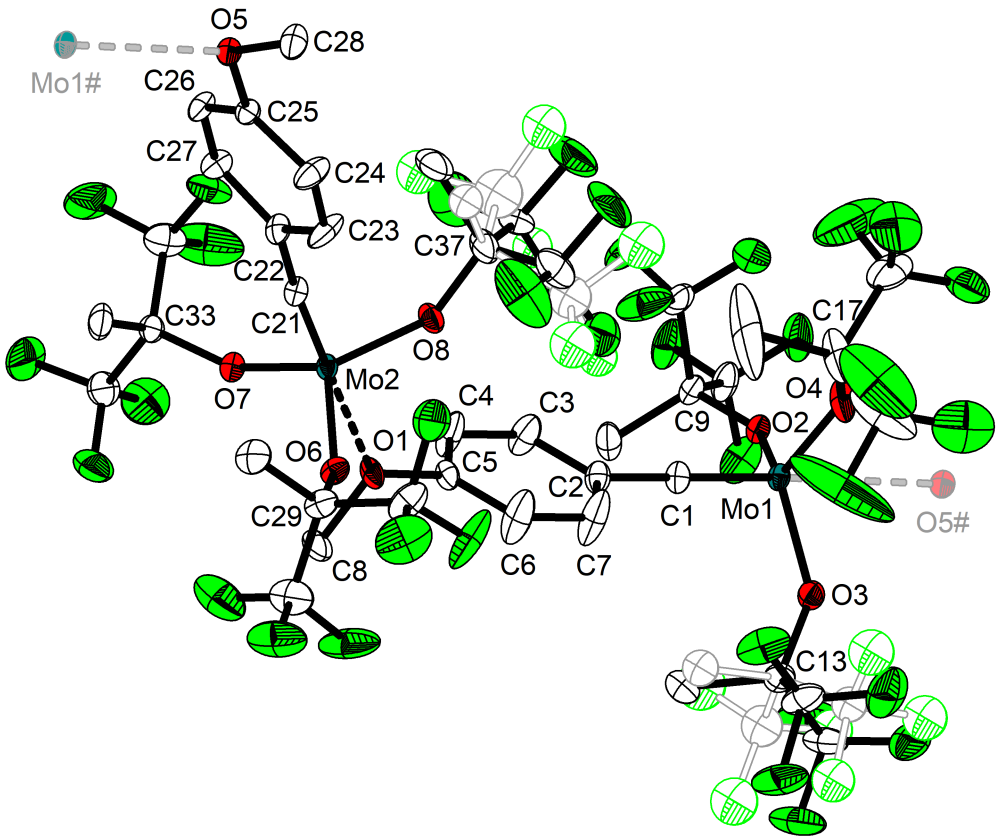

Figure 79. Molecular structure of **2** showing the two independent molecules with thermal displacement parameters drawn at the 50% probability level. Hydrogen atoms are omitted for clarity. Relevant atoms of neighbouring molecules (Mo1#, O5#) and the minor component of the two disordered $C(CF_3)_2Me$ groups are indicated using paler colours. Selected bond lengths (Å) and angles (deg): Mo–C1 1.750(3), Mo2–C21 1.753(3), Mo1–O2 1.9052(19), Mo2–O6 1.908(2), Mo1–O3 1.900(2), Mo2–O7 1.906(2), Mo1–O4 1.896(2), Mo2–O8 1.905(2), Mo1···O5# 2.7241(19), Mo2···O1 2.4723(19), C1–C2 1.452(4), C21–C22 1.449(4); C1–Mo1–O2 104.27(11), C21–Mo2–O6 102.84(11), C1–Mo1–O3 103.74(12), C21–Mo2–O7 103.14(11), C1–Mo1–O4 102.47(11), C21–Mo2–O8 101.79(11), C1–Mo1···O5# 174.28(10), C21–Mo2···O1 179.44(11), O2–Mo1–O3 114.68(9), O6–Mo2–O7 112.57(9), O2–Mo1–O4 111.61(10), O6–Mo2–O8 117.61(9), O2–Mo1···O5# 81.44(7), O6–Mo2···O1 77.15(7), O3–Mo1–O4 117.88(10), O7–Mo2–O8 115.98(9), O3–Mo1···O5# 73.33(7), O7–Mo2···O1 77.36(8), O4–Mo1···O5# 75.13(7), O8–Mo2···O1 77.75(8), Mo1–C1–C2 175.1(2), Mo2–C21–C22 175.1(2), Mo2···O1–C5 128.67(16), Mo1#···O5–C25 118.41(16).

Preparation of tris((1,1,1,3,3,3-hexafluoro-2-(trifluoromethyl)-2-propanyl)oxy)(tetrahydrofuran-*κO*)(4-methoxybenzylidyne) molybdenum(VI), [**21**(thf)]

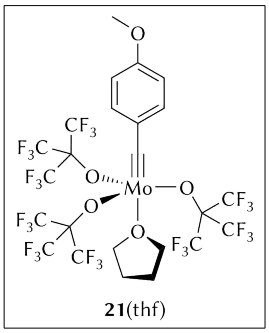

21(thf)

A solution of K-**20** (411 mg, 1.50 mmol, 3 equiv) in THF (7 mL) was added to a stirred solution of **13** (272 mg, 0.50 mmol) in THF (3 mL), and the reddish-brown mixture was stirred overnight at ambient temperature. The volatiles were removed under reduced pressure, and the brown residue was dried under dynamic vacuum. It was then extracted repeatedly with *n*-pentane (total amount 40 mL), filtered through D.E., and the frit was washed with more *n*-pentane (3 × 10 mL) to give a yellow filtrate. Removal of the solvent in high vacuum afforded the product as a brown solid. Yield: 79% (0.39 g, 0.39 mmol).

1. Elemental analysis

$C_{24}H_{15}F_{27}MoO_5$	C [%]	H [%]
Found	29.00	1.39
Calc.	29.05	1.52

2. NMR spectroscopy

	solvent: C_6D_6
δ_H (400.4 MHz, 297 K)	1.32 (br s, $\nu_{½}$ = 13 Hz, 4H, THF), 3.09 (s, 3H, OCH_3), 3.72 (br s, $\nu_{½}$ = 65 Hz, 4H, THF), 6.38 (d, 2H, $^3J_{HH}$ = 9.0 Hz, 2 × Ar-*H*), 7.14 (d, 2H, 2 × Ar-*H*). The coupling constant for the resonance at 7.15 ppm was not determined because of overlapping with the solvent signal.
δ_C (100.7 MHz, 298 K)	25.2 (br, $\nu_{½}$ = 14 Hz, THF), 54.8 (OCH_3), 71.2 (br m, $\nu_{½}$ ≈ 70 Hz, THF), 85.5 (dec, $^2J_{CF}$ = 29 Hz, $C(CF_3)_3$), 112.8 (*m*-*C*H), 121.6 (q, $^1J_{CF}$ = 293 Hz, CF_3), 134.0 (*o*-*C*H), 137.9 (br, $\nu_{½}$ ≈ 20 Hz, *i*-C_q), 161.8 (*p*-C_qO), 315.2 (br, $\nu_{½}$ ≈ 35 Hz, *C*≡Mo). The outer lines of the dectet were not observed.
δ_F (376.8 MHz, 298 K)	–72.34

3. X-ray crystal structure determination

Crystallisation attempts from concentrated *n*-pentane solutions at –35 °C afforded red crystals of [**21**(thf)] (see Figure 34, p 63).

Special features/exceptions: The structure suffers from severe disorder. It can be concluded that the structure is qualitatively correct, but it could not be refined satisfactorily. For this reason, structural parameters are not included.

empirical formula	$C_{24}H_{15}F_{27}MoO_5$
M_w	992.30
wavelength/Å	1.54184
T/K	100(2)
cryst. size/mm³	0.20 × 0.08 × 0.04
cryst. system	monoclinic
space group	$P2_1/n$
a/Å	10.79820(2)
b/Å	17.33437(5)
c/Å	17.63111(4)
α/°	90
β/°	93.9351(2)
γ/°	90
V/Å³	3 292.41(4)
identification code	oscar28
Z	4
ρ_{calc}/(Mg m^{-3})	1.856
μ/mm^{-1}	4.99
F(000)	1776
reflections collected	188 581
indep. reflections (R_{int})	6 896 (0.0454)
parameters	498
restraints	21
goodness-of-fit on F^2	1.142
R_1 ($I > 2\sigma(I)$)	0.0492
wR_2 (all reflections)	0.1375
max and min $\Delta\rho$/(e Å^{-3})	2.341 and −1.462

Preparation of (acetonitrile-*κN*)tris((1,1,1,3,3,3-hexafluoro-2-methyl-2-propanyl)oxy)(2,4,6-trimethylbenzylidyne)molybdenum(VI), 22

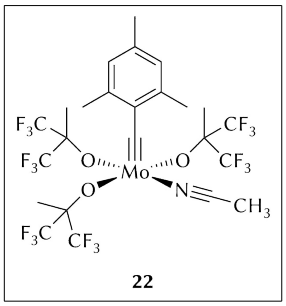

22

To a stirred solution of **1** (30.0 mg, 39 µmol) in *n*-pentane (0.5 mL) was added a solution of acetonitrile (1.6 mg, 39 µmol, 1 equiv) in toluene (0.2 mL), which resulted in an immediate colour change to red. The mixture was filtered through a glass microfibre filter, washed with *n*-pentane (2 × 0.2 mL + 0.1 mL) and stored for 4 d at –35 °C, after which red crystals formed. The supernatant was decanted, and residual solvent was evaporated in the glove-box at normal pressure and room temperature,† which resulted in a visual loss of crystallinity caused by the release of solvated toluene. Yield: 78% (24.7 mg, 30.4 µmol).

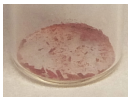

1. NMR experiment

A solution of **1** (28.5 mg, 37 µmol) in benzene-d_6 (0.6 mL) was treated with acetonitrile-d_3 (1.6 mg, 37 µmol, 1 equiv), which immediately turned red. Yield: quantitative.

2. Elemental analysis

$C_{24}H_{23}F_{18}MoNO_3$	C [%]	H [%]	N [%]
Found	35.50	2.72	1.99
Calc.	35.53	2.86	1.73

† Evaporation under dynamic vacuum induced the release of acetonitrile.

3. NMR spectroscopy

	solvent: C_6D_6
δ_H (600.1 MHz, 303 K)	0.54 (s, 3H, CH_3CN), 1.71 (s, 9H, 3 × C(CH_3)(CF_3)$_2$), 2.03 (s, 3H, *p*-CH_3), 2.59 (s, 6H, 2 × *o*-CH_3), 6.54 (s, 2H, 2 × *m*-*H*)
δ_C (150.9 MHz, 303 K)	−0.20 (*C*H$_3$CN), 18.56 (C(*C*H$_3$)(CF$_3$)$_2$), 19.71 (*o*-*C*H$_3$), 21.04 (*p*-*C*H$_3$), 83.77 (sep, $^2J_{CF}$ = 28.9 Hz, *C*(CH$_3$)(CF$_3$)$_2$), 124.70 (q, $^1J_{CF}$ = 288.9 Hz, *C*F$_3$), 124.88 (CH$_3$*C*N), 128.30 (*m*-*C*H), 140.26 (*p*-C_qCH$_3$), 141.48 (*i*-C_q), 142.31 (*o*-C_qCH$_3$), 315.14 (*C*≡Mo)
δ_F (470.8 MHz, 298 K)	−76.5

4. Alkyne metathesis

The catalytic activity was tested according to the general procedure for the metathesis of alkyne **Y**-Me on a 0.250 mmol scale. Special remarks: compound **22** does not immediately dissolve in toluene but 0.5 min after addition. Isolated yield: 97%.

5. X-ray crystal structure determination

From the solution used in the NMR reaction, the solvent was removed, and the residue was dissolved in *n*-pentane. Red–colourless dichroic single-crystals were obtained by storing this solution at –35 °C.

Special features and exceptions: The two toluene molecules (only one half of the molecules is found in the independent unit) are disordered over an inversion centre each and were refined on two positions.

empirical formula	$C_{31}H_{28}D_3F_{18}MoNO_3$	identification code	oscar33
M_w	906.53	Z	4
wavelength/Å	0.71073	ρ_{calc}/(Mg m^{-3})	1.628
T/K	130(2)	μ/mm^{-1}	0.480
cryst. size/mm^3	0.35 × 0.30 × 0.12	F(000)	1808
cryst. system	monoclinic	reflections collected	265 447
space group	$P2_1/n$	indep. reflections (R_{int})	11 410 (0.0507)
a/Å	12.7489(2)	parameters	465
b/Å	19.8808(3)	restraints	8
c/Å	14.5468(3)	goodness-of-fit on F^2	1.082
α/°	90	R_1 ($I > 2\sigma(I)$)	0.0320
β/°	91.057(2)	wR_2 (all reflections)	0.0711
γ/°	90	max and min $\Delta\rho$/(e Å^{-3})	0.788 and −0.542
V/Å^3	3 686.39(11)		

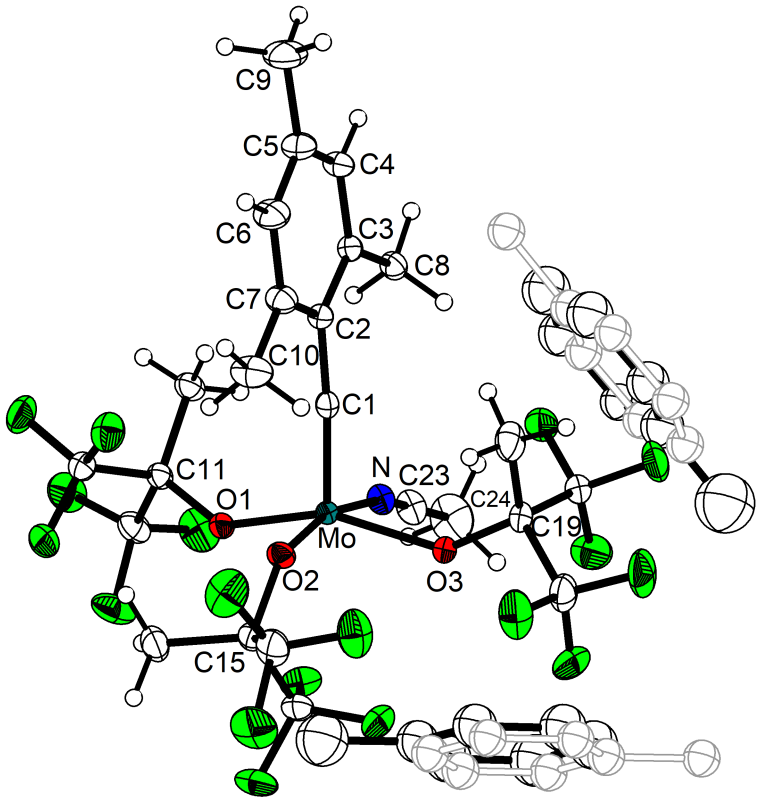

Figure 80. Molecular structure of **22**·C_7H_8 with thermal displacement parameters drawn at the 50% probability level. Hydrogen atoms of the solvent molecules are omitted for clarity. The minor component of the disordered solvent molecules is depicted using a paler colour.

Preparation of ((2,4,6-trimethoxy)benzonitrile-*κN*)tris((1,1,1,3,3,3-hexafluoro-2-methyl-2-propanyl)oxy)(2,4,6-trimethylbenzylidyne)molybdenum(VI), 24

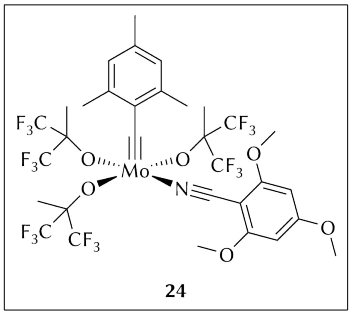

To a stirred solution of **1** (36.0 mg, 47 µmol) in toluene (2.0 mL) was added 2,4,6-trimethoxybenzonitrile (9.0 mg, 47 µmol, 1 equiv) as a solid, resulting in a rapid colour change to red. The mixture was stirred for 1 h, and then the solvent was removed under reduced pressure. *n*-Pentane (10 mL) was added; the mixture was subjected to a freeze-thaw cycle, the solvent was removed, and the residue was dried under dynamic vacuum to give a pale red solid. Yield: 89% (40 mg, 42 µmol).

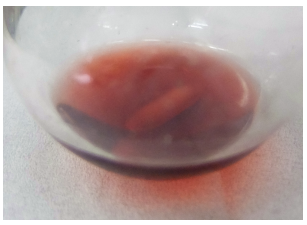

1. Elemental analysis

$C_{32}H_{31}F_{18}MoNO_6$	C [%]	H [%]	N [%]
Found	39.51	2.81	1.61
Calc.	39.89	3.24	1.45

2. NMR spectroscopy

	solvent: C_6D_6
δ_H (300.1 MHz, 297 K)	1.95 (br s, $\nu_{½} \approx 20$ Hz, 9H, 3 × C(CH_3)(CF_3)), 2.07 (s, 3H, *p*-CH_3), 2.78 (s, 6H, 2 × *o*-CH_3), 3.06 (s, 6H, 2 × *o*-OCH_3), 3.10 (s, 3H, *p*-OCH_3), 5.50 (s, 2H, 2 × *m*-*H* (nitrile)), 6.61 (m, 2H, 2 × *m*-*H*)
δ_C (150.9 MHz, 303 K)	18.8 (br, $\nu_{½} \approx 250$ Hz, C(*C*H_3)(CF_3)$_2$), 19.98 (*o*-*C*H_3), 21.08 (*p*-*C*H_3), 55.11 (*p*-O*C*H_3), 55.42 (*o*-O*C*H_3), 82.12 (*i*-C_q (nitrile)), 83.81 (sep, $^2J_{CF}$ = 29 Hz, *C*(CH$_3$)(CF_3)$_2$), 90.61 (*m*-*C*H (nitrile)), 121.53 (*C*N), 124.98 (q, $^1J_{CF}$ = 289 Hz, *C*F_3), 128.35 (*m*-*C*H), 139.62 (*p*-C_qCH$_3$), 141.45 (*i*-C_q), 142.55 (*o*-C_qCH$_3$), 164.96 (*o*-C_qOCH$_3$), 167.08 (br, $\nu_{½} \approx 50$ Hz, *p*-C_qOCH$_3$), 314.22 (*C*≡Mo)
δ_F (282.5 MHz, 298 K)	−76.5
	solvent: toluene-d_8
δ_H (600.1 MHz, 303 K)	1.95 (br s, ν½ ≈ 31 Hz, 9H, 3 × C(CH_3)(CF_3)), 2.05 (s, 3H, *p*-CH_3), 2.73 (s, 6H, 2 × *o*-CH_3), 3.13 (s, 6H, 2 × *o*-OCH_3), 3.14 (s, 3H, *p*-OCH_3), 5.47 (s, 2H, 2 × *m*-*H* (nitrile)), 6.57 (m, 2H, 2 × *m*-*H*)
δ_C (150.9 MHz, 303 K)	18.8 (br, $\nu_{½} \approx 150$ Hz, C(*C*H_3)(CF_3)$_2$), 19.98 (*o*-*C*H_3), 21.03 (*p*-*C*H_3), 55.15 (*p*-O*C*H_3), 55.42 (*o*-O*C*H_3), 80.77 (*i*-C_q (nitrile)), 83.82 (sep, $^2J_{CF}$ = 29 Hz, *C*(CH$_3$)(CF_3)$_2$), 90.64 (*m*-*C*H (nitrile)), 124.90 (*C*N), 124.96 (q, $^1J_{CF}$ = 288 Hz, *C*F_3), 128.24 (*m*-*C*H), 139.67 (*p*-C_qCH$_3$), 141.46 (*i*-C_q), 142.51 (*o*-C_qCH$_3$), 165.34 (*o*-C_qOCH$_3$), 167.94 (br, $\nu_{½} \approx 50$ Hz, *p*-C_qOCH$_3$), 314.29 (*C*≡Mo)
δ_F (376.8 MHz, 298 K)	−76.58

3. X-ray crystal structure determination

Deep red–light pink dichroic single-crystals (prisms) of **24** · C_6D_6 were obtained from a solution in benzene-d_6 at ambient temperature (see Figure 37, p 70).

Special features and exceptions: One badly resolved regions of residual electron density was tentatively identified as one molecule of deuterobenzene, but could not be refined satisfactorily. For this reason the program *Squeeze*[271] was used to remove mathematically the effects of the solvents. Derived parameters such as the molecular weight correspond to four molecules of deuterobenzene per cell.

empirical formula	$C_{38}H_{31}D_6F_{18}MoNO_6$	identification code	oa37fr
M_w	1047.67	Z	4
wavelength/Å	1.54184	ρ_{calc}/(Mg m^{-3})	1.621
T/K	100(2)	μ/mm^{-1}	3.656
cryst. size/mm^3	0.22 × 0.18 × 0.06	F(000)	2096
cryst. system	monoclinic	reflections collected	87554
space group	$P2_1/n$	indep. reflections (R_{int})	8885 (0.0536)
a/Å	12.82078(15)	parameters	532
b/Å	22.2437(2)	restraints	0
c/Å	14.99380(15)	goodness-of-fit on F^2	1.035
α/°	90	R_1 ($I > 2\sigma(I)$)	0.0276
β/°	93.6058(10)	wR_2 (all reflections)	0.0699
γ/°	90	max and min $\Delta\rho$/(e Å^{-3})	0.289 and −0.787
V/Å^3	4267.48(8)		

4. Alkyne metathesis

The catalytic activity was tested according to the general procedure for the metathesis of alkyne **Y**-Me on a 0.250 mmol scale.

Preparation of (acetone-*κO*)tris((1,1,1,3,3,3-hexafluoro-2-methyl-2-propanyl)oxy) (2,4,6-trimethylbenzylidyne)molybdenum(VI), 25

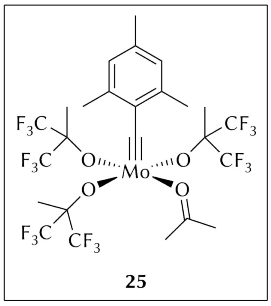

25

To a stirred solution of **1** (30 mg, 39 µmol) in *n*-pentane (0.5 mL) was added an excess of acetone (5 mg, 0.09 mmol, ~2.2 equiv), resulting in a rapid colour change to red. The mixture was placed overnight in the glove-box freezer (–35 °C) for crystallisation. The red crystals thus obtained were isolated by decantation, and solvent traces were evaporated in the glove-box at normal pressure and room temperature. Yield: 77% (25 mg, 30 µmol).

1. Elemental analysis

$C_{25}H_{26}F_{18}MoO_4$	C [%]	H [%]
Found	36.40	3.30
Calc.	36.25	3.16

2. NMR spectroscopy

	solvent: C_6D_6
δ_H (600.1 MHz, 303 K)	1.54 (s, 6H, acetone-CH_3), 1.67 (br s, $\nu_{½}$ = 3.7 Hz, 9H, 3 × C(CH_3)(CF_3)), 2.02 (s, 3H, *p*-CH_3), 2.61 (s, 6H, 2 × *o*-CH_3), 6.53 (m, 2H, 2 × *m*-*H*)
δ_C (150.9 MHz, 303 K)	18.59 (C(*C*H_3)(CF_3)$_2$), 19.73 (*o*-*C*H_3), 21.05 (*p*-*C*H_3), 29.89 (acetone-*C*H_3), 83.63 (sep, $^2J_{CF}$ = 30 Hz, *C*(CH_3)(CF_3)$_2$), 124.49 (q, $^1J_{CF}$ = 288 Hz, *C*F_3), 128.35 (*m*-*C*H), 140.26 (*p*-$C_q$$CH_3$), 141.98 (*i*-$C_q$), 142.59 (br, $\nu_{½}$ = 11 Hz, *o*-$C_q$$CH_3$), 218.42 (br, $\nu_{½}$ = 10 Hz, acetone-C_q), 314.20 (*C*≡Mo)
δ_F (188.3 MHz, 300 K)	–76.8

3. Alkyne metathesis

The catalytic activity was tested according to the general procedure for the metathesis of alkyne **Y**-Me on a 0.250 mmol scale. Isolated yield: 85%.

4. X-ray crystal structure determination

Red–yellow dichroic single-crystals of **25**-d_6‡ were obtained from a solution in *n*-pentane at –35 °C.

empirical formula	$C_{25}H_{20}D_6F_{18}MoO_4$	identification code	oscar32
M_w	834.44	Z	4
wavelength/Å	0.71073	ρ_{calc}/(Mg m^{-3})	1.753
T/K	100(2)	μ/mm^{-1}	0.556
cryst. size/mm^3	0.22 × 0.20 × 0.06	F(000)	1648
cryst. system	monoclinic	reflections collected	181847
space group	$P2_1/n$	indep. reflections (R_{int})	7794 (0.0673)
a/Å	9.9261(2)	parameters	441
b/Å	16.9005(3)	restraints	0
c/Å	18.9292(4)	goodness-of-fit on F^2	1.148
α/°	90	R_1 ($I > 2\sigma(I)$)	0.0385
β/°	98.792(2)	wR_2 (all reflections)	0.0823
γ/°	90	max and min $\Delta\rho$/(e Å^{-3})	0.528 and –0.528
V/Å^3	3138.16(11)		

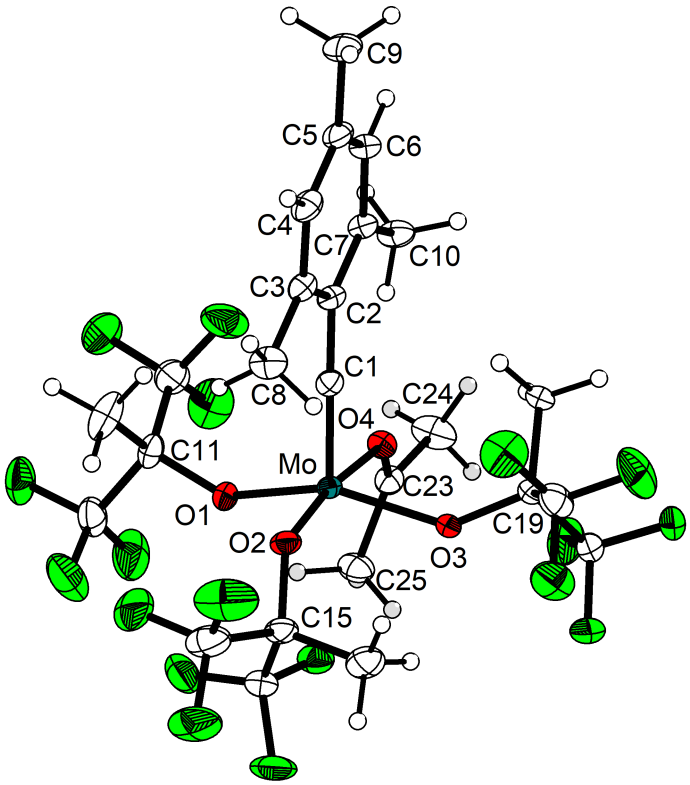

Figure 81. Molecular structure of **25**-d_6 with thermal displacement parameters drawn at the 50% probability level. Selected bond lengths (Å) and angles (deg): Mo–C1 1.739(2), Mo–O1 1.9487(15), Mo–O2 1.9494(15), Mo–O3 1.9496(15), Mo–O4 2.2166(15), O4–C23 1.231(3), C1–C2 1.446(3); C1–Mo–O1 105.27(8), C1–Mo–O2 96.99(8), C1–Mo–O3 105.07(8), C1–Mo–O4 91.85(8), O1–Mo–O2 97.39(7), O1–Mo–O3 143.92(6), O1–Mo–O4 81.15(6), O2–Mo–O3 97.86(6), O2–Mo–O4 171.10(6), O3–Mo–O4 78.79(6), Mo–C1–C2 177.45(17), Mo–O4–C23 132.99(15).

‡ For this particular batch acetone-d_6 was used to generate complex **25**.

Preparation of tris((1,1,1,3,3,3-hexafluoro-2-methyl-2-propanyl)oxy)(pyridine-κN)(2,4,6-trimethylbenzylidyne)molybdenum(VI), 26

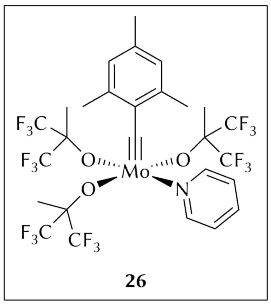

26

A solution of **1** (60 mg, 78 μmol) in toluene (1.5 mL) was treated with pyridine (0.07 mL, 0.07 g, 0.87 mmol, ~10 equiv), which resulted in an immediate colour change to red. The mixture was stirred for 1 h, and the solvent was removed under reduced pressure. The reddish residue was washed with *n*-pentane (5 mL) at 0 °C; it was then dissolved in *n*-pentane at ambient temperature, filtered through a glass microfibre filter and stored at –35 °C, which resulted in the precipitation of a solid. The supernatant was decanted, and the solid was dried under dynamic vacuum to give the product as a purple-red solid. Yield: 47% (31 mg, 36 μmol).

1. NMR experiment

NMR spectroscopic analyses of the crude product show the presence of bis(mesityl)acetylene (**27**), *n*-pentane and other impurities.

2. Elemental analysis

$C_{27}H_{25}F_{18}MoNO_3$	C [%]	H [%]	N [%]
Found	38.18	3.12	1.75
Calc.	38.18	2.97	1.65

3. NMR spectroscopy

	solvent: C_6D_6
δ_H (300.3 MHz, 298)	1.70 (s, 9H, 3 × C(CH_3)(CF_3)$_2$), 2.04 (s, 3H, *p*-CH_3), 2.70 (s, 6H, 2 × *o*-CH_3), 6.51 (br s, $\nu_{½}$ ≈ 35 Hz, 2H, py), 6.56 (m, 2H, 2 × *m*-*H*), 6.77 (br s, $\nu_{½}$ ≈ 25 Hz, 1H, py), 8.60 (br s, $\nu_{½}$ = 48 Hz, 2H, py)
δ_C (75.5 MHz, 298 K)	18.6 (C(*C*H$_3$)(CF$_3$)$_2$), 20.7 (*o*-*C*H$_3$), 21.0 (*p*-*C*H$_3$), 84.1 (sep, $^2J_{CF}$ = 29 Hz, *C*(CH$_3$)(CF$_3$)$_2$), 124.5 (br, $\nu_{½}$ ≈ 70 Hz, py), 124.7 (q, $^1J_{CF}$ = 289 Hz, *C*F$_3$), 128.6 (*m*-*C*H), 138.8 (br, $\nu_{½}$ ≈ 40 Hz, py), 140.6 (*p*-C_qCH$_3$), 141.6 (*i*-C_q), 143.2 (*o*-C_qCH$_3$), 150.2 (br, $\nu_{½}$ ≈ 13 Hz, py), 312.0 (*C*≡Mo). The outer lines of the septet and one pyridine resonance were not observed.

4. X-ray crystal structure determination

Storing of the mother liquor at –35 °C gave colourless crystals of bis(mesityl)acetylene (**27**); the structure has been determined before (cf. Figure 57).

5. Alkyne metathesis

The catalytic activity was tested according to the general procedure for the metathesis of alkyne **Y**-Me on a 0.250 mmol scale. The last sample was measured after 120 min.

Preparation of *mer*-(2,2′-bipyridine-κ^2N,N')tris((1,1,1,3,3,3-hexafluoro-2-methyl-2-propanyl)oxy)(2,4,6-trimethylbenzylidyne)molybdenum(VI), 28

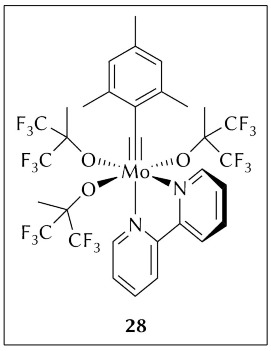

28

A solution of **1** (77 mg, 100 µmol) in toluene (2.0 mL) was treated with 2,2′-bipyridine (20.3 mg, 130 µmol, 1.3 equiv), which resulted in a colour change to brown. The mixture was stirred overnight, and the solvent was removed under reduced pressure. The brownish residue was washed with *n*-pentane (9 mL), and the residue was dried in high vacuum to give the product as a pale brown solid. Yield: 95% (88 mg, 95 µmol).

1. Elemental analysis

Triplicate analysis as usual, but the last sample was handled in air for about 0.5 h. The values in parentheses provide an average of the three analyses.

$C_{32}H_{28}F_{18}MoN_2O_3$	C [%]	H [%]	N [%]
Found	41.64, 41.45, 41.50 (41.53)	2.82, 2.76, 2.87 (2.81)	2.85, 2.93, 3.11 (2.96)
Calc.	41.48	3.05	3.02

2. NMR spectroscopy

	solvent: C_6D_6
δ_H (300.3 MHz, 298 K)	1.49 (sep, $^4\mathcal{J}_{HF}$ = 1.1 Hz, 6H, 2 × *cis*-C(CH_3)(CF_3)$_2$), 2.12 (s, 3H, *p*-CH_3), 2.17 (sep, $^4\mathcal{J}_{HF}$ = 1.1 Hz, 3H, *trans*-C(CH_3)(CF_3)$_2$), 2.96 (s, 6H, 2 × *o*-CH_3), 6.35 (m, 1H, bipy), 6.48 (m, 1H, bipy), 6.71 (m, 2H, 2 × *m*-*H*), 6.89 (m, 2H, bipy), 6.97 (m, 1H, bipy), 7.08 (m, 1H, bipy), 8.81 (m, 1H, bipy), 9.29 (m, 1H, bipy)
δ_C (75.5 MHz, 298 K)	17.5 (2 × *cis*-C(*C*H$_3$)(CF$_3$)$_2$), 18.9 (*trans*-C(*C*H$_3$)(CF$_3$)$_2$), 20.9 (*p*-*C*H$_3$), 21.0 (2 × *o*-*C*H$_3$), 82.6–85.4 (m, 3 × *C*(CH$_3$)(CF$_3$)$_2$), 121.3 (bipy-*C*H), 121.8 (bipy-*C*H), 124.5 (q, $^1\mathcal{J}_{CF}$ = 290 Hz, C(CH$_3$)(*C*F$_3$)$_2$), 124.9 (bipy-*C*H), 125.1 (q, $^1\mathcal{J}_{CF}$ = 291 Hz, 2 × C(CH$_3$)(*C*F$_3$)$_2$), 125.2 (bipy-*C*H), 128.6 (*m*-*C*H), 138.5 (bipy-*C*H), 139.1 (*o*-C_qCH$_3$), 139.6 (bipy-*C*H), 140.3 (2 × *p*-C_qCH$_3$), 143.3 (*i*-C_q), 148.4 (bipy-*C*H), 152.0 (bipy-C_q), 153.8 (bipy-C_q), 156.4 (bipy-*C*H), 306.4 (*C*≡Mo). Two septets overlapped at about δ_C = 84 ppm and some of the outer lines were not observed.
δ_F (282.5 MHz, 298 K)	−76.9 (q, $^4\mathcal{J}_{FF}$ = 10.5 Hz, 6F), −76.3 (q, $^4\mathcal{J}_{FF}$ = 10.5 Hz, 6F), −75.8 (s, 6F)

3. Alkyne metathesis

The catalytic activity was tested according to the general procedure for the metathesis of alkyne **Y**-Me (0.252 mmol). The first samples were measured at t = 2 min, t = 4 min, and t = 7 min, and the last two samples were measured at t = 120 min and t = 24 h.

4. X-ray crystal structure determination

Purple–violet dichroic single-crystals (plates) were obtained by diffusion of cyclohexane into a benzene solution of **28** (see Figure 39, p 75).

Special features/exceptions: The compound crystallises only by chance in a chiral (Sohncke) space group and is *not* enantiomerically pure.

empirical formula	$C_{32}H_{28}F_{18}MoN_2O_3$	identification code	oa43fr
M_w	926.50	Z	2
wavelength/Å	1.54184	ρ_{calc}/(Mg m^{-3})	1.772
T/K	100(2)	μ/mm^{-1}	4.343
cryst. size/mm³	0.20 × 0.18 × 0.05	F(000)	924
cryst. system	monoclinic	reflections collected	108 753
space group	$P2_1$	indep. reflections (R_{int})	7 249 (0.0569)
a/Å	10.18878(10)	parameters	511
b/Å	13.08954(12)	restraints	1
c/Å	13.72962(15)	goodness-of-fit on F^2	1.022
α/°	90	R_1 ($I > 2\sigma(I)$)	0.0253
β/°	108.4667(10)	wR_2 (all reflections)	0.0651
γ/°	90	absolute structure parameter	−0.022(5)
V/Å³	1736.79(3)	max and min $\Delta\rho$/(e Å^{-3})	0.259 and −0.758

Preparation of tris((1,1,1,3,3,3-hexafluoro-2-methyl-2-propanyl)oxy)(2,4,6-trimethylbenzylidyne)(trimethylphosphane-*κP*)molybdenum(VI), 29

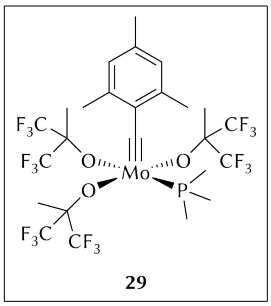

29

In an NMR tube, a solution of **1** (50 mg, 65 µmol) in benzene-d_6 (0.6 mL) was treated with trimethylphosphane (5 mg, 65 µmol, 1 equiv), which resulted in an immediate colour change to red. The mixture was transferred into a Schlenk-flask, the NMR tube was rinsed with toluene, and the solvents were removed under dynamic vacuum. The deep red residue was washed with cold *n*-pentane (3 mL) and dried in high vacuum to give a red solid. Yield: NMR solution, quantitative; isolated, 71% (39 mg, 46 µmol).

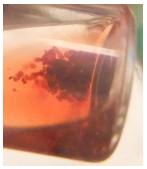

1. NMR spectroscopy

	solvent: C_6D_6
δ_H (400.4 MHz, 298 K)	1.12 (d, $^2J_{HP}$ = 9.1 Hz, 9H, P(CH_3)$_3$), 1.64 (br s, $\nu_{½}$ = 4.1 Hz, 6H, 2 × C(CH_3)(CF$_3$)$_2$), 1.67 (br m, $\nu_{½}$ = 4.0 Hz, 3H, C(CH_3)(CF$_3$)$_2$), 1.96 (s, 3H, *p*-CH_3), 2.57 (s, 6H, 2 × *o*-CH_3), 6.51 (m, 2H, 2 × *m*-*H*)
δ_C (100.7 MHz, 299 K)	14.4 (d, $^1J_{CP}$ = 23 Hz, P(*C*H$_3$)$_3$), 16.8 (2 × *cis*-C(*C*H$_3$)(CF$_3$)$_2$), 19.1 (2 × *o*-*C*H$_3$), 20.7 (*trans*-C(*C*H$_3$)(CF$_3$)$_2$), 21.2 (*p*-*C*H$_3$), 83.0 (sep, $^2J_{CF}$ = 28 Hz, 2 × *cis*-*C*(CH$_3$)(CF$_3$)$_2$), 84.1 (sep, $^2J_{CF}$ = 28 Hz, *trans*-*C*(CH$_3$)(CF$_3$)$_2$), 124.7 (q, $^1J_{CF}$ = 290 Hz, *trans*-C(CH$_3$)(*C*F$_3$)$_2$), 124.8, 125.1 (2 × q, $^1J_{CF}$ = 287 Hz, $^1J_{CF}$ = 289 Hz, 2 × *cis*-C(CH$_3$)(*C*F$_3$)$_2$), 128.6 (d, $^5J_{CP}$ = 1 Hz, 2 × *m*-*C*H), 140.6 (d, $^3J_{CP}$ = 3 Hz, *i*-C_q), 142.0 (d, $^6J_{CP}$ = 1 Hz, *p*-C_qCH$_3$), 145.1 (d, $^4J_{CP}$ = 2 Hz, 2 × *o*-C_qCH$_3$), 323.3 (d, $^2J_{CP}$ = 26 Hz, *C*≡Mo). The outer lines of the septets were not observed.
δ_F (376.7 MHz, 298 K)	−78.1 (q, $^4J_{FF}$ = 9.1 Hz, 6F), −76.6 (m, 6F), −75.5 (s, 6F)
δ_P (162.1 MHz, 299 K)	−0.82 (sep, $^5J_{PF,cis}$ = 4.7 Hz)

2. Elemental analysis

$C_{25}H_{29}F_{18}MoO_3P$	C [%]	H [%]
Found	35.26	3.44
Calc.	35.48	3.45

3. Alkyne metathesis

The catalytic activity was tested according to the general procedure for the metathesis of alkyne **Y**-Me on a 0.250 mmol scale. The last two samples were measured at t = 120 min and t = 375 min.

4. X-ray crystal structure determination

Red–pink dichroic plates were obtained from an *n*-pentane solution at –35 °C.

empirical formula	$C_{25}H_{29}F_{18}MoO_3P$
M_w	846.39
wavelength/Å	0.71073
T/K	100(2)
cryst. size/mm³	0.25 × 0.20 × 0.08
cryst. system	orthorhombic
space group	*Pccn*
a/Å	32.8336(8)
b/Å	14.8711(3)
c/Å	13.2624(3)
α/°	90
β/°	90
γ/°	90
V/Å³	6 475.7(3)

identification code	oa39fr
Z	8
ρ_{calc}/(Mg m^{-3})	1.736
μ/mm^{-1}	0.586
F(000)	3 376
reflections collected	106 996
indep. reflections (R_{int})	10 451 (0.0636)
parameters	442
restraints	0
goodness-of-fit on F^2	1.033
R_1 ($I > 2\sigma(I)$)	0.0370
wR_2 (all reflections)	0.0822
max and min $\Delta\rho$/(e Å^{-3})	0.892 and –0.522

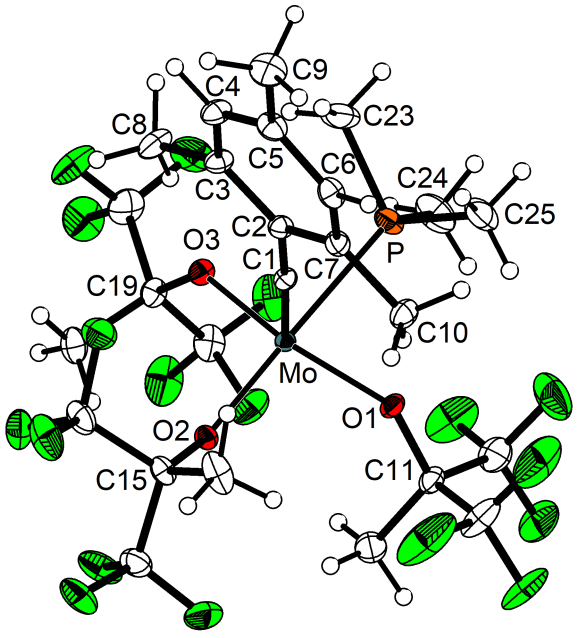

Figure 82. Molecular structure of **29** with thermal displacement parameters drawn at the 50% probability level. For selected bond lengths and angles, see Figure 40, p 78.

Preparation of tris((1,1,1,3,3,3-hexafluoro-2-methyl-2-propanyl)oxy)(1,3,4,5-tetramethylimidazolin-2-ylidene-*κC*)(2,4,6-trimethylbenzylidyne)molybdenum(VI), 30

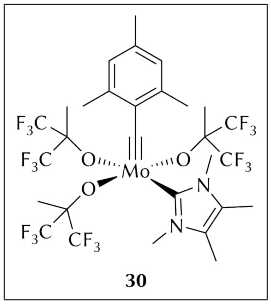

30

A stirred solution of **1** (77.0 mg, 100.0 μmol) in toluene (2.0 mL) was treated with 1,3,4,5-tetramethylimidazolin-2-ylidene (12.4 mg, 100.0 μmol, 1.0 equiv), which resulted in an immediate colour change to wine-red. After 30 min, the solvent was removed, and the deep violet residue was washed with *n*-pentane (4 mL) and dried in high vacuum to yield a red-violet solid. Yield: 97% (87 mg, 97 μmol).

1. NMR experiment

A solution of **1** (48.4 mg, 62.8 μmol) in benzene-d_6 (0.6 mL) was treated with 1,3,4,5-tetramethylimidazolin-2-ylidene (7.8 mg, 62.8 μmol, 1.0 equiv), which immediately turned wine-red. Yield: quantitative.

2. Elemental analysis

Two triplicate analyses. Some samples were exposed to air for a certain period of time.

$C_{29}H_{32}F_{18}MoN_2O_3$		C [%]	H [%]	N [%]
Found	(under argon)	39.07, 39.12	3.45, 3.40	3.35, 3.17
	(air, 1 h)	38.67	3.36	3.17
	(air, 24 h)	38.80, 38.73, 38.91	3.63, 3.64, 3.68	3.21, 3.25, 3.24
Calc.		38.94	3.61	3.13

3. NMR spectroscopy

	solvent: C_6D_6
δ_H (600.1 MHz, 303 K)	1.31 (s, 6H, 2 × NHC-CCH_3), 1.68 (s, 6H, 2 × C(CH_3)(CF$_3$)$_2$), 1.85 (s, 3H, C(CH_3)(CF$_3$)$_2$), 2.07 (s, 3H, *p*-CH_3), 2.79 (s, 6H, 2 × *o*-CH_3), 3.06 (br s, $\nu_{½}$ = 72 Hz, 3H, NHC-NCH_3), 3.39 (br s, $\nu_{½}$ = 72 Hz, 3H, NHC-NCH_3), 6.62 (m, 2H, 2 × *m*-*H*)
δ_C (150.9 MHz, 303 K)	8.13 (br m, $\nu_{½}$ = 113 Hz, 2 × NHC-CCH_3), 18.36 (C(CH_3)(CF$_3$)$_2$), 18.89 (2 × C(CH_3)(CF$_3$)$_2$), 20.87 (*p*-CH_3), 21.31 (2 × *o*-CH_3), 33.29 (br, $\nu_{½}$ = 64 Hz, NHC-NCH_3), 36.76 (br, $\nu_{½}$ = 65 Hz, NHC-NCH_3), 83.36 (sep, $^2J_{CF}$ = 27.8 Hz, 3 × C(CH$_3$)(CF$_3$)$_2$), 123.5, 124.6 (2 × br, $\nu_{½}$ ≈ 50 Hz, 2 × NHC-C_qCH$_3$), 124.44, 124.75 (2 × q, $^1J_{CF}$ = 291 Hz, $^1J_{CF}$ = 289 Hz, 2 × *cis*-C(CH$_3$)(CF$_3$)$_2$), 125.23 (q, $^1J_{CF}$ = 290 Hz, *trans*-C(CH$_3$)(CF$_3$)$_2$), 128.62 (2 × *m*-*C*H), 138.86 (*p*-C_qCH$_3$), 140.59 (2 × *o*-C_qCH$_3$), 141.80 (*i*-C_q), 186.60 (NHC-NC_qN), 305.51 (C≡Mo)
δ_F (376.7 MHz, 298 K)	−76.8 (app q, $^{4,\,app}J_{FF}$ = 8.0 Hz, 6F), −76.7 (br s, 12F)

4. X-ray crystal structure determination

Deep red–pale purple dichroic single-crystals were obtained by slow evaporation of the NMR solution.

empirical formula	$C_{29}H_{32}F_{18}MoN_2O_3$	identification code	oa40fr
M_w	894.51	Z	4
wavelength/Å	0.71073	ρ_{calc}/(Mg m^{-3})	1.722
T/K	100(2)	μ/mm^{-1}	0.512
cryst. size/mm^3	0.26 × 0.20 × 0.12	F(000)	1792
cryst. system	monoclinic	reflections collected	180 664
space group	$P2_1/n$	indep. reflections (R_{int})	10 592 (0.0555)
a/Å	11.1192(2)	parameters	488
b/Å	18.4687(3)	restraints	0
c/Å	16.8262(3)	goodness-of-fit on F^2	1.041
α/°	90	R_1 ($I > 2\sigma(I)$)	0.0288
β/°	93.212(2)	wR_2 (all reflections)	0.0645
γ/°	90	max and min $\Delta\rho$/(e Å^{-3})	0.542 and −0.473
V/Å^3	3 449.94(10)		

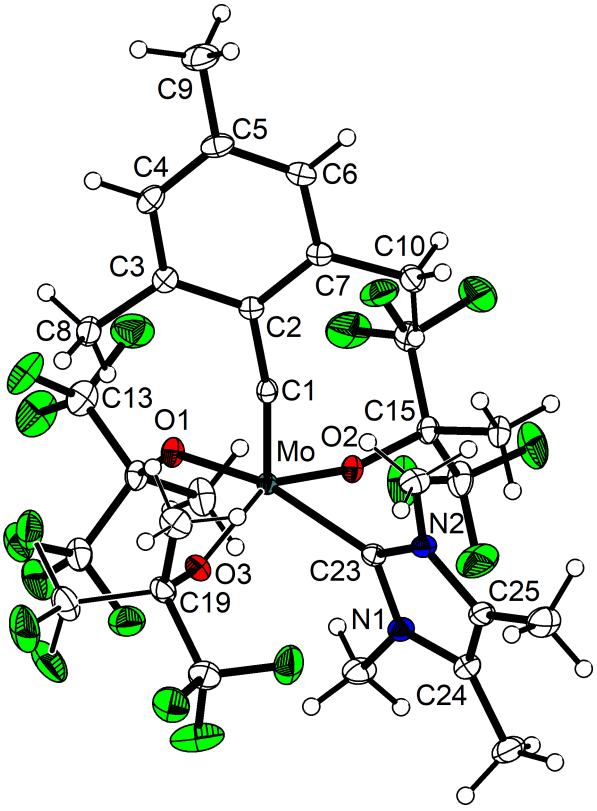

Figure 83. Molecular structure of **30** with thermal displacement parameters drawn at the 50% probability level. For selected bond lengths and angles, see Figure 43, p 83.

5. Alkyne metathesis

The catalytic activity was tested according to the general procedure for the metathesis of alkyne **Y**-Me on a 0.250 mmol scale. The first samples were measured at t = 2 min, t = 4 min, and t = 7 min, and the last sample was measured at t = 120 min.

Reaction of complex 1 with 3-hexyne

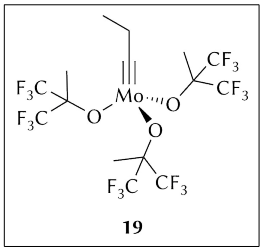

19

A solution of **1** (89 mg, 0.116 mmol) in *n*-hexane (3 mL) was treated with a solution of 3-hexyne (90 mg, 1.10 mmol, 9.5 equiv) in *n*-hexane (7 mL). The mixture turned brown, and a white precipitate formed. After filtration, the solid was washed with *n*-hexane (2 × 2 mL) and then dried under dynamic vacuum to give a polymeric material (14 mg; see picture). The solvent was removed from the filtrate, and the brown residue was analysed by NMR spectroscopy. Further attempts to purify the product through crystallisation were unsuccessful.

1. NMR spectroscopy

19	solvent: C_6D_6
δ_H (300.1 MHz, 297 K)	0.56 (t, $^3J_{HH}$ = 7.5 Hz, 3H, CH_2CH_3), 1.53 (s, 9H, 3 × $C(CH_3)(CF_3)_2$), 2.43 (q, $^3J_{HH}$ = 7.5 Hz, 2H, CH_2CH_3)
δ_C (75.5 MHz, 298 K)	12.2 (CH_2CH_3), 19.3 ($C(CH_3)(CF_3)_2$), 44.9 (CH_2CH_3), 83.6 (sep, $^2J_{CF}$ = 30 Hz, $C(CH_3)(CF_3)_2$), 123.5 (q, $^1J_{CF}$ = 288 Hz, $C(CH_3)(CF_3)_2$), 313.1 (C≡Mo). The outer lines of the septet were not observed.
δ_F (188.3 MHz, 300 K)	−78.0

Additional signals are assigned to bis(mesityl)acetylene (**27**, see p 198).

2. GPC

Polymer sample	$\overline{M}_n$ [g mol^{-1}]	$\overline{M}_w$ [g mol^{-1}]	$Đ$	X_n	X_w
1.5 mg / mL (THF)	738	1277	1.73	9	16
2 mg / mL (THF)	750	1753	2.34	9	21

Preparation of (benzylidyne)tris((1,1,1,3,3,3-hexafluoro-2-methyl-2-propanyl)oxy)molybdenum(VI), 32

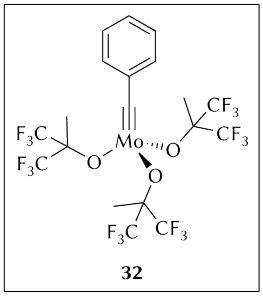

32

A solution of **1** (77 mg, 0.10 mmol) in toluene (0.9 mL) was treated with diphenylacetylene (17.8 mg, 0.10 mmol, 1 equiv) in toluene (0.1 mL) and stirred for 1 h. After removing the solvent under dynamic vacuum, the brown residue was dissolved in *n*-pentane (<1 mL), filtered through glass fibre, and stored for 2 d at –35 °C for crystallisation. The brown crystals thus obtained were separated from the supernatant and dried in high vacuum (57 mg). NMR analyses revealed a mixture of complex **32** (~89%, ~51 mg, ~70% yield) and minor amounts of 2-mesityl-1-phenylacetylene (~11%, ~6 mg). Recrystallisation in *n*-pentane (0.5 mL) afforded pure **32** as pale brown needles. Isolated yield: 53% (39 mg, 54 µmol).

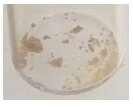

1. Elemental analysis

$C_{19}H_{14}F_{18}MoO_3$	C [%]	H [%]
Found	31.43	2.02
Calc.	31.34	1.94

2. NMR spectroscopy

	solvent: C_6D_6
δ_H (600.1 MHz, 303 K)	1.58 (s, 9H, 3 × CH_3), 6.77 (m, 1H, *p-H*), 6.87 (m, 2H, 2 × *m-H*), 7.05 (m, 2H, 2 × *o-H*)
δ_C (150.9 MHz, 303 K)	19.51 (3 × *C*H_3), 84.57 (sep, $^2J_{CF}$ = 30 Hz, 3 × *C*(CH_3)(CF_3)$_2$), 123.29 (q, $^1J_{CF}$ = 287 Hz, 6 × *C*F_3), 128.63 (2 × *m-C*H), 129.71 (2 × *o-C*H), 130.50 (*p-C*H), 145.01 (*i-C*$_q$), 299.21 (*C*≡Mo)
δ_F (376.1 MHz, 299 K)	–78.0

3. X-ray crystal structure determination

Single-crystals suitable for X-ray diffraction analysis were obtained from a saturated *n*-hexane solution at –35 °C. The structure is illustrated in Figure 44, p 88.

empirical formula	$C_{19}H_{14}F_{18}MoO_3$
M_w	728.24
wavelength/Å	1.54184
T/K	100(2)
cryst. size/mm³	0.20 × 0.08 × 0.06
cryst. system	orthorhombic
space group	*Pbca*
a/Å	18.4399(4)
b/Å	12.3991(3)
c/Å	22.2428(5)
α/°	90
β/°	90
γ/°	90
V/Å³	5 085.5(2)

identification code	oscar09
Z	8
ρ_{calc}/(Mg m^{-3})	1.902
μ/mm^{-1}	5.694
F(000)	2 848
reflections collected	94 837
indep. reflections (R_{int})	5 268 (0.0504)
parameters	373
restraints	0
goodness-of-fit on F^2	1.029
R_1 ($I > 2\sigma(I)$)	0.0380
wR_2 (all reflections)	0.1030
max and min $\Delta\rho$/(e Å^{-3})	1.378 and –1.287

4. Alkyne metathesis

The catalytic activity was tested according to the general procedure for the metathesis of internal alkyne **Y**-Me (0.253 mmol) and terminal alkyne **Y**-H (0.250 mmol). No sample was measured at t = 15 min.

Preparation of (benzylid[^{13}C]yne)tris((1,1,1,3,3,3-hexafluoro-2-methyl-2-propanyl)oxy)molybdenum(VI), 32′

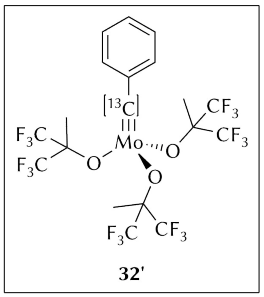

32′

This compound was synthesised analogously to unlabelled complex **32** but using 50 mol% of (1,2-$^{13}C_2$)-diphenylacetylene. For convenience, the procedure is reproduced here. A mixture of diphenylacetylene (26.1 mg, 0.15 mmol) and (1,2-$^{13}C_2$)-diphenylacetylene (27.7 mg, 0.15 mmol) in toluene (2 mL) was added to a solution of **1** (231.1 mg, 0.3 mmol) in toluene (1 mL), and the mixture was stirred for 1 h. After removal of the solvent under reduced pressure, the brown residue was dissolved in *n*-pentane (2.5 mL) and stored for 2 d at –35 °C for crystallisation. The obtained deep brown crystals were separated from the supernatant and dried in high vacuum (172 mg). NMR analysis revealed a mixture of complex **32′** (~91%, ~156 mg, ~71% yield) and minor amounts of 2-mesityl-1-phenyl-1-^{13}C-ethyne (~9%, ~16 mg). Recrystallisation of the mixture (100 mg) in *n*-pentane (1 mL) afforded pale brown crystals of pure **32′**. Isolated yield: 43% (55 mg, 75 μmol). Complex **32′** was thus 50% ^{13}C-enriched at the alkylidyne carbon atom.

1. NMR spectroscopy

	solvent: C_6D_6
δ_H (600.1 MHz, 303 K)	1.58 (s, 9H, 3 × CH_3), 6.77 (m, 1H, *p-H*), 6.86 (m, 2H, 2 × *m-H*), 7.04 (m, 2H, 2 × *o-H*)
δ_C (150.9 MHz, 303 K)	19.51 (3 × CH_3), 84.57 (sep, $^2J_{CF}$ = 30 Hz, 3 × $C(CH_3)(CF_3)_2$), 123.28 (q, $^1J_{CF}$ = 287 Hz, 6 × CF_3), 128.63 (d, $^3J_{CC}$ = 4 Hz, 2 × *m-C*H), 129.71 (2 × *o-C*H), 130.50 (*p-C*H), 145.00 (d, $^1J_{CC}$ = 43 Hz, *i-*C_q), 299.22 (*C*≡Mo). The outer lines of the septet were not observed.
δ_F (188.3 MHz, 300 K)	–78.0

Additional signals in the $^{13}C\{^1H\}$ NMR spectrum account for the ^{13}C-substituted atom in residual amounts (<1%) of (1,2-$^{13}C_2$)-diphenylacetylene (δ_C = 90.18 ppm) and 2-mesityl-1-phenyl-1-^{13}C-ethyne (δ_C = 97.79 ppm).

Preparation of [1,3-bis(4-methylpiperidin-1-yl)-2-(2,4,6-trimethylphenyl)-1-propene-3-ylium-1,3-diyl]tris(1,1,1,3,3,3-hexafluoro-2-methyl-2-propanolate)molybdenum(IV), 35

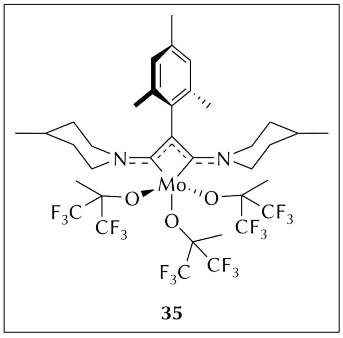

35

To a precooled (–40 °C) solution of **1** (236 mg, 306 μmol) in *n*-pentane (4 mL) was added a solution of **34** (71 mg, 322 μmol, 1.05 equiv) in *n*-pentane (1 mL). The colour changed to deep red immediately, and a crystalline dark precipitate formed. The solution was stored overnight at –30 °C, and the supernatant was removed with a syringe at the same temperature. Solvent traces were allowed to evaporate for one week in the glove-box freezer (–35 °C). Yield: 72% (219 mg, 221 μmol).

1. Elemental analysis

$C_{36}H_{44}F_{18}MoN_2O_3$	C [%]	H [%]	N [%]
Found	43.31	4.59	3.04
Calc.	43.65	4.48	2.83

2. NMR spectroscopy

solvent: toluene-d_8

δ_H (400.4 MHz, 244 K): –9.29 ($\nu_{½}$ = 26.7 Hz, 2H, *rac*-**35**: 2 × 3,5-CH*H*), –7.03 ($\nu_{½}$ = 23.9 Hz, 2H, *meso*-**35**: 2 × 3,5-CH*H*), –3.15 ($\nu_{½}$ = 34.6 Hz, 2H, *meso*-**35**: 2 × 3,5-CH*H*), –2.90 ($\nu_{½}$ = 34.0 Hz, 2H, *rac*-**35**: 2 × 3,5-CH*H*), 1.02 ($\nu_{½}$ = 39.9 Hz, 4H, *meso*-**35**: 2 × 4-C*H*, *rac*-**35**: 2 × 4-C*H*), 1.53 ($\nu_{½}$ = 12.0 Hz, 6H, *meso*-**35**: 2 × 4-CH_3), 1.69 ($\nu_{½}$ = 12.2 Hz, 6H, *rac*-**35**: 2 × 4-CH_3), 2.79 ($\nu_{½}$ = 39.3 Hz, 2H, *meso*-**35**: 2 × 3,5-CH*H*), 2.96 ($\nu_{½}$ = 4.9 Hz, 3H, *rac*-**35**: *p*-CH_3), 3.18 ($\nu_{½}$ = 37.3 Hz, 2H, *rac*-**35**: 2 × 3,5-CH*H*), 3.67 ($\nu_{½}$ = 5.1 Hz, 3H, *meso*-**35**: *p*-CH_3), 4.82 ($\nu_{½}$ = 22.1 Hz, 2H, *rac*-**35**: 2 × 3,5-CH*H*), 5.27 ($\nu_{½}$ = 21.0 Hz, 2H, *meso*-**35**: 2 × 3,5-CH*H*), 6.95 ($\nu_{½}$ ≈ 15 Hz, 6H, *rac*-**35**: 2 × *o*-CH_3), 7.19 ($\nu_{½}$ = 20.1 Hz, 3H, *meso*-**35**: *o*-CH_3), 7.82 ($\nu_{½}$ = 18.3 Hz, 3H, *meso*-**35**: *o*-CH_3), 9.38 ($\nu_{½}$ = 298 Hz, 6H, *meso*-**35**: 2 × C(CH_3)$(CF_3)_2$), 11.2–11.7 (app d, $\nu_{½}$ = 226 Hz, 4H, *meso*-**35**: 4 × 2,6-CH*H*), 16.14 ($\nu_{½}$ = 133 Hz, 3H, *meso*-**35**: C(CH_3)$(CF_3)_2$), 23.40 ($\nu_{½}$ = 54.9 Hz, 2H, *rac*-**35**: 2 × 2,6-CH*H*), 25.10 ($\nu_{½}$ = 13.6 Hz, 1H, *meso*-**35**: *m*-*H*), 25.17 ($\nu_{½}$ = 13.6 Hz, 1H, *meso*-**35**: *m*-*H*), 25.64 ($\nu_{½}$ = 14.5 Hz, 2H, *rac*-**35**: 2 × *m*-*H*), 25–26 (very br, $\nu_{½}$ ≈ 470 Hz, ~4H, *rac*-**35**: 2 × 2,6-CH*H*), 27.37 ($\nu_{½}$ = 44.9 Hz, 2H, *meso*-**35**: 2 × 2,6-CH*H*), 42.64 ($\nu_{½}$ = 92.6 Hz, 2H, *meso*-**35**: 2 × 2,6-CH*H*), 48.11 ($\nu_{½}$ = 184 Hz, 2H, *rac*-**35**: 2 × 2,6-CH*H*)

δ_C (100.7 MHz, 244 K): 17.0 ($\nu_{½}$ = 7.1 Hz, *meso*-**35**: *p*-CH_3), 18.6 ($\nu_{½}$ = 7.1 Hz, *rac*-**35**: *p*-CH_3), 31.3 ($\nu_{½}$ = 9.6 Hz, *meso*-**35**: 2 × 4-CH_3), 32.3 ($\nu_{½}$ = 10.2 Hz, *rac*-**35**: 2 × 4-CH_3), 61.6 ($\nu_{½}$ = 20.3 Hz, *meso*-**35**: 2 × 3,5-CH_2), 65.2 ($\nu_{½}$ = 16.5 Hz, *rac*-**35**: 2 × 3,5-CH_2), 71.8 ($\nu_{½}$ = 19.3 Hz, *rac*-**35**: 2 × 3,5-CH_2), 71.9 ($\nu_{½}$ = 19.3 Hz, *meso*-**35**: 2 × 4-C*H*), 73.5 ($\nu_{½}$ = 18.7 Hz, *rac*-**35**: 2 × 4-C*H*), 81.6 ($\nu_{½}$ = 24.6 Hz, *meso*-**35**: 2 × 3,5-CH_2), 92.7 ($\nu_{½}$ = 36 Hz, *meso*-**35**: *o*-CH_3), 105.5 ($\nu_{½}$ = 38 Hz, *rac*-**35**: *o*-CH_3), 108.9 ($\nu_{½}$ = 30 Hz, *meso*-**35**: *o*-CH_3), 139.4 ($\nu_{½}$ = 8.0 Hz, *rac*-**35**: *p*-C_qCH_3), 143.4 ($\nu_{½}$ = 8.7 Hz, *meso*-**35**: *p*-C_qCH_3), 182.1 ($\nu_{½}$ = 49 Hz, *meso*-**35**: *m*-C*H*), 186.9 ($\nu_{½}$ = 45 Hz, *meso*-**35**: *m*-C*H*), 190.3 ($\nu_{½}$ = 49 Hz, *rac*-**35**: *m*-C*H*), 224.9 ($\nu_{½}$ ≈ 100 Hz, *o*-C_qCH_3, uncertain assignment)

δ_F (376.8 MHz, 244 K): –1.4 ($\nu_{½}$ ≈ 2 700 Hz), 20.5 ($\nu_{½}$ ≈ 2 400 Hz), 38.8 ($\nu_{½}$ ≈ 1000 Hz)

Table 5. ^{1}H NMR chemical shifts (ppm) of *meso*-**35** at various temperatures; solvent: toluene-d_8.

	mesityl ring			4-methylpiperidinyl rings				
T / °C	***m*-H**[a]	***o*-CH_3**[a]	***p*-CH_3**	4-CH_3	4-CH	3,5-CH_2[c]	2,6-CH_2[c]	O(CF_3)$_2$CH_3[g]
−93	31.9, 32.2	10.8[b]	4.5	1.8	0.5	−8.6, −4.9, −,[d] 6.3	11.6,[e] 35.3, 51.7	12.3, 24.5
−83	30.7, 30,9	10.2[b]	4.3	1.7	0.6	−8.5, −4.5, −,[d] 6.1	11.5,[e] 33.3, 49.6	11.9, 22.7
−72	29.3, 29,4	9.3, 9.6	4.1	1.7	0.7	−8.2, −4.1, 2.9, 5.9	11.3,[e] 31.4, 47.8	11.6, 20.8
−61	28.1, 28.2	8.6, 9.1	4.0	1.6	0.8	−7.9, −3.8, 2.8, 5.7	11.4,[e] 30.1, 46.3	11.1, 19.3
−47	26.9[b]	8.0, 8.6	3.9	1.6	0.9	−7.6, −3.5, 2.8, 5.5	11.4,[e] 28.9, 44.7	10.4, 18.0
−40	25.9, 25.9	7.5, 8.1	3.8	1.6	1.0	−7.3, −3.3, 2.8, 5.4	11.5,[e,f] 28.0, 43.5	9.7, 16.9
−29	25.1, 25.2	7.2, 7.8	3.7	1.5	1.0	−7.0, −3.2, 2.8, 5.3	11.4,[e,f] 27.4, 42.7	9.4, 16.1
−13	23.5, 23.6	6.5, 7.2	3.5	1.5	1.1	−6.5, −2.8, 2.8, 5.0	11.3,[e,f] 25.8, 40.3	8.7, 13.6
−2	22.6, 22.8	6.2, 6.9	3.4	1.5	1.2	−6.2, −2.6, 2.7, 4.9	11.3,[e,f] 25.2, 39.5	8.6, 12.7
10	21.9, 22.1	6.0, 6.6	3.3	1.5	1.3	−5.9, −2.5, 2.7, 4.8	11.3,[e,f] 24.6, 38.6	8.3, −[h]

[a] Two inequivalent positions; [b] Overlapped resonances; [c] All four hydrogen atoms in these positions are diastereotopic, each resonance integrates to 2H; [d] One resonance is missing because of overlap; [e] Unclear assignment, presumably two resonances (4H); [f] Apparent doublet; [g] Unclear assignments, because the integrals do not fit for all temperatures. The first resonance presumably integrates to 6H, and the second presumably integrates to 3H; [h] One resonance was not observed because of line broadening.

Table 6. ^{1}H NMR chemical shifts (ppm) of *rac*-**35** at various temperatures; solvent: toluene-d_8.

	mesityl ring			4-methylpiperidinyl rings				
T / °C	***m*-H**	***o*-CH_3**	***p*-CH_3**	4-CH_3	4-CH	3,5-CH_2[b]	2,6-CH_2[c]	O(CF_3)$_2$CH_3[e]
−93	35.2	9.9	2.7	2.0	0.4	−12.3, −4.1, 3.8, 5.7	28.7, −,[d] 52.7[a]	12.3, 24.5
−83	33.1	9.3	2.8	1.9	0.5	−11.8, −3.9, 3.7, 5.5	27.6, −,[d] 52.2	11.9, 22.7
−72	31.0	8.6	2.9	1.9	0.6	−11.2, −3.6, 3.6, 5.3	26.3, −,[d] 51.7	11.6, 20.8
−61	29.3	8.1	2.9	1.8	0.7	−10.6, −3.4, 3.4, 5.2	25.4, *29*, 51.0	11.1, 19.3
−47	27.8	7.6	3.0	1.8	0.9	−10.1, −3.2, 3.3, 5.0	24.5, *28*, 49.9	10.4, 18.0
−40	26.5	7.2	3.0	1.7	1.0	−9.6, −3.0, 3.2, 4.9	23.9, *26*, 48.8	9.7, 16.9
−29	25.6	7.0	3.0	1.7	1.0	−9.3, −2.9, 3.2, 4.8	23.4, *26*, 48.1	−[f]
−13	23.8	6.4	3.0	1.6	1.1	−8.4, −2.6, 3.0, 4.6	22.2, *24*, 45.8	−[f]
−2	22.9	6.1	3.0	1.6	1.2	−8.0, −2.5, 3.0, 4.5	21.8, *23*, 44.8	−[f]
10	22.0[a]	5.9	2.9	1.5	1.3	−7.6, −2.4, 2.9, 4.4	21.4, *22*, 43.8	−[f]

[a] Estimated value because of overlap; [b] All four hydrogen atoms in these positions are diastereotopic, each resonance integrates to 2H; [c] Unclear assignments because of overlap. Four resonances are expected because of diastereotopic hydrogen atoms in these positions: Two resonances (2 × 2H) can be easily identified, whereas the other two are very broad and overlap with themselves and other resonances; thus, estimated values are given here in italics; [d] One resonance is missing because of overlap; [e] Unclear assignments, because the integral does not fit for all temperatures; [f] This resonance was not observed because of line broadening.

3. X-ray crystal structure determination

Single-crystals suitable for XRD analysis were obtained from a concentrated *n*-pentane solution at –35 °C.

empirical formula	$C_{36}H_{44}F_{18}MoN_2O_3$	identification code	oscar07
M_w	990.67	Z	2
wavelength/Å	1.54184	ρ_{calc}/(Mg m^{-3})	1.617
T/K	100(2)	μ/mm^{-1}	3.744
cryst. size/mm^3	0.20 × 0.08 × 0.05	F(000)	948
cryst. system	triclinic	reflections collected	92 647
space group	$P\bar{1}$	indep. reflections (R_{int})	8 408 (0.0810)
a/Å	11.2300(6)	parameters	569
b/Å	12.6831(6)	restraints	112
c/Å	15.8296(10)	goodness-of-fit on F^2	1.038
α/°	101.495(5)	R_1 ($I > 2\sigma(I)$)	0.0492
β/°	110.382(6)	wR_2 (all reflections)	0.1279
γ/°	95.857(4)	max and min $\Delta\rho$/(e Å^{-3})	0.777 and –1.421
V/Å^3	2 034.68(19)		

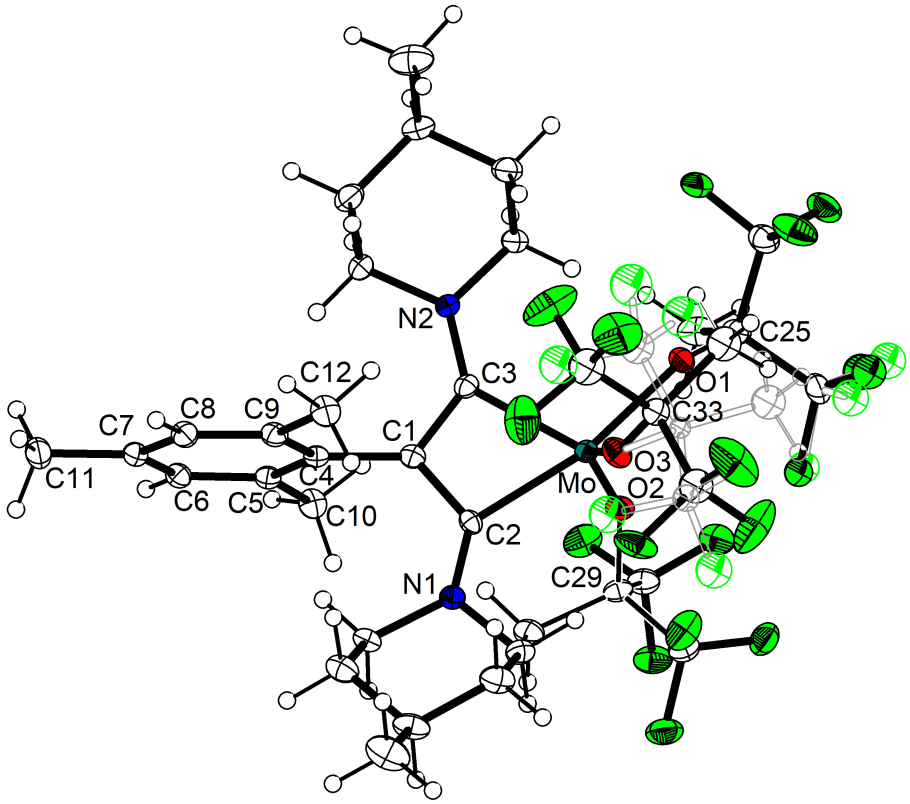

Figure 84. Molecular structure of **35** with thermal displacement parameters drawn at the 30% probability level. Alternative disordered positions of some groups are depicted using paler colours. Selected bond lengths (Å) and angles (deg): Mo–C2 2.166(3), Mo–C3 2.138(3), Mo–O1 2.089(2), Mo–O2 1.936(2), Mo–O3 1.912(3), C1–C2 1.423(5), C1–C3 1.413(4), C1–C4 1.499(4), N1–C2 1.323(4), N2–C3 1.322(4); C2–Mo–C3 62.71(12), C2–Mo–O1 167.65(11), C2–Mo–O2 100.55(10), C2–Mo–O3 89.09(11), C3–Mo–O1 105.91(11), C3–Mo–O2 110.72(11), C3–Mo–O3 109.43(12), O1–Mo–O2 87.78(9), O1–Mo–O3 90.61(10), O2–Mo–O3 138.64(11), Mo–C2–C1 95.5(2), Mo–C2–N1 136.2(2), C1–C2–N1 128.2(3), Mo–C3–C1 97.1(2), Mo–C3–N2 132.0(2), C1–C3–N2 130.9(3), C2–C1–C3 104.3(3), C2–C1–C4 128.5(3), C3–C1–C4 126.8(3).

4. Alkyne metathesis

The metathesis of the diaminoacetylene **34** with diphenylacetylene was attempted using **1** as the catalysis initiator. To a stirred solution of diphenylacetylene (18 mg, 100 µmol) and **34** (22 mg, 100 µmol) in C_6D_6 (0.6 mL) was added 1 mol% of **1** (0.8 mg, 1 µmol), which resulted in an immediate colour change to red. The reaction mixture was analysed by NMR spectroscopy, revealing only the presence of the starting materials even after 24 h, heating at 50 °C, or further addition of 1 mol% of **1**.

Preparation of [1,3-bis(diethylamine)-2-(2,4,6-trimethylphenyl)-1-propene-3-ylium-1,3-diyl]tris(1,1,1,3,3,3-hexafluoro-2-methyl-2-propanolate)molybdenum(IV), 36

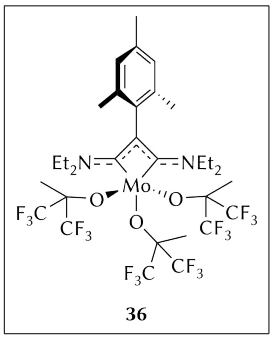

36

To a precooled (–30 °C) solution of **1** (56.6 mg, 73.5 µmol) in *n*-pentane (0.6 mL) was added a solution of **33** (12.4 mg, 73.5 µmol, 1.00 equiv) in *n*-pentane (0.15 mL). The colour changed to deep red immediately, and an oily dark precipitate formed. The supernatant was decanted, filtered through a glass microfibre filter and stored overnight at –35 °C, after which deep red crystals formed. The supernatant was removed with a syringe, and solvent traces were allowed to evaporate for one week in the glove-box freezer (–35 °C). Yield: 33% (23 mg, 24.5 µmol).

1. NMR experiment

For the NMR spectroscopy studies, a precooled (–30 °C) solution of **33** (9.8 mg, 58.2 µmol, 1.00 equiv) in toluene-d_8 (0.2 mL) was added in a vial to a precooled (–30 °C) solution of **1** (44.8 mg, 58.2 µmol) in toluene-d_8 (0.2 mL), which resulted in an immediate colour change to deep red. The mixture was transferred into an NMR tube, the vial was washed with toluene-d_8 (4 × 0.05 mL), and the tube was flame sealed and stored at –80 °C.

2. Elemental analysis

$C_{32}H_{40}F_{18}MoN_2O_3$	C [%]	H [%]	N [%]
Found	41.54	4.45	2.91
Calc.	40.95	4.30	2.98

3. NMR spectroscopy

	solvent: toluene-d_8
δ_H (400.4 MHz, 273 K)	−1.28 ($\nu_{½}$ = 16.0 Hz, 6H, 2 × CH_2CH_3), 1.96 ($\nu_{½}$ = 3.7 Hz, 3H, *p*-CH_3), 3.50 ($\nu_{½}$ = 19.0 Hz, 6H, 2 × CH_2-CH_3), 10.26 ($\nu_{½}$ = 58.8 Hz, 9H, 3 × $C(CH_3)(CF_3)_2$), 13.01 ($\nu_{½}$ = 22.5 Hz, 6H, 2 × *o*-CH_3), 16.91 ($\nu_{½}$ = 6.2 Hz, 2H, 2 × *m*-*H*), 23.82 ($\nu_{½}$ = 36.3 Hz, 4H, 2 × CH_2CH_3), 25.81 ($\nu_{½}$ ≈ 135 Hz, 4H, 2 × CH_2CH_3)
δ_F (376.8 MHz, 273 K)	−2.4 ($\nu_{½}$ = 182 Hz)

4. X-ray crystal structure determination

Single-crystals suitable for XRD analysis were obtained after recrystallisation from a concentrated *n*-pentane solution at –35 °C.

empirical formula	$C_{32}H_{40}F_{18}MoN_2O_3$	identification code	oscar31
M_w	938.60	Z	2
wavelength/Å	1.54184	ρ_{calc}/(Mg m^{-3})	1.622
T/K	100(2)	μ/mm^{-1}	3.927
cryst. size/mm³	0.18 × 0.15 × 0.04	F(000)	948
cryst. system	triclinic	reflections collected	119 615
space group	$P\bar{1}$	indep. reflections (R_{int})	8 009 (0.0556)
a/Å	12.5635(5)	parameters	555
b/Å	12.6072(4)	restraints	98
c/Å	12.7731(4)	goodness-of-fit on F^2	1.040
α/°	88.000(2)	R_1 ($I > 2\sigma(I)$)	0.0318
β/°	73.097(3)	wR_2 (all reflections)	0.0833
γ/°	82.987(3)	max and min $\Delta\rho$/(e Å^{-3})	0.793 and −0.876
V/Å³	1921.25(11)		

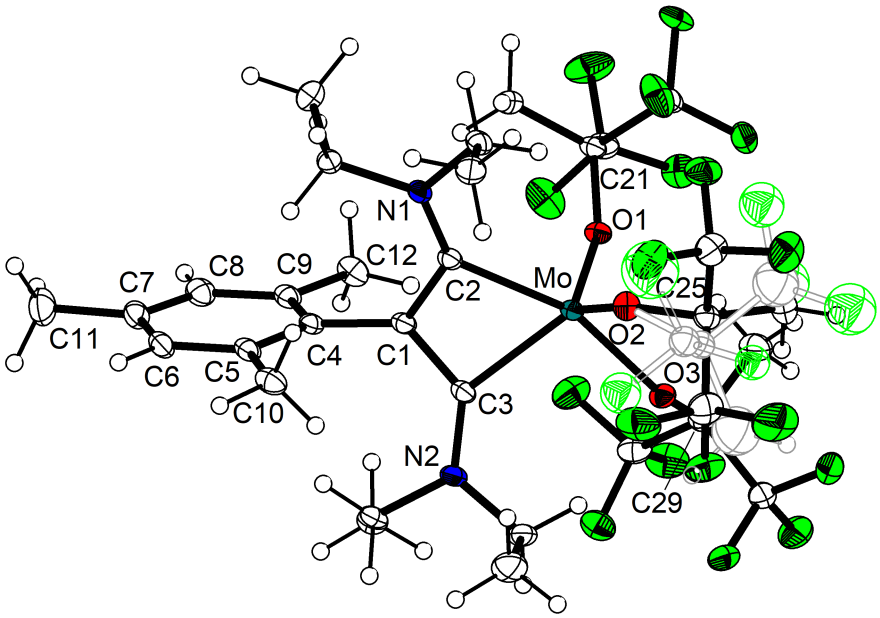

Figure 85. Molecular structure of **36** with thermal displacement parameters drawn at the 30% probability level. The minor component of the disordered alkoxide ligand (at O2) is depicted using paler colours. Selected bond lengths (Å) and angles (deg): Mo–C2 2.1422(2), Mo–C3 2.1203(19), Mo–O1 1.9413(14), Mo–O2 1.9084(15), Mo–O3 2.0787(15), C1–C2 1.433(3), C1–C3 1.413(3), C1–C4 1.499(3), N1–C2 1.324(3), N2–C3 1.324(3); C2–Mo–C3 61.96(8), C2–Mo–O1 99.03(7), C2–Mo–O2 98.15(7), C2–Mo–O3 159.67(7), C3–Mo–O1 119.58(7), C3–Mo–O2 115.32(7), C3–Mo–O3 97.82(7), O1–Mo–O2 124.29(6), O1–Mo–O3 89.04(6), O2–Mo–O3 92.49(6), Mo–C2–C1 92.76(13), Mo–C2–N1 138.15(15), C1–C2–N1 128.9(2), Mo–C3–C1 94.25(13), Mo–C3–N2 133.52(16), C1–C3–N2 131.8(2), C2–C1–C3 100.87(18), C2–C1–C4 129.27(19), C3–C1–C4 128.99(18).

Preparation of *mer*-(benzylidyne)(2,2′-bipyridine-κ^2*N,N′*)tris((1,1,1,3,3,3-hexafluoro-2-methyl-2-propanyl)oxy)molybdenum(VI), 42

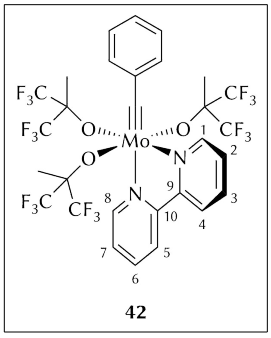

42

A solution of **1** (38.5 mg, 50 µmol) in *n*-hexane (0.7 mL) was treated with phenylacetylene (7 mg, 70 µmol, 1.4 equiv), which resulted in precipitation of an orange solid. Addition of a solution of 2,2′-bipyridine (31.2 mg, 200 µmol, 4 equiv) in dichloromethane (0.3 mL) caused the partial dissolution of the precipitate and a colour change to deep brown. Filtration of the mixture through a glass microfibre filter and storage overnight at –30 °C yielded a crude product as a brown crystalline material. A second crop of crystals was obtained from the decanted mother liquor at –30 °C.

1. Elemental analysis

$C_{29}H_{22}F_{18}MoN_2O_3$	C [%]	H [%]	N [%]
Found	38.31	3.11	5.48
Calc.	39.38	2.51	3.17

The elemental composition found is outside the range viewed as establishing analytical purity, and suggests the presence of one or more impurities.

2. NMR spectroscopy

	solvent: C_6D_6
δ_H (400.4 MHz, 297 K)	1.81 (m, 6H, 2 × *cis*-C(CH_3)(CF$_3$)$_2$), 2.09 (m, 3H, *trans*-C(CH_3)(CF$_3$)$_2$), 6.45 (m, 1H, 2-*H*), 6.53 (m, 1H, 7-*H*), 6.83 (m, 1H, 6-*H*), 6.84 (m, 1H, *p*-*H*), 6.92 (m, 1H, 3-*H*), 6.95 (m, 1H, 5-*H*), 7.08 (m, 1H, 4-*H*), 7.12 (m, 2H, 2 × *m*-*H*), 7.44 (m, 2H, 2 × *o*-*H*), 8.97 (m, 1H, 8-*H*), 9.16 (br d, $^3J_{HH}$ = 5.4 Hz, 1H, 1-*H*)
δ_C (100.7 MHz, 298 K)	18.4 (2 × *cis*-C(*C*H$_3$)(CF$_3$)$_2$), 19.7 (*trans*-C(*C*H$_3$)(CF$_3$)$_2$), 83.65 (sep, $^2J_{CF}$ = 28 Hz, 2 × *cis*-*C*(CH$_3$)(CF$_3$)$_2$), 83.67 (sep, $^2J_{CF}$ = 29 Hz, *trans*-*C*(CH$_3$)(CF$_3$)$_2$), 121.3 (5-*C*H), 122.0 (4-*C*H), 124.3 (2-*C*H), 124.61 (q, $^1J_{CF}$ = 290 Hz, *cis*-C(CH$_3$)(*C*F$_3$)$_2$), 124.63 (q, $^1J_{CF}$ = 289 Hz, *cis*-C(CH$_3$)(*C*F$_3$)$_2$), 125.0 (q, $^1J_{CF}$ = 289 Hz, *trans*-C(CH$_3$)(*C*F$_3$)$_2$), 125.5 (7-*C*H), 128.6 (*m*-*C*H), 128.9 (*p*-*C*H), 130.7 (*o*-*C*H), 137.9 (6-*C*H), 139.4 (3-*C*H), 143.9 (*i*-C_q), 147.4 (8-*C*H), 150.6 (10-C_q), 153.6 (9-C_q), 156.3 (1-*C*H), 292.4 (*C*≡Mo). Some of the outer lines of the septets were not observed.
δ_F (376.7 MHz, 297 K)	–78.3 (m, 6F), –76.7 (q, $^4J_{FF}$ = 10.3 Hz, 6F), –76.6 (m, 6F)

3. X-ray crystal structure determination

After a first crop of product precipitated from the reaction mixture, pale red–brown dichroic single-crystals were obtained from the decanted mother liquor (*n*-hexane/dichloromethane) at –30 °C.

Special features and exceptions: Two of the C(CF$_3$)$_2$Me groups (at O1 and O3) are disordered and were refined on two positions.

empirical formula	$C_{29}H_{22}F_{18}MoN_2O_3$	identification code	oscar13
M_w	884.43	Z	2
wavelength/Å	1.54184	ρ_{calc}/(Mg m^{-3})	1.798
T/K	100(2)	μ/mm^{-1}	4.585
cryst. size/mm³	0.15 × 0.10 × 0.05	F(000)	876
cryst. system	triclinic	reflections collected	116 825
space group	$P\bar{1}$	indep. reflections (R_{int})	6 769 (0.0447)
a/Å	10.8104(3)	parameters	599
b/Å	11.9449(3)	restraints	173
c/Å	12.7687(3)	goodness-of-fit on F^2	1.040
α/°	82.618(2)	R_1 ($I > 2\sigma(I)$)	0.0272
β/°	89.680(2)	wR_2 (all reflections)	0.0694
γ/°	87.294(2)	max and min $\Delta\rho$/(e Å^{-3})	0.486 and −0.813
V/Å³	1633.31(7)		

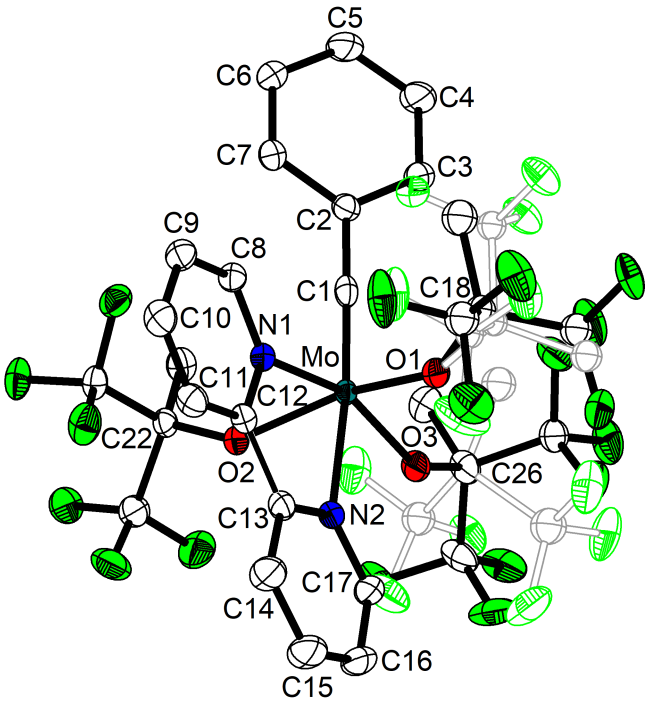

Figure 86. Molecular structure of **42** with thermal displacement parameters drawn at the 50% probability level. Hydrogen atoms are omitted for clarity. The minor component of disordered $C(CF_3)_2Me$ ligands (at O1 and O3) are depicted using paler colours. For selected bond lengths and angles, see Figure 55, p 107.

Preparation of mer-(2,2′-bipyridine-κ²N,N′)tris((1,1,1,3,3,3-hexafluoro-2-methyl-2-propanyl)oxy)(hexylidyne)molybdenum(VI), 43

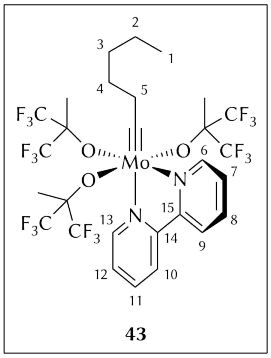

43

To a solution of **1** (120 mg, 156 µmol) in *n*-hexane (3 mL) was added a solution of 1-heptyne (30 mg, 312 µmol, 2.0 equiv) in *n*-hexane (3 mL), which resulted in an immediate colour change to red. After stirring for 5 min, the mixture was concentrated to ~4 mL under reduced pressure and filtered through a glass microfibre filter from a deep brownish residue. The filtrate

was stored at –30 °C, filtered through a glass microfibre filter, and divided in two. To one half a solution of 2,2′-bipyridine (18 mg, 115 µmol, ~1.5 equiv) in dichloromethane (0.2 mL) and more *n*-hexane (0.3 mL) was added, and the mixture was stored for several months at –30 °C, which resulted in the formation of **43** as block-shaped red crystals. The other half was also stored for several months at –30 °C, which yielded bis(mesityl)acetylene (**27**) as colourless needles.

1. Elemental analysis

$C_{28}H_{28}F_{18}MoN_2O_3$	C [%]	H [%]	N [%]
Found	38.13	2.98	3.62
Calc.	38.28	3.21	3.19

2. NMR spectroscopy

	solvent: C_6D_6
δ_H (600.1 MHz, 303 K)	0.88 (t, $^3J_{HH}$ = 7.4 Hz, 3H, 1-CH_3), 1.04 (m, 2H, 3-CH_2), 1.19 (m, 2H, 2-CH_2), 1.58 (m, 2H, 4-CH_2), 1.77 (m, 6H, 2 × *cis*-C(CH_3)(CF_3)$_2$), 2.02 (m, 3H, *trans*-C(CH_3)(CF_3)$_2$), 3.19 (m, 2H, 5-CH_2), 6.50 (app ddd, $^{3,app}J_{HH}$ = 7.6 Hz, $^{3,app}J_{HH}$ = 5.0 Hz, $^{4,app}J_{HH}$ = 1.0 Hz, 1H, 12-*H*), 6.57 (app ddd, $^{3,app}J_{HH}$ = 7.5 Hz, $^{3,app}J_{HH}$ = 5.5 Hz, $^{4,app}J_{HH}$ = 1.3 Hz, 1H, 7-*H*), 6.81 (app td, $^{3,app}J_{HH}$ = 7.8 Hz, $^{4,app}J_{HH}$ = 1.8 Hz, 1H, 11-*H*), 6.92–6.97 (m, 2H, 10-*H,* 8-*H*), 7.07 (br d, $^3J_{HH}$ = 8.0 Hz, 1H, 9-*H*), 8.87 (app ddd, $^{3,app}J_{HH}$ = 5.0 Hz, $^{4,app}J_{HH}$ = 1.8 Hz, $^{5,app}J_{HH}$ = 0.8 Hz, 1H, 13-*H*), 8.96 (br dm, $^3J_{HH}$ = 5.1 Hz, 1H, 6-*H*)
δ_C (150.9 MHz, 303 K)	14.06 (1-*C*H$_3$), 18.51 (2 × *cis*-C(*C*H$_3$)(CF$_3$)$_2$), 19.51 (*trans*-C(*C*H$_3$)(CF$_3$)$_2$), 22.39 (2-*C*H$_2$), 28.15 (4-*C*H$_2$), 31.63 (3-*C*H$_2$), 49.01 (5-*C*H$_2$), 83.04 (sep, $^2J_{CF}$ = 28 Hz, 3 × *C*(CH$_3$)(CF$_3$)$_2$), 121.14 (10-*C*H), 121.94 (9-*C*H), 124.06 (7-*C*H), 124.76 (q, $^1J_{CF}$ = 289 Hz, 3 × C(CH$_3$)(*C*F$_3$)$_2$), 125.28 (12-*C*H), 137.71 (11-*C*H), 139.13 (8-*C*H), 147.42 (13-*C*H), 150.63 (14-C_q), 153.49 (15-C_q), 156.64 (6-*C*H), 305.95 (*C*≡Mo). The outer lines of the septet were not observed.
δ_F (376.7 MHz, 297 K)	–78.4 (m, 6F), –76.7 (sep, $^4J_{FF}$ = 2.4 Hz, 6F), –76.5 (q, $^4J_{FF}$ = 10.1 Hz, 6F)

3. X-ray crystal structure determination

Red single-crystals were obtained from an *n*-hexane/dichloromethane solution at –30 °C. The structure is illustrated in Figure 56, p 109.

empirical formula	$C_{28}H_{28}F_{18}MoN_2O_3$	identification code	oscar10
M_w	878.46	Z	4
wavelength/Å	0.71073	ρ_{calc}/(Mg m^{-3})	1.736
T/K	100(2)	μ/mm^{-1}	0.524
cryst. size/mm^3	0.25 × 0.20 × 0.15	F(000)	1752
cryst. system	monoclinic	reflections collected	101211
space group	$P2_1/n$	indep. reflections (R_{int})	10083 (0.0367)
a/Å	13.33127(10)	parameters	473
b/Å	18.7544(3)	restraints	0
c/Å	13.4454(2)	goodness-of-fit on F^2	1.064
α/°	90	R_1 ($I > 2\sigma(I)$)	0.0243
β/°	90.516(2)	wR_2 (all reflections)	0.0560
γ/°	90	max and min $\Delta\rho$/(e Å^{-3})	0.580 and –0.448
V/Å^3	3361.48(8)		

In addition, a few green–brown dichroic crystals of a decomposition product with the formula [Mo(≡O)(bipy)(OC(CF$_3$)$_2$Me)$_3$], **45**, were obtained and analysed by X-ray diffraction:

empirical formula	$C_{22}H_{17}F_{18}MoN_2O_4$
M_w	811.32
wavelength/Å	0.71073
T/K	100(2)
cryst. size/mm³	0.30 × 0.22 × 0.15
cryst. system	triclinic
space group	$P\bar{1}$
a/Å	9.7583(2)
b/Å	11.0938(3)
c/Å	28.4008(7)
α/°	90.759(2)
β/°	99.848(2)
γ/°	111.874(2)
V/Å³	2 801.17(12)

identification code	oscar11
Z	4
ρ_{calc}/(Mg m^{-3})	1.924
μ/mm^{-1}	0.623
F(000)	1596
reflections collected	185 412
indep. reflections (R_{int})	16 852 (0.0406)
parameters	853
restraints	0
goodness-of-fit on F^2	1.100
R_1 ($I > 2\sigma(I)$)	0.0295
wR_2 (all reflections)	0.0610
max and min $\Delta\rho$/(e Å^{-3})	0.491 and −0.624

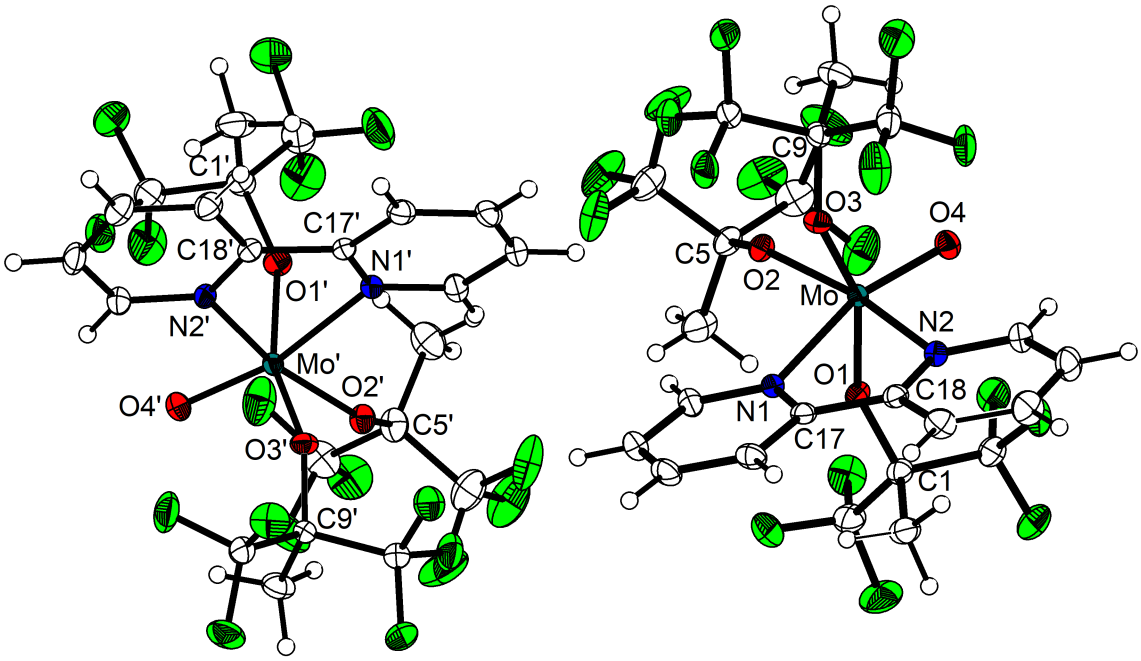

Figure 87. Molecular structure of **45** showing the two independent molecules with thermal displacement parameters drawn at the 50% probability level. Selected bond lengths (Å) and angles (deg): Mo–N1 2.3077(13), Mo′–N1′ 2.3146(13), Mo–N2 2.2389(13), Mo′–N2′ 2.2181(13), Mo–O1 1.9827(11), Mo′–O1′ 1.9886(11), Mo–O2 1.9561(11), Mo′–O2′ 1.9496(11), Mo–O3 1.9808(11), Mo′–O3′ 1.9856(11), Mo–O4 1.6730(11), Mo′–O4′ 1.6748(11), N1–C17 1.342(2), N1′–C17′ 1.347(2), N2–C18 1.3578(19), N2′–C18′ 1.3575(19), C17–C18 1.473(2), C17′–C18′ 1.477(2); N1–Mo–N2 70.27(5), N1′–Mo′–N2′ 70.81(5), N1–Mo–O1 82.74(4), N1′–Mo′–O1′ 83.43(5), N1–Mo–O2 94.40(5), N1′–Mo′–O2′ 92.80(5), N1–Mo–O3 76.34(4), N1′–Mo′–O3′ 76.37(4), N1–Mo–O4 157.03(5), N1′–Mo′–O4′ 158.78(5), N2–Mo–O1 98.76(5), N2′–Mo′–O1′ 94.65(5), N2–Mo–O2 162.14(5), N2′–Mo′–O2′ 162.40(5), N2–Mo–O3 81.61(5), N2′–Mo′–O3′ 82.27(5), N2–Mo–O4 86.76(5), N2′–Mo′–O4′ 88.05(5), O1–Mo–O2 87.93(4), O1′–Mo′–O2′ 89.60(5), O1–Mo–O3 157.66(5), O1′–Mo′–O3′ 159.47(5), O1–Mo–O4 101.02(5), O1′–Mo′–O4′ 100.54(5), O2–Mo–O3 85.96(5), O2′–Mo′–O3′ 87.76(5), O2–Mo–O4 108.31(5), O2′–Mo′–O4′ 107.98(5), O3–Mo–O4 101.30(5), O3′–Mo′–O4′ 99.64(5), Mo–N1–C17 117.98(10), Mo′–N1′–C17′ 117.77(10), Mo–N2–C18 119.45(10) Mo′–N2′–C18′ 120.51(10), N1–C17–C18 114.66(13), N1′–C17′–C18′ 114.63(13), N2–C18–C17 115.47(13), N2′–C18′–C17′ 115.57(13).

Preparation of (2,2′-bipyridine-κ^2N,N')[1-(2,4,6-trimethylphenyl)-1-octene-1,2-diyl-3-ylidene-κ^3C]bis(1,1,1,3,3,3-hexafluoro-2-methyl-2-propanolate)molybdenum(VI), 46

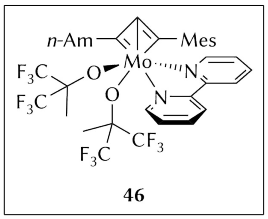

46

To a precooled (–40 °C) solution of **1** (77 mg, 0.10 mmol) in diethyl ether (6 mL) was added a solution of 1-heptyne (10.6 mg, 0.11 mmol. 1.1 equiv) in diethyl ether (1 mL). The mixture turned red immediately; Et_3N (0.14 mL, 101 mg, 1 mmol, 10 equiv) was added at once, and the mixture was stirred for 10 min at –40 °C. The cooling bath was removed, and 2,2′-bipyridine (63 mg, 0.4 mmol, 4 equiv) was added as the mixture warmed up to ambient temperature. The solution quickly turned brownish-violet. The solvent was removed, the residue was extracted first with *n*-pentane (2 mL) and then with dichloromethane (2 mL), and both fractions were filtered through a glass microfibre filter. The deep violet filtrates were stored for several weeks at –30 °C, whereby large block-shaped deep red crystals of **46** precipitated from the dichloromethane solution. Yield: 77% (65 mg, 77 μmol).

In addition, a dark solid deposited from the *n*-pentane solution; the supernatant was decanted and stored at –30 °C, from which red crystals of **43** were obtained. Finally, the residue was recrystallised in *n*-pentane at –30 °C, which gave a mixture of colourless and violet crystals not suitable for X-ray diffraction analysis.

1. NMR spectroscopy

	solvent: C_6D_6
δ_H (400.4 MHz, 296 K)	0.68 (s, 6H, 2 × C(CH_3)(CF_3)$_2$), 1.05 (t, $^3J_{HH}$ = 7.4 Hz, 3H, CH_2CH_3), 1.56 (m, 2H, CH_2CH_3), 1.81 (m, 2H, $CH_2CH_2CH_3$), 2.35 (s, 3H, *p*-CH_3), 2.42 (m, 2H, $MoCCH_2CH_2$), 2.75 (s, 6H, 2 × *o*-CH_3), 4.36 (t, $^3J_{HH}$ = 7.4 Hz, 3H, $MoCCH_2$), 6.66 (m, 2H, bipy), 6.87 (m, 1H, bipy), 7.04 (m, 1H, bipy), 7.14 (m, 2H, 2 × *m*-*H*), 7.25 (m, 1H, bipy), 7.31 (m, 1H, bipy), 9.91 (br d, $^3J_{HH}$ = 4.4 Hz, 1H, bipy), 9.97 (br d, $^3J_{HH}$ = 5.0 Hz, 1H, bipy)
δ_C (100.7 MHz, 299 K)	14.4 (CH_2CH_3), 17.1 (2 × C(CH_3)(CF_3)$_2$), 21.2 (*p*-CH_3), 21.4 (2 × *o*-CH_3), 23.2 (CH_2CH_3), 32.2 ($CH_2CH_2CH_3$), 32.3 ($MoCCH_2CH_2$), 41.2 ($MoCCH_2$), 79.8 (sep, $^2J_{CF}$ = 28 Hz, 2 × *C*(CH_3)(CF_3)$_2$), 121.5 (bipy-*C*H), 121.9 (bipy-*C*H), 124.3 (q, $^1J_{CF}$ = 289 Hz, 2 × C(CH_3)(*C*F_3)$_2$), 124.8 (bipy-*C*H), 125.3 (bipy-*C*H), 129.5 (2 × *m*-*C*H), 137.4 (*p*-$C_q$$CH_3$), 137.7 (2 × *o*-$C_q$$CH_3$), 138.3 (bipy-*C*H), 138.8 (bipy-*C*H), 139.5 (*i*-C_q), 153.2 (bipy-*C*H), 153.3 (bipy-*C*H), 153.6 (bipy-C_q), 154.7 (bipy-C_q), 200.7 (β-C_q), 213.9 (Mes–C_q), 228.0 (*n*-Am–C_q). The outer lines of the septet were not observed.
δ_F (376.7 MHz, 298 K)	–78.3 (q, $^4J_{FF}$ = 9.9 Hz, 6F), –77.9 (q, $^4J_{FF}$ = 9.8 Hz, 6F)

Additional signals belong to uncoordinated bipy and minor side-products.

2. X-ray crystal structure determination

Deep red crystals were obtained from a concentrated diethyl ether solution at –30 °C.

Special features and exceptions: First attempts to record data at 100 K led to degradation of the crystals, possibly because of a destructive phase transition. The mesityl moiety is disordered and was refined over two positions; ISOR restrains were applied. The pentyl chain is disordered over several positions and was refined over three positions; ISOR and SADI restraints were applied. Five reflections with Error/ESDs over –10 were omitted.

empirical formula	$C_{39}H_{46}F_{12}MoN_2O_3$
M_w	914.72
wavelength/Å	0.71073
T/K	130(2)
cryst. size/mm³	0.30 × 0.25 × 0.06
cryst. system	monoclinic
space group	$P2_1/c$
a/Å	12.8542(3)
b/Å	24.7063(5)
c/Å	12.6445(3)
α/°	90
β/°	96.146(2)
γ/°	90
V/Å³	3 992.57(16)
identification code	oscar22
Z	4
ρ_{calc}/(Mg m^{-3})	1.522
μ/mm^{-1}	0.424
F(000)	1872
reflections collected	211 464
indep. reflections (R_{int})	12 224 (0.0607)
parameters	678
restraints	283
goodness-of-fit on F^2	1.064
R_1 ($I > 2\sigma(I)$)	0.0518
wR_2 (all reflections)	0.1323
max and min $\Delta\rho$/(e Å^{-3})	0.573 and –0.836

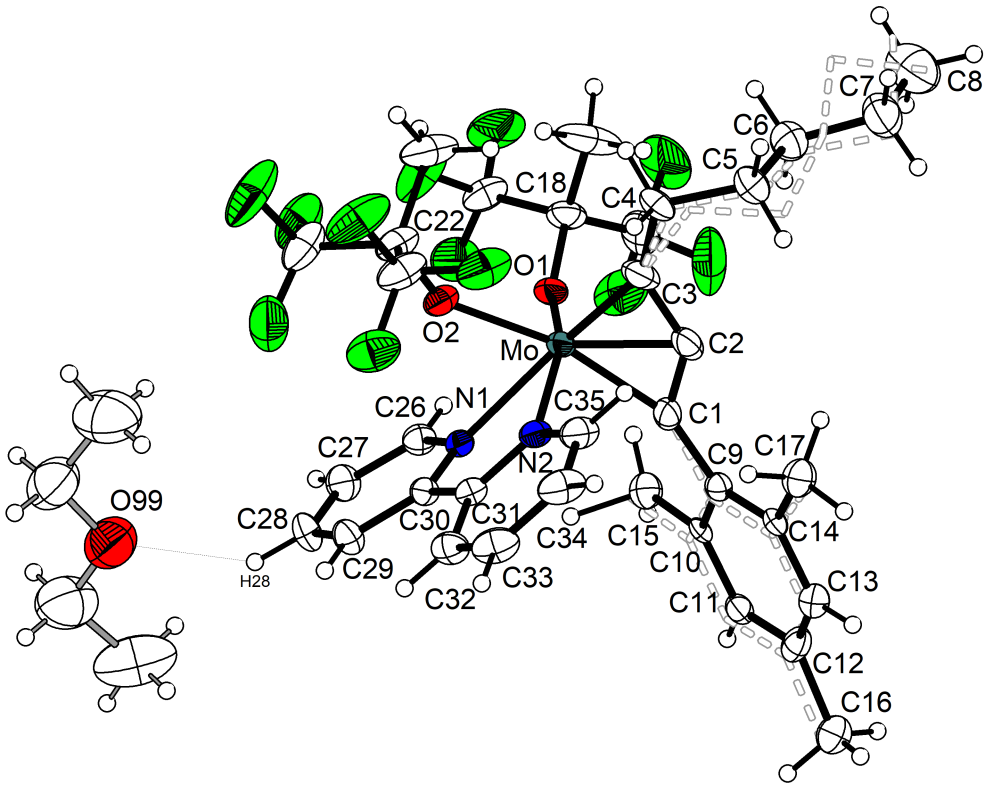

Figure 88. Molecular structure of **46**·Et_2O with thermal displacement parameters drawn at the 50% probability level. The pentyl chain (at C3) and the mesityl group (at C1) are disordered; for clarity, the minor components are depicted as a wireframe model using dashed bonds and paler colours. The short contact H28···O99 is drawn explicitly as a dotted bond. Selected bond lengths (Å) and angles (deg): Mo–C1 2.006(3), Mo–C2 2.020(3), Mo–N1 2.3128(19), Mo–N2 2.251(2), Mo–C3 1.925(3), Mo–O1 1.9614(18), Mo–O2 2.0785(18), N1–C30 1.349(3), N2–C31 1.349(3), C1–C2 1.363(4), C2–C3 1.404(5), C3–C4 1.635(8), C3–C4A 1.428(16), C3–C4B 1.40(3), C1–C9 1.390(5), C1–C9A 1.580(5), C30–C31 1.480(3), O99···H28 2.4350(38); C1–Mo–C2 39.58(13), C1–Mo–C3 81.18(13), C2–Mo–C3 41.61(14), C1–Mo–N1 99.03(9), C1–Mo–N2 85.51(9), C1–Mo–O1 99.10(10), C1–Mo–O2 164.46(9), C2–Mo–N1 137.15(10), C2–Mo–N2 90.17(10), C2–Mo–O1 106.16(11), C2–Mo–O2 143.83(12), C3–Mo–N1 165.61(11), C3–Mo–N2 93.81(11), C3–Mo–O1 106.60(11), C3–Mo–O2 104.07(12), N1–Mo–N2 71.92(7), N1–Mo–O1 87.62(7), N1–Mo–O2 72.20(7), N2–Mo–O1 159.51(7), N2–Mo–O2 79.59(7), O1—Mo—O2 93.43(7), Mo–C1–C2 70.76(17), Mo–C2–C1 69.66(16), Mo–C2–C3 65.57(16), Mo–C3–C2 72.83(17), C1–C2–C3 135.2(3), Mo–C1–C9 158.2(3), Mo–C1–C9A 149.8(3), C2–C1–C9 125.2(4), C2–C1–C9A 139.1(3), Mo–C3–C4 148.7(3), Mo–C3–C4A 168.6(7), Mo–C3–C4B 157.9(9), C2–C3–C4 135.3(4), C2–C3–C4A 116.6(6), C2–C3–C4B 129.2(9), Mo–N1–C30 115.54(15), Mo–N2–C31 118.01(16), N1–C30–C31 115.8(2), N2–C31–C30 116.6(2).

5.3.5. Alkynes

Preparation of bis(4-methylpiperidino)acetylene, 34

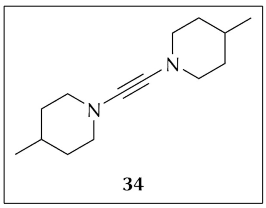

34

The literature protocol[236] was adapted as follows. A solution of *n*-BuLi (2.5 M in hexanes, 6.53 mL, 16.35 mmol, 1.1 equiv) was added dropwise to a stirred solution of 1,1-di(4-methylpiperidino)-2,2-dibromoethene (5.65 g, 14.86 mmol, 1.0 equiv) in *n*-hexane (60 mL), which resulted in the formation of a white precipitate (LiBr). After 30 min the excess *n*-BuLi was quenched with dimethylformamide (1 mL), and the mixture was filtered through D.E. and washed with *n*-hexane (10 mL + 2 × 5 mL). The yellow filtrate was collected in a silylated flask (the flask was rinsed with a 5% chlorodimethylsilane solution in chloroform and then with water prior to drying), and the volatiles were removed in high vacuum, affording a yellowish residue. After bulb-to-bulb distillation under low pressure (3 Pa), **34** was obtained as a colourless crystalline solid and stored in a silylated flask at –30 °C. Yield: 79% (2.57 g, 11.66 mmol). Spectroscopic data are in agreement with the literature.[236]

Preparation of bis(diethylamino)acetylene, 33

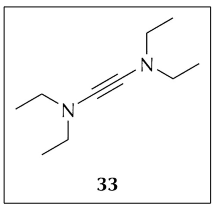

33

The literature protocols[225,272] were adapted as follows. To a precooled (–80 °C) solution of trichloroethylene (6.570 g, 50.0 mmol) in diethyl ether (50 mL) was carefully added dropwise over a period of 45 min a solution of lithium diethylamide (3.954 g, 50.0 mmol, 1.0 equiv) in diethyl ether (50 mL). After addition was completed, the orange solution was stirred for 2 h and allowed to warm gradually to room temperature, leaving a turbid brown mixture. The mixture was cooled again to –80 °C, and a solution of lithium diethylamide (3.954 g, 50.0 mmol, 1.0 equiv) in diethyl ether (50 mL) was slowly added over a period of 45 min under exclusion of light. The mixture was stirred for 1 h and allowed to warm gradually to 0 °C, resulting in a brown mixture. At this temperature, the solvent was partially removed (approx. 100 mL) at low pressure (besides the solvent, a yellow substance was collected in the cold trap that decomposes in contact with air). The deep maroon mixture was cooled to –80 °C again, and a solution of lithium diethylamide (4.349 g, 55.0 mmol, 1.1 equiv) in diethyl ether (50 mL) was slowly added over 45 min under exclusion of light. The reaction mixture was then allowed to warm gradually to 0 °C, and the solvent was partially removed (approx. 100 mL). The

brown mixture was filtered through D.E. and washed with diethyl ether (4 × 5 mL). The solvent was removed at 0 °C, and the brown residue was purified by bulb-to-bulb distillation (40–70 °C, 5 Pa), affording **33** as a pale yellow liquid. Yield: 48% (4.000 g, 23.8 mmol). Spectroscopic data are in agreement with the literature.[225]

Preparation of *meso*–1,2-dibromo-1,2-diphenylethane and 1,2-diphenylacetylene

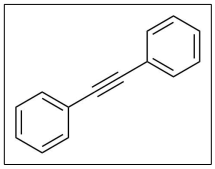

meso-1,2-Dibromo-1,2-diphenylethane and 1,2-diphenylacetylene were synthesised based on published procedures.[217,218] Inert conditions are not required for these syntheses. Yield from 250 mg (1.387 mmol) *trans*-stilbene: *meso*-1,2-dibromo-1,2-diphenylethane, 84% (395 mg, 1.162 mmol); 1,2-diphenylacetylene, 52% (129 mg, 0.724 mmol).

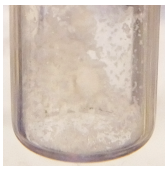

1. NMR spectroscopy

Spectroscopic data of *meso*-1,2-dibromo-1,2-diphenylethane[273] and 1,2-diphenylacetylene[212] are in agreement with the literature.

Preparation of (1,2-$^{13}C_2$)-1,2-diphenylacetylene

The procedure for the synthesis of this compound is analogous to that for 1,2-diphenylacetylene. For convenience, the synthesis is included herein. Inert conditions are not required.

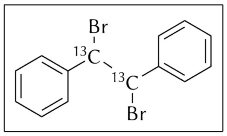

trans-(1,2-$^{13}C_2$)-stilbene (250 mg, 1.37 mmol) was dissolved in glacial acetic acid (3 mL) at 140 °C in a 10 mL round-bottom flask fitted with a reflux condenser. The reflux was stopped, and the reflux condenser was briefly removed before adding pyridinium tribromide (496 mg, 1.55 mmol, 1.13 equiv) in glacial acetic acid (2 mL) through a funnel. Refluxing for 6 min at 140 °C gave a colourless precipitate. After cooling down to ~40 °C on a water bath, the product (*meso*-1,2-dibromo-1,2-diphenyl($^{13}C_2$)ethane) was collected on a Hirsch funnel, washed with cold (0 °C) water (3 × 1.1 mL) and cold (0 °C) acetone (2 × 1.1 mL), and dried in high vacuum. Yield: 87% (407 mg, 1.19 mmol).

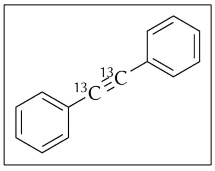

In a 10 mL round-bottom flask, KOH (386 mg, ~85 m%, ~6 mmol, ~5 equiv) and triethylene glycol (2 mL) were added to the obtained *meso*-1,2-dibromo-1,2-diphenyl($^{13}C_2$)ethane (407 mg, 1.19 mmol), and the mixture was heated for 8 min at 195 °C. The brown solution was cooled down to ~40 °C on a water bath, and water (5 mL) was added to precipitate (1,2-$^{13}C_2$)-1,2-diphenylacetylene as a colourless solid. The flask was then kept for 30 min at 0 °C before collecting the solid on a Hirsch funnel and washing it with ethanol (70 v%, 1 + 0.5 mL). Crystallisation in ethanol (95 v%, 1.9 mL) at 3 °C and drying in high vacuum for 3 h afforded 94 mg of colourless crystals. Additional 13 mg of product were obtained from the supernatant after concentration and recrystallisation at 3 °C. Total yield: 50% (107 mg, 0.59 mmol), 43% from *trans*-(1,2-$^{13}C_2$)-stilbene.

1. NMR spectroscopy

meso–1,2-dibromo-1,2-diphenyl($^{13}C_2$)ethane	solvent: dimethyl sulphoxide-d_6
δ_H (600.1 MHz, 303 K)	6.15 (d, $^1\mathcal{J}_{HC}$ = 155 Hz, 2H, 2 × ^{13}C*H*), 7.35 (m, 2H, 2 × *p-H*), 7.43 (app t, $^{3,app}\mathcal{J}_{HH}$ = 7.5 Hz, 4H, 4 × *m-H*), 7.70 (m, 4H, 4 × *o-H*)

(1,2-$^{13}C_2$)-diphenylacetylene	solvent: chloroform-d_3
δ_H (600.1 MHz, 303 K)	7.31–7.38 (m, 6H, 2 × *p-H*, 4 × *m-H*), 7.52–7.56 (m, 4H, 4 × *o-H*)
δ_C (150.9 MHz, 303 K)	89.33 (s, 2 satellites ($^1\mathcal{J}_{CC}$ = 52 Hz), 2 × $^{13}C\equiv$), 123.25 (app t, $^{1-2,app}\mathcal{J}_{CC}$ = 52 Hz, *i-C*$_q$), 128.26 (s, 2 × *p-C*H), 128.34 (app t, $^{3-4,app}\mathcal{J}_{CC}$ = 3 Hz, 4 × *m-C*H), 131.61 (app t, $^{2-3,app}\mathcal{J}_{CC}$ = 2 Hz, 4 × *o-C*H)

2. High-resolution mass spectrometry

$C_{12}{}^{13}C_2H_{10}$: Found, 180.08496; calc., 180.08574 ($\Delta m/m$ = 4.31 ppm).

Characterisation of bis(mesityl)acetylene, 27

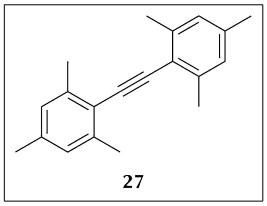
27

In several experiments, bis(mesityl)acetylene (**27**) was obtained either as a by-product (e.g. see p 180, p 189) or as a decomposition product (e.g. see p 174).

1. NMR spectroscopy

NMR data of **27** has been reported in different occasions for chloroform-d_3 samples.[249,250,274,275] The corresponding chemical shifts in benzene-d_6 are listed below.

	solvent: C_6D_6
δ_H (300.3 MHz, 298 K)	2.12 (s, 3H, *p*-CH_3), 2.53 (s, 6H, 2 × *o*-CH_3), 6.78 (s, 2H, 2 × *m*-*H*)
δ_C (75.5 MHz, 298 K)	21.3 (*p*-CH_3), 21.7 (*o*-CH_3), 96.0 ($C_q \equiv C_q$), 121.5 (*i*-C_q), 128.2 (*m*-CH), 137.5 (*p*-$C_q CH_3$), 140.1 (*o*-$C_q CH_3$)

2. X-ray crystal structure determination

Colourless needles of **27** were observed several times, for instance, in the preparation of **26**, **43**, or **44**. X-ray diffraction analysis was executed on a single-crystal obtained from an *n*-hexane solution at –30 °C during work-up in the synthesis of **44**. The molecular structure is depicted in Figure 57.

empirical formula	$C_{20}H_{22}$
M_w	262.38
wavelength/Å	1.54184
T/K	100(2)
cryst. size/mm³	0.15 × 0.10 × 0.05
cryst. system	monoclinic
space group	$P2_1/n$
a/Å	13.6567(7)
b/Å	7.7846(4)
c/Å	15.0132(8)
α/°	90
β/°	107.431(6)
γ/°	90
V/Å³	1522.79(14)

identification code	oscar08
Z	4
ρ_{calc}/(Mg m^{-3})	1.144
μ/mm^{-1}	0.476
F(000)	568
reflections collected	26 355
indep. reflections (R_{int})	3147 (0.0434)
parameters	187
restraints	0
goodness-of-fit on F^2	1.038
R_1 ($I > 2\sigma(I)$)	0.0469
wR_2 (all reflections)	0.1328
max and min $\Delta\rho$/(e Å^{-3})	0.327 and –0.196

General procedure for alkyne cross-metathesis

1. Self-metathesis of 5-(benzyloxy)-2-pentyne, Y-Me

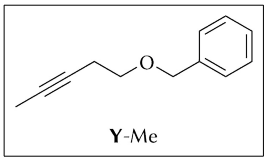

Y-Me

A mixture of **Y**-Me (0.25 mmol), *n*-decane (0.25 mmol), molecular sieves (250 mg), and toluene (1.25 mL, 200 mM) was stirred for 10 min before adding the catalyst (1 mol%, 2.5 μmol) as a solid. Aliquots (0.05 mL) for GC analysis were taken at t = 0 min (prior to addition of catalyst) and at specified time intervals (usually 1, 2, 3, 4, 5, 10, 15, 20, 40, and 60 min). The samples were filtered through a small pad of neutral alox, and the product was eluted with diethyl ether (1 mL) and analysed by GC. *RT*(*n*-decane) = 5.1 min, *RT*(**Y**-Me) = 12.2 min, *RT*(**47**) = 22.5 min.

To determine isolated yields, a larger aliquot (0.35 mL, 28% of the total) was taken after the last sample, it was passed through a pad of neutral alox, the product was eluted with diethyl ether (5 × 1 mL) and, after removal of the solvents under reduced pressure, it was dried in high vacuum. Alternatively, the procedure described above was repeated without *n*-decane, and the scale was doubled (0.50 mmol substrate). The mixture was then stirred for 1 h at ambient temperature, followed by filtration through a short column of neutral alox, and the product was eluted with diethyl ether (5 × 2 mL) and, after removal of the solvents under reduced pressure, it was dried in high vacuum.

2. Self-metathesis of 4-(benzyloxy)-1-butyne, Y-H

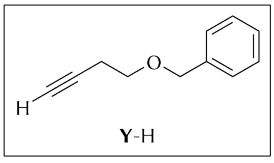

Y-H

A mixture of **Y**-H (0.25 mmol), *n*-decane (0.25 mmol), molecular sieves (250 mg), and toluene (12.5 mL, 20 mM) was stirred for 10 min before adding the catalyst (1 mol%, 2.5 μmol) as a solid. Aliquots (0.05 mL) for GC analysis were taken at t = 0 min (prior to addition of catalyst) and at specified time intervals (usually 1, 2, 3, 4, 5, 10, 20, 40, and 60 min). The samples were filtered through a small pad of neutral alox, and the product was eluted with diethyl ether (1 mL) and analysed by GC. *RT*(**Y**-H) = 9.8 min.

6 Abbreviations and Acronyms

General abbreviations and acronyms

ACM	alkyne cross-metathesis
ADIMET	acyclic diyne metathesis
ARCO	Atlantic Richfield Company
BASF	Badische Anilin- & Soda-Fabrik
bipy	2,2′-bipyridine
Bn	benzyl
Bz	benzoyl
calc	calculated
cat.	catalyst
coord.	coordinated
cryst.	crystal
Cy	cyclohexyl
D.E.	diatomaceous earth
DFT	density functional theory
DME	1,2-dimethoxyethane
DPMCBD	deprotiometallacyclobutadiene
DYCM	diyne cross-metathesis
ECP	effective core potentials
EI	electron ionisation
ELSD	evaporative light scattering detector
EPR	electron paramagnetic resonance
FID	flame ionization detector

GC	gas chromatography
GPC	gel permeation chromatography
HOMO	highest occupied molecular orbital
HPLC	high-performance liquid chromatography
Im^{Me_4}	1,3,4,5-tetramethylimidazolin-2-ylidene
indep.	independent
*i*Pr	2-propyl, isopropyl
l.s.	least-square
LUMO	lowest occupied molecular orbital
MAS	magic angle spinning
MCBD	metallacyclobutadiene
MCP	metallacyclopropen
MCPD	metallacyclopentadiene
Mes	2,4,6-trimethylphenyl, mesityl
MS	mass spectrometry
NACM	nitrile–alkyne cross-metathesis
Naph	1-naphthyl
NCM	nitrile cross-metathesis
NHC	*N*-heterocyclic carbenes
$NIm^{t\text{-}Bu}$	1,3-di-tert-butylimidazolin-2-iminato
NMR	nuclear magnetic resonance
PhD	Doctor of Philosophy
phen	1,10-phenanthroline
pip	piperidin-1-yl
pip^{Me}	4-methylpiperidin-1-yl
PPN	bis(triphenylphosphine)iminium
py	pyridine
quin	quinuclidine

RCAM	ring-closing alkyne metathesis
RCDYM	ring-closing diyne metathesis
ROAMP	ring-opening alkyne metathesis polymerisation
RT	retention time
SHOP	Shell Higher Olefin Process
$SiO_{2\,(700)}$	at 700 °C partially dehydroxylated silica
SOMC	surface organometallic chemistry
SOMO	singly occupied molecular orbital
SQUID	superconducting quantum interference device
TAM	terminal alkyne metathesis
THF	tetrahydrofuran
TMS	trimethylsilyl
TOBA	*N,N,N*-tri(2-oxidobenzyl)amine
TOF	turnover frequency
TON	turnover number
VE	valence electrons
VT	variable temperature

Abbreviations related to NMR spectroscopy

${}^{n}J_{AB}$	coupling constant between atoms A and B separated by *n* bonds
ppm	parts per milion
app	apparent
br	broad
d	doublet
dec	dectet
m	multiplet
q	quartet
s	singlet
sep	septet
t	triplet
i	*ipso*
m	*meta*
o	*ortho*
p	*para*
COSY	COrrelated SpectroscopY
DEPT	Distortions Enhancement by Polarisation Transfer
EXSY	EXchange SpectroscopY
HMBC	Heteronuclear Multiple Bond Correlation
HSQC	Heteronuclear Single Quantum Coherence
NOESY	Nuclear Overhauser Enhancement SpectroscopY
ROESY	Rotating frame Overhause Effect SpectroscopY

7 Acknowledgements

In a couple of years, I will probably have forgotten all the effort (and some sleep deprivation) it took me to complete this thesis. What I will certainly not forget are all the people who gave me a hand and contributed to the success of this project.

In the first place, I wish to express my deep gratitude to my advisor, Matthias Tamm, for his trust and the freedom given to me to explore my own ideas in the lab, but also for guiding me all these years. In addition, he brought the CaSuS doctoral program to Braunschweig, and encouraged me to participate in it.

I would like to acknowledge Prof. Daniel B. Werz for agreeing to review this dissertation and be a member of the examining committee. I am also thankful to Christian Kleeberg for his willingness to chair the Thesis committee.

For the successful cooperation that concluded with a co-authorship in a high-impact journal I am indebted to Prof. Christophe Copéret (ETH Zürich) and his coworkers.

My warmest thanks go to the following people: Kristof, Jeroen, Celine and Ludwig, who proofread some parts of this thesis, for their helpful comments and constructive criticism; Tobi, Daniel, and Celine for the great time we all had during the ISOM; Andrea (everyone has a bad day!) for her empathy, tenderness and good will; Phong, because during his first-year lab course I presumed that he would became a great chemist, and he did not disappoint me; Kristof (Rakkatakka!), Jeroen (he also survived without a TV!), Peter ("don't go home too late!"), and Richi ("el Comandante!") for their jokes, happiness and welcoming spirit; Martin and Jenni, for their teamwork and involvement in the JCF; Miguel, for his daily lessons on terrible music; Andy, for installing in me the fascination for organometallic chemistry; Sascha, for his virtuosity, immense knowledge and priceless tips and tricks; René and Vicky, for their patience and commitment; Alex and Adi, for pleasant conversations and fruitful discussions (especially at unseemly hours); Ismael and Muazzez, for their affection, friendliness and delicious food; and all current and past lab colleagues, for keeping cool and responding with humour to my chronic lateness and my obsession with order.

I am also in debt to all the students I had the pleasure to supervise in the lab, whose valuable work and constant dedication contributed significantly to improve this thesis.

Some techniques require a level of expertise beyond my ambition: Kai and Banny (DFT), Dirk (SQUID), Christian (powder diffraction) and Prof. Jones (XRD), you all have my gratitude!

Without the assistance of the technical, analytical and administration staff, this thesis would probably have never exist, and I am obliged to them for this. Special thanks go to Conny (Scorpio, of course), Janin (invaluable glove-box first-aid service), Jürgen (the art of custom-made!), Michael (we will remember you), and Mr Schröpfer (if it was made of glass, he would be able to make it); and a warm word of thanks goes to Ms Miehe and Ms Giere.

There is not enough space here to thank all my friends individually, but among all people I met at the TU Braunschweig, I am really happy to have met two. A very special thanks to Eliza, for her enthusiasm and her cooking skills, and to Lukas, for his sympathetic ear and the tardy meals after a late-night session.

My family and friends, so close and yet so far (Barcelona, Berlin, Oldenburg, Switzerland, London, Singapore, Canberra), had to cope with my destiny and were always there giving me lots of love, advice and good reasons to eat out or go for a drink. I am very lucky to have you all!

Last, but surely not least, I want to thank my dear Almut for her love and unconditional support, and for being the perfect mother for our lovely Clara. Thank you, you are incredible!

> *What we accomplished, […], came through basic research without really knowing exactly how we were proceeding; we ultimately came to realise, step by step, that our basic research was leading to something really useful.*
>
> *— Richard R. Schrock, American chemist and Nobel laureate (b. 1945)*

8 References

[1] J. M. Thomas, *Philos. Trans. R. Soc., A* **2015**, *373*, No. 20140288.

[2] J. J. Berzelius, *Jahresbericht über die Fortschritte der physischen Wissenschaften*; Laupp, Tübingen (Germany), **1836**.

[3] H. Hildebrand, NobelPrize.org, Nobel Media AB 2019. *The Nobel Prize in Chemistry 1909: Award Ceremony Speech*, can be found under https://www.nobelprize.org/prizes/chemistry/1909/ceremony-speech/ (accessed Mar 9, 2019).

[4] BASF Catalysts. *What is a Catalyst?* (2017), can be found under https://www.catalysts.basf.-com/about-us/what-is-a-catalyst (accessed Mar 9, 2019).

[5] I. Chorkendorff, J. W. Niemantsverdriet, *Concepts of Modern Catalysis and Kinetics*, 2nd ed.; Wiley-VCH Verlag GmbH & Co. KGaA, Weinheim (Germany), **2007**.

[6] BASF Catalysts, press photo BASF. *BASF catalysts* (12.11.2009), can be found under https://www.flickr.com/photos/basf/7460836832 (accessed Mar 9, 2019).

[7] D. Steinborn, *Grundlagen der metallorganischen Komplexkatalyse*, 1st ed.; B. G. Teubner Verlag, Wiesbaden (Germany), **2007**.

[8] N. Calderon, H. Y. Chen, K. W. Scott, *Tetrahedron Lett.* **1967**, *8*, 3327–3329.

[9] For an early review, see N. Calderon, *Acc. Chem. Res.* **1972**, *5*, 127–132.

[10] R. Streck, *Industrial Aspects of Olefin Metathesis/Polymerization Catalysts*. In *Olefin Metathesis and Polymerization Catalysts: Synthesis, Mechanism and Utilization* (Eds.: Y. İmamoğlu, B. Zümreoğlu-Karan, A. J. Amass), Springer, Dordrecht (Netherlands), **1990**, 439–515.

[11] C. Janiak, H.-J. Meyer, D. Gudat, P. Kurz, *Riedel Moderne Anorganische Chemie*, 5th ed.; De Gruyter, Berlin (Germany), Boston (MA, USA), **2018**.

[12] NobelPrize.org, Nobel Media AB 2019. *The Nobel Prize in Chemistry 2005*, can be found under https://www.nobelprize.org/prizes/chemistry/2005/summary/ (accessed Mar 9, 2019).

[13] For a selection, see *Alkene Metathesis in Organic Synthesis, Topics in Organometallic Chemistry*, Vol. 1, A. Fürstner (Ed.); Springer, Berlin (Germany), **1998**, and references 14–17.

[14] A. Fürstner, *Angew. Chem. Int. Ed.* **2000**, *39*, 3012–3043; *Angew. Chem.,* **2000,** *112,* 3140–3172.

[15] R. H. Grubbs, *Handbook of Metathesis*; Wiley-VCH Verlag GmbH, **2003**.

[16] R. R. Schrock, *Angew. Chem. Int. Ed.* **2006**, *45*, 3748–3759; *Angew. Chem.,* **2006,** *118,* 3832–3844.

[17] *Olefin Metathesis*, K. Grela (Ed.); John Wiley & Sons, Hoboken, NJ, USA, **2014**.

[18] *Handbook of Metathesis: Catalyst Development*, Vol. 1, R. H. Grubbs (Ed.); Wiley-VCH Verlag GmbH & Co. KGaA, Weinheim (Germany), **2003**.

[19] J. S. Kingsbury, J. P. A. Harrity, P. J. Bonitatebus, A. H. Hoveyda, *J. Am. Chem. Soc.* **1999**, *121*, 791–799.

[20] Y. Ginzburg, N. G. Lemcoff, *Hoveyda-Type Olefin Metathesis Complexes*. In *Olefin Metathesis* (Ed.: K. Grela), John Wiley & Sons, Hoboken, NJ, USA, **2014**, 437–451.

[21] M. Barbasiewicz, *Novel Concepts in Catalyst Design—A Case Study of Development of Hoveyda-Type Complexes*. In *Olefin Metathesis* (Ed.: K. Grela), John Wiley & Sons, Hoboken, NJ, USA, **2014**, 475–481.

[22] D. Astruc, *New J. Chem.* **2005**, *29*, 42–56.

[23] W. Zhang, J. S. Moore, *Adv. Synth. Catal.* **2007**, *349*, 93–120.

[24] A. Fürstner, *Angew. Chem. Int. Ed.* **2013**, *52*, 2794–2819; *Angew. Chem.,* **2013,** *125,* 2860–2887.

[25] A. Fürstner, *Alkyne Metathesis in Organic Synthesis*. In *Modern Alkyne Chemistry* (Eds.: B. M. Trost, C.-J. Li), Wiley-VCH Verlag GmbH & Co. KGaA, Weinheim (Germany), **2015**, 69–112.

[26] F. Pennella, R. L. Banks, G. C. Bailey, *Chem. Commun. (London)* **1968**, 1548–1549.

[27] A. Mortreux, M. Blanchard, *J. Chem. Soc., Chem. Commun.* **1974**, 786–787.

[28] T. J. Katz, J. McGinnis, *J. Am. Chem. Soc.* **1975**, *97*, 1592–1594.

[29] E. O. Fischer, G. Kreis, C. G. Kreiter, J. Müller, G. Huttner, H. Lorenz, *Angew. Chem. Int. Ed. Engl.* **1973**, *12*, 564–565; *Angew. Chem.,* **1973,** *85,* 618–620.

[30] D. N. Clark, R. R. Schrock, *J. Am. Chem. Soc.* **1978**, *100*, 6774–6776.

[31] R. R. Schrock, *Acc. Chem. Res.* **1986**, *19*, 342–348.

[32] R. R. Schrock, *Chem. Rev.* **2002**, *102*, 145–180.

[33] J. H. Wengrovius, J. Sancho, R. R. Schrock, *J. Am. Chem. Soc.* **1981**, *103*, 3932–3934.

[34] X. Wu, M. Tamm, *Beilstein J. Org. Chem.* **2011**, *7*, 82–93.

[35] R. R. Schrock, *Chem. Commun.* **2013**, *49*, 5529–5531.

[36] J. Sancho, R. R. Schrock, *J. Mol. Catal.* **1982**, *15*, 75–79.

[37] S. F. Pedersen, R. R. Schrock, M. R. Churchill, H. J. Wasserman, *J. Am. Chem. Soc.* **1982**, *104*, 6808–6809.

[38] M. R. Churchill, J. W. Ziller, J. H. Freudenberger, R. R. Schrock, *Organometallics* **1984**, *3*, 1554–1562.

[39] J. H. Freudenberger, R. R. Schrock, M. R. Churchill, A. L. Rheingold, J. W. Ziller, *Organometallics* **1984**, *3*, 1563–1573.

[40] H. Ehrhorn, M. Tamm, *Chem. Eur. J.* **2019**, *25*, 3190–3208.

[41] Y. Jin, Q. Wang, P. Taynton, W. Zhang, *Acc. Chem. Res.* **2014**, *47*, 1575–1586.

[42] T. Lindel, *Nachr. Chem.* **2000**, *48*, 1242–1244.

[43] A. Fürstner, P. W. Davies, *Chem. Commun.* **2005**, 2307–2320.

[44] G. Mata, B. Wölfl, A. Fürstner, *Chem. Eur. J.* **2019**, *25*, 246–254.

[45] B. Wölfl, G. Mata, A. Fürstner, *Chem. Eur. J.* **2019**, *25*, 255–259.

[46] B. N. Bhawal, B. Morandi, *Isr. J. Chem.* **2018**, *58*, 94–103.

[47] W. Zhang, S. Kraft, J. S. Moore, *J. Am. Chem. Soc.* **2004**, *126*, 329–335.

[48] L. Kloppenburg, D. Song, U. H. F. Bunz, *J. Am. Chem. Soc.* **1998**, *120*, 7973–7974.

[49] J. Heppekausen, R. Stade, R. Goddard, A. Fürstner, *J. Am. Chem. Soc.* **2010**, *132*, 11045–11057.

[50] W. Zhang, J. S. Moore, *J. Am. Chem. Soc.* **2004**, *126*, 12796–12796.

[51] W. Zhang, S. M. Brombosz, J. L. Mendoza, J. S. Moore, *J. Org. Chem.* **2005**, *70*, 10198–10201.

[52] W. Zhang, H. M. Cho, J. S. Moore, S. E. Denmark, C. R. Butler, *Org. Synth.* **2007**, *84*, 177–191.

[53] C. Elschenbroich, *Organometallchemie*, 6th ed.; B. G. Teubner Verlag, Wiesbaden (Germany), **2008**.

[54] W. A. Nugent, J. M. Mayer, *Metal-ligand multiple bonds: The chemistry of transition metal complexes containing oxo, nitrido, imido, alkylidene, or alkylidyne ligands*; John Wiley & Sons, New York, NY (USA), **1988**.

[55] M. Cui, R. Lin, G. Jia, *Chem. Asian J.* **2018**, *13*, 895–912, and references cited therein.

[56] B. E. Bursten, *J. Am. Chem. Soc.* **1983**, *105*, 121–122.

[57] T. Woo, E. Folga, T. Ziegler, *Organometallics* **1993**, *12*, 1289–1298.

[58] F. Erdman, III, D. B. Lawson, *J. Organomet. Chem.* **2005**, *690*, 4939–4944.

[59] C. H. Suresh, G. Frenking, *Organometallics* **2012**, *31*, 7171–7180.

[60] For theoretical calculations, see J. Zhu, G. Jia, Z. Lin, *Organometallics* **2006**, *25*, 1812–1819.

[61] S. Beer, K. Brandhorst, C. G. Hrib, X. Wu, B. Haberlag, J. Grunenberg, P. G. Jones, M. Tamm, *Organometallics* **2009**, *28*, 1534–1545.

[62] C. Bittner, H. Ehrhorn, D. Bockfeld, K. Brandhorst, M. Tamm, *Organometallics* **2017**, *36*, 3398–3406.

[63] D. P. Estes, C. P. Gordon, A. Fedorov, W.-C. Liao, H. Ehrhorn, C. Bittner, M. L. Zier, D. Bockfeld, K. W. Chan, O. Eisenstein, C. Raynaud, M. Tamm, C. Copéret, *J. Am. Chem. Soc.* **2017**, *139*, 17597–17607.

[64] K. Weiss, *Catalytic Reactions of Carbyne Complexes*. In *Carbyne Complexes*, VCH Verlagsgesellschaft, Weinheim (Germany), New York, NY (USA), **1988**, 205–228.

[65] H. Strutz, J. C. Dewan, R. R. Schrock, *J. Am. Chem. Soc.* **1985**, *107*, 5999–6005.

[66] S. Sarkar, K. P. McGowan, S. Kuppuswamy, I. Ghiviriga, K. A. Abboud, A. S. Veige, *J. Am. Chem. Soc.* **2012**, *134*, 4509–4512.

[67] C. D. Roland, H. Li, K. A. Abboud, K. B. Wagener, A. S. Veige, *Nat. Chem.* **2016**, *8*, 791–796.

[68] R. R. Schrock, S. F. Pedersen, M. R. Churchill, J. W. Ziller, *Organometallics* **1984**, *3*, 1574–1583.

[69] L. G. McCullough, R. R. Schrock, *J. Am. Chem. Soc.* **1984**, *106*, 4067–4068.

[70] A. Bray, A. Mortreux, F. Petit, M. Petit, T. Szymanska-Buzar, *J. Chem. Soc., Chem. Commun.* **1993**, 197–199.

[71] A. Mortreux, F. Petit, M. Petit, T. Szymanska-Buzar, *J. Mol. Catal. A* **1995**, *96*, 95–105.

[72] O. Coutelier, A. Mortreux, *Adv. Synth. Catal.* **2006**, *348*, 2038–2042.

[73] O. Coutelier, G. Nowogrocki, J.-F. Paul, A. Mortreux, *Adv. Synth. Catal.* **2007**, *349*, 2259–2263.

[74] M. R. Churchill, J. W. Ziller, *J. Organomet. Chem.* **1985**, *286*, 27–36.

[75] R. R. Schrock, J. H. Freudenberger, M. L. Listemann, L. G. McCullough, *J. Mol. Catal.* **1985**, *28*, 1–8.

[76] T. J. Katz, T. H. Ho, N. Y. Shih, Y. C. Ying, I. W. van Stuart, *J. Am. Chem. Soc.* **1984**, *106*, 2659–2668.

[77] A. Mayr, K. S. Lee, M. A. Kjelsberg, D. van Engen, *J. Am. Chem. Soc.* **1986**, *108*, 6079–6080, and references cited therein.

[78] R. R. Schrock, Z. J. Tonzetich, A. G. Lichtscheidl, P. Müller, F. J. Schattenmann, *Organometallics* **2008**, *27*, 3986–3995, and references cited therein.

[79] L. G. McCullough, R. R. Schrock, J. C. Dewan, J. C. Murdzek, *J. Am. Chem. Soc.* **1985**, *107*, 5987–5998.

[80] R. R. Schrock, J. S. Murdzek, J. H. Freudenberger, M. R. Churchill, J. W. Ziller, *Organometallics* **1986**, *5*, 25–33.

[81] L. G. McCullough, M. L. Listemann, R. R. Schrock, M. R. Churchill, J. W. Ziller, *J. Am. Chem. Soc.* **1983**, *105*, 6729–6730.

[82] J. H. Freudenberger, R. R. Schrock, *Organometallics* **1986**, *5*, 1411–1417.

[83] M. R. Churchill, J. W. Ziller, *J. Organomet. Chem.* **1985**, *281*, 237–248.

[84] J. Heppekausen, R. Stade, A. Kondoh, G. Seidel, R. Goddard, A. Fürstner, *Chem. Eur. J.* **2012**, *18*, 10281–10299.

[85] D. Melcher, *Entwicklung neuartiger Katalysatoren für die Alkinmetathese und die Butadiinmetathese-Depolymerisation*, PhD thesis, Technische Universität Braunschweig, Braunschweig (Germany), **2017**.

[86] F. J. Feher, M. Green, A. G. Orpen, *J. Chem. Soc., Chem. Commun.* **1986**, 291–293.

[87] E. V. Anslyn, M. J. Brusich, W. A. Goddard, III, *Organometallics* **1988**, *7*, 98–105.

[88] U. H. F. Bunz, L. Kloppenburg, *Angew. Chem. Int. Ed.* **1999**, *38*, 478–481; *Angew. Chem.,* **1999,** *111,* 503–505.

[89] J. C. López, J. Plumet, *Eur. J. Org. Chem.* **2011**, *2011*, 1803–1825.

[90] A. Fürstner, G. Seidel, *Angew. Chem. Int. Ed.* **1998**, *37*, 1734–1736; *Angew. Chem.,* **1998,** *110,* 1758–1760.

[91] For an example in natural product synthesis, see K. J. Ralston, H. C. Ramstadius, R. C. Brewster, H. S. Niblock, A. N. Hulme, *Angew. Chem. Int. Ed.* **2015**, *54*, 7086–7090; *Angew. Chem.,* **2015,** *127,* 7192–7196.

[92] A. Fürstner, *Alkyne Metathesis.* In *Handbook of Metathesis, Vol. 2* (Ed.: R. H. Grubbs), Wiley-VCH Verlag GmbH & Co. KGaA, Weinheim (Germany), **2003**, 432–462.

[93] A. Fürstner, *Chem. Commun.* **2011**, *47*, 6505–6511.

[94] U. H. F. Bunz, K. P. C. Vollhardt, *Acyclic Diyne Metathesis Utilizing in Situ Transition Metal Catalysts: An Efficient Access to Alkyne-Bridged Polymers.* In *Handbook of Metathesis, Vol. 3* (Ed.: R. H. Grubbs), Wiley-VCH Verlag GmbH & Co. KGaA, Weinheim (Germany), **2003**, 354–374.

[95] H. Yang, Y. Jin, Y. Du, W. Zhang, *J. Mater. Chem. A* **2014**, *2*, 5986–5993.

[96] O. Š. Miljanić, K. P. C. Vollhardt, G. D. Whitener, *Synlett* **2003**, 29–34.

[97] W. Zhang, J. S. Moore, *Angew. Chem. Int. Ed.* **2006**, *45*, 4416–4439; *Angew. Chem.,* **2006,** *118,* 4524–4548.

[98] H. Yang, Y. Zhu, Y. Du, D. Tan, Y. Jin, W. Zhang, *Mater. Chem. Front.* **2017**, *1*, 1369–1372.

[99] U. H. F. Bunz, *Chem. Rev.* **2000**, *100*, 1605–1644.

[100] M. Ortiz, C. Yu, Y. Jin, W. Zhang, *Top. Curr. Chem.* **2017**, *375*, No. 69.

[101] R. R. Schrock, *The Discovery and Development of High Oxidation State Alkylidyne Complexes for Alkyne Metathesis.* In *Handbook of Metathesis, Vol. 1* (Ed.: R. H. Grubbs), Wiley-VCH Verlag GmbH & Co. KGaA, Weinheim (Germany), **2003**, 173–189.

[102] U. H. F. Bunz, *Science* **2005**, *308*, 216–217.

[103] R. R. Schrock, *Chem. Commun.* **2005**, 2773–2777.

[104] A. Mortreux, O. Coutelier, *J. Mol. Catal. A* **2006**, *254*, 96–104.

[105] R. R. Schrock, C. Czekelius, *Adv. Synth. Catal.* **2007**, *349*, 55–77.

[106] M. Tamm, X. Wu, *Chem. Today* **2010**, *28*, 60–63.

[107] K. Jyothish, W. Zhang, *Angew. Chem. Int. Ed.* **2011**, *50*, 8478–8480; *Angew. Chem.,* **2011,** *123,* 8628–8630.

[108] C. Deraedt, M. d'Halluin, D. Astruc, *Eur. J. Inorg. Chem.* **2013**, 4881–4908.

[109] J. S. Murdzek, R. R. Schrock, *High Oxidation State Alkylidyne Complexes*. In *Carbyne Complexes*, VCH Verlagsgesellschaft, Weinheim (Germany), New York, NY (USA), **1988**, 147–203.

[110] B. Haberlag, X. Wu, K. Brandhorst, J. Grunenberg, C. G. Daniliuc, P. G. Jones, M. Tamm, *Chem. Eur. J.* **2010**, *16*, 8868–8877.

[111] A. Mayr, G. A. McDermott, *J. Am. Chem. Soc.* **1986**, *108*, 548–549.

[112] G. A. McDermott, A. M. Dorries, A. Mayr, *Organometallics* **1987**, *6*, 925–931.

[113] E. O. Fischer, A. Maasböl, *Chem. Ber.* **1967**, *100*, 2445–2456.

[114] E. O. Fischer, *Adv. Organomet. Chem.* **1976**, *14*, 1–32, and references cited therein.

[115] K. H. Dötz, J. Stendel, *Chem. Rev.* **2009**, *109*, 3227–3274, and references cited therein.

[116] E. O. Fischer, U. Schubert, *J. Organomet. Chem.* **1975**, *100*, 59–81.

[117] D. Himmelreich, E. O. Fischer, *Z. Naturforsch. B* **1982**, *37*, 1218–1218.

[118] S. J. Dossett, A. F. Hill, J. C. Jeffery, F. Marken, P. Sherwood, F. G. A. Stone, *J. Chem. Soc., Dalton Trans.* **1988**, 2453–2465.

[119] M. H. Chisholm, F. A. Cotton, M. Extine, B. R. Stults, *J. Am. Chem. Soc.* **1976**, *98*, 4477–4485.

[120] *Multiple Bonds Between Metal Atoms*, 3rd ed., F. A. Cotton, C. A. Murillo, R. A. Walton (Eds.); Springer US, Boston, MA, **2005**.

[121] H. Ehrhorn, J. Schlösser, D. Bockfeld, M. Tamm, *Beilstein J. Org. Chem.* **2018**, *14*, 2425–2434.

[122] R. R. Schrock, M. L. Listemann, L. G. Sturgeoff, *J. Am. Chem. Soc.* **1982**, *104*, 4291–4293.

[123] R. R. Schrock, *Science* **1983**, *219*, 13–18.

[124] M. L. Listemann, R. R. Schrock, *Organometallics* **1985**, *4*, 74–83.

[125] I. A. Latham, L. R. Sita, R. R. Schrock, *Organometallics* **1986**, *5*, 1508–1510.

[126] M. H. Chisholm, B. K. Conroy, B. W. Eichhorn, K. Folting, D. M. Hoffman, J. C. Huffman, N. S. Marchant, *Polyhedron* **1987**, *6*, 783–792.

[127] M. H. Chisholm, *Chem. Rec.* **2001**, *1*, 12–23.

[128] J. Sun, C. K. Simpson, M. D. Hopkins, A. S. Hock, R. R. Schrock, *Tungsten Benzylidyne Complexes*. In *Inorganic Syntheses* (Eds.: G. S. Girolami, A. P. Sattelberger), John Wiley & Sons, Hoboken, NJ (USA), **2014**, 134–138.

[129] H. Strutz, R. R. Schrock, *Organometallics* **1984**, *3*, 1600–1601.

[130] J. M. Blackwell, J. S. Figueroa, F. H. Stephens, C. C. Cummins, *Organometallics* **2003**, *22*, 3351–3353.

[131] R. L. Gdula, M. J. A. Johnson, *J. Am. Chem. Soc.* **2006**, *128*, 9614–9615.

[132] A. D. Finke, J. S. Moore, *Chem. Commun.* **2010**, *46*, 7939–7941.

[133] A. M. Geyer, M. J. Holland, R. L. Gdula, J. E. Goodman, M. J. A. Johnson, J. W. Kampf, *J. Organomet. Chem.* **2012**, *708–709*, 1–9.

[134] A. Fürstner, C. Mathes, C. W. Lehmann, *Chem. Eur. J.* **2001**, *7*, 5299–5317, and references cited therein.

[135] W. Zhang, S. Kraft, J. S. Moore, *Chem. Commun.* **2003**, 832–833.

[136] W. Zhang, Y. Lu, J. S. Moore, G. Seidel, A. Fürstner, *Org. Synth.* **2007**, *84*, 163–176.

[137] Y. Du, H. Yang, C. Zhu, M. Ortiz, K. D. Okochi, R. Shoemaker, Y. Jin, W. Zhang, *Chem. Eur. J.* **2016**, *22*, 7959–7963, and references cited therein.

[138] S. W. von Kugelgen, R. Sifri, D. E. Bellone, F. R. Fischer, *J. Am. Chem. Soc.* **2017**, *139*, 7577–7585.

[139] K. V. Bukhryakov, R. R. Schrock, A. H. Hoveyda, C. Tsay, P. Müller, *J. Am. Chem. Soc.* **2018**, *140*, 2797–2800.

[140] B. Haberlag, M. Freytag, P. G. Jones, M. Tamm, *Adv. Synth. Catal.* **2014**, *356*, 1255–1265.

[141] S. Beer, C. G. Hrib, P. G. Jones, K. Brandhorst, J. Grunenberg, M. Tamm, *Angew. Chem. Int. Ed.* **2007**, *46*, 8890–8894; *Angew. Chem.,* **2007,** *119,* 9047–9051.

[142] J. H. Oskam, H. H. Fox, K. B. Yap, D. H. McConville, R. O'Dell, B. J. Lichtenstein, R. R. Schrock, *J. Organomet. Chem.* **1993**, *459*, 185–198.

[143] R. R. Schrock, R. T. DePue, J. D. Fellmann, C. J. Schaverien, J. C. Dewan, A. H. Liu, *J. Am. Chem. Soc.* **1988**, *110*, 1423–1435.

[144] S. Lysenko, B. Haberlag, C. G. Daniliuc, P. G. Jones, M. Tamm, *ChemCatChem* **2011**, *3*, 115–118.

[145] S. Lysenko, J. Volbeda, P. G. Jones, M. Tamm, *Angew. Chem. Int. Ed.* **2012**, *51*, 6757–6761; *Angew. Chem.,* **2012,** *124,* 6861–6865.

[146] S. T. Li, T. M. Schnabel, S. Lysenko, K. Brandhorst, M. Tamm, *Chem. Commun.* **2013**, *49*, 7189–7191.

[147] T. M. Schnabel, D. Melcher, K. Brandhorst, D. Bockfeld, M. Tamm, *Chem. Eur. J.* **2018**, *24*, 9022–9032.

[148] F. Ungeheuer, A. Fürstner, *Chem. Eur. J.* **2015**, *21*, 11387–11392.

[149] S. Schaubach, K. Gebauer, F. Ungeheuer, L. Hoffmeister, M. K. Ilg, C. Wirtz, A. Fürstner, *Chem. Eur. J.* **2016**, *22*, 8494–8507.

[150] K. Jyothish, W. Zhang, *Angew. Chem. Int. Ed.* **2011**, *50*, 3435–3438; *Angew. Chem.,* **2011,** *123,* 3497–3500.

[151] K. Jyothish, Q. Wang, W. Zhang, *Adv. Synth. Catal.* **2012**, *354*, 2073–2078.

[152] H. Yang, Z. Liu, W. Zhang, *Adv. Synth. Catal.* **2013**, *355*, 885–890.

[153] Q. Wang, C. Zhang, B. C. Noll, H. Long, Y. Jin, W. Zhang, *Angew. Chem. Int. Ed.* **2014**, *53*, 10663–10667; *Angew. Chem.,* **2014,** *126,* 10839–10843.

[154] Q. Wang, C. Yu, H. Long, Y. Du, Y. Jin, W. Zhang, *Angew. Chem. Int. Ed.* **2015**, *54*, 7550–7554; *Angew. Chem.,* **2015,** *127,* 7660–7664.

[155] Y. Du, H. Yang, J. M. Whiteley, S. Wan, Y. Jin, S.-H. Lee, W. Zhang, *Angew. Chem. Int. Ed.* **2016**, *55*, 1737–1741; *Angew. Chem.,* **2016,** *128,* 1769–1773.

[156] Q. Wang, C. Yu, C. Zhang, H. Long, S. Azarnoush, Y. Jin, W. Zhang, *Chem. Sci.* **2016**, *7*, 3370–3376.

[157] B. Haberlag, M. Freytag, C. G. Daniliuc, P. G. Jones, M. Tamm, *Angew. Chem. Int. Ed.* **2012**, *51*, 13019–13022; *Angew. Chem.,* **2012,** *124,* 13195–13199.

[158] D. P. Estes, C. Bittner, Ò. Àrias, M. Casey, A. Fedorov, M. Tamm, C. Copéret, *Angew. Chem. Int. Ed.* **2016**, *55*, 13960–13964; *Angew. Chem.,* **2016,** *128,* 14166–14170.

[159] S. W. von Kugelgen, D. E. Bellone, R. R. Cloke, W. S. Perkins, F. R. Fischer, *J. Am. Chem. Soc.* **2016**, *138*, 6234–6239.

[160] P. Persich, J. Llaveria, R. Lhermet, T. de Haro, R. Stade, A. Kondoh, A. Fürstner, *Chem. Eur. J.* **2013**, *19*, 13047–13058.

[161] R. Lhermet, A. Fürstner, *Chem. Eur. J.* **2014**, *20*, 13188–13193.

[162] H. Ehrhorn, *Katalytische Metathese von Alkinen: Entwicklung neuer Katalysatoren*; Springer, Wiesbaden (Germany), **2017**.

[163] S. Hötling, C. Bittner, M. Tamm, S. Dähn, J. Collatz, J. L. M. Steidle, S. Schulz, *Org. Lett.* **2015**, *17*, 5004–5007.

[164] J. Willwacher, A. Fürstner, *Angew. Chem. Int. Ed.* **2014**, *53*, 4217–4221; *Angew. Chem.,* **2014,** *126,* 4301–4305.

[165] D. W. Paley, D. F. Sedbrook, J. Decatur, F. R. Fischer, M. L. Steigerwald, C. Nuckolls, *Angew. Chem. Int. Ed.* **2013**, *52*, 4591–4594; *Angew. Chem.,* **2013,** *125,* 4689–4692.

[166] A. Mortreux, N. Dy, M. Blanchard, *J. Mol. Catal.* **1976**, *1*, 101–109.

[167] For a recent example, see J. Geng Lopez, M. Zaranek, P. Pawluc, R. M. Gauvin, A. Mortreux, *Oil Gas Sci. Technol.* **2016**, *71*, 20–20.

[168] N. G. Pschirer, U. H. F. Bunz, *Tetrahedron Lett.* **1999**, *40*, 2481–2484.

[169] K. Grela, J. Ignatowska, *Org. Lett.* **2002**, *4*, 3747–3749.

[170] V. Sashuk, J. Ignatowska, K. Grela, *J. Org. Chem.* **2004**, *69*, 7748–7751.

[171] M. Koy, I. Elser, J. Meisner, W. Frey, K. Wurst, J. Kästner, M. R. Buchmeiser, *Chem. Eur. J.* **2017**, *23*, 15484–15490.

[172] K. Grela, A. Michrowska, M. Bieniek, *Chem Rec.* **2006**, *6*, 144–156.

[173] H. Jeong, S. W. von Kugelgen, D. E. Bellone, F. R. Fischer, *J. Am. Chem. Soc.* **2017**, *139*, 15509–15514.

[174] F. H. Allen, *Acta Crystallogr., Sect. B: Struct. Sci.* **2002**, *58*, 380–388.

[175] W. J. Doucette, J. Kim, J. A. Kautz, S. L. Gipson, *Inorg. Chim. Acta* **2000**, *304*, 237–240.

[176] Ò. Àrias, H. Ehrhorn, J. Härdter, P. G. Jones, M. Tamm, *Organometallics* **2018**, *37*, 4784–4800.

[177] F. H. Allen, O. Kennard, D. G. Watson, L. Brammer, A. G. Orpen, R. Taylor, *J. Chem. Soc., Perkin Trans. 2* **1987**, S1–S19.

[178] $\tau_4 = (360 - \alpha - \beta)/141$, where α and β represent the two largest angles around the metal atom. The values range between idealised square-planar ($\tau_4 = 0$), seesaw ($\tau_4 = 0–0.85$), trigonal-pyramidal ($\tau_4 = 0.85$), and tetrahedral ($\tau_4 = 1$) geometries. See L. Yang, D. R. Powell, R. P. Houser, *Dalton Trans.* **2007**, 955–964.

[179] K. H. Dötz, H. Larbig, K. Harms, *Chem. Ber.* **1992**, *125*, 2143–2148.

[180] P. Pyykkö, M. Atsumi, *Chem. Eur. J.* **2009**, *15*, 186–197.

[181] H.-P. Abicht, K. Issleib, *J. Organomet. Chem.* **1977**, *132*, 327–331.

[182] K. H. Dötz, M. Popall, *Angew. Chem. Int. Ed. Engl.* **1987**, *26*, 1158–1160; *Angew. Chem.,* **1987,** *99,* 1220–1221, and references cited therein.

[183] K. H. Dötz, M. Popall, *Chem. Ber.* **1988**, *121*, 665–672.

[184] K. H. Dötz, H.-G. Erben, W. Staudacher, K. Harms, G. Müller, J. Riede, *J. Organomet. Chem.* **1988**, *355*, 177–191.

[185] K. H. Dötz, M. Popall, G. Müller, K. Ackermann, *J. Organomet. Chem.* **1990**, *383*, 93–111.

[186] M. Jaeger, R. Stumpf, C. Troll, H. Fischer, *Chem. Commun.* **2000**, 931–932.

[187] R. Stumpf, N. Burzlaff, B. Weibert, H. Fischer, *J. Organomet. Chem.* **2002**, *651*, 66–71.

[188] $\tau_5 = (\alpha - \beta)/60$, where α and β represent the two largest angles around the metal atom. The values range between idealised square-pyramidal ($\tau_5 = 0$) and trigonal-bipyramidal ($\tau_5 = 1$) geometries. See A. W. Addison, T. N. Rao, J. Reedijk, J. van Rijn, G. C. Verschoor, *J. Chem. Soc., Dalton Trans.* **1984**, 1349–1356.

[189] A. G. Orpen, L. Brammer, F. H. Allen, O. Kennard, D. G. Watson, R. Taylor, *J. Chem. Soc., Dalton Trans.* **1989**, S1–S83.

[190] Most of the work described in this subchapter was conducted as part of a Bachelor's thesis supervised by the author of this dissertation; see J. Härdter, *Synthese von para-Methoxybenzylidin-Molybdänkomplexen*, Bachelor's thesis, Technische Universität Braunschweig, Braunschweig (Germany), **2015**.

[191] C. Lorber, L. Vendier, *Organometallics* **2010**, *29*, 1127–1136.

[192] P. Pyykkö, S. Riedel, M. Patzschke, *Chem. Eur. J.* **2005**, *11*, 3511–3520.

[193] This compound has been independently prepared by R. R. Schrock and coworkers; see F. Zhai, K. V. Bukhryakov, R. R. Schrock, A. H. Hoveyda, C. Tsay, P. Müller, *J. Am. Chem. Soc.* **2018**, *140*, 13609–13613.

[194] S. S. Batsanov, *Inorg. Mater.* **2001**, *37*, 871–885.

[195] A. M. Geyer, R. L. Gdula, E. S. Wiedner, M. J. A. Johnson, *J. Am. Chem. Soc.* **2007**, *129*, 3800–3801.

[196] A. M. Geyer, E. S. Wiedner, J. B. Gary, R. L. Gdula, N. C. Kuhlmann, M. J. A. Johnson, B. D. Dunietz, J. W. Kampf, *J. Am. Chem. Soc.* **2008**, *130*, 8984–8999.

[197] J. H. Freudenberger, R. R. Schrock, *Organometallics* **1986**, *5*, 398–400.

[198] Z. J. Tonzetich, Y. C. Lam, P. Müller, R. R. Schrock, *Organometallics* **2007**, *26*, 475–477.

[199] R. L. Gdula, M. J. A. Johnson, N. W. Ockwig, *Inorg. Chem.* **2005**, *44*, 9140–9142.

[200] R. R. Schrock, J. Y. Jamieson, J. P. Araujo, P. J. Bonitatebus, Jr., A. Sinha, L. P. H. Lopez, *J. Organomet. Chem.* **2003**, *684*, 56–67.

[201] X. Wu, *New Tungsten Alkylidyne Complexes as Catalysts for Alkyne Metathesis*, PhD Thesis, Technische Universität Braunschweig, Braunschweig (Germany), **2011**.

[202] G. R. Fulmer, A. J. M. Miller, N. H. Sherden, H. E. Gottlieb, A. Nudelman, B. M. Stoltz, J. E. Bercaw, K. I. Goldberg, *Organometallics* **2010**, *29*, 2176–2179.

[203] M. Bindl, R. Stade, E. K. Heilmann, A. Picot, R. Goddard, A. Fürstner, *J. Am. Chem. Soc.* **2009**, *131*, 9468–9470.

[204] For example, see X. Bantreil, R. A. M. Randall, A. M. Z. Slawin, S. P. Nolan, *Organometallics* **2010**, *29*, 3007–3011, and references cited therein.

[205] P. M. Hauser, M. Hunger, M. R. Buchmeiser, *ChemCatChem* **2018**, *10*, 1829–1834.

[206] N. Kuhn, T. Kratz, *Synthesis*, *1993*, 561–562.

[207] W. E. Buhro, M. H. Chisholm, *Adv. Organomet. Chem.* **1987**, *27*, 311–369.

[208] Also known as ynediamines. For example, see H. G. Viehe, *Ynamines.* In *Chemistry of Acetylenes* (Ed.: H. G. Viehe), M. Dekker, New York, NY (USA), **1969**, 861–912.

[209] For example, see W. W. Seidel, M. J. Meel, M. Schaffrath, T. Pape, *Eur. J. Org. Chem.* **2007**, 3526–3532.

[210] S. Beer, *Entwicklung neuartiger Katalysatoren für die Alkinmetathese*, PhD Thesis, Technische Universität Braunschweig, Braunschweig (Germany), **2008**.

[211] H. Ehrhorn, D. Bockfeld, M. Freytag, T. Bannenberg, C. E. Kefalidis, L. Maron, M. Tamm, *Organometallics* **2019**, *38*, 1627–1639.

[212] C. Feng, T.-P. Loh, *Chem. Commun.* **2010**, *46*, 4779–4781.

[213] For a review, see C. Copéret, A. Comas-Vives, M. P. Conley, D. P. Estes, A. Fedorov, V. Mougel, H. Nagae, F. Núñez-Zarur, P. A. Zhizhko, *Chem. Rev.* **2016**, *116*, 323–421.

[214] H. Weissman, K. N. Plunkett, J. S. Moore, *Angew. Chem. Int. Ed.* **2006**, *45*, 585–588; *Angew. Chem.,* **2006,** *118,* 599–602, and references cited therein.

[215] N. Merle, M. Taoufik, M. Nayer, A. Baudouin, E. Le Roux, R. M. Gauvin, F. Lefebvre, J. Thivolle-Cazat, J.-M. Basset, *J. Organomet. Chem.* **2008**, *693*, 1733–1737.

[216] M. Genelot, N. P. Cheval, M. Vitorino, E. Berrier, J.-M. Weibel, P. Pale, A. Mortreux, R. M. Gauvin, *Chem. Sci.* **2013**, *4*, 2680–2685.

[217] L. F. Fieser, K. L. Williamson, *Organic Experiments*, 7th ed.; D. C. Heath and Company, Lexington, MA (USA), **1992**.

[218] D. W. Mayo, R. M. Pike, D. C. Forbes, *Microscale Organic Laboratory: with Multistep and Multiscale Synthesis*, 6th ed.; John Wiley & Sons, Hoboken, NJ (USA), **2015**.

[219] R. Gleiter, D. B. Werz, *Chem. Rev.* **2010**, *110*, 4447–4488.

[220] A. Fürstner, C. Mathes, *Org. Lett.* **2001**, *3*, 221–223.

[221] D. Villemin, M. Héroux, V. Blot, *Tetrahedron Lett.* **2001**, *42*, 3701–3703.

[222] P. van de Weghe, P. Bisseret, N. Blanchard, J. Eustache, *J. Organomet. Chem.* **2006**, *691*, 5078–5108.

[223] R. B. King, C. A. Harmon, *Inorg. Chem.* **1976**, *15*, 879–885.

[224] J. Heck, K.-A. Kriebisch, W. Massa, S. Wocadlo, *J. Organomet. Chem.* **1994**, *482*, 81–84.

[225] S. R. Klopfenstein, C. Kluwe, K. Kirschbaum, J. A. Davies, *Can. J. Chem.* **1996**, *74*, 2331–2339.

[226] A. C. Filippou, T. Rosenauer, *Angew. Chem. Int. Ed.* **2002**, *41*, 2393–2396; *Angew. Chem.,* **2002,** *114,* 2499–2502.

[227] A. R. Petrov, T. Bannenberg, C. G. Daniliuc, P. G. Jones, M. Tamm, *Dalton Trans.* **2011**, *40*, 10503–10512.

[228] Ò. Àrias, A. R. Petrov, T. Bannenberg, K. Altenburger, P. Arndt, P. G. Jones, U. Rosenthal, M. Tamm, *Organometallics* **2014**, *33*, 1774–1786.

[229] For examples in main-group chemistry, see Y. N. Lebedev, U. Das, O. Chernov, G. Schnakenburg, A. C. Filippou, *Chem. Eur. J.* **2014**, *20*, 9280–9289, and references 230–235.

[230] H. Kelch, S. Kachel, M. A. Celik, M. Schäfer, B. Wennemann, K. Radacki, A. R. Petrov, M. Tamm, H. Braunschweig, *Chem. Eur. J.* **2016**, *22*, 13815–13818.

[231] R. Bertermann, H. Braunschweig, M. A. Celik, T. Dellermann, H. Kelch, *Chem. Commun.* **2016**, *52*, 13249–13252.

[232] J. Böhnke, H. Braunschweig, A. Deißenberger, T. Dellermann, R. D. Dewhurst, J. O. C. Jiménez-Halla, S. Kachel, H. Kelch, D. Prieschl, *Chem. Commun.* **2017**, *53*, 12132–12135.

[233] L. Winner, A. Hermann, G. Bélanger-Chabot, O. F. González-Belman, J. O. C. Jiménez-Halla, H. Kelch, H. Braunschweig, *Chem. Commun.* **2018**, *54*, 8210–8213.

[234] A. Hofmann, A. Lamprecht, O. F. González-Belman, R. D. Dewhurst, J. O. C. Jiménez-Halla, S. Kachel, H. Braunschweig, *Chem. Commun.* **2018**, *54*, 1639–1642.

[235] H. Kelch, S. Kachel, J. Wahler, M. A. Celik, A. Stoy, I. Krummenacher, T. Kramer, K. Radacki, H. Braunschweig, *Chem. Eur. J.* **2018**, *24*, 15387–15391.

[236] A. R. Petrov, C. G. Daniliuc, P. G. Jones, M. Tamm, *Chem. Eur. J.* **2010**, *16*, 11804–11808.

[237] R. Knorr, *Chem. Rev.* **2004**, *104*, 3795–3850.

[238] J. Torres-Alacan, U. Das, B. Wezisla, M. Straßmann, A. C. Filippou, P. Vöhringer, *Chem. Eur. J.* **2015**, *21*, 17184–17190.

[239] B. Wezisla, J. Lindner, U. Das, A. C. Filippou, P. Vöhringer, *Angew. Chem. Int. Ed.* **2017**, *56*, 6901–6905; *Angew. Chem.,* **2017,** *129,* 7005–7009.

[240] M. B. Smith, J. March, *Advanced organic chemistry: Reactions, mechanisms, and structure*, 6th ed.; John Wiley & Sons, Hoboken, NJ (USA), **2007**.

[241] C. J. Adams, K. M. Anderson, I. M. Bartlett, N. G. Connelly, A. G. Orpen, T. J. Paget, H. Phetmung, D. W. Smith, *J. Chem. Soc., Dalton Trans.* **2001**, 1284–1292.

[242] R. R. Schrock, S. W. Seidel, N. C. Mösch-Zanetti, K.-Y. Shih, M. B. O'Donoghue, W. M. Davis, W. M. Reiff, *J. Am. Chem. Soc.* **1997**, *119*, 11876–11893.

[243] H. F. King, R. E. Stanton, H. Kim, R. E. Wyatt, R. G. Parr, *J. Chem. Phys.* **1967**, *47*, 1936–1941.

[244] Z. Lin, M. B. Hall, *Organometallics* **1994**, *13*, 2878–2884.

[245] R. P. Hughes, J. W. Reisch, A. L. Rheingold, *Organometallics* **1985**, *4*, 1754–1761.

[246] D. Lloyd, H. McNab, *Angew. Chem. Int. Ed. Engl.* **1976**, *15*, 459–468; *Angew. Chem.,* **1976,** *88,* 496–504.

[247] U. Nubbemeyer, *Science of Synthesis*, **2008**, *32*, Section 32.3.4.1.5.5, 275–275.

[248] A. Fürstner, M. Alcarazo, H. Krause, *Org. Synth.* **2009**, *86*, 298–307.

[249] K. Park, G. Bae, J. Moon, J. Choe, K. H. Song, S. Lee, *J. Org. Chem.* **2010**, *75*, 6244–6251.

[250] X. Li, F. Yang, Y. Wu, *RSC Adv.* **2014**, *4*, 13738–13741.

[251] J. S. Murdzek, L. Blum, R. R. Schrock, *Organometallics* **1988**, *7*, 436–441.

[252] A. Mayr, G. A. McDermott, A. M. Dorries, *Organometallics* **1985**, *4*, 608–610.

[253] J.-J. Cho, J. T. Park, *Bull. Korean Chem. Soc.* **1995**, *16*, 1130–1132.

[254] W. L. F. Armarego, C. L. L. Chai, *Purification of Laboratory Chemicals*, 7th ed.; Butterworth-Heinemann, Amsterdam (Netherlands), **2013**.

[255] G. M. Sheldrick, *Acta Crystallogr., Sect. A: Found. Crystallogr.* **2008**, *64*, 112–122.

[256] G. M. Sheldrick, *Acta Crystallographica Section A* **2015**, *71*, 3–8.

[257] G. M. Sheldrick, *Acta Crystallogr., Sect. C: Struct. Chem.* **2015**, *71*, 3–8.

[258] K. Brandenburg. *DIAMOND, Version 4.3.0*; Crystal Impact GbR, Bonn (Germany), **2016**.

[259] M. J. Frisch, G. W. Trucks, H. B. Schlegel, G. E. Scuseria, M. A. Robb, J. R. Cheeseman, G. Scalmani, V. Barone, B. Mennucci, G. A. Petersson, H. Nakatsuji, M. Caricato, X. Li, H. P. Hratchian, A. F. Izmaylov, J. Bloino, G. Zheng, J. L. Sonnenberg, M. Hada, M. Ehara, K. Toyota, R. Fukuda, J. Hasegawa, M. Ishida, T. Nakajima, Y. Honda, O. Kitao, H. Nakai, T. Vreven, J. A. Montgomery, Jr., J. E. Peralta, F. Ogliaro, M. Bearpark, J. J. Heyd, E. Brothers, K. N. Kudin, V. N. Staroverov, R. Kobayashi, J. Normand, K. Raghavachari, A. Rendell, J. C. Burant, S. S. Iyengar, J. Tomasi, M. Cossi, N. Rega, J. M. Millam, M. Klene, J. E. Knox, J. B. Cross, V. Bakken, C. Adamo, J. Jaramillo, R. Gomperts, R. E. Stratmann, O. Yazyev, A. J. Austin, R. Cammi, C. Pomelli, J. W. Ochterski, R. L. Martin, K. Morokuma, V. G. Zakrzewski, G. A. Voth, P. Salvador, J. J. Dannenberg, S. Dapprich, A. D. Daniels, Ö. Farkas, J. B. Foresman, J. V. Ortiz, J. Cioslowski, D. J. Fox. *Gaussian 09, Revision D.01*; Gaussian Inc., Wallingford, CT (USA), **2009**.

[260] A. D. Becke, *Phys. Rev. A* **1988**, *38*, 3098–3100.

[261] C. Lee, W. Yang, R. G. Parr, *Phys. Rev. B* **1988**, *37*, 785–789.

[262] D. Andrae, U. Häußermann, M. Dolg, H. Stoll, H. Preuß, *Theoret. Chim. Acta* **1990**, *77*, 123–141.

[263] M. D. Walter, M. Schultz, R. A. Andersen, *New J. Chem.* **2006**, *30*, 238–246.

[264] G. A. Bain, J. F. Berry, *J. Chem. Educ.* **2008**, *85*, 532–536.

[265] E. Hünerhoff, *Prax. Naturwiss., Chem.* **1973**, *22*, 156–157.

[266] J. S. Lum, L. Tahsini, J. A. Golen, C. Moore, A. L. Rheingold, L. H. Doerrer, *Chem. Eur. J.* **2013**, *19*, 6374–6384.

[267] R. E. A. Dear, W. B. Fox, R. J. Fredericks, E. E. Gilbert, D. K. Huggins, *Inorg. Chem.* **1970**, *9*, 2590–2591.

[268] J. Betz, W. Bauer, *J. Am. Chem. Soc.* **2002**, *124*, 8699–8706.

[269] F. A. Cotton, S. A. Koch, M. Millar, *Inorg. Chem.* **1978**, *17*, 2087–2093.

[270] S. Harder, J. Boersma, L. Brandsma, J. A. Kanters, A. J. M. Duisenberg, J. H. van Lenthe, *Organometallics* **1990**, *9*, 511–516.

[271] A. L. Spek, *Acta Crystallogr., Sect. C: Struct. Chem.* **2015**, *71*, 9–18.

[272] G. Himbert, H. Naßhan, S. Kosack, *Synlett* **1991**, 117–118.

[273] National Institute of Advanced Industrial Science and Technology. *SDBSWeb*, can be found under https://sdbs.db.aist.go.jp (accessed Mar 30, 2019).

[274] C. J. Cooksey, J. L. Courtneidge, A. G. Davies, P. S. Gregory, J. C. Evans, C. C. Rowlands, *J. Chem. Soc., Perkin Trans. 2* **1988**, 807–813.

[275] W. Zhang, H. Wu, Z. Liu, P. Zhong, L. Zhang, X. Huang, J. Cheng, *Chem. Commun.* **2006**, 4826–4828.